



RCSI

UNIVERSITY
OF MEDICINE
AND HEALTH
SCIENCES

Royal College of Surgeons in Ireland

repository@rcsi.com

The Development of Bilayered Collagen-GAG Scaffolds for Applications in Airway Modelling and Tissue Regeneration

AUTHOR(S)

Cian O'Leary

CITATION

O'Leary, Cian (2016): The Development of Bilayered Collagen-GAG Scaffolds for Applications in Airway Modelling and Tissue Regeneration. Royal College of Surgeons in Ireland. Thesis.
<https://doi.org/10.25419/rcsi.10809959.v1>

DOI

[10.25419/rcsi.10809959.v1](https://doi.org/10.25419/rcsi.10809959.v1)

LICENCE

CC BY-NC-SA 4.0

This work is made available under the above open licence by RCSI and has been printed from <https://repository.rcsi.com>. For more information please contact repository@rcsi.com

URL

https://repository.rcsi.com/articles/thesis/The_Development_of_Bilayered_Collagen-GAG_Scaffolds_for_Applications_in_Airway_Modelling_and_Tissue_Regeneration/10809959/1



**The Development of Bilayered Collagen-GAG Scaffolds
for Applications in Airway Modelling and Tissue
Regeneration**

Cian O'Leary BPharm MPharm MPSI

School of Pharmacy and Dept. of Anatomy

A thesis submitted to the School of Postgraduate Studies, Faculty of
Medicine and Health Sciences, Royal College of Surgeons in Ireland,
in fulfilment of the requirements for the degree of

Doctor of Philosophy

April 2016

Supervisors

Prof. Sally-Ann Cryan

Prof. Fergal J. O'Brien

Declaration

I declare that this thesis, which I submit to RCSI for examination in consideration of the award of a higher degree of Doctor of Philosophy, is my own personal effort. Where any of the content presented is the result of input or data from a related collaborative research programme this is duly acknowledged in the text such that it is possible to ascertain how much of the work is my own. I have not already obtained a degree in RCSI or elsewhere on the basis of this work. Furthermore, I took reasonable care to ensure that the work is original, and, to the best of my knowledge, does not breach copyright law, and has not been taken from other sources except where such work has been cited and acknowledged within the text.

Signed _____

Student Number _____

Date _____

Abstract

Today, lung disease and major airway trauma are a significant global healthcare concern with limited treatment options. Incurable airway diseases such as asthma, chronic obstructive pulmonary disease, cystic fibrosis and idiopathic pulmonary fibrosis contribute to an enormous clinical and socioeconomic burden. At the core of many of these debilitating conditions, epithelial cell dysfunction and persistent inflammatory damage to respiratory tissue play a central role in their pathophysiology. In order to identify new therapies that can cure these diseases and repair or replace damaged tissue, physiologically-representative *in vitro* models must be developed for improved drug development, in addition to new surgical interventions for extensive lung tissue injury. Tissue engineering strategies have the potential to provide such complex *in vitro* models as well as next generation biocompatible tissue replacement treatments.

The overall goal of this PhD project was to develop a novel tissue-engineered 3D *in vitro* model of the tracheobronchial region with potential applications in respiratory drug development and respiratory tissue regeneration. Specifically, this thesis sought to investigate the potential of collagen-glycosaminoglycan (CG) scaffolds as a 3D substrate for the growth and differentiation of a bronchial epithelial cell line and to develop a novel bilayered CG scaffold as an *in vitro* co-culture model for both a bronchial epithelial cell line and primary tracheobronchial epithelial cells. A final objective was to manufacture an all-*trans* retinoic acid-eluting bilayered scaffold as a platform technology for tracheal tissue regeneration.

This thesis initially investigated the ability of a fully-porous collagen-chondroitin-6-sulphate scaffold to support the growth and differentiation of the Calu-3 epithelial cell line under two sets of respiratory culture conditions: air-liquid interface (ALI) culture and liquid-liquid interface (LLI) culture. Scaffolds not only supported cell growth, but also had a direct influence on increasing epithelial mucin secretion when compared to culture on standard polymeric cell inserts at an ALI. The scaffold was verified as a suitable substrate for a novel tracheobronchial *in vitro* model, although the formation of a robust ciliated epithelial barrier was not possible on the porous biomaterial. Accordingly, the thesis next focused on the manufacture of a bilayered scaffold structure that mimicked tracheobronchial

tissue architecture and composition. This bilayered collagen-hyaluronate (CHyA-B) scaffold was composed of a thin, densely-packed film top-layer for epithelial monolayer culture and a porous submucosal layer for 3D co-culture with lung fibroblasts. The scaffold design succeeded in resolving the major limitation of the fully-porous biomaterial by facilitating the formation of a confluent and continuous Calu-3 cell monolayer with suitable epithelial barrier integrity. Furthermore, this cell barrier was ciliated, pseudostratified in morphology and maintained enhanced mucin secretion, with organotypic localisation above a submucosal analogue of co-cultured fibroblasts and scaffold.

This study validated the CHyA-B scaffold as an innovative platform technology to generate a physiologically-representative 3D tracheobronchial *in vitro* model. In order to apply this novel 3D culture system as an organotypic physiological representation of the tracheobronchial region, the next stage of the project progressed to using a primary tracheobronchial epithelial cell co-culture with lung fibroblasts. As well as supporting Calu-3 epithelial cells, the CHyA-B scaffold also supported the growth and differentiation of primary tracheobronchial epithelial cells in the successful development of an organotypic 3D co-culture model with the formation of a ciliated pseudostratified epithelium that secreted mucus and exhibited a physiologically-relevant barrier integrity.

Having developed the CHyA-B scaffold as a 3D *in vitro* co-culture model with primary epithelial cells and lung fibroblasts, the final study in this thesis investigated the potential of the scaffold as a platform technology for tracheal tissue regeneration. For this application, *all-trans* retinoic acid (atRA) was incorporated into the film layer of the scaffold as a potential enhancer of rapid functional epithelialisation of the CHyA-B scaffold that is critical for tracheal implants. This atRA-CHyA-B scaffold was successfully manufactured and displayed stable retention of the drug in the film layer prior to its release in physiological buffer. The drug-loaded film layer of this scaffold enhanced mucociliary gene expression of tracheobronchial epithelial cells and with future studies, the atRA-CHyA-B scaffold can potentially pioneer the development of a novel and biocompatible device to address a currently unmet clinical need in tracheal replacement.

In conclusion, this thesis has successfully developed a bilayered collagen-glycosaminoglycan scaffold with applications in both airway modelling and tissue regeneration. This scaffold holds potential as a biofabricated template that provides a physiologically-relevant 3D *in vitro* model to develop novel therapeutics, perform toxicological analysis of inhalable formulations and generate more sophisticated disease models for understanding and treating respiratory disease. Finally, this scaffold can also be applied as a novel technology with enhanced functional epithelialisation for tracheal tissue regeneration as an advanced medical device that can potentially overcome the limitations of current tracheal implants.

Table of Contents

Declaration.....	2
Abstract.....	3
Acknowledgements.....	16
Publications, grants, prizes and presentations related to thesis.....	18
List of abbreviations.....	22
List of figures.....	26
List of tables.....	29
List of equations.....	29

Chapter 1: Introduction and literature review

1.1. The respiratory system: respiratory disease and drug development.....	32
1.1.1. <i>Overview: the burden of respiratory disease and injury</i>	32
1.1.2. <i>Anatomy and physiology of the respiratory tract</i>	33
1.1.2.1. <i>Anatomy and physiology of the conducting zone of the respiratory tract</i>	34
1.1.2.2. <i>Anatomy and physiology of the respiratory zone of the respiratory tract</i>	35
1.1.3. <i>Treatment of respiratory disease</i>	36
1.1.3.1. <i>Pharmacotherapy</i>	37
1.1.3.2. <i>Surgical intervention</i>	38
1.1.3.3. <i>The development of novel treatments</i>	39
1.2. Current respiratory drug development models.....	41
1.2.1. <i>Cell culture models</i>	42
1.2.2. <i>Animal models</i>	44
1.2.3. <i>Limitations of current cell culture and animal models</i>	45
1.3. Tissue engineering and the respiratory system.....	47
1.3.1. <i>Tissue engineering: an alternative approach to respiratory drug development and the treatment respiratory disease</i>	47
1.3.2. <i>Cell sources for respiratory tissue engineering and regeneration</i>	49

1.3.2.1. Endogenous lung stem cell populations of the of the respiratory tract.....	49
1.3.2.2. Other lung stem cell populations.....	51
1.3.3. Signalling factors for respiratory tissue engineering and regeneration.....	52
1.3.3.1. Hepatocyte growth factor (HGF).....	52
1.3.3.2. Bone morphogenetic protein 4 (BMP4).....	53
1.3.3.3. Keratinocyte growth factor (KGF).....	54
1.3.3.4. All-trans retinoic acid (atRA).....	54
1.3.4. Biomaterials for respiratory tissue engineering and regeneration.....	55
1.3.4.1. Biomaterials for alveolar tissue engineering and regeneration.....	55
1.3.5. Biomaterials for tracheobronchial tissue engineering and regeneration.....	58
1.3.5.1. Hydrogels.....	58
1.3.5.2. Decellularised tissue.....	61
1.3.5.3. Porous polymeric scaffolds.....	63
1.4. The Tissue Engineering Research Group (TERG): collagen-based scaffolds for tissue engineering and regeneration.....	68
1.5. Thesis objectives.....	70

Chapter 2: The assessment of CG scaffolds as a 3D substrate for the growth and differentiation of a bronchial epithelial cell line

2.1. Introduction.....	72
2.2. Materials and Methods.....	74
2.2.1. Collagen-chondroitin-6-sulphate (CCS) scaffold fabrication.....	74
2.2.1.1. Scaffold manufacture.....	74
2.2.1.2. Chemical crosslinking.....	74
2.2.2. Epithelial cell culture on CCS scaffolds.....	75
2.2.2.1. Cell line and culture medium.....	75
2.2.2.2. Air-liquid interface (ALI) culture on CCS scaffolds.....	76
2.2.2.3. Liquid-liquid interface (LLI) culture on CCS scaffolds.....	77
2.2.3. Epithelial cell growth on CCS scaffolds.....	77

2.2.4. Epithelial cell differentiation on CCS scaffolds.....	77
2.2.4.1. Mucin expression.....	77
2.2.4.2. Tight junction formation.....	78
2.2.4.3. Epithelial ciliation.....	79
2.2.4.4. Expression of genetic markers of epithelial differentiation.....	79
2.2.5. Cell morphology and migration on CCS scaffolds.....	79
2.2.6. Data analysis.....	80
2.3. Results.....	81
2.3.1. Epithelial cell growth on CCS scaffolds.....	81
2.3.2. Mucin expression on CCS scaffolds.....	82
2.3.3. Tight junction formation on CCS scaffolds.....	83
2.3.4. Ciliation on CCS scaffolds.....	84
2.3.5. Expression of genetic markers of cellular differentiation on CCS scaffolds.....	85
2.3.5.1. Expression of MUC5AC on CCS scaffolds.....	85
2.3.5.2. Expression of ZO-1 on CCS scaffolds.....	86
2.3.5.3. Expression of FOXJ1 on CCS scaffolds.....	87
2.3.6. Cell morphology and migration on CCS scaffolds.....	89
2.4. Discussion.....	90
2.5. Conclusion.....	95

Chapter 3: The development of a bilayered CG scaffold as a substrate for a bronchial epithelial cell line 3D *in vitro* co-culture model

3.1. Introduction.....	98
3.2. Materials and Methods.....	100
3.2.1. Bilayered collagen-hyaluronate (CHyA-B) scaffold manufacture.....	100
3.2.1.1. Collagen-hyaluronate (CHyA) film layer fabrication.....	100
3.2.1.2. Bilayered scaffold manufacture.....	100
3.2.1.3. Chemical crosslinking.....	101
3.2.2. CHyA-B scaffold characterisation.....	101

3.2.2.1. Scaffold ultrastructure.....	101
3.2.2.2. Interfacial adhesion strength.....	101
3.2.2.3. Mechanical testing.....	102
3.2.2.4. Pore size analysis.....	102
3.2.3. Calu-3 epithelial cell culture on CHyA-B scaffolds.....	103
3.2.3.1. Cell source and culture medium.....	103
3.2.3.2. Epithelial cell monoculture.....	104
3.2.3.3. Epithelial cell co-culture with fibroblasts.....	105
3.2.4. Cell morphology and migration.....	106
3.2.4.1. Histology.....	106
3.2.4.2. Scanning electron microscopy (SEM).....	106
3.2.5. Calu-3 epithelial cell differentiation on CHyA-B scaffolds.....	107
3.2.5.1. Immunofluorescence.....	107
3.2.5.2. Transmission electron microscopy (TEM).....	107
3.2.5.3. Expression of genetic markers of epithelial cell differentiation.....	108
3.2.6. Evaluation of Calu-3 epithelial cell barrier integrity.....	108
3.2.6.1. Transepithelial electrical resistance (TEER) measurement.....	108
3.2.6.2. Fluorescein isothiocyanate (FITC)-labelled dextran permeability assay.....	109
3.2.7. Data analysis.....	109
3.3. Results.....	111
3.3.1. CHyA-B scaffold characterisation.....	111
3.3.1.1. Scaffold ultrastructure.....	111
3.3.1.2. Interfacial adhesion strength.....	112
3.3.1.3. Mechanical testing.....	112
3.3.1.4. Pore size analysis.....	114
3.3.2. Calu-3 epithelial cell monoculture on CHyA-B scaffolds.....	116
3.3.2.1. Cell morphology and migration.....	116
3.3.2.2. Mucin expression.....	118

3.3.2.3. <i>Tight junction formation</i>	119
3.3.2.4. <i>Epithelial ciliation</i>	121
3.3.3. <i>Expression of genetic markers of epithelial cell differentiation</i>	122
3.3.3.1. <i>The effect of CHyA-B scaffolds on epithelial cell gene expression</i>	122
3.3.3.2. <i>The effect of time on epithelial cell gene expression</i>	124
3.3.4. <i>Calu-3 epithelial cell co-culture with fibroblasts on CHyA-B scaffolds</i>	126
3.3.4.1. <i>Cell morphology and migration</i>	126
3.3.4.2. <i>Mucin expression</i>	128
3.3.4.3. <i>Tight junction formation</i>	129
3.3.4.4. <i>Epithelial ciliation</i>	130
3.3.5. <i>Evaluation of Calu-3 epithelial cell barrier integrity</i>	131
3.3.5.1. <i>TEER measurement</i>	131
3.3.5.2. <i>FITC-labelled dextran permeability assay</i>	131
3.4. Discussion.....	133
3.5. Conclusion.....	141

Chapter 4: The development of a 3D primary tracheobronchial epithelial cell-derived co-culture system for applications in respiratory in vitro modelling

4.1. Introduction.....	144
4.2. Materials and Methods.....	146
4.2.1. <i>Bilayered collagen-hyaluronate (CHyA-B) scaffold fabrication</i>	146
4.2.1.1. <i>CHyA-B scaffold manufacture</i>	146
4.2.1.2. <i>Chemical crosslinking</i>	146
4.2.2. <i>Primary tracheobronchial epithelial cell culture on CHyA-B scaffolds</i>	147
4.2.2.1. <i>Cell source and culture medium</i>	147
4.2.2.2. <i>Epithelial cell monoculture</i>	147
4.2.2.3. <i>Epithelial cell co-culture with fibroblasts</i>	148
4.2.3. <i>Cell morphology and migration</i>	148
4.2.4. <i>Primary tracheobronchial epithelial cell differentiation on CHyA-B scaffolds</i>	149

4.2.4.1. Immunofluorescence.....	149
4.2.4.2. Scanning electron microscopy (SEM).....	149
4.2.4.3. Transmission electron microscopy (TEM).....	149
4.2.4.4. Expression of genetic markers of epithelial differentiation.....	150
4.2.5. Evaluation of primary tracheobronchial epithelial cell barrier integrity.....	150
4.2.5.1. Transepithelial electrical resistance (TEER) measurement.....	150
4.2.5.2. Fluorescein isothiocyanate (FITC)-labelled dextran permeability assay.....	150
4.2.6. Data analysis.....	151
4.3. Results.....	152
4.3.1. Primary tracheobronchial epithelial cell monoculture on CHyA-B scaffolds.....	152
4.3.1.1. Cell morphology and migration.....	152
4.3.1.2. Mucin expression.....	153
4.3.1.3. Tight junction formation.....	154
4.3.1.4. Epithelial ciliation.....	155
4.3.1.5. Epithelial ultrastructure- SEM.....	156
4.3.1.6. Epithelial ultrastructure- TEM.....	157
4.3.2. Primary tracheobronchial epithelial cell co-culture with fibroblasts on CHyA-B scaffolds.....	158
4.3.2.1. Cell morphology and migration.....	158
4.3.2.2. Mucin expression.....	160
4.3.2.3. Tight junction formation.....	161
4.3.2.4. Epithelial ciliation.....	163
4.3.2.5. Epithelial ultrastructure- SEM.....	164
4.3.2.6. Epithelial ultrastructure- TEM.....	166
4.3.3. Expression of genetic markers of epithelial differentiation.....	167
4.3.4. Evaluation of primary tracheobronchial epithelial cell barrier integrity.....	168
4.3.4.1. TEER measurement.....	168
4.3.4.2. FITC-labelled dextran permeability assay.....	168
4.4. Discussion.....	170

4.5.	Conclusion.....	177
------	-----------------	-----

Chapter 5: The manufacture of an all-*trans* retinoic acid-eluting bilayered scaffold as a platform technology for airway tissue regeneration

5.1.	Introduction.....	180
5.2.	Materials and Methods.....	182
5.2.1.	<i>All-trans retinoic acid-loaded bilayered collagen-hyaluronate (atRA-CHyA-B) scaffold fabrication</i>	182
5.2.1.1.	<i>All-trans retinoic acid-loaded collagen-hyaluronate (atRA-CHyA) film manufacture</i>	182
5.2.1.2.	<i>atRA-CHyA-B scaffold manufacture</i>	182
5.2.1.3.	<i>Chemical crosslinking</i>	182
5.2.2.	<i>atRA-CHyA film and atRA-CHyA-B scaffold characterisation</i>	183
5.2.2.1.	<i>Fourier transform infrared spectroscopy (FTIR)</i>	183
5.2.2.2.	<i>atRA encapsulation efficiency</i>	183
5.2.2.3.	<i>atRA in vitro release</i>	185
5.2.2.4.	<i>High performance liquid chromatographic (HPLC) analysis</i>	185
5.2.3.	<i>Primary tracheobronchial epithelial cell culture</i>	185
5.2.3.1.	<i>Cell source and culture medium</i>	185
5.2.3.2.	<i>Primary tracheobronchial epithelial cell culture on atRA-CHyA films</i>	186
5.2.3.3.	<i>Primary tracheobronchial epithelial cell culture on atRA-CHyA-B scaffolds</i>	187
5.2.4.	<i>Epithelial cell viability on atRA-CHyA films and atRA-CHyA-B scaffolds</i>	187
5.2.4.1.	<i>Cell growth on atRA-CHyA films and atRA-CHyA-B scaffolds</i>	187
5.2.4.2.	<i>Cell morphology and migration on atRA-CHyA-B scaffolds</i>	187
5.2.5.	<i>Primary tracheobronchial epithelial cell differentiation on atRA-CHyA films and atRA-CHyA-B scaffolds</i>	188
5.2.5.1.	<i>Immunofluorescence</i>	188
5.2.5.2.	<i>Expression of genetic markers of epithelial differentiation</i>	188
5.2.5.3.	<i>Scanning electron microscopy (SEM)</i>	189
5.2.5.4.	<i>Transmission electron microscopy (TEM)</i>	189

5.2.6. <i>Data analysis</i>	189
5.3. Results.....	190
5.3.1. <i>atRA-CHyA film characterisation</i>	190
5.3.1.1. <i>atRA-CHyA film manufacture and stability</i>	190
5.3.1.2. <i>atRA-CHyA film encapsulation efficiency</i>	192
5.3.1.3. <i>In vitro release of atRA from atRA-CHyA films</i>	194
5.3.2. <i>Primary tracheobronchial epithelial cell culture on atRA-CHyA films</i>	196
5.3.2.1. <i>Epithelial cell growth</i>	196
5.3.2.2. <i>Mucin expression</i>	197
5.3.2.3. <i>Epithelial ciliation</i>	198
5.3.2.4. <i>Expression of genetic markers of epithelial differentiation</i>	199
5.3.3. <i>atRA-CHyA-B scaffold characterisation</i>	200
5.3.3.1. <i>atRA-CHyA-B scaffold manufacture and atRA encapsulation efficiency</i>	200
5.3.3.2. <i>In vitro release of atRA from atRA-CHyA-B scaffolds</i>	200
5.3.4. <i>Primary tracheobronchial epithelial cell culture on atRA-CHyA-B scaffolds</i>	202
5.3.4.1. <i>Epithelial cell growth</i>	202
5.3.4.2. <i>Cell morphology and migration</i>	202
5.3.4.3. <i>Mucin expression</i>	204
5.3.4.4. <i>Epithelial ciliation</i>	206
5.3.4.5. <i>Epithelial ultrastructure- SEM</i>	208
5.3.4.6. <i>Epithelial ultrastructure- TEM</i>	210
5.3.4.7. <i>Expression of genetic markers of epithelial differentiation</i>	211
5.4. Discussion.....	212
5.5. Conclusion.....	219

Chapter 6: Thesis discussion and conclusions

6.1. Overview.....	221
6.2. Chapter 2: The assessment of CG scaffolds as a 3D substrate for the growth and differentiation of a bronchial epithelial cell line.....	223
6.3. Chapter 3: The development of a bilayered CG scaffold as a substrate for a bronchial epithelial cell line 3D in vitro co-culture model.....	225
6.4. Chapter 4: The development of a 3D primary tracheobronchial epithelial cell-derived co-culture system for applications in respiratory in vitro modelling.....	227
6.5. Chapter 5: The manufacture of an all- <i>trans</i> retinoic acid-eluting bilayered scaffold as a platform technology for airway tissue regeneration.....	229
6.6. Future work.....	231
6.7. Thesis conclusions.....	234
Bibliography.....	236
Appendices.....	267

“It’s the repetition of affirmations that leads to belief. And once that belief becomes a deep conviction, things begin to happen”

- Muhammad Ali

Acknowledgements

Well lads, where to begin with all of the acknowledgements?

Firstly, I would like to thank my two supervisors, Prof. Sally-Ann Cryan and Prof. Fergal O'Brien for all of their help in guiding me with this project. Beyond being two top individuals who are a pleasure to work with irrespective of any supervision or research matters, I really appreciated the perfect blend of faith and autonomy that you granted me throughout the years, in combination with helpful guidance and direction when I needed it most. That goes for both this PhD project, career guidance and everything in between! A major thank you must also be said for the time and effort that you both put into reviewing this thesis, particularly in the midst of the very hectic schedules you both lead within the college and also with new arrivals to the family outside of work. Sally, if anything, I hope that you were able to use this thesis as an effective bedtime story to get Roisín to sleep!

There are so many charming individuals who I've encountered in the TERG lab over the years, it's tricky to keep track of the many, many people who have helped along the way and made this group such a great one to be part of. In no particular order, I'd like to thank Alan, Arlyng, Amro, Andrew, Cathal, Caroline C, Christina, Claire, Dave, Emily, Garry, Gemma, Gillian, Joanne O'D, Joanne R/S, Johnny G, Johnny O'B, Laura, Liam, Matt (that Tissue Eng C paper is legendary; let it never be forgotten), Nicola, Orlaith, Paula, Rachel, Rob, Rosie, Rukmani, Sara, Seóna, Tanya, Tati, Tijnna, Will Lack and Will Whyte. I know that when I normally am writing all these names down in sequence, it is to send an ice-cold email about the state of the lab or some mishap, so thanks for enduring those, among many of my other grumpy habits; you're all great! Past members of the group without who I would be lost also must be mentioned: Adolfo, Alan Hibbs, Amos, Cai, Elaine, Erica, Emmet T, Gregory and Ryan; the first six of you in particular helped me find my feet when I was a complete headless chicken in the lab in the early days, so thanks so very much! Special mentions amongst current members to Andrew and Alan for all the laughs, chewing the fat about film formulation ideas, other science talk and mechanical prop assistance, Garry for research advice across the board and lastly to Johnny O'B, for preventing the place from burning down, the laughs over pints and stringing the occasional silky set piece together out on the pitch on

Wednesday lunch-times. If anyone's name has been omitted by accident then you are no less forgotten; please forgive me and my current state of exhaustion for the error and chase me down for a pint to make it up to you!

Of course Hugh and Irene, I haven't forgotten you guys, it's just that the BioAT group has to get a paragraph all to itself. I have been really lucky to have started off in RCSI with such a stellar crew in BioAT who made the whole experience unreal! Too many memories make me smile as I write this: Claire and our bonding over meatloaf in Maynooth, Sinéad and her amazing button-sewing skills, a few late-night sessions in Ross' plush surroundings, discussing grilled meat and other culinary treats with Valerio in Porto, serious dance battles with Irene, ridiculous science banter with Cormac up in the third floor office, a bit of Huttese and every taboo topic under the sun with Eanna, and most recently, helping Tadhg in his campaign to bring down Jim Corr for being rude. Hugh bey, between our shoddy attempts at Movember, hazardous Christmas parties, foggy discussions about ruling the academic world and tip-top banter back in your gaff on multiple occasions, I only have to say this: you are a gent.

Final thanks go to a few others outside of TERG, namely to Graeme and Emmet in Chemistry for loads of help with analytical methods, the technician crew in Pharmacy (don't give up on QPR, Pete), Karen in Physiology for some proof-reading and just for being a lovely friend over the last decade and to Brenton Cavanagh for the training in confocal microscopy. Proper respect goes to long-time chum Anna Kelly for helping me get MatLab and for her tremendous patience and kindness towards this slob of a housemate. I'd also like to thank Prof. James Kirkpatrick and his lab group for the fantastic experience I had over in his lab in Mainz. A big thanks also goes out to Pharmacy pals John, Michelle and Sam who have helped me immensely with the new job and also endured me in all my charming glory at the tail end of my lab work and writing up when I needed to vent!

Finally, I also must graciously acknowledge the funding sources for this project and the School of Postgraduate Studies for their assistance in managing the BioAT programme. This work is funded under the PRTL Cycle 5 & co-funded through the European Regional Development Fund, part of the European Union Structural Funds Programme 2007-2013.

Publications, grants, prizes and presentations related to thesis

Journal publications

O'Leary C., Cavanagh B., Unger R. E., Kirkpatrick C. J., O'Dea S., O'Brien F. J., Cryan S. A. (2016) The development of a tissue-engineered tracheobronchial epithelial model using a bilayered collagen-hyaluronate scaffold. *Biomaterials*; 85: 111-27. (doi: 10.1016/j.biomaterials.2016.01.065).

O'Leary, C., Gilbert, J. L., O'Dea, S., O'Brien, F. J. and Cryan, S. A. (2015) Respiratory tissue engineering: current status and opportunities for the future. *Tissue Engineering Part B Reviews*; 21: 323-44. (doi: 10.1089/ten.teb.2014.0525).

Grants

European Molecular Biology Organisation (EMBO) Short Term Fellowship Award to fund a three month research visit to Mainz, Germany.

BioAT PhD Scholars programme, funded under the PRTL Cycle 5 & co-funded through the European Regional Development Fund, part of the European Union Structural Funds Programme 2007-2013.

Prizes

2nd Prize Poster Presentation: Tissue Engineering and Regenerative Medicine International Society, European Conference 2013 Student and Young Investigator Section Awards, Istanbul, Turkey. Collagen-based scaffolds for three-dimensional airway models.

1st Prize Oral Presentation in the Experienced Researcher Category- Tissue Engineering: The 20th Annual Conference of the Section of Bioengineering of the Royal Academy of Medicine in Ireland (RAMI), Limerick, Ireland. Bilayered collagen-GAG scaffolds for respiratory tissue engineering.

2nd Prize Oral Presentation in the Regenerative Medicine Category: Young Life Scientists Ireland (YLSI) Conference, Dublin, Ireland. A tissue-engineering approach to improve airway in vitro models: the development of a collagen-GAG bilayered scaffold.

International conference proceedings

O'Leary C., Unger R. E., Kirkpatrick C. J., O'Brien F. J., Cryan S. A. (2015) Bilayered collagen-hyaluronate scaffolds: a novel platform for 3D in vitro respiratory tissue modelling. In: Proceedings of the Fourth World Congress of the Tissue Engineering and Regenerative Medicine International Society, Boston, USA. Abstract published in Tissue Engineering Part A 21 (Suppl. 1): 1076.

O'Leary, C.; O'Brien, F.J. and Cryan, S.A. (2015) The development of all-trans retinoic acid-loaded collagen-hyaluronic acid films for respiratory tissue regeneration. In: Proceedings of the Annual Meeting of the Controlled Release Society, Edinburgh, Scotland: 500.

O'Leary, C.; O'Dea, S.; O'Brien, F.J. and Cryan, S.A. (2013) Development of tissue engineered scaffolds for airway modelling and regeneration. In: Proceedings of the Asia-Pacific Chapter of the Tissue Engineering and Regenerative Medicine International Society, Shanghai-Wuzhen, China: S39-O-5.

O'Leary, C.; O'Dea, S.; O'Brien, F.J. and Cryan, S.A. (2013) Collagen-based scaffolds for three-dimensional airway models. In: Proceedings of the European Chapter of the Tissue Engineering and Regenerative Medicine International Society, Istanbul, Turkey: CLL-P1-59.

National conference proceedings

O'Leary C., Unger R. E., Kirkpatrick C. J., O'Dea S., O'Brien F. J., Cryan S. A. (2015) Bilayered collagen scaffolds for respiratory in vitro modelling: engineering novel drug development platforms. In: Proceedings of the BioAnalysis and Therapeutics PhD Programme Annual Research Day, Dublin, Ireland: 13.

O'Leary, C.; O'Dea, S.; O'Brien, F.J. and Cryan, S.A. (2015) Collagen-hyaluronate bilayered Scaffolds: An advanced in vitro model for respiratory drug development. In: Proceedings of the Royal College of Surgeons in Ireland Annual Research Day, Dublin, Ireland: PG2+ P47.

O'Leary C., O'Dea S., O'Brien F. J., Cryan S. A. (2014) Airway epithelium culture on bilayered collagen-GAG scaffolds: developing a novel respiratory drug development tool with tissue engineering. In: Proceedings of the BioAnalysis and Therapeutics PhD Programme Annual Research Day, Dublin, Ireland: 18.

O'Leary C., O'Dea S., O'Brien F. J., Cryan S. A. (2014) A tissue-engineering approach to improve airway in vitro models: the development of a collagen-GAG bilayered scaffold. In: Proceedings of the Young Life Scientists Ireland (YLSI) Conference, Dublin, Ireland: OP5C.

O'Leary, C.; O'Dea, S.; O'Brien, F.J. and Cryan, S.A. (2014) Airway Epithelial cell culture on bilayered collagen-glycosaminoglycan Scaffolds. In: Proceedings of the Royal College of Surgeons in Ireland Annual Research Day, Dublin, Ireland: PHD P32.

O'Leary, C.; O'Dea, S.; O'Brien, F.J. and Cryan, S.A. (2014) Bilayered collagen-GAG scaffolds for respiratory tissue engineering: improving tracheobronchial scaffold design. In: Proceedings of the 20th Annual Conference of the Section of Bioengineering of the Royal Academy of Medicine in Ireland, M. Walsh (Ed.), Limerick, Ireland: TE14.

O'Leary, C.; O'Dea, S.; O'Brien, F.J. and Cryan, S.A. (2013) Improving in vitro airway models with tissue engineering: three-dimensional culture of bronchial epithelium on collagen-based scaffolds. In: Proceedings of the Anatomical Society Summer Meeting on Form and Function in Regenerative Medicine, Dublin, Ireland: A3.

O'Leary, C.; O'Dea, S.; O'Brien, F.J. and Cryan, S.A. (2013) Novel three-dimensional culture of respiratory epithelium: an innovative tool for respiratory drug development. In: Proceedings of the BioAnalysis and Therapeutics PhD Programme Annual Research Day, Maynooth, Ireland: 18.

O'Leary, C.; O'Dea, S.; O'Brien, F.J. and Cryan, S.A. (2013) Markers of epithelial differentiation in a novel in vitro 3D airway model. In: Proceedings of the Royal College of Surgeons in Ireland Annual Research Day, Dublin, Ireland: PHD P39.

O’Leary, C.; O’Dea, S.; O’Brien, F.J. and Cryan, S.A. (2013) Towards the development of collagen-based scaffolds for airway modelling: effects of mean pore size & cross-linking. In: Proceedings of the 19th Annual Conference of the Section of Bioengineering of the Royal Academy of Medicine in Ireland, D. Kelly and C. Buckley (Eds.), Enfield, Ireland: 69.

O’Leary C.; Matsiko A.; O’Dea S.; O’Brien F.J. and Cryan S.A. (2012) The development of collagen scaffolds for applications in airway modelling & regeneration. Royal Irish Academy Life Sciences Workshop, “Emerging Treatments for Lung Diseases: Progress, Challenges and Opportunities from an Irish Perspective,” Dublin, Ireland.

O’Leary C.; O’Dea S.; O’Brien F.J. and Cryan S.A. (2012) The development of “smart” collagen scaffolds for applications in airway modelling and regeneration. In: Proceedings of the BioAnalysis and Therapeutics PhD Programme Annual Research Day, Dublin Ireland: 2.

List of abbreviations

2D	Two-dimensional
3D	Three-dimensional
ALI	Air-liquid interface
ANOVA	Analysis of variance
AT	Alveolar epithelial cell
ATMP	Advanced therapeutic medicinal product
atRA	All- <i>trans</i> retinoic acid
atRA-CHyA-B	All- <i>trans</i> retinoic acid-loaded bilayered collagen-hyaluronate
atRA-CHyA	All- <i>trans</i> retinoic acid-loaded collagen-hyaluronate
BASC	Bronchioalveolar stem cell
BDP	Beclomethasone dipropionate
BEBM	Bronchial epithelial basal medium
BEGM	Bronchial epithelial growth medium
BIV	β -tubulin IV
BM-MSC	Bone marrow-derived mesenchymal stem cell
BMP	Bone morphogenetic protein
BPE	Bovine pituitary extract
BSA	Bovine serum albumin
CCS	Collagen-chondroitin-6-sulphate
cDNA	Complementary deoxyribonucleic acid
CF	Cystic fibrosis
CFTR	Cystic fibrosis transmembrane conductance regulator

CG	Collagen-glycosaminoglycan
CHyA	Collagen-hyaluronate
CHyA-B	Bilayered collagen-hyaluronate
COPD	Chronic obstructive pulmonary disease
DASC	Distal alveolar stem cell
DAPI	4', 6-diamidino-2-phenylindole
DC	Decellularised
DHT	Dehydrothermal
DMEM	Dulbecco's modified Eagle's medium
DMSO	Dimethylsulphoxide
DNA	Deoxyribonucleic acid
DPBS	Dulbecco's phosphate buffered saline
dsDNA	Double-stranded deoxyribonucleic acid
ECM	Extracellular matrix
EDAC	1-ethyl-3-(3-dimethylaminopropyl)carbodiimide hydrochloride
EGF	Epidermal growth factor
EMT	Epithelial-mesenchymal transition
ESC	Embryonic stem cell
FDA	Food and Drug Administration
FGF	Fibroblast growth factor
Fig.	Figure
FITC	Fluorescein isothiocyanate
FTIR	Fourier transform infrared spectroscopy/spectroscopic

GAG	Glycosaminoglycan
GF	Growth factor
H&E&FG	Haematoxylin and eosin and fast green
hAFSC	Human amniotic fluid stem cell
HBSS	Hank's buffered salt solution
HGF	Hepatocyte growth factor
HPLC	High-performance liquid chromatography/chromatographic
HUVEC	Human umbilical vein endothelial cell
HyA	Hyaluronate
IgG	Immunoglobulin G
IL-1	Interleukin-1
IL-8	Interleukin-8
IPF	Idiopathic pulmonary fibrosis
iPSC	Induced pluripotent stem cell
KGf	Keratinocyte growth factor
LLI	Liquid-liquid interface
LPS	Lipopolysaccharide
LR	London resin
MNC	Mononuclear cell
mRNA	Messenger ribonucleic acid
MSC	Mesenchymal stem cell
MUC5AC	Mucin 5AC
NHBE	Normal human bronchial epithelial

NHS	N-hydroxysuccinimide
PC	Polycarbonate
PCL	Poly-ε-caprolactone
PCU	Poly-(carbonate-urea)urethane
PET	Polyethylene terephthalate
PF127	Pluronic F127
PGA	Polyglycolic acid
PLGA	Poly(lactic-co-glycolic) acid
POSS	Polyhedral oligomeric silsesquioxane
PTFE	Polytetrafluoroethylene
PU	Polyurethane
qRT-PCR	Quantitative reverse transcriptase-polymerase chain reaction
RCSI	Royal College of Surgeons in Ireland
RHAMM	Receptor for hyaluronan-mediated motility
RNA	Ribonucleic acid
RT-PCR	Reverse transcriptase-polymerase chain reaction
SPC	Surfactant protein C
SEM	Scanning electron microscopy OR Standard error of the mean
SR	Slow-release
T ₃	Triiodothyronine
TE	Tissue engineering OR Tris-ethylenediaminetetraacetic acid
TEM	Transmission electron microscopy
TERG	Tissue Engineering Research Group

TGFβ	Transforming growth factor beta
TGFβ1	Transforming growth factor beta-1
VATS	Video-assisted thoracoscopic surgery
ZO-1	Zonula occludens-1
®	Registered trademark

List of figures

Figure 1.1: The respiratory tract.....	34
Figure 1.2: British guideline on the management of asthma in adults.....	38
Figure 1.3: The drug development process timeline.....	40
Figure 1.4: Models for inhalational drug discovery	41
Figure 1.5: Conventional cell insert culture of respiratory epithelial cells.....	44
Figure 1.6: The extracellular matrix component of the respiratory tract.....	46
Figure 1.7: Endogenous epithelial progenitor cells of the lung	50
Figure 1.8: Macroscopic image of collagen scaffolds manufactured by the Tissue Engineering Research Group (TERG)	69
Figure 2.1: Calu-3 epithelial cell culture conditions examined for in vitro experiments	76
Figure 2.2: Calu-3 cell growth on collagen-chondroitin-6-sulphate scaffolds	81
Figure 2.3: Mucin expression by Calu-3 cells cultured on collagen-chondroitin-6-sulphate scaffolds	82
Figure 2.4: Zonula occludens-1 (ZO-1) expression by Calu-3 cells cultured on collagen-chondroitin-6-sulphate scaffolds	83
Figure 2.5: Scanning electron micrographs of Calu-3 cells cultured on collagen-chondroitin-6-sulphate scaffolds	84
Figure 2.6: MUC5AC mRNA expression by Calu-3 cells on collagen-chondroitin-6-sulphate scaffolds.....	86
Figure 2.7: ZO-1 mRNA expression by Calu-3 cells on collagen-chondroitin-6-sulphate scaffolds	87
Figure 2.8: FOXJ1 mRNA expression by Calu-3 cells on collagen-chondroitin-6-sulphate scaffolds	88
Figure 2.9: Migration of Calu-3 cells into collagen-chondroitin-6-sulphate scaffolds.....	89
Figure 3.1: Calu-3 epithelial cell and Wi38 fibroblast air-liquid interface (ALI) culture models examined for in vitro experiments.....	104
Figure 3.2: Bilayered collagen-hyaluronate scaffold ultrastructure	111

Figure 3.3: Mechanical properties of bilayered collagen-hyaluronate scaffolds	113
Figure 3.4: Pore size analysis of bilayered collagen-hyaluronate scaffolds	115
Figure 3.5: Calu-3 cell monoculture on bilayered collagen-hyaluronate scaffolds	117
Figure 3.6: MUC5AC expression by Calu-3 cells in monoculture on bilayered collagen-hyaluronate (CHyA-B) scaffolds.....	118
Figure 3.7: ZO-1 expression by Calu-3 cells in monoculture on bilayered collagen-hyaluronate (CHyA-B) scaffolds.....	120
Figure 3.8: Transmission electron microscopy images of Calu-3 cells in monoculture on bilayered collagen-hyaluronate (CHyA-B) scaffolds	121
Figure 3.9: The effect of bilayered collagen-hyaluronate (CHyA-B) scaffolds on the relative mRNA expression of Calu-3 cells in monoculture	123
Figure 3.10: The effect of time on the relative mRNA expression of Calu-3 cells in monoculture.....	125
Figure 3.11: Co-culture on bilayered collagen-hyaluronate scaffolds	127
Figure 3.12: MUC5AC expression by Calu-3 cells in co-culture on bilayered collagen-hyaluronate (CHyA-B) scaffolds.....	128
Figure 3.13: ZO-1 expression by Calu-3 cells in co-culture on bilayered collagen-hyaluronate (CHyA-B) scaffolds.....	129
Figure 3.14: Transmission electron microscopy (TEM) images of Calu-3 cells in co-culture on bilayered collagen-hyaluronate (CHyA-B) scaffolds	130
Figure 3.15: Calu-3 epithelial cell barrier integrity in monoculture and co-culture on bilayered collagen-hyaluronate (CHyA-B) scaffolds	132
Figure 4.1: Primary tracheobronchial epithelial cell monoculture on bilayered collagen-hyaluronate (CHyA-B) scaffolds.....	152
Figure 4.2: MUC5AC expression on primary tracheobronchial epithelial cells in monoculture on bilayered collagen-hyaluronate (CHyA-B) scaffolds.....	153
Figure 4.3: ZO-1 expression on primary tracheobronchial epithelial cells in monoculture on bilayered collagen-hyaluronate (CHyA-B) scaffolds	154
Figure 4.4: β -tubulin IV (BIV) expression on primary tracheobronchial epithelial cells in monoculture on bilayered collagen-hyaluronate (CHyA-B) scaffolds.....	155
Figure 4.5: Ultrastructural analysis of primary tracheobronchial epithelial cells in monoculture on bilayered collagen-hyaluronate (CHyA-B) scaffolds using scanning electron microscopy.....	156
Figure 4.6: Ultrastructural analysis of primary tracheobronchial epithelial cells in monoculture on bilayered collagen-hyaluronate (CHyA-B) scaffolds using transmission electron microscopy.....	157
Figure 4.7: Primary tracheobronchial epithelial cell co-culture on bilayered collagen-hyaluronate scaffolds.....	159
Figure 4.8: MUC5AC expression on primary tracheobronchial epithelial cells in co-culture on bilayered collagen-hyaluronate (CHyA-B) scaffolds	160

Figure 4.9: ZO-1 expression on primary tracheobronchial epithelial cells in co-culture on bilayered collagen-hyaluronate (CHyA-B) scaffolds	162
Figure 4.10: β -tubulin IV (BIV) expression on primary tracheobronchial epithelial cells in co-culture on bilayered collagen-hyaluronate (CHyA-B) scaffolds.....	163
Figure 4.11: Ultrastructural analysis of primary tracheobronchial epithelial cells in co-culture on bilayered collagen-hyaluronate (CHyA-B) scaffolds using scanning electron microscopy	165
Figure 4.12: Ultrastructural analysis of primary tracheobronchial epithelial cells in co-culture on bilayered collagen-hyaluronate (CHyA-B) scaffolds using transmission electron microscopy	166
Figure 4.13: Expression of genetic markers of primary tracheobronchial epithelial differentiation in co-culture on bilayered collagen-hyaluronate (CHyA-B) scaffolds.....	167
Figure 4.14: Primary tracheobronchial epithelial cell barrier integrity in monoculture and co-culture on bilayered collagen-hyaluronate (CHyA-B) scaffolds.....	169
Figure 5.1: Primary tracheobronchial epithelial cell air-liquid interface (ALI) culture models examined for in vitro experiments	186
Figure 5.2: The manufacture of stable all-trans retinoic acid-loaded collagen-hyaluronate (atRA-CHyA) films for a range of concentrations	191
Figure 5.3: All-trans retinoic acid (atRA) release from atRA-loaded collagen-hyaluronate (atRA-CHyA) films	195
Figure 5.4: Primary tracheobronchial epithelial cell viability on all-trans retinoic acid-loaded collagen-hyaluronate (atRA-CHyA) films.....	196
Figure 5.5: MUC5AC expression in primary tracheobronchial epithelial cells on all-trans retinoic acid-loaded collagen-hyaluronate (atRA-CHyA) films	197
Figure 5.6: β -tubulin IV (BIV) expression in primary tracheobronchial epithelial cells on all-trans retinoic acid-loaded collagen-hyaluronate (atRA-CHyA) films	198
Figure 5.7: The effect of all-trans retinoic acid (atRA) incorporation into CHyA films on the relative mRNA expression of primary tracheobronchial epithelial cells.....	199
Figure 5.8: Bilayered all-trans retinoic acid-loaded collagen-hyaluronate (atRA-CHyA-B) scaffold characterisation	201
Figure 5.9: Primary tracheobronchial epithelial cell viability on bilayered all-trans retinoic acid-loaded collagen-hyaluronate (atRA-CHyA-B) scaffolds	203
Figure 5.10: MUC5AC expression in primary tracheobronchial epithelial cells on bilayered all-trans retinoic acid-loaded collagen-hyaluronate (atRA-CHyA-B) scaffolds	205
Figure 5.11: β -tubulin IV (BIV) expression in primary tracheobronchial epithelial cells on bilayered all-trans retinoic acid-loaded collagen-hyaluronate (atRA-CHyA-B) scaffolds	207
Figure 5.12: Ultrastructural analysis of primary tracheobronchial epithelial cells on bilayered all-trans retinoic acid-loaded collagen-hyaluronate (atRA-CHyA-B) scaffolds using scanning electron microscopy	209

Figure 5.13: Ultrastructural analysis of primary tracheobronchial epithelial cells on bilayered all-trans retinoic acid-loaded collagen-hyaluronate (atRA-CHyA-B) scaffolds using transmission electron microscopy.....210

Figure 5.14: The effect of bilayered all-trans retinoic acid-loaded collagen-hyaluronate (atRA-CHyA-B) scaffolds on the relative mRNA expression of primary tracheobronchial epithelial cells211

List of tables

Table 1.1: Prominent epithelial cell sources for respiratory cell culture models.....43

Table 1.2: Biomaterials used in alveolar tissue engineering.....56

Table 1.3: Hydrogels used in tracheobronchial tissue engineering.....60

Table 1.4: Decellularised tissue used in tracheobronchial tissue engineering.....63

Table 1.5: Porous polymeric scaffolds used in tracheobronchial tissue engineering.....67

Table 5.1: Concentration of all-trans retinoic acid (atRA) loading in collagen-hyaluronate (CHyA) films.....193

Table 5.2: Encapsulation efficiency of all-trans retinoic acid (atRA) loading in collagen-hyaluronate (CHyA) films.....193

List of equations

Equation 1:
$$Porosity (\%) = \left(1 - \frac{\rho_{scaffold}}{\rho_{solid}}\right) \times 100$$

Equation 2:
$$P_{app} = F \times \left(\frac{1}{A \times C_0}\right)$$

Chapter 1: Introduction and literature review

The literature review in this chapter has been partially published as O’Leary et al.,
Respiratory tissue engineering: current status and opportunities for the future. *Tissue Eng*
Part B Rev, 2015; 21:323-44.

1.1.	The respiratory system: respiratory disease and drug development.....	32
1.1.1.	Overview: the burden of respiratory disease and injury	32
1.1.2.	Anatomy and physiology of the respiratory tract.....	33
1.1.2.1.	Anatomy and physiology of the conducting zone of the respiratory tract	34
1.1.2.2.	Anatomy and physiology of the respiratory zone of the respiratory tract.....	35
1.1.3.	Treatment of respiratory disease.....	36
1.1.3.1.	Pharmacotherapy.....	37
1.1.3.2.	Surgical intervention	38
1.1.3.3.	The development of novel treatments	39
1.2.	Current respiratory drug development models.....	41
1.2.1.	Cell culture models.....	42
1.2.2.	Animal models	44
1.2.3.	Limitations of current cell culture and animal models	45
1.3.	Tissue engineering and the respiratory system	47
1.3.1.	Tissue engineering: an alternative approach to respiratory drug development and the treatment respiratory disease	47
1.3.2.	Cell sources for respiratory tissue engineering and regeneration	49
1.3.2.1.	Endogenous lung stem cell populations of the of the respiratory tract.....	49
1.3.2.2.	Other lung stem cell populations.....	51
1.3.3.	Signalling factors for respiratory tissue engineering and regeneration.....	52
1.3.3.1.	Hepatocyte growth factor (HGF)	52
1.3.3.2.	Bone morphogenetic protein 4 (BMP4)	53
1.3.3.3.	Keratinocyte growth factor (KGF).....	54
1.3.3.4.	All-trans retinoic acid (atRA)	54
1.3.4.	Biomaterials for respiratory tissue engineering and regeneration	55
1.3.4.1.	Biomaterials for alveolar tissue engineering and regeneration	55
1.3.5.	Biomaterials for tracheobronchial tissue engineering and regeneration.....	58
1.3.5.1.	Hydrogels.....	58
1.3.5.2.	Decellularised tissue	61
1.3.5.3.	Porous polymeric scaffolds	63

1.4. The Tissue Engineering Research Group (TERG): collagen-based scaffolds for tissue engineering and regeneration.....68

1.5. Thesis objectives.....70

1.1. The respiratory system: respiratory disease and drug development

1.1.1. Overview: the burden of respiratory disease and injury

Today, lung disease and major airway trauma are a major global healthcare concern with limited treatment options. Incurable airway diseases such as asthma, chronic obstructive pulmonary disease (COPD), cystic fibrosis (CF) and idiopathic pulmonary fibrosis (IPF) contribute significantly to an enormous clinical and socioeconomic burden. COPD, in particular, has been identified as the fourth leading cause of mortality worldwide [1]. Survival rates for CF decrease steadily beyond forty years, primarily as a result of death from respiratory causes in 68% of cases [2, 3], while for patients diagnosed with IPF, the median survival is approximately 2.5-3.5 years post-diagnosis [4]. Additionally, tracheal, bronchial and other lung cancers are predicted to become the sixth leading cause of mortality by 2030 [5]. From an economic standpoint, these debilitating conditions also bring with them a heavy toll: COPD alone costs an estimated €38.6 billion in the European Union and has combined costs of approximately \$50 billion in the United States [1]. Indeed, chronic lung disease and major airway trauma constitute a significant clinical problem that must be addressed to improve patient survival, quality of life and reduce overloaded healthcare budgets. Unfortunately, treatment options for such conditions are primarily palliative, focused mainly on symptomatic inhalable treatments (Section 1.1.3); ultimately, restoration or replacement of damaged lung tissue is required for success.

Epithelial cell dysfunction and persistent inflammatory damage to respiratory tissue play a central role in the pathophysiology of these debilitating conditions. The epithelium in the respiratory tract is of critical importance for the maintenance of homeostasis, with key roles in lining the airways for protection, mediating interaction with the external environment and in regulating innate immune responses [6, 7]. In asthma, for example, the disruption of this homeostasis contributes to a weakened epithelial barrier, impaired healing responses and chronic release of growth factors (GFs) into the microenvironment that remodel the airways and propagate tissue inflammation [8]. CF is rooted in defective ion transport across epithelia that drives bacterial colonisation and inflammation in the lungs [9], while a chronic injury response from alveolar epithelial cells leads to dysregulation of epithelial-fibroblast communication, pathological fibroproliferation

and collagen deposition in IPF [10]. Of course, the extracellular matrix (ECM) of the larger airways can also be adversely altered in chronic asthma by fibrosis in the submucosal region [8, 11] and degraded fragments from ECM itself can actually augment the inflammatory cascade to worsen lung damage in cases of COPD and CF [9]. Accordingly, in order to identify new therapies that can successfully ameliorate and cure such respiratory diseases, effective drug targeting of epithelial tissue and restoration of its normal function is a significant factor in the design of therapeutics.

This thesis will seek to improve the identification and translation of new therapies through the development of a novel three-dimensional (3D) *in vitro* model to provide a physiologically-representative system for advanced drug development and disease modelling. Additionally, the potential of this model to act as a platform technology for respiratory tissue regeneration will also be investigated. To this end, tissue engineering strategies that are described in Section 1.3 will be employed in its fabrication. Before these can be outlined, however, it is crucial to first consider the relevant cells, ECM composition and respiratory tract tissue architecture in order to understand the tissue being modelled and to provide a more complete understanding of the interplay between the epithelium and the other components of the lungs (Section 1.1.2). Thereafter, Section 1.2 reviews current treatments for respiratory disease and the models used to develop these treatments to identify the limitations of current models and how this PhD project can potentially provide an alternative solution for respiratory drug development.

1.1.2. Anatomy and physiology of the respiratory tract

The lungs are the essential organs of the respiratory tract that enable animals to exchange oxygen and carbon dioxide with the environment to facilitate respiration within cells and tissue. The human respiratory tract contains nearly 50 different cell types along its hierarchical structure [12] in distinct proximal (conducting) and distal (respiratory) zones [13]. The larger proximal airways include the trachea, bronchi and bronchioles of greater than 2mm in diameter; these regions are reinforced by cartilaginous rings to prevent collapse (Fig. 1.1; [14]). The distal airways, composed of non-cartilaginous conducting airways with an internal diameter of less than 2mm, include the bronchioles and the alveoli, the structural units at the end of the respiratory tree that are responsible for gas exchange in the

respiratory zone. The diverse range of cell types spread across the airways is primarily separated into these defined regions as a reflection of their functionality.

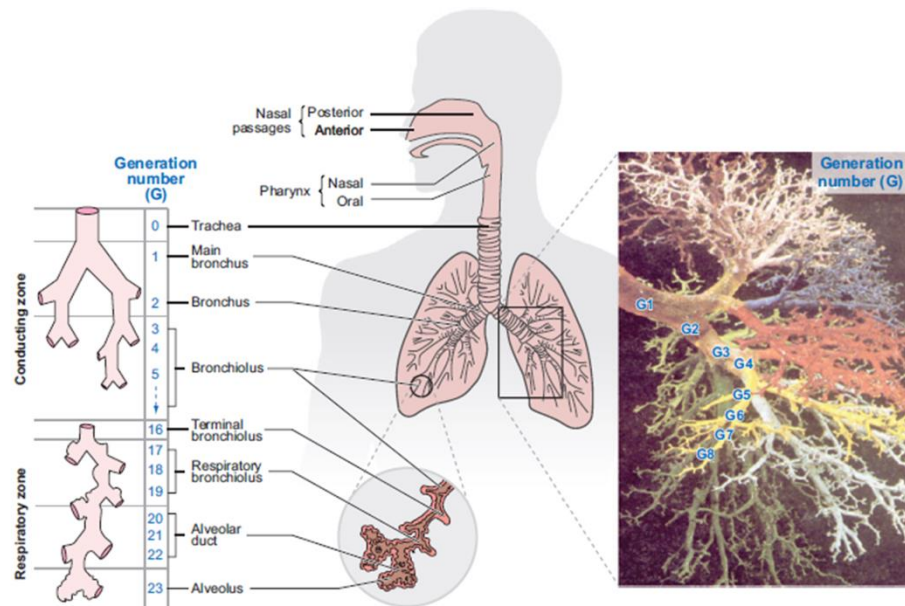


Figure 1.1: The respiratory tract. The tract contains nearly 50 different cell types in a three-dimensional branching arrangement across two distinct zones. Adapted from [14].

1.1.2.1. Anatomy and physiology of the conducting zone of the respiratory tract

Within the tracheobronchial region or conducting zone of the respiratory tract, a pseudostratified epithelial layer composed of three main cell types- ciliated epithelial cells, goblet cells and basal cells- is supported by the ECM of pulmonary interstitium and cartilage in a specific 3D structure and branching patterns [15]. These cells perform an essential role in innate host defence by providing a physical barrier and by producing mucus and serous secretions that allow the body to clear environmental toxins and infectious agents entering the conducting airways following inhalation. The respiratory epithelium operates as an interface between the host and its external environment [6, 7]; in this regard, cells present along the walls of the tract have a barrier function, preventing the easy passage of potentially pathogenic substances. Mucus-producing cells assist in this defensive activity, trapping foreign bodies so that they can be removed by the ciliary action of the pseudostratified columnar epithelium. The presence of a mucus layer also acts as a diffusional buffer to protect the cells from noxious gases that may be inhaled. In addition to mucus expression, the epithelium can secrete a host of other signalling molecules and inflammatory mediators to recruit immune cells that elicit

an appropriate response to pathogen infection or invasion, including IL-1, IL-8 and leukotrienes (reported in [6]). Descending further down the proximal region through the branching bronchioles towards the alveoli, the pseudostratified epithelial layer is replaced by a cell monolayer composed of Clara cells (also known as club cells) and neuroendocrine cells with a concomitant reduction in the density of mucus-secreting cells and ciliated epithelia.

The fibro-cartilaginous ECM found below the epithelium hosts a range of cellular and non-cellular components. Smooth muscle cells, fibroblasts, chondrocytes and inflammatory cells constitute the cellular content, mediating muscle contraction, matrix composition and signalling processes. Non-cellular molecules such as collagen, elastin and various glycosaminoglycans (GAGs) modulate structural support and morphogenesis in tandem with GFs and morphogens such as epidermal growth factor (EGF), bone morphogenetic proteins (BMPs) and fibroblast growth factors (FGFs) [16-19], which can dictate cell differentiation. A continuous network of fibrillar collagen I and III supports the epithelium and airway smooth muscle [17], reinforced by a series of C-shaped cartilage rings located along the outside of the upper respiratory tract. This cartilage is hyaline in nature, composed predominantly of type II collagen and proteoglycans including aggrecan, decorin, biglycan and fibromodulin [20, 21]; it conveys increased structural integrity to the trachea and bronchi, preventing airway collapse and ensuring transit of inhaled air to the alveoli [16]. The ECM architectural design in the conducting region allows for longitudinal flexibility but lateral rigidity [22], a mechanical combination that preserves large airway patency and functionality.

1.1.2.2. Anatomy and physiology of the respiratory zone of the respiratory tract

Exchange of oxygen and carbon dioxide that is essential for survival occurs in the respiratory zone in the distal airways. The alveolar sacs themselves are populated by squamous type I pneumocytes (also known as alveolar epithelial cells) to mediate gas exchange and surfactant-secreting cuboidal type II pneumocytes [23]. Type I pneumocytes occupy approximately 93% of the surface area of the alveoli; this cell population has adapted to maximise rapid gas transfer to and from the bloodstream by adopting a thin squamoid shape and by residing at a close proximity to capillaries, reducing the gaseous diffusion barrier to approximately 1µm in thickness. The surfactant produced by type II cells is critical for reducing

surface tension within the alveolar sacs from 70mN/m to 22-23mN/m, preventing their collapse during breathing [24, 25].

The ECM of the alveolar region complements the cellular functionality, consisting of thin fused capillary and alveolar epithelial basement membranes to maximise gas exchange between the respiratory tract and blood [17]. This membrane is rich in fibronectin and the proteoglycan perlecan which can influence type II pneumocyte behaviour [26, 27]. The ECM protein composition changes in the distal airways relative to the conducting region, with an increased elastin component providing more recoil in the airway walls in response to influx and efflux of air. Collagen, elastin and GAGs provide the lower parenchymal region of the airways with viscoelastic behaviour to withstand expansion and contraction during tidal ventilation [28, 29]. As elastin fibres are stretched during tidal breathing, collagen fibres coiled around them uncrimp and reduce excessive strain on the elastin, preventing excessive stretch during alveolar expansion and ensuring elastic recoil following exhalation [30].

1.1.3. Treatment of respiratory disease

Current treatments for chronic respiratory conditions focus primarily on retarding disease progression through lifestyle modification, pharmacotherapy and, in severe cases, surgical intervention. While the mainstay of asthma and COPD treatment is provided through inhaled medicines [31], CF requires a multi-faceted approach using a plethora of inhaled and oral antibacterial agents, enzyme supplementation and anti-inflammatory treatments for effective management [32]. Effective drug therapy for IPF, on the other hand, has only recently started to show promise [33]. The principal surgical interventions for major airway trauma and chronic lung disease are tracheal resection, lung volume reduction and lung transplantation. Ideally, new therapeutics that can actually cure, rather than delay, lung deterioration need to be developed as the prevalence and burden of such diseases continue to grow; thus, in addition to a review of the pharmacological and surgical management, this section also outlines the drug development process as a prelude to an analysis of the current respiratory models available for developing novel inhalable therapies.

1.1.3.1. Pharmacotherapy

Broadly speaking, pharmacological management of asthma and COPD by inhalable therapeutics can be classified under two categories: “relievers” and “preventers” [31]. Drugs falling within the first set include β_2 -adrenoreceptor agonists and muscarinic receptor antagonists that act as bronchodilators to relieve symptoms of breathlessness, wheezing and coughing. Preventers, on the other hand, do not provide immediate relief for patients but act as anti-inflammatory agents to reduce tissue damage and remodelling within the respiratory tract in the longer-term; prominent drug classes include inhaled corticosteroids and leukotriene receptor antagonists. There is a lot of overlap between the medications used for asthma and COPD, with clinical guidelines outlining various algorithms for treatment regimens based on the severity of disease (e.g. see Fig. 1.2 for the UK guidelines for asthma management; [34]).

Pharmacotherapy for CF and IPF involves different medicines in addition to the classical relief/prevention dogma of asthma and COPD. As well as the various therapeutics previously mentioned for CF (Section 1.1.3), an interesting pharmacological intervention involves the use of nebulised hypertonic saline to reverse the thinning of the tenacious mucus layer that impairs ciliary action in CF [32]. This simple formulation of highly-concentrated salt draws out water into the respiratory tract by osmosis and can aid in the restoration of mucociliary clearance within the tracheobronchial region. A more recent breakthrough for a sub-population of CF patients has been the approval of the oral drug ivacaftor that acts to potentiate cystic fibrosis transmembrane conductance regulator (CFTR) activity in airway epithelial cells [35, 36]; the enormous cost of this drug, however, limits its widespread implementation [37]. The treatment of IPF has also experienced a paradigm shift with the advent of the novel drugs pirfenidone and nintedanib that antagonise excessive fibrosis and GF signalling [10, 33]. Notably, beyond targeting CFTR activity with ivacaftor, almost none of the current pharmacological treatments specifically target epithelial cell dysfunction.

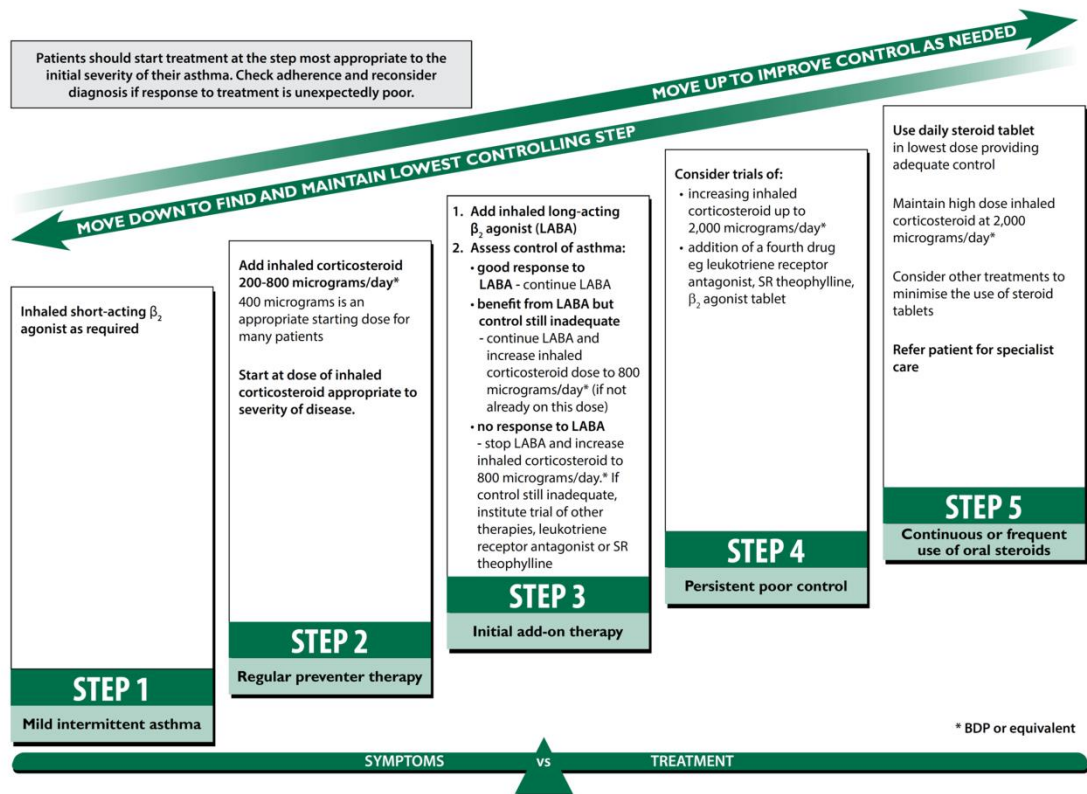


Figure 1.2: British guideline on the management of asthma in adults. The guideline lists the main inhaled therapies available for treatment of respiratory disease. Adapted from [34]. BDP: Beclomethasone dipropionate; SR: Slow-release.

1.1.3.2. Surgical intervention

For cases of extensive tracheobronchial injury due to cancer, stenosis, infection or congenital abnormalities, resection of the malignant tissue with primary anastomosis is indicated [38, 39]. This approach, however, is restricted by the size of the segment that can be excised, rendering lesions greater than half the length of the trachea in adults and one third in children inoperable. To date, these cases have been treated primarily with autografts, allografts and artificial prosthetics [40]. Unfortunately, allograft transplantation is limited by the complications of immunosuppressive treatment, while artificial prostheses are associated with numerous issues, including device migration and dislodgement, material degradation and failure, tissue granulation and tracheal stenosis [41]. Consequently, novel approaches inspired by tissue engineering have emerged in the last decade that seek to address this unmet clinical need (Section 1.3).

For patients with severe lung disease who meet the criteria for surgery, lung volume reduction and transplantation are two possible interventions. The objective of lung volume reduction is to remove regions of parenchymal respiratory tissue that no longer contribute to gas exchange in hyper-inflated lungs so that the remaining functional tissue can restore elasticity and engage in more efficient oxygen uptake [42]. This has been conventionally performed by median sternotomy and excision, video-assisted thoracoscopic surgery (VATS) or endobronchial valves, though new procedures involving bronchoscopic thermal vapour ablation and lung volume reduction coils show potential as less invasive procedures. Transplantation of one or two of the lungs themselves is performed most frequently in COPD patients, though elderly sufferers of CF and IPF can also be candidates [32, 42]. Bilateral sequential lung transplantation is most commonly indicated, where each lung is consecutively removed and replaced during the course of the operation [43]. Sadly, lung transplantation is associated with a 5 year mortality of approximately 50% post-transplantation, in addition to the iatrogenic complications of post-operative immunosuppression [44]. Therefore, the development of new therapeutics that can prevent patients from reaching this stage of disease severity would be a better alternative to this high-risk procedure that also requires a ready supply of donor lung tissue.

1.1.3.3. The development of novel treatments

The process for the development of novel respiratory drugs follows the same convention as that of other drugs (Fig. 1.3; [45]). Thousands of candidate molecules progress through stages of identification, optimisation, pre-clinical and clinical steps prior to drug approval by the regulatory body. This process has an enormous attrition rate, with 85% of investigational new drugs failing in early clinical trials and only half of the remaining 15% obtaining approval after Phase III trials [46]. Coupled with the average length of 12.5 years that it takes to successfully bring a new drug to market, this process can cost upwards of \$1 billion [47]. The major contributors to the failure of lead candidates include lack of drug efficacy and toxicity issues [48]. The disconnect between pre-clinical *in vitro* models, animal models and subsequent human trials is an important contributor to this poor rate of clinical translation. More advanced tools for translation to address this disparity could hold the answer to streamlining the drug development pipeline

and to improving the successful translation of new therapeutics, including those for currently incurable respiratory diseases.

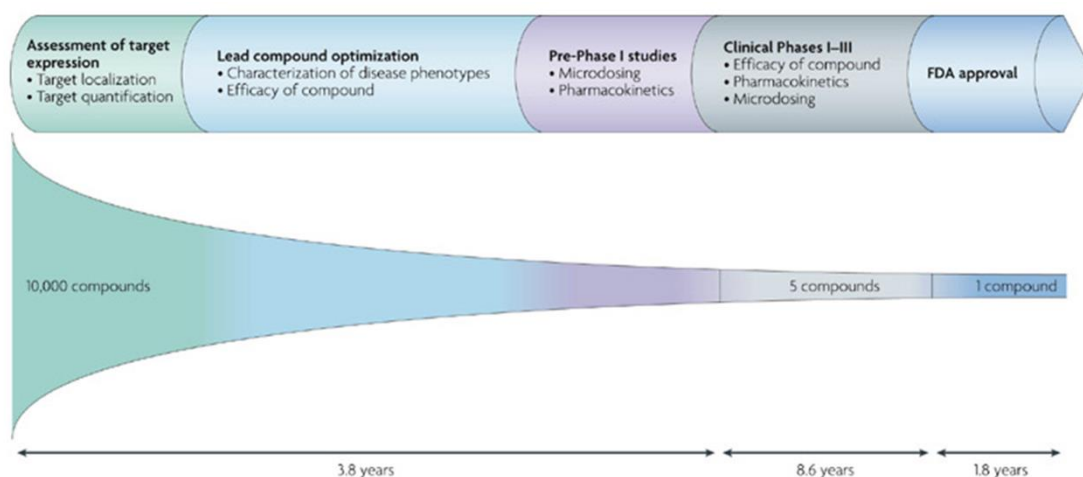


Figure 1.3: The drug development process timeline. Thousands of compounds progress through stages of identification, optimisation, pre-clinical and clinical steps prior to drug approval by the regulatory body. Adapted from [45]. FDA: Food and Drug Administration.

From an industrial perspective, the respiratory tract is not only an important system to consider for the development of novel inhalable products for the local treatment of chronic lung disease, but it is also a very attractive route for systemic drug delivery to treat a range of non-respiratory diseases. This is due to a large absorptive surface area, thin alveolar epithelium barrier, high blood flow and relatively low drug-degrading metabolic activity [49]. Indeed, this route could be of great interest for delivery of complex biotechnology medicines and advanced therapeutic medicinal products (ATMPs). When considered with the potential of epithelial dysfunction as a target for the treatment of respiratory disease, the improvement of current preclinical models of respiratory epithelial tissue in healthy and diseased states could reveal novel strategies to identify therapeutic targets and maximise drug delivery through a route of administration that has invested industrial interest. In order for this objective to be realised, an examination of the current models for respiratory drug discovery is warranted to assess the shortcomings that should be addressed in a new model system.

1.2. Current respiratory drug development models

Current models for respiratory drug discovery and delivery consist of a range of *in vitro*, *ex vivo* and *in vivo* approaches that aim to obtain valuable preclinical data on aspects of drug deposition and absorption (Fig. 1.4; [50]), as well as efficacy and toxicity. *In vitro* studies include analysis of aerosol deposition and cell culture models to predict the anatomical regions to which the inhaled therapeutic travels, in addition to drug transport and toxicological assessment, while the *ex vivo* isolated perfused lung can provide the same readouts with relevance to a physiologically intact architecture. Animal models are of course an essential component of all preclinical testing and novel lung imaging techniques, coupled with *in silico* computational methods, can be employed for further analysis of an inhalable product in human patients at the clinical trial stage. Analysis of aerosol deposition and the isolated perfused lung have been recently reviewed by Nahar and colleagues and within the same research group, Patel et al. have published an informative discussion of *in silico* computational approaches [50, 51]. For the purposes of this thesis, the discussion of respiratory models focuses on cell culture and animal models. Although each model has its own advantages and disadvantages, an examination of their major limitations identifies the potential for an innovative approach to develop novel and effective respiratory models.

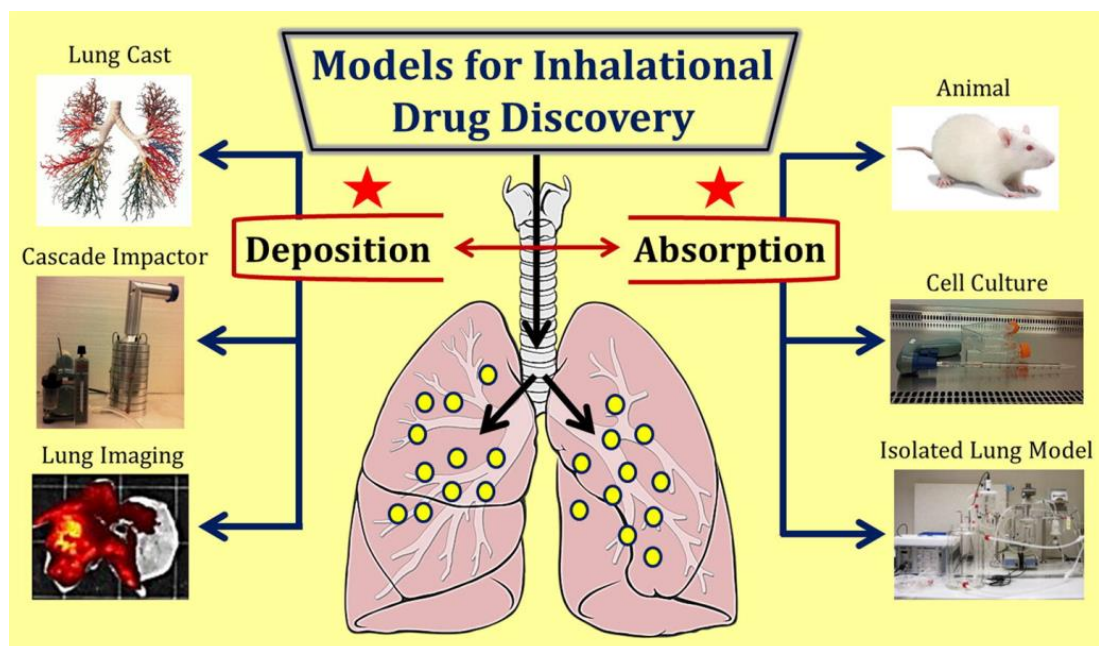


Figure 1.4: Models for inhalational drug discovery. Adapted from [50].

1.2.1. Cell culture models

Respiratory cell culture models incorporate a range of immortalised cell lines or primary epithelial cells for mechanistic, drug transport and toxicity studies. As is the case with cell culture models for other organ tissues, immortalised cell lines are useful as a supply of steadily proliferating and phenotypically stable cells. This in turn facilitates consistency in assay design and a subsequent improvement in comparison between respiratory drug candidates [52]. Respiratory cell lines have chiefly been derived from either lung carcinoma or by virally-transformed epithelium (Table 1.1). Bronchial cells feature predominantly, owing in general to their propensity to form tight junctions and, particularly in the case of the Calu-3 epithelial cell line, the ability to secrete an apical mucus layer under certain conditions akin to secretions present *in vivo* [53].

Of course, the inherent immortal nature of a cell line indicates that differences exist between cell lines and native cells [54, 55]; the Calu-3 cell line, for example, may exhibit features of bronchial epithelial cells, but it has been derived from a pulmonary carcinoma [56]. Accordingly, there is a drive towards the increased implementation of primary respiratory cells that can exhibit all of the organotypic hallmarks of the *in vivo* epithelium. Indeed, the efficacy of ivacaftor on potentiating chloride and sodium transport was analysed using primary tracheobronchial epithelial cell culture with both normal and diseased primary bronchial epithelial cells [35], ultimately contributing to its approval. The requirement for complex culture conditions and the rapid dedifferentiation of these cells *in vitro*, however, remain a challenge. Donor variability is an additional well-known issue with primary cells. Furthermore, the artificial *in vitro* culture environment can limit primary cell functionality, as described in Section 1.2.3.

Table 1.1: Prominent epithelial cell sources for respiratory cell culture models.

Cell Type	Features	Studies
<u>Bronchial cell lines</u>		
16HBE14o-	Transformed bronchial cell line Tight junction formation Limited ciliation and mucus secretion	[57-60]
BEAS-2B	Transformed bronchial cell line Cytochrome P450 metabolic activity Lack tight junctions, ciliation and mucus secretion	[61]
Calu-3	Derived from adenocarcinoma of the lung Tight junction formation and mucus secretion Limited ciliation	[53, 56, 62]
<u>Bronchiolar cell lines</u>		
NCI-H441	Derived from adenocarcinoma of the lung Tight junction formation post-dexamethasone stimulation Limited ciliation	[63-65]
<u>Alveolar cell lines</u>		
A549	Derived from adenocarcinoma of the lung Surfactant secretion Potential for tight junction formation	[66-68]
<u>Primary cells</u>		
NHBE cells	Obtained from tracheobronchial tissue Tight junction formation, mucus secretion and ciliation Donor variability and limited passage number	[69, 70]
MatTek EpiAirway® Epithelix MucilAir®	Specialised primary cell culture models Tight junction formation, mucus secretion and ciliation Long lifespan Expensive	[71, 72]

Whatever the cell source, current cell-based *in vitro* models of the respiratory tract typically consist of an epithelial monolayer cultured on a semipermeable membrane insert at an air-liquid interface (ALI) to induce cell polarisation, differentiation and mucus production (Fig. 1.5; [13, 54]). This model is referred to as cell insert or “transwell” culture in reference to one of the main cell insert products supplied. The semipermeable membranes are available in a range of polymeric materials, including polycarbonate (PC) and polyethylene terephthalate (PET) [71]. Other modifications to enhance epithelial differentiation with this model includes the use of collagen coating [73] and co-culture with other cell types found in the relevant region of the respiratory tract [60, 64, 68]. Overall, the cell insert culture model is viewed as the principal cell culture model for respiratory drug discovery and toxicology.

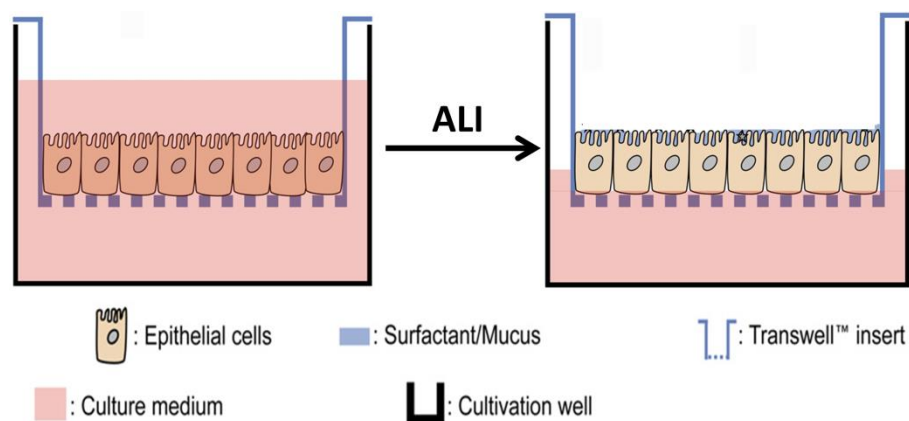


Figure 1.5: Conventional cell insert culture of respiratory epithelial cells. Epithelial cells are initially seeded onto a semipermeable membrane and exposed to air-liquid interface (ALI) conditions. Adapted from [13].

1.2.2. Animal models

Animal models for respiratory drug discovery primarily consist of rodent models, though larger animals are also employed. Mice, rats, and guinea pigs are commonly used because of cheaper storage and handling costs compared to larger animals, the capacity for larger sample size numbers in studies, and the availability of beneficial imaging and molecular technologies that can be used with such rodent species (reported in [74] and [75]). While the use of small animals is pragmatic and cost-effective, issues related to the size of dose that can be administered to animals can present a challenge, particularly in cases of drug candidates with limited aqueous solubility or for those that require the inhalation of a larger quantity of drug. Furthermore, blood, urine and other samples that are taken for pharmacokinetic analyses have a limited extractable volume from small creatures. In these cases, larger animals such as pigs, sheep or primates can be more useful, though the use of such species will come at an additional cost and will require acceptable ethical justification [76]. Thus, the rational selection of an animal species warrants consideration of the disease or treatment that is being modelled, study design and sampling, in addition to study endpoints.

The method of aerosol administration is a key factor in the design of animal studies for drug delivery to the lungs and will impact on the accuracy of the results obtained [74]. Inhalable agents can be administered to animals by passive inhalation methods through the use of a whole-body exposure chamber, such as in animal models of cigarette smoke exposure [77], or by nasal methods [78].

Alternatively, intratracheal instillation of a drug solution and insufflation are common techniques. The former method is regularly performed to deliver inhalable agents in drug testing and can also be used to induce emphysema in rodent disease models with elastase, as described by March and colleagues above, while insufflation can be useful for the evaluation of dry powder formulations [79, 80]. In summary, a range of animal models and means of drug administration to the respiratory tract exist, but it is paramount to carefully design animal trials with due consideration to the species and mode of inhalation for there to be any chance of translatable outcomes to humans. Of course, due to differences between humans and animal, this may not always be possible.

1.2.3. Limitations of current cell culture and animal models

ALI culture has played a significant role in the *in vitro* recapitulation of the *in vivo* respiratory environment. This model positions the cells at the border of an apical compartment reminiscent of the respiratory tract lumen and a basolateral side representing vascular supply of nutrients [71]; as a result, it has facilitated increased expression of cilia in primary cells and differences in barrier and mucus-secreting properties of cell lines [53, 81]. However, the conducting and respiratory regions both have a prominent extracellular component that is absent in cell insert models (Fig. 1.6; [13]), which can result in an oversimplification of the airway barrier that renders this drug development tool lacking in physiological relevance [82, 83]. For example, culture on polymeric inserts can alter cell growth and phenotype, with different proliferation rates, protein expression and cellular differentiation observed when different compositions of natural and synthetic substrates are utilised [73, 84-86]. Inadequate data obtained from the use of synthetic cell substrates can increase the risk of drug candidate failure due to poor *in vitro-in vivo* correlation between the apparent pharmacokinetic and pharmacodynamic characteristics of the compound, culminating in great expense and time lost that delay the development process of new medicines. With this in mind, complex, physiologically-representative *in vitro* models must be developed to address the inadequacies of current model platforms.

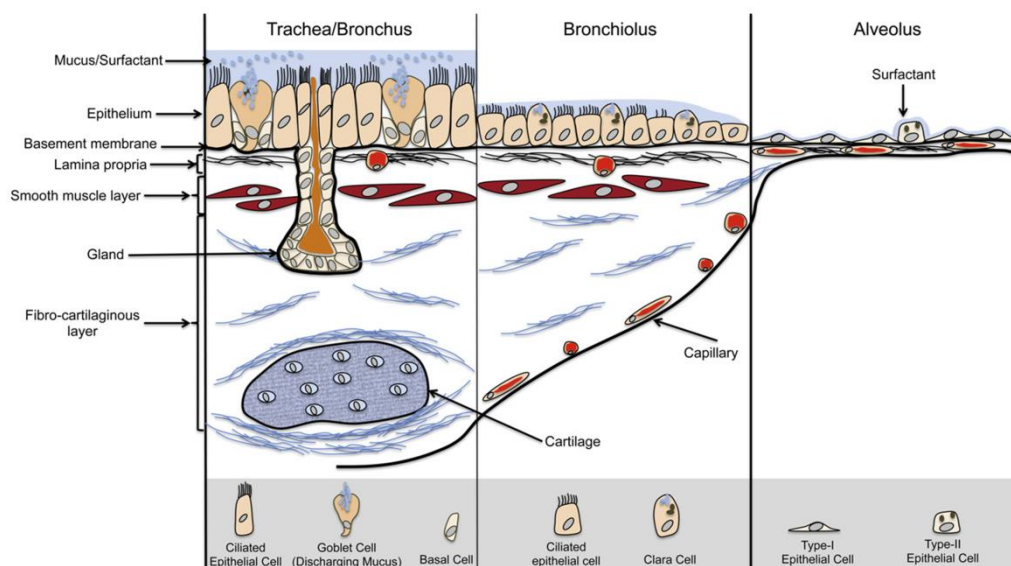


Figure 1.6: The extracellular matrix component of the respiratory tract. Adapted from [13].

In vivo animal models also suffer from other significant limitations, in addition to those alluded to in Section 1.2.2. While their use can provide toxicological information that might not be currently attainable with *in vitro* models, some animal species used in preclinical testing are not always suitable for human respiratory drug research because of interspecies structural and physiological differences. Firstly, despite the fact that aerosol deposition in lungs is influenced by particle size, airflow patterns and the airway geometry [51], branching divisions within the respiratory tract and the relative position of the right and left main bronchi are not equivalent between humans and common animal models [87]. As a result, the assessment of drug disposition in animals can inaccurately reflect that in humans and have consequences for reliable estimation of tracheobronchial and alveolar drug exposure. From a histological perspective, the differential distribution of submucosal glands and cell types in mice could contribute to different lung healing responses and mucus secretions [88]. Immunological differences between species are perhaps of even more significance. Novel treatments for asthma that showed promise in animal studies, for example, have failed when brought forward for clinical trials [75], while extreme systemic inflammatory responses occurred in human volunteers to novel agents that were originally safe in animals in the tragic case of the phase I trial of TGN1412 [89]. Indeed, the discordance between inflammatory pathways and the immune system between rodents and humans is clearly evident in the lack of a model that efficiently demonstrates the respiratory

pathophysiology of asthma and cystic fibrosis [32, 90]. Ultimately, the failure of such novel drugs is due to an incomplete and/or ineffective preclinical assessment in both animal and human tissues; the development of innovative methods for creating effective human tissue models could therefore synergise with current animal studies to successfully improve predictive validity of drug compounds in humans and increase the number of successfully formulated inhalable therapeutics.

Thus, combined with the drive to implement the reduction, refinement and replacement of animal models in research [91, 92], more sophisticated models based on 3D human normal and diseased tissue are required. Novel microfluidic approaches have created a “lung-on-a-chip technology” to model the bronchioalveolar region [93, 94]. Tissue engineering strategies, as discussed in the following section, might greatly advance the realisation of *in vitro* models that incorporate an ECM component into respiratory models, and this approach forms the focus of this PhD project.

1.3. Tissue engineering and the respiratory system

1.3.1. Tissue engineering: an alternative approach to respiratory drug development and the treatment respiratory disease

Advances in the field of tissue engineering (TE) have the potential to overcome the shortcomings of current respiratory *in vitro* models and airway disease treatments. TE is principally concerned with the reconstruction of tissue equivalents to replace physiologic tissue function lost due to disease or injury for regenerative medicine purposes [95]. Respiratory TE has recently flourished from the pioneering studies of 3D cell culture substrates by Douglas and colleagues [96] to the landmark case concerning a tissue-engineered tracheal transplant using acellular donor tissue re-seeded with autologous epithelial cells and bone marrow-derived mesenchymal stem cells (BM-MSCs; [97, 98]). The success of this *ex vivo* engineered tracheobronchial tissue highlighted the potential of TE strategies for respiratory tissue regeneration. Such strategies provide an opportunity for integrating the co-culture of multiple airway cell types that can be seeded in the correct tissue architecture to recapitulate the physiological environment, as well as facilitating the vascularisation of new tissue formed to consolidate viable respiratory

regeneration. Moreover, a TE approach can also be utilised to improve *in vitro* cell culture models in respiratory drug development. TE-based *in vitro* models incorporate the prominent extracellular component that is absent in current cell insert models and can consequently induce the formation of an *in vitro* organotypic epithelium through the use of ECM proteins as a substrate [99, 100]. Furthermore, the ECM analogue architecture provides a 3D framework for submucosal cell culture instead of flat two-dimensional (2D) surfaces. This can influence cell behaviour through biomechanical signalling pathways and cytoskeletal rearrangement [101]; as a result, paracrine factor release from embedded fibroblasts or BM-MSCs can replicate epithelial-mesenchymal cell-cell communication that occurs in the microenvironment of the native respiratory tract within an *in vitro* setting.

In order to apply TE strategies towards the development of novel *in vitro* models and innovative implants for tissue regeneration, it is crucial to implement the tissue engineering triad in their design [102, 103]. Firstly, the appropriate cells of the pertinent region of the respiratory tract must be present for acceptable *in vitro* representation or *in vivo* regeneration of the tissue. Stem cells, cell lines and primary cells can all be used depending on whether the final application is for *in vitro* modelling or tissue restoration. Cell sources are reviewed in Section 1.3.2 and the cell types used throughout this PhD project are identified. Secondly, TE strategies utilise biomechanical cues and growth factors (GFs) to provide signals to these cells to induce functional tissue formation. For respiratory TE, several GFs and drugs that can induce tissue repair and cellular differentiation are outlined in Section 1.3.3, including the drug all-*trans* retinoic acid (atRA) that is investigated in Chapter 5. Finally, in order for the cells to form correct respiratory tissue architecture, the use of a 3D scaffold to act as a structural framework for tissue formation is the cornerstone of successful airway TE. Given that the main goal of this PhD is to develop a novel scaffold of the tracheobronchial region for potential applications in respiratory drug development and respiratory tissue regeneration, Sections 1.3.4 and 1.3.5 extensively review the types of biomaterials that have been manufactured as scaffolds for respiratory TE. Through examination of these biomaterials, the choice of scaffold for this thesis is identified and justified.

1.3.2. Cell sources for respiratory tissue engineering and regeneration

In order to implement a successful respiratory tissue TE-based approach to heal or replace physiological tissue, scaffolds should ideally include progenitor cell populations for *ex vivo* culture or recruit them following implantation so that a regenerative response can be recapitulated and enhanced *in vivo*. Recent advances in our understanding of lung stem cell biology have identified potential pools of cell types that could be utilised for regenerative purposes in line with tissue engineered biomaterials [104]. Respiratory epithelial cells have a low rate of cell turnover but following injury to the surface of the tract, a rapid response is initiated to restore the epithelial barrier [105]. Distinct groups of progenitors appear to marshal reparative processes in distinct regions of the lungs, while some evidence also points to the recruitment of a universal stem cell population that can assist in the repair along the entire respiratory tract [106]. Endogenous mesenchymal progenitors include FGF10-releasing mesenchymal cells (reported in [107]), but knowledge of these cells is limited and the literature is focused on airway epithelial progenitors at present. All cell sources are of interest from a tissue-engineering perspective because whether the desired cell population is derived from a pool of stem cell progenitors, currently residing epithelia or a combination of both, the result is the same: regeneration of respiratory tissue that can perform adequate re-epithelialisation, and possible prevention of remodelling at the site that contributes to fibrosis, loss of lung function and respiratory disease [108].

1.3.2.1. Endogenous lung stem cell populations of the of the respiratory tract

Stem cells involved in airway development and repair processes can be broadly divided into two classifications: endogenous progenitor cells specific to a respiratory region and exogenous stem cells that arise from extrapulmonary tissue or embryonic stem cells. Within the first set (Fig. 1.7), basal cells have been identified as multipotent progenitors of the tracheal and bronchial epithelium [109, 110], a variant Clara cell subpopulation in the bronchus and bronchioles [111] and type II alveolar cells in the alveolar regions [112]; the capacity to act as progenitors appears to be an additional role along with the basic cellular functions outlined in Section 1.1 and evidence suggests that following injury to the lung, mechanisms are triggered to activate this regenerative capacity [113]. Basal cells occupy

approximately 30% of the pseudostratified epithelium of the lung and facilitate ciliated columnar epithelial attachment to the basement membrane [114], in addition to other potential roles in inflammatory processes and neurogenic signalling [115]. Different ratios of ciliated cells:Clara cells are derived from the basal progenitors depending on the different type of insult to the upper respiratory tract; for example, more basal cells differentiate into Clara cells following their selective depletion with naphthalene [109, 110]. Clara cells in their own right, as well as a subpopulation of naphthalene-resistant variant Clara cell, are capable of renewing the tracheobronchial and bronchiolar epithelium [111]. It is hypothesised that Clara cells provide a transiently amplifying population in response to injury while basal cells are longer-term progenitors of ciliated, secretory and Clara cell types.

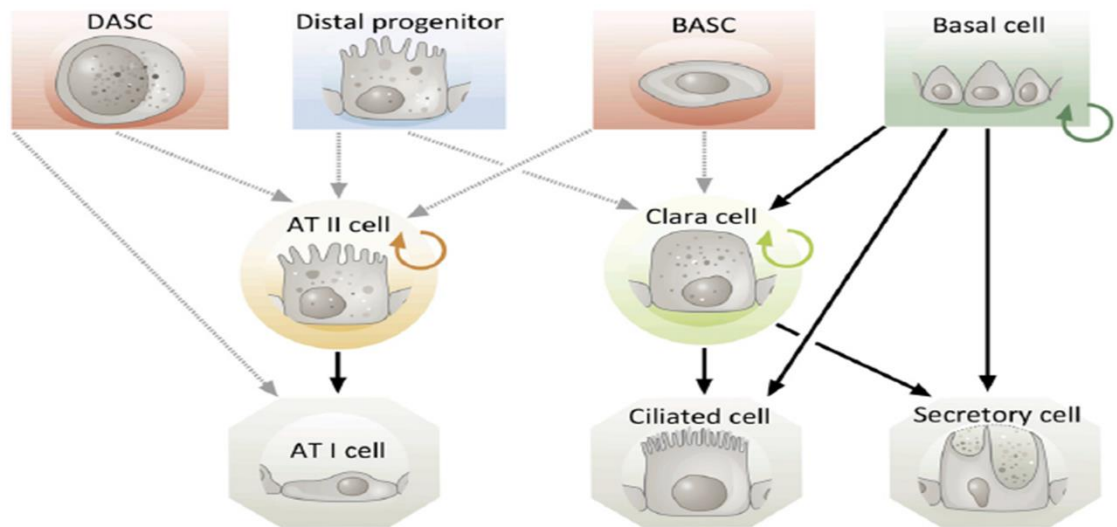


Figure 1.7: Endogenous epithelial progenitor cells of the lung. Gray dashed lines indicate that definitive *in vivo* evidence of lineage data is missing. Adapted from [116]. AT: Alveolar epithelial cell; BASC: Bronchioalveolar stem cell; DASC: Distal alveolar stem cell.

In the alveolar region of the respiratory tract, type II alveolar epithelial cells are widely referred to as the progenitor for type I cells. It has been shown to be the case that in addition to their surfactant-producing function, these cells can give rise to type I pneumocytes both under homeostatic conditions and in response to bleomycin-induced injury [117, 118]. Indeed, surfactant protein C+ (SPC+) type II cells have been recently confirmed as alveolar progenitors and as long-term stem cells in the adult lung [119]. Additional progenitors of the respiratory zone include a

putative bronchioalveolar stem cell niche population and two distinct distal progenitor populations [120-122].

1.3.2.2. Other lung stem cell populations

Other sources of lung stem cell populations include a reported multipotent lung stem, embryonic stem cells (ESCs), human amniotic fluid stem cells (hAFSCs) and BM-MSCs. In contrast to the multitude of progenitor cells described above that have regional restrictions, a report by Kajstura et al. has claimed to identify a multipotent lung stem cell with not only the potential to differentiate into any cell of epidermal origin, but also of mesodermal origin [106]. This study assessed a c-kit+ population for the properties of clonality, self-renewal and engraftment through serial transplantation into mouse lungs. While of great interest from a respiratory regeneration perspective as a universal lung stem cell, this work has been met with some consternation over the choice of controls, lack of lineage tracing and the choice of cellular markers [123], with further investigation warranted. Alternatively, pluripotent ESCs have been tested for induction into tracheobronchial and alveolar epithelial cells by various methods [124-127], while hAFSCs have been primarily investigated for their potential to differentiate into alveolar epithelial cell populations [128].

BM-MSCs are a widely investigated multipotent cell population that is a possible source of cells for respiratory regeneration. Repopulation of alveolar regions with bone marrow-derived stem cells has been demonstrated from analysis of sex-mismatched transplant tissue in humans [129, 130], while surgeries using aortic allografts as tracheal replacements provide evidence of MSC involvement [131]. Of course, the most successful tracheal TE transplants reported have also employed BM-MSCs, either by pre-seeding the acellular tracheal tissue *ex vivo* [97] or by recruiting them intraoperatively with pharmacological agents [132]. BM-MSCs are an alternative cell source that is easier to obtain in larger numbers than other stem cells, less difficult to culture *in vitro* and has a more favourable safety profile. With improved standardisation of cell isolation and maintenance practice (reviewed in [133]), MSCs could be a universally successful therapeutic option for respiratory TE strategies.

The local airway progenitors and stem cell populations reviewed above are not investigated with the novel scaffold developed in this thesis, but it is nonetheless important to understand their potential for the repair of lung tissue that has been damaged by chronic respiratory disease. As our knowledge of the lineage commitment mechanisms of these various stem cells increases, the techniques and methods used to induce epithelial or mesenchymal commitment will improve and could be combined with scaffolds (including that developed in this thesis) to maximise *in vivo* or *ex vivo* tissue regeneration strategies in future studies. For the purposes of this PhD project, however, the Calu-3 cell line and primary tracheobronchial epithelial cells outlined in Section 1.2.1 are investigated in culture upon the scaffolds developed through the course of the thesis.

1.3.3. Signalling factors for respiratory tissue engineering and regeneration

Healing processes in the airways require complex coordination of a range of GFs for processes such as proliferation, differentiation and vascularisation of tissue to restore functionality [82]. Further delineation of specific GFs in the respiratory tract, their mechanisms of action, as well as their temporal release in morphogenesis, tissue development and responses to injury, could be incorporated into tissue modelling or regenerative medicine strategies for the airways. While not as extensively studied as in other regenerative medicine applications, several GFs and other molecules have been identified that hold the potential to progress the field of respiratory TE; these include hepatocyte growth factor (HGF), BMP4, keratinocyte growth factor (KGF) and all-*trans* retinoic acid (atRA).

1.3.3.1. Hepatocyte growth factor (HGF)

Of all the GFs with regenerative potential for lung tissue, HGF is of particular interest as a therapeutic agent with clinical application for the treatment of pulmonary fibrosis. This GF has been detected at higher levels in patients suffering from pulmonary fibrosis [134], suggesting its role in the physiological response to chronic injury, while other studies have revealed the presence of defective HGF production by fibroblasts in COPD [135]. Within the respiratory tract, HGF plays a role in the modulation of alveolar epithelial and endothelial apoptosis, as well as fibroblast differentiation into pro-fibrotic myofibroblasts [136]. Increasing the levels of HGF, either by gene transfection or by intratracheal

administration, has reduced lung fibrosis in models of pulmonary fibrosis and emphysema [137-141]. Mechanisms of reparative action determined in these studies confirmed an anti-apoptotic effect on alveolar epithelial cells, reduction of pro-inflammatory molecules, decreases in transforming growth factor beta-1 (TGF β 1)-mediated epithelial-mesenchymal transition (EMT) and reduction in collagen deposition. Indeed, recognition of HGF's role in regenerating respiratory tissue has instigated several clinical trials for the use of small molecule HGF-mimetics for the treatment of acute lung injury and pulmonary fibrosis (reviewed in [142]). Recent evidence suggests that HGF can be supplied to the damaged airways by BM-MSCs [143], suggesting that this is one mechanism of healing through which such stem cells bring about their paracrine reparative effects. Overall, HGF has been identified as a significant signalling GF in respiratory epithelial-fibroblast crosstalk and is of interest from a tissue regeneration perspective.

1.3.3.2. Bone morphogenetic protein 4 (BMP4)

In the airways, BMPs- notably, BMP4- have been identified for their roles in lung development and airway healing following acute injury [144, 145]. BMPs regulate proliferation, differentiation, angiogenesis, apoptosis and regeneration across the body [146] and this has been exploited for tissue regeneration purposes, such as the soak-loaded recombinant BMP2 commercial bone graft substitute, INFUSE® [147]. BMP4 has been previously identified as a modulator of lung branching morphogenesis and proximal-distal differentiation of ciliated and secretory epithelial cells [148]; perhaps of greater interest from a tracheal tissue regeneration perspective, however, BMP signalling is more active in the conducting airways after parturition and is upregulated following asthmatic injury [149]. The canonical signalling pathway of BMP has been attributed to EMT processes in human bronchial cell lines and primary murine airway epithelial cells that are temporarily activated during wound repair and epithelial damage [145, 150, 151]. Accordingly, the short-term induction of this pathway through the use of BMPs by tissue-engineered constructs for tracheobronchial implantation could herald a novel application for a family of GFs that has been traditionally associated with osteogenesis [152].

1.3.3.3. Keratinocyte growth factor (KGF)

KGF, also known as FGF7, mediates epithelial proliferation in the respiratory tract, particularly during morphogenesis and repair in acute lung injury [153]. Increased transcription and translation of KGF within fibroblasts occurs in response to pro-inflammatory cytokines such as IL-1, and this increased expression could stimulate epithelial repair following injury via paracrine action [154]. Moreover, KGF-induced epithelial growth by autocrine release from tracheobronchial epithelial cells might also contribute to the healing response [155]. The protein appears to induce its restorative effects by stimulating epithelial cell growth, inhibition of apoptosis, mobilisation and attraction of circulating progenitor cells, as well as restoration of epithelial barrier integrity by cytoskeletal stabilisation and protection of Clara cells [156-158]. Although this GF has not been considered in the development of any tissue-engineered respiratory scaffold for tracheobronchial regeneration to date, future studies incorporating KGF into scaffolds could potentially yield an enhancement in epithelialisation of the implanted constructs.

1.3.3.4. All-trans retinoic acid (atRA)

Derived from vitamin A, atRA is a low molecular weight molecule that is employed as an anti-cancer drug and as a media supplement for primary airway epithelial cell culture [69, 159]. It is generated from retinol *in vivo* by several oxidative reactions and operates in conjunction with FGF10 signalling to regulate morphogenic branching processes in the developing lung [160]. In adults, atRA has been investigated as a drug for the reversal of COPD-induced alveolar injury with recorded reductions in alveolar enlargement; data in human and animal trials, however, have been mixed [78, 161-165]. While investigations into alveolar tissue regeneration have not been conclusive, the potential for atRA-induced regeneration of the conducting airways has largely been unexplored and its regenerative potential for tracheobronchial tissue could hold promise. From a TE perspective, the application of atRA provides a significantly cheaper alternative to macromolecular GF biomolecules and also has the advantage of targeting a pathway that is not mediated by paracrine and autocrine peptides in the airways [166, 167]. In this regard, an atRA-loaded regenerative implant could enhance epithelial repair and functionalisation to synergise with GF release by cells in the local *milieu* and provide a multimodal approach to targeting cell signals, rather

than just “piggybacking” GF molecular pathways. The major challenge for such an implant, however, is the unfavourable physicochemical properties of atRA that limit its integration into a scaffold. This challenge is addressed in Chapter 5 of the thesis.

1.3.4. Biomaterials for respiratory tissue engineering and regeneration

The majority of respiratory TE research has focused on the use of biomaterial scaffolds for 3D airway *in vitro* modelling or for the fabrication of regenerative implants. Scaffolds employed are typically composed of natural polymeric materials (e.g. collagen), donor ECM (decellularised (DC) tissue), synthetic polymeric materials (e.g. poly- ϵ -caprolactone (PCL)) and composites of synthetic and natural materials. All these categories have been employed in engineering both the tracheobronchial region and alveolar region of the airways in a variety of formulations, including hydrogels, porous polymeric sponges, and DC constructs. The choice of scaffold type has often reflected the TE application in mind, with most 3D *in vitro* modelling applications investigating hydrogel-based formulations while *ex vivo* culture and other regenerative approaches favouring the use of acellular ECM material and porous polymeric scaffolds.

1.3.4.1. Biomaterials for alveolar tissue engineering and regeneration

The first report concerned with biomaterials and respiratory TE investigated 3D modelling of histotypic alveoli [96]. Since then, alveolar TE has seen a trend where earlier studies focused on hydrogels with some porous polymeric scaffolds and more recent research has expanded on the use of acellular whole lungs to preserve alveolar architecture. This PhD is focused on TE of the tracheobronchial region (Section 1.3.5) and consequently, biomaterials for alveolar TE are only reviewed in brief to provide context to the entire field of respiratory TE. A summary is provided in Table 1.2; for a more comprehensive review of these biomaterials, the reader is referred to [168].

Table 1.2: Biomaterials used in alveolar tissue engineering. FGF: Fibroblast growth factor; GAG: Glycosaminoglycan.

Cell-Scaffold System	Notes	Studies
<u>Hydrogels</u>		
Rabbit foetal lung cells on Matrigel®-based hydrogel	Thick gel required for alveolar structures to form and persist for 22 days; surfactant production	[169]
Murine foetal lung cells on Matrigel®-based hydrogel	Foetal lung and alveolar histological features observed with high seeding in Matrigel; surfactant gene expression; combinations of FGF 2/7/10 induced epithelial cell budding and endothelial network formation	[170, 171]
Rat primary type II pneumocytes on collagen type I hydrogel	Cellular aggregates developed into alveolar structures with flattened and cuboidal cell morphology; surfactant production	[172]
<u>Decellularised tissue: whole-lung</u>		
Rat foetal lung cells, human umbilical vein endothelial cells and A549 alveolar epithelial cells on acellular rat lung	Perfusion decellularisation preserved lung architecture; ventilation of cell-seeded tissue performed in vitro; in vivo orthotopic transplantation of pre-cultured construct maintained without ventilation support for 6 hours	[173]
Rat primary lung epithelial cells and rat lung microvascular endothelial cells on acellular rat lung	Perfusion decellularisation preserved lung architecture; ventilation of cell-seeded tissue performed in vitro; epithelial cells expressed alveolar markers by 8 days; transplantation of pre-cultured construct maintained for up to 2 hours	[174]
Mouse foetal lung cells and embryonic stem cells on acellular mouse and rat lung	Perfusion decellularisation preserved lung architecture and extracellular matrix components; expression of markers for type II alveolar epithelial cells, endothelial cells, smooth muscle cells and Clara cells observed in bioreactor culture	[175, 176]
Rhesus primary bone marrow-derived mesenchymal stem cells and adipose-derived stem cell on acellular primate lung	Perfusion decellularisation preserved lung architecture and extracellular matrix components; cellular attachment, elongation and proliferation observed over 7 days in culture	[177]
Murine embryonic stem cells, human foetal lung cells, porcine primary bone marrow-derived mesenchymal stem cells and human alveolar epithelial cells on acellular porcine and human lung	Perfusion decellularisation preserved lung architecture and extracellular matrix components; cellular attachment and proliferation observed after 7 days; alveolar epithelial cells expressed alveolar markers	[178]
Human primary bronchial epithelial cells, human primary bone marrow-derived mesenchymal stem cells, human lung fibroblasts and CBF12 human vascular endothelial cells on acellular human lung	Decellularisation of fibrotic lungs was inefficient; coating tissue sections with pleural mimic increased cellular retention and adherence to scaffold	[179]
<u>Porous polymeric scaffolds</u>		
Rat foetal lung cells on gelatin sponge disc	Cellular aggregates developed into alveolar structures with microvilli and lamellar bodies	[96, 180]
Rat foetal lung cells on Gelfoam®	Pre-culture with cells prior to implantation necessary for vascularisation and alveolar unit formation in scaffold in vivo	[181]
Rat foetal lung cells on collagen-GAG scaffolds	Alveolar structures formed with surfactant production in vitro; extracellular matrix deposition around alveolar units	[182]
Ovine somatic lung progenitor cells on PGA mesh-pluronic F127 hydrogel	Cells expressed alveolar features in vitro on PGA scaffolds; foreign body reaction in vivo prevented by combination with hydrogel	[183]

Hydrogel scaffolds have been investigated as an environment for forming 3D alveolar structures for distal airway modelling, where epithelial cells have been cultured within the gel matrix. One of the first studies reporting the use of a gel scaffold for the support of airway cell culture by Blau et al. described the formation of spherical clusters of foetal rabbit type 2 pneumocytes around a central lumen within reconstituted basement membrane (Matrigel®) [169]. The propensity for type 2 alveolar cells to form these alveolar-like structures *in vitro* has been replicated with other species [170, 171] and with type I collagen gels [172]. Analysis of markers of differentiation indicated the transition from type II alveolar epithelial cells to flattened type I cells in 3D culture. However, encased alveolar units described above are infeasible for *in vivo* tissue regeneration or replacement as their successful integration with the surrounding airway branches is unlikely. Therefore, the utility of hydrogel scaffolds of the alveolar region lies principally in its role as a tool for basic research in the study of processes such as alveolar morphogenesis and progression of disease.

Alternatively, DC whole lung is an interesting possibility for alveolar tissue regeneration using acellular cadaveric donor tissue. Donor tissue can have its antigenic components removed by various steps of detergent addition to leave a natural scaffold maintaining tissue architecture and embedded signalling factors [184], allowing for the re-seeding of the biomaterial with the recipient's cells. Since the publication of two studies outlining the preparation and transplantation of acellular rat lungs using primary epithelial and vascular cells and foetal airway cells [173, 174], parallel investigations have been conducted with murine [175, 176], primate [177] and more recently in human tissue [178, 179, 185], as well as analysis with different stem cell populations such as BM-MSCs [186]. While these studies highlight the potential of this TE strategy, the requirement for vast quantities of multiple cell types and standardisation of tissue quality, storage and DC methods [185, 187-190] makes this form of therapy far from clinic-worthy at present. For now, a more plausible and beneficial clinical application for could be as a sophisticated *in vitro* drug delivery platform that could provide information on drug deposition fate in the lungs following pulmonary administration [191] and analysis of systemic absorption, given that the vascular and airway systems remain intact and independent of each other in the DC organ.

Porous polymeric scaffolds, a third type of biomaterial, were utilised in the first reports of respiratory TE [96, 180]. Since then, further research of foetal lung cell culture on other materials such as the purified gelatin product Gelfoam® [181], highly-porous lyophilised collagen-glycosaminoglycan (CG) scaffolds [182], and a composite of polyglycolic acid (PGA) mesh and Pluronic F127 (PF127) gel [183] have shown promise for alveolar modelling and regeneration applications. Overall, porous polymeric scaffolds can remedy the regenerative limitations of hydrogel scaffolds by providing a structure in which the struts of the pores can provide a framework for alveolar cells to grow on and a hollow pore to develop in to the luminal airway on the apical side of the cells, with the correct tailoring of pore size and interconnectivity within the construct.

1.3.5. Biomaterials for tracheobronchial tissue engineering and regeneration

While it is relevant to consider the biomaterials used in alveolar TE because of the overlap with the type of polymers and manufacturing methods with tracheobronchial TE, the main goal of this PhD is to develop a novel scaffold of the tracheobronchial region for potential applications in respiratory drug development and respiratory tissue regeneration using a TE-based approach. Therefore, the use of hydrogels, DC tissue and porous polymeric scaffolds for bioengineering the conducting zone of the respiratory tract are reviewed in detail here.

1.3.5.1. Hydrogels

Hydrogels are the most investigated biomaterial for tracheobronchial TE. Primary tracheobronchial epithelial cells cultured at an ALI upon a type I collagen gel, either as a gel alone or as a set gel suspension containing fibroblasts, has been shown to enhance cellular proliferation and differentiation to yield an organotypic pseudostratified epithelium [100, 192-194]. The 3D multicellular environment, including hydrogel composition and mechanical properties, can have a prominent influence on respiratory epithelial cells. Pageau et al., for example, discovered that a collagen concentration range of 2mg/ml-3mg/ml was optimal for the co-culture model to prevent excessive fibroblast-induced contraction [100]. This study also identified that the change of fibroblast cell type affected the epithelial cell phenotype and contractile properties. Additionally, other studies have shown that Matrigel®, a basement membrane analogue derived from mouse sarcoma cells [195], induced the formation of spheroid-like structures from human bronchial

epithelial cells within the gel and displayed alveolar and pulmonary acinar characteristics when used as the cellular substrate, similar to its effects on type 2 pneumocytes [196, 197]. Further improvements have been made to hydrogel models by introducing lateral physical strain with a customised culture plate and T-cells from healthy and asthmatic donors to better mimic airway mechanical forces and understand inflammatory disease, respectively [198, 199].

While collagen-based hydrogels are undoubtedly the most common choice of biomaterial for *in vitro* respiratory TE applications to date, other natural polymers and composites have been considered as gel structures. Risbud and colleagues, for example, validated the immunocompatibility of a chitosan-gelatin hydrogel through a 7-day culture period with macrophages and found that the biocompatible material supported the growth of human primary respiratory epithelial cells [200]. Cornelissen et al. directly compared fibrin hydrogels to those made from collagen in a bid to create a biomaterial that could be derived from autologous blood in a patient [201]; fibrin was found to be equivalent to collagen as a material for tracheal epithelial cell culture, highlighting its potential as a substrate for engineering the tracheobronchial region. Overall, hydrogel models of the conducting zone have demonstrated efficacy as an ECM mimic of the proximal airways. Table 1.3 provides a summary of hydrogel biomaterials for tracheobronchial TE.

Table 1.3: Hydrogels used in tracheobronchial tissue engineering. PCL: Poly- ϵ -caprolactone; PLGA, Polylactic(co-glycolic) acid.

Cell-Scaffold System	Notes	Studies
<u>Collagen hydrogels</u>		
Human primary bronchial epithelial and fibroblastic cells	Serum-free medium supplemented with retinoic acid was best for bronchial tissue culture	[192]
Immortalised human primary bronchial epithelial cells; IMR-90 fibroblasts	Keratinocyte feeder layer media used; multipotent immortalised cells achieved in culture	[193, 196]
Canine and porcine primary tracheal-bronchial epithelial cells	Use of collagen enhanced ciliogenesis; metachronal ciliary beating observed	[194]
Human primary bronchial epithelial cells; IMR-90 and LuCAF fibroblasts	Higher concentration of collagen (3mg/ml) reduced gel contraction; fibroblast type influenced epithelial cell features	[100]
Human bronchial epithelial cells; IMR-90 fibroblasts; human primary eosinophils	Combined 50% lateral strain and activated eosinophils induced epithelial layer thickening	[198]
Human primary bronchial epithelial, fibroblastic cells and T-cells	Co-culture system influenced the survival of T-cells	[199]
Human primary bronchial epithelial cells; human primary tracheal, dermal, nasal and gingival fibroblasts	Gingival and tracheal fibroblasts induced normalised tracheal epithelium	[202]
Rat primary lung fibroblasts and bone marrow-derived mesenchymal stem cells	Three-layered collagen-fibroblast hydrogel was reinforced with rings of osteogenically-induced stem cells; animals survived approx. 24 hours post-implantation	[203]
<u>Other hydrogels</u>		
Matrigel®-based hydrogel; human primary bronchial epithelial cells	Culture on or within hydrogel induced pulmonary acinar formation	[197]
Chitosan-gelatin hydrogel; human primary tracheal epithelial cells; J774 macrophage cells	Cells cultured on hydrogel had similar viability and cell marker expression to culture on tissue culture plastic	[200]
Fibrin hydrogel; ovine primary tracheal epithelial cells	Hydrogel was found to be non-inferior to a collagen gel for the culture and barrier formation of respiratory cells	[201]
Fibrin-hyaluronan-PLGA gel; rabbit primary auricular and articular chondrocytes	Pre-cultured gel showed integration with tissue in a partial tracheal defect; cartilage formation, epithelialisation and ciliary beating detected; PLGA reinforced gel strength	[204, 205]
Fibrin-PCL gel; rabbit primary bone marrow-derived mesenchymal stem cells	Pre-cultured gel reinforced with a PCL mesh showed integration with tissue in a partial tracheal defect; cartilage formation, epithelialisation and ciliary beating detected	[206]

In spite of their widespread use as an ECM mimic of the tracheobronchial region, hydrogel scaffolds suffer from one major disadvantage- their high water content [207]. As a result, the gel materials are viscoelastic in nature and are awkward to handle; furthermore, they suffer from weak mechanical properties, requiring extended *ex vivo* culture periods and combinations with synthetic polymers to reduce scaffold collapse *in vivo* [203-206]. Thus, their role in the design of tracheobronchial constructs for *in vivo* regeneration is quite limited and their use is generally restricted to *in vitro* airway reconstruction for disease modelling. Indeed, one of the reasons that the scaffolds in this thesis are investigated is due to their superior mechanical and handling properties when compared to hydrogels. That said, the employment of hydrogels as a cell delivery agent could be a promising regenerative approach for the airways in the future. In this role, the material might act to enhance delivery and retention of mesenchymal stem cells to the damaged tissue [208-210], providing an *in situ* reservoir of GF-secreting cells that can repair damaged respiratory tissue by paracrine action [211, 212].

1.3.5.2. Decellularised tissue

The use of DC tissue for tracheobronchial TE and regeneration has increased significantly since the clinical report of Macchiarini et al. [97, 98]. A proof-of-concept study of this method with a cell-seeded tissue-engineered patch of porcine jejunal segment demonstrated that the presence of both epithelial cell and mesenchymal cell types were necessary to prevent stenosis and infection in the graft [213, 214]. More recent work has delivered success with intraoperative-based seeding and eliminating the use of a bioreactor through use of pharmacological cell boosting agents [215, 216]. Other notable approaches towards tracheal regeneration using donor tissue include pre-vascularisation of donor tracheae within the recipient patient's forearm to allow autologous vessel growth prior to tracheal implantation [217, 218] and the use of autogenous and allogeneic aortas as a means to induce *in situ* tracheal regeneration [219-225]. Indeed, in the case of the latter strategy, a clinical trial was completed in September 2015 using this construct, though no study results have been released to date [226].

DC trachea is not without its drawbacks, however. Ultimately, the use of tissue-based scaffolds suffers from the same major limitation as transplantation- the requirement for donors. For widespread clinical application, mass-production of

this type of material becomes an implausible challenge at present. Furthermore, donor tissue segments may be limited in their dimensions, which may not fit all recipients depending on the location and size of the injury. For acellular trachea, the process of decellularisation can weaken the tissue mechanical properties in spite of retention of architecture, increasing the risk of graft collapse following implantation *in vivo* [227]. The ideal method of decellularisation also remains to be determined, with differences seen in structural integrity and ECM composition between the three most popular protocols [228]. Tissue heterogeneity due to long-term storage prior to surgical implantation is another caveat that must be taken into account [229]. Finally, there is the risk of disease transmission between donor and recipient. Thus, although they show great promise, acellular material is not the conclusive solution for tracheobronchial tissue regeneration just yet. Accordingly, the novel scaffold developed in this thesis is investigated for its potential as an alternative platform for tracheobronchial regeneration in Chapter 5. A summary of DC tissue for tracheobronchial TE is provided in Table 1.4.

Table 1.4: Decellularised tissue used in tracheobronchial tissue engineering.

Cell-Scaffold System	Notes	Studies
<u>Decellularised tissue: tracheobronchial</u>		
Human primary tracheal fibroblast and muscle cells on porcine jejunum	Autologous cells pre-cultured in a decellularised porcine jejunal segment integrated with host tissue with epithelialisation of the luminal surface	[213]
Porcine primary tracheal epithelial cells and bone marrow-derived mesenchymal stem cells on trachea	Bioreactor pre-culture with both epithelial cells and stem cells required to prevent in vivo collapse of a decellularised tracheal construct	[214]
Human primary tracheal epithelial cells and bone marrow-derived mesenchymal stem cells on trachea	Successful replacement of a damaged bronchus with a pre-cultured decellularised trachea; first human case with a tissue-engineered airway transplant	[97, 98]
Porcine primary mononuclear cells and tracheal epithelial cells on trachea	Intraoperative seeding of decellularised trachea was boosted with post-operative regenerative therapy led to cartilage formation and epithelisation in vivo	[215]
Human primary mononuclear cells and nasal epithelial cells on trachea	First report of the intraoperative seeding procedure of decellularised trachea used in humans	[216]
Unseeded tracheal allograft with controlled immunosuppression	Scaffold pre-vascularised in patient's forearm fascia and transferred to airway to become the first vascularised tracheal transplant	[217, 218]
Unseeded allogeneic aorta	Implantation in airways induced in situ tracheal regeneration; fresh and cryopreserved aorta examined	[219-225]

1.3.5.3. Porous polymeric scaffolds

Porous polymeric scaffolds hold the potential to address the supply and compatibility issues of donor tissue and to further improve the *in vitro* representation of the tissue architecture and composition of the tracheobronchial region, creating more fibrous structures that are reminiscent of the tracheobronchial tissue architecture (Section 1.1.2). These scaffolds are typically sponge-like materials that are composed of either naturally-occurring polymers, synthetic polymers or a composite of natural and synthetic material [230]. Synthetic and composite polymeric materials have been explored as biomaterials in TE because of their potential to produce constructs with more customisable biocompatible and biodegradable properties than some natural substrates, with

manufacturing techniques such as freeze-drying, electrospinning and 3D printing involved in scaffold production, as discussed below.

Synthetic materials have been tested alone as the source material for tracheobronchial scaffolds for both *in vitro* modelling and *in vivo* regeneration applications. A novel approach of individually manufacturing electrospun layers of PET for culture of epithelial, fibroblastic and dendritic cellular components of the scaffold before stacking them to create a combined immunocompetent “triculture” system with appropriate cell localisation has been designed [231]. Initial findings have indicated that 3D co-culture with the fibroblasts has enhanced epithelial cell functionality, while immune responses following allergen exposure showed favourable dendritic cell migration. *In vivo* regeneration of a segmental tracheal defect has shown potential with pre-vascularisation of a chondrocyte-seeded PGA-silicone construct in the sternohyoid muscle prior to implantation in the trachea [232], while a well-characterised electrospun PET-polyurethane scaffold pre-cultured with MSCs demonstrated cell attachment and expression of markers of epithelial differentiation in a rodent model [233]. In what has become a prominent case in the media, a proof-of-concept study was conducted in a 36 year old male with a polyhedral oligomeric silsesquioxane (POSS)-poly-(carbonate-urea)urethane (PCU) scaffold processed by an extrusion-phase inversion method [234]. Computed tomography scans and virtual imaging of the patient’s airway were employed to match the construct dimensions to the site of implant to ultimately achieve the first *in vivo* implantation of a synthetic graft in man. The validity of this study and indeed the true merits of this synthetic scaffold, however, have been cast in doubt following recent investigations into potential misconduct and negligence [235-239].

Synthetic materials are not without their limitations. Firstly, these polymers can lack suitable ligands that are required for initial cell adherence and repopulation of constructs, as well as subsequent growth and differentiation. This drawback can typically be overcome through coating the material with ECM proteins to enhance cell attachment, such as with the integrin ligand RGD peptide [240]. Of greater concern, perhaps, are issues with the biocompatibility and biodegradability of synthetic materials, where the presence of foreign material or its by-products can induce damaging pro-inflammatory responses *in vivo*. Implantation of a synthetic

scaffold can induce a foreign body reaction that encapsulates the biomaterial in a fibrotic capsule, rendering it useless for tissue regeneration [241], while for materials like poly(lactic-co-glycolic acid) (PLGA), acidic metabolic products can elicit tissue damage in its local environment in the body [242]. Finally, prolonged or absent rates of material degradation in tandem with replacement with host tissue can be a challenge for implanted synthetic scaffolds.

The combination of synthetic materials with natural polymers can benefit from the synergy of natural cell-binding ligands and robust synthetic mechanical properties. PCL is an example of a polymer that can support respiratory cells with the advantage of being suitable for a range of fabrication methods and different cell types in conjunction with natural polymers. Electrospun mixtures of decorin, gelatin and PCL, for example, created a highly fibrillar network that supported primary human airway epithelial cells expressing markers and morphological features of a differentiated airway epithelium [243]. Freeze-dried PCL-type II collagen scaffolds cultured with chondrocytes in a bioreactor were grafted into rabbits and maintained for a mean period of 52 days [244]. Certain combinations of natural materials can also reinforce the mechanical properties of one natural material alone, such as the incorporation of electrospun silk fibroin into a dense collagen tubular construct [245]. In this study, the inclusion of the silk mesh not only provided increased mechanical strength, but also introduced a fibrous component that can mimic tracheobronchial architecture; such a scaffold holds promise for future *ex vivo* bioreactor culture for tracheobronchial tissue regeneration.

When natural materials have been used alone to produce porous polymeric scaffolds for tracheobronchial TE, collagen has been the popular choice. Non-woven collagen scaffolds have been shown to sustain growth of human nasal epithelium in 3D *in vitro* culture [246], while other *in vitro* work by Pfenninger and colleagues has also validated the use of collagen for tracheal engineering through analysis of a collagen membrane [99]. Concerning the use of porous collagen scaffolds for *in vivo* regeneration of partial tracheal defects, collagen sponges coated with a type I collagen vitrigel can reproducibly induce *in vivo* formation of rat tracheal epithelium, as well as supporting tissue repair by *ex vivo* culture of epithelial cell and fibroblast co-culture prior to implantation [247-249]. Vitrification of the hydrogel involves drying a “traditional” collagen hydrogel in order to form a

more robust glass-like material that can be subsequently rehydrated and utilised for TE applications [250]. Although these studies highlight the potential of collagen as the principal component for a naturally-derived porous polymeric scaffold, it has not been investigated in this physical form as extensively as hydrogels. Therefore, the research in this thesis aims to improve our knowledge on the use of this form of collagen biomaterial for tracheobronchial TE applications.

Overall, porous polymeric scaffolds can offer a balance between improved handling and mechanical properties and the ability to tailor scaffolds to customisable sizes and shapes to match different airway dimensions. Ultimately, they can potentially surpass the limitations of hydrogels and DC tissue encountered with TE of the conducting zone of the respiratory tract. For tracheal tissue regeneration using biomaterials, the achievement of gradual replacement of the biomaterial with functional neotissue that can integrate and grow with the patient, particularly in cases of neonatal or paediatric tracheal injury [132, 251], is the ideal objective for porous polymeric scaffolds. Natural porous polymeric scaffolds have the capability to achieve this goal and are therefore an interesting method to pursue for the development of novel scaffolds for tracheobronchial tissue healing. A summary of porous polymeric scaffolds is provided in Table 1.5.

Table 1.5: Porous polymeric scaffolds used in tracheobronchial tissue engineering. GAG: Glycosaminoglycan; PCL: Poly- ϵ -caprolactone; PET: Polyethylene terephthalate; PGA: Polyglycolic acid; PLGA: Polylactic(co-glycolic) acid; POSS-PCU: Polyhedral oligomeric silsesquioxane- poly(carbonate-urea)urethane; PU: Polyurethane.

Cell-Scaffold System	Notes	Studies
<u>Porous polymeric scaffolds</u>		
Calu-3 bronchial epithelial cells, MRC-5 fibroblasts and human primary dendritic cells on an electrospun PET scaffold	Inclusion of fibroblasts enhanced epithelial barrier strength, mucus secretion and healing; dendritic cells responded to immunostimulation	[231]
Rabbit primary auricular chondrocytes on PGA-silicone scaffold	Vascularisation of pre-cultured scaffold in subcutaneous tissue before tracheal implantation reduced tissue granulation and improved cartilage strength	[232]
Rat primary bone marrow-derived mesenchymal stem cells on electrospun PET-PU scaffolds	1:1 polymer ratio optimal for mechanical properties; cell attachment dependent on PET	[233]
Human primary mononuclear cells on electrospun POSS-PCU scaffold	Pre-cultured scaffold boosted with post-operative regenerative therapy led to cartilage formation and epithelialisation in vivo	[234]
Human primary tracheobronchial epithelial cells on electrospun PCL-gelatin-decorin scaffold	Scaffolds supported adherence and growth of epithelial cells; scaffolds did not induce T-cell proliferation or cytokine release	[243]
Rabbit primary articular chondrocytes on freeze-dried PCL-type II collagen tubular scaffold	Dynamic culture improved cartilage cell number, alignment and collagen and GAG content on scaffold. Rabbits survived a mean 52 days following in vivo implantation	[244]
Mouse primary bone marrow-derived mesenchymal stem cells seeded on silk fibroin-collagen scaffold	Pulsatile and laminar flow induced differences in cell alignment and differentiation on scaffold	[245]
Human primary nasal epithelial cells on collagen sponge	Non-woven collagen scaffold supported the growth of respiratory epithelium; a hyaluronic acid derivative membrane was found to be non-adherent for cells	[246]
Rat primary tracheal epithelial cells; rat primary tracheal and gingival fibroblasts; rat primary adipose-derived stem cells on a vitrigel-coated collagen sponge with polypropylene mesh	Scaffolds integrated into tissue at a partial tracheal defect site with reepithelialisation; gingival fibroblasts, adipose cells and basic fibroblast growth factor hastened healing	[247-249]

1.4. The Tissue Engineering Research Group (TERG): collagen-based scaffolds for tissue engineering and regeneration

As can be inferred from the plethora of studies in Section 1.3 that utilise collagen as a biomaterial substrate, this protein is one of the most popular natural polymers within TE. As the most abundant structural protein *in vivo*, collagen is biocompatible and bioresorbable in nature, along with extensive cell adhesive properties [252]. Collagens form a large protein family containing more than 40 genes encoding various alpha chains which can form at least 29 members [253]. Within this family, type I collagen forms the bedrock of the ECM of many tissues, including the tracheobronchial region [17]. Collagen I is fibrillar in structure, composed of a distinctive heterotrimeric left-handed helix. The repeating Gly-X-Y amino acid sequence in its primary structure is critical to the formation of the polypeptide and resultant fibrils [27]. The inclusion of the small glycine residue in every third position in the primary sequence facilitates the interaction between adjacent collagen alpha subunits by reducing steric hindrance and permits the formation of the collagen triple-helix with the glycine residues pointed inwards towards the central axis. Furthermore, this conformation causes the other amino acid side chains to project outwards which maximises their availability for association with other collagen molecules and different ECM components. Overall, this fibrillar structure confers stability and tensile strength to the molecule. Indeed, as a natural polypeptide that is plentiful, more robust than other natural biomolecules and rich with cell-adhesive regions such as the integrin-binding GFOGER sequence [254], type I collagen exhibits excellent properties as the core biomaterial for porous polymeric scaffolds of natural origin.

Accordingly, the Tissue Engineering Research Group (TERG) in the Royal College of Surgeons in Ireland (RCSI) has utilised type I collagen as the principal component in porous scaffolds for a range of TE applications (Fig. 1.8). Collagen-glycosaminoglycan (CG) scaffolds manufactured by our group have consistently demonstrated the ability to facilitate cell growth and differentiation [255-259] and fully-porous constructs have enhanced the healing of bone and cartilage in both small and large animal models [260-263]. Indeed, one of these scaffolds based on a composite of collagen and hydroxyapatite, HydroxyColl®, has received CE marking and human clinical trial approval and is being commercialised by

SurgaColl® Technologies Ltd., a spin-out company from TERG. Such scaffolds have since been further specialised through the addition of therapeutic nucleic acids and proteins to enhance regeneration [264-269] and new organ systems have been investigated [270, 271]. However, beyond the alveolar TE study mentioned in Section 1.3.4.3 [182], CG scaffolds have not yet been widely investigated for respiratory applications.

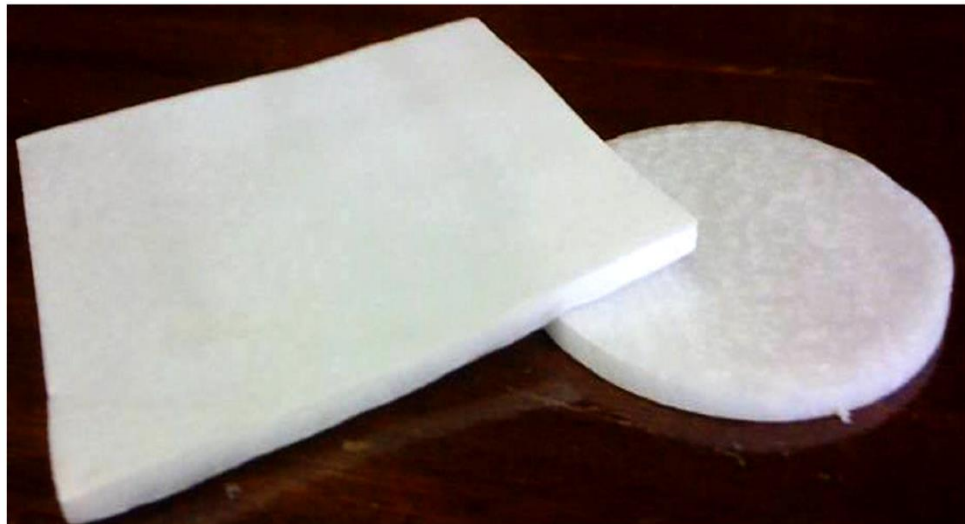


Figure 1.8: Macroscopic image of collagen scaffolds manufactured by the Tissue Engineering Research Group (TERG). Image adapted from [272].

To summarise, the literature review in this chapter has outlined the potential for respiratory TE to overcome the shortcomings of current respiratory *in vitro* models and airway disease treatments. The development of scaffolds of the tracheobronchial region of the respiratory tract could have applications for assessing drug toxicity, efficacy and disease modelling using a 3D *in vitro* system, as well as for tracheal tissue regeneration in cases of extensive damage to the conducting zone of the airways. Naturally-derived porous polymeric biomaterials can provide the ECM component lacking in current cell culture models and also a 3D framework for submucosal co-culture; in addition, they do not suffer from the supply limitations of DC tissue or the mechanical frailty of hydrogels. In spite of this, collagen-based porous scaffolds have not been extensively studied for such applications to date. Therefore, this thesis will investigate the use of CG scaffolds that shown great benefit in other TE applications and tailor them as a 3D analogue of tracheobronchial tissue.

1.5. Thesis objectives

The overall goal of the research presented in this PhD project is to develop a novel *in vitro* 3D model of the tracheobronchial region for potential applications in respiratory drug development and respiratory tissue regeneration. The central hypothesis of this thesis is that collagen-glycosaminoglycan (CG) scaffolds can be used as a platform to create an improved and physiologically-relevant tracheobronchial analogue that can be validated through *in vitro* characterisation and comparative studies with conventional cell insert models. In order to accomplish this goal, the following specific objectives were pursued:

1. Investigation of the potential of a porous CG scaffold as a 3D substrate for the growth and differentiation of a bronchial epithelial cell line (Chapter 2).
2. The development of a bilayered CG scaffold as a substrate for a bronchial epithelial cell line 3D *in vitro* co-culture model. This scaffold consisted of a thin film top-layer for epithelial monolayer culture and a porous sub-mucosal layer for 3D culture of fibroblasts (Chapter 3).
3. The development of a 3D primary tracheobronchial epithelial cell-derived co-culture system for applications in respiratory *in vitro* modelling (Chapter 4).
4. The manufacture of an all-*trans* retinoic acid-eluting bilayered scaffold as a platform technology for airway tissue regeneration (Chapter 5).

Chapter 2: The assessment of CG scaffolds as a 3D substrate for the growth and differentiation of a bronchial epithelial cell line

2.1.	Introduction	72
2.2.	Materials and Methods	74
2.2.1.	<i>Collagen-chondroitin-6-sulphate (CCS) scaffold fabrication</i>	74
2.2.1.1.	<i>Scaffold manufacture</i>	74
2.2.1.2.	<i>Chemical crosslinking</i>	74
2.2.2.	<i>Epithelial cell culture on CCS scaffolds</i>	75
2.2.2.1.	<i>Cell line and culture medium</i>	75
2.2.2.2.	<i>Air-liquid interface (ALI) culture on CCS scaffolds</i>	76
2.2.2.3.	<i>Liquid-liquid interface (LLI) culture on CCS scaffolds</i>	77
2.2.3.	<i>Epithelial cell growth on CCS scaffolds</i>	77
2.2.4.	<i>Epithelial cell differentiation on CCS scaffolds</i>	77
2.2.4.1.	<i>Mucin expression</i>	77
2.2.4.2.	<i>Tight junction formation</i>	78
2.2.4.3.	<i>Epithelial ciliation</i>	79
2.2.4.4.	<i>Expression of genetic markers of epithelial differentiation</i>	79
2.2.5.	<i>Cell morphology and migration on CCS scaffolds</i>	79
2.2.6.	<i>Data analysis</i>	80
2.3.	Results	81
2.3.1.	<i>Epithelial cell growth on CCS scaffolds</i>	81
2.3.2.	<i>Mucin expression on CCS scaffolds</i>	82
2.3.3.	<i>Tight junction formation on CCS scaffolds</i>	83
2.3.4.	<i>Ciliation on CCS scaffolds</i>	84
2.3.5.	<i>Expression of genetic markers of cellular differentiation on CCS scaffolds</i>	85
2.3.5.1.	<i>Expression of MUC5AC on CCS scaffolds</i>	85
2.3.5.2.	<i>Expression of ZO-1 on CCS scaffolds</i>	86
2.3.5.3.	<i>Expression of FOXJ1 on CCS scaffolds</i>	87
2.3.6.	<i>Cell morphology and migration on CCS scaffolds</i>	89
2.4.	Discussion	90
2.5.	Conclusion	95

2.1. Introduction

To date, the majority of three-dimensional (3D) tracheobronchial culture systems have capitalised on the favourable properties of natural polymers to fabricate scaffolds that support respiratory epithelial proliferation and differentiation, particularly in co-culture with other cell types (Section 1.3.2). Natural polymers provide numerous cell-binding structural motifs to facilitate cell attachment that support 3D cell and tissue culture growth in a biocompatible material with relatively non-toxic biodegradability when compared to porous synthetic scaffolds [27, 102]. However, for the most part, hydrogels are the favoured form of scaffold substrate in these studies, the selection of which presents limitations of their own. Hydrogels have a high water content [207] and their resultant viscoelastic nature reduces their ease of handling and in many cases, their mechanical strength. Alternatively, the use of porous, sponge-like scaffolds can offer more robust and practical constructs for more convenient and reproducible 3D culture, as well as further improving upon the *in vitro* representation of the fibrous tissue architecture and composition of the conducting region of the respiratory tract. Moreover, these porous structures are not restricted by the supply and compatibility issues of donor tissue-derived scaffolds. Thus, further development of naturally-derived porous polymeric scaffolds for applications in tracheobronchial modelling should be investigated with appropriate selection of the material source itself.

Collagen-glycosaminoglycan scaffolds (CG) are one set of naturally-derived porous polymeric biomaterials that could be developed for 3D tracheobronchial modelling (Section 1.4). These scaffolds, manufactured by our group, have consistently demonstrated the ability to facilitate cell growth and differentiation, particularly in the fields of bone and cartilage regeneration [255-258, 273]. They have tuneable mechanical properties through implementation of different crosslinking methods to reinforce intermolecular bonds [274] and their pore size can be tailored by altering the freezing temperature of a controlled lyophilisation process [275]. Previous reports have identified that CG scaffolds with mean pore diameters of 325µm and 120µm can influence attachment, proliferation and migration of a pre-osteoblastic cell line [276], but the influence of pore structure has not yet been examined for tracheobronchial cell culture modelling.

Accordingly, one focus of the research presented in this chapter was to study the

influence of these scaffold characteristics on airway cell behaviour in order to identify the optimal properties for 3D tracheobronchial tissue culture.

Two other relevant scaffold characteristics that were considered in this chapter were scaffold stiffness and the choice of glycosaminoglycan (GAG) in the CG scaffold co-polymer. The stiffness of a cell substrate can significantly influence cell activity, including cell spreading, migration, and in the case of stem cells, lineage commitment [277]. CG scaffolds can be made mechanically stiffer through chemical crosslinking with 1-ethyl-3-(3-dimethylaminopropyl)carbodiimide hydrochloride (EDAC). EDAC crosslinking involves coupling reactions between carboxylic and amine groups within the collagen molecule [278] and use of 6mM EDAC per gram collagen has been previously shown to modulate cell numbers and distribution within CG scaffolds [274]. Thus, the influence of EDAC crosslinking on Calu-3 cell distribution within CG scaffolds was also investigated in this chapter. Another consideration taken into account for this study was the choice of GAG that composed the CG polymer. Chondroitin-6-sulphate has predominantly been the choice of GAG incorporated into CG scaffolds and has demonstrated favourable outcomes in a number of applications, from pioneering work by Yannas and colleagues in the field of skin regeneration [279] to bone tissue engineering applications in our laboratory [255, 274, 280, 281]. Accordingly, CG scaffolds composed of a co-polymer of type I collagen and chondroitin-6-sulphate were chosen for use with a bronchial epithelial cell line in this chapter.

In order to evaluate the ability of CG scaffolds to support respiratory epithelium and to identify the ideal scaffold culture parameters for a tracheobronchial culture system, the Calu-3 cell line was selected as our cell type in Chapter 2. This bronchial epithelial cell line is derived from an adenocarcinoma of the lung [56] and was chosen as it is a well-established *in vitro* cell line that is used in respiratory drug development models to represent the respiratory tract [54, 282]. Calu-3 cells are known to differentiate by forming tight junctions in both air-liquid interface (ALI) conditions and in standard media-covered cell culture (liquid-liquid interface; LLI) conditions, in addition to the expression of mucins and cilia at an ALI. All of these features are key components of the differentiated respiratory epithelial barrier [53]. It is currently unknown if 3D culture on a CG substrate will have any effect on the functionality of this cell line.

The central hypothesis of this thesis is that porous polymeric scaffolds derived from natural sources have the potential to act as improved substrates for the development of 3D tracheobronchial *in vitro* models. Accordingly, the major objective of Chapter 2 was to assess the potential of CG scaffolds as a 3D substrate for the growth and differentiation of a bronchial epithelial cell line. Specifically, two aims were pursued:

1. To analyse Calu-3 growth and differentiation on CG scaffolds under ALI and LLI culture conditions.
2. To examine the effect of mean pore size on cell growth, differentiation and monolayer formation.

2.2. Materials and Methods

2.2.1. Collagen-chondroitin-6-sulphate (CCS) scaffold fabrication

2.2.1.1. Scaffold manufacture

CCS scaffolds were fabricated using a lyophilisation process as previously described [255]. A suspension of 0.5% microfibrillar bovine tendon collagen (Integra Life Sciences, Plainsboro, NJ) and 0.044% shark-derived chondroitin-6-sulphate (Sigma-Aldrich, Arklow, Ireland) in 0.05M acetic acid (Sigma) was blended at 15,000rpm and 4°C for 3.5 hours using an Ultra Turrax T18 Overhead blender (IKA Works Inc., Wilmington, NC). It was subsequently degassed under a vacuum to remove all air bubbles created from the homogenising process. This suspension slurry was pipetted into a stainless steel grade 304 SS pan and frozen (Virtis Genesis 25EL, Biopharma, Winchester, UK) at a constant cooling rate of 1°C/minute to a final freezing temperature of either -10°C or -40°C. The frozen sheet was then sublimated under a vacuum for 17 hours at 0°C. These temperatures yielded scaffolds with mean pore sizes of 325µm and 120µm, respectively [275]. After freeze-drying, the scaffolds were crosslinked and sterilised using a dehydrothermal (DHT) process at 105°C for 24 hours in a vacuum oven at 50mTorr (VacuCell 22, MMM, Germany) [283].

2.2.1.2. Chemical crosslinking

DHT-crosslinked CCS scaffolds were chemically crosslinked using EDAC (Sigma) for certain experiments in order to increase their mechanical strength. Scaffolds

were cut into discs and pre-hydrated for 30 minutes in Dulbecco's Phosphate Buffered Saline (DPBS; Sigma) before they were added to a mixture of 6mM EDAC per gram of CCS scaffold for 2 hours [274]. N-hydroxysuccinimide (NHS; Sigma) was included as a catalyst at a molar ratio of 2.5M EDAC:1M NHS [278]. The scaffolds were then washed three times with DPBS to remove any residual cytotoxic product and stored in DPBS at 4°C until use. All steps were performed under sterile conditions.

2.2.2. Epithelial cell culture on CCS scaffolds

2.2.2.1. Cell line and culture medium

The Calu-3 bronchial epithelium cell line (ATCC, Middlesex, UK) was used for scaffold culture experiments. The cells were cultured in a 1:1 mixture of Dulbecco's modified Eagle's medium (DMEM; Sigma) and Ham's F12 medium (Sigma) supplemented with 10% foetal bovine serum (Biosera, Ringmer, UK), 2mM L-glutamine (Sigma), 14mM sodium bicarbonate (Sigma) and 100U/ml penicillin/streptomycin (Sigma). Cells were used between passages 25-50 and grown at 37°C and 5% CO₂ under a humidified atmosphere. Unless otherwise stated, all cell culture incubation steps were also performed in these conditions. A summary of the cell culture conditions for ALI and LLI culture outlined below (Sections 2.2.2.2 and 2.2.2.3) is provided in Figure 2.1.

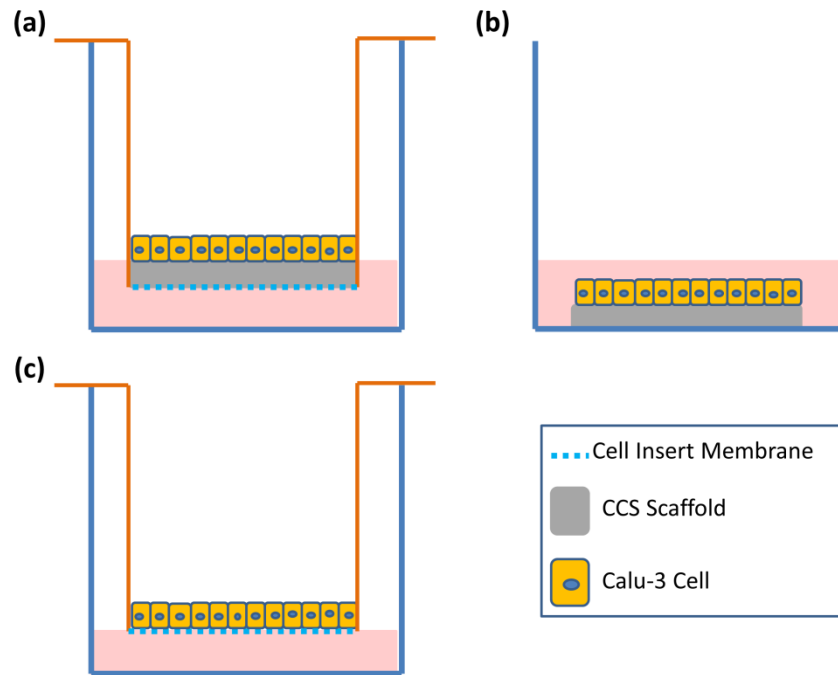


Figure 2.1: Calu-3 epithelial cell culture conditions examined for in vitro experiments. (a) Calu-3 cell culture on a collagen-chondroitin-6-sulphate (CCS) scaffold at an air-liquid interface (ALI). The scaffold is inserted into a Transwell® insert prior to cell seeding and the cells are fed with culture medium (pink) from the basolateral compartment following ALI induction. (b) Calu-3 cell culture on a CCS scaffold at a liquid-liquid interface (LLI). The cell-seeded scaffolds are submerged in culture medium. (c) Calu-3 cell culture on a cell insert polymeric membrane. The cells are seeded directly into a Transwell® insert and cultured at an ALI under the same conditions as CCS scaffold culture at an ALI.

2.2.2.2. Air-liquid interface (ALI) culture on CCS scaffolds

The ability of CCS scaffolds to support the growth and differentiation of the Calu-3 cell line was assessed under ALI conditions. 12mm-diameter cut scaffolds were pre-hydrated in DPBS, inserted into Transwell® inserts (Corning Costar, NY) and seeded with 2×10^5 cells on the apical side of the scaffold. Briefly, scaffolds were preconditioned with culture medium and 50µl of a cell suspension containing the desired number of cells was pipetted slowly onto the scaffold surface.

Subsequently, the scaffold was incubated for 15 minutes to allow for cell attachment. Following this, 600µl of media was added to the apical compartment of the insert and 1200µl to the basolateral compartment. 3 days later, media was removed from the top layer to introduce an ALI and the cells were fed from the basolateral compartment with 600µl media for the remainder of the culture period, with media replaced every 2-3 days (Fig. 2.1a). For certain experiments, cells

were also seeded directly onto the cell inserts at a density of 5×10^5 cells per cm^2 . Cell insert culture was performed under ALI conditions as outlined above (Fig. 2.1c).

2.2.2.3. Liquid-liquid interface (LLI) culture on CCS scaffolds

The ability of CCS scaffolds to support the growth and differentiation of the Calu-3 cell line was assessed under LLI conditions. 12mm-diameter cut scaffolds were seeded in 24-well plates as described above. Following incubation for cell attachment, samples were covered in 2ml of media (Fig. 2.1b). Media was replaced every 2-3 days.

2.2.3. Epithelial cell growth on CCS scaffolds

Cellular growth was quantified using a Quant-IT Picogreen® dsDNA assay kit (Molecular Probes, Invitrogen, UK). Cell-seeded scaffolds were washed three times with DPBS, flash frozen in liquid nitrogen and placed on ice. Each sample was lysed in 550 μl of 0.01% β -mercaptoethanol (Sigma) in RLT lysis buffer (Qiagen, Crawley, UK) for 20 minutes, homogenised using an Ultra Turrax T18 Overhead blender and centrifuged at 12,000rpm for 2.5 minutes through a homogeniser spin column (Omega Biotek, Norcross, GA) to remove any residual scaffold. 50 μl of the lysate was assayed for double-stranded DNA (dsDNA) content as a measure of cell viability and the remaining volume was stored at -80°C for analysis of gene expression (Section 2.2.4.4). For dsDNA quantification, the lysates were diluted 1/25 in tris-ethylenediaminetetraacetic acid (TE) solution and incubated with the Picogreen reagent. Fluorescence excitation was read at 485nm and emission at 538nm.

2.2.4. Epithelial cell differentiation on CCS scaffolds

2.2.4.1. Mucin expression

Cell-seeded scaffolds were stained with alcian blue and safranin-O to assess mucin expression, an essential feature of a functional respiratory epithelium [284], by Calu-3 cells on CCS scaffolds. Samples were washed three times with DPBS and fixed for 30 minutes in 10% neutral buffered formalin (Sigma). Subsequently, they were processed using an automated tissue processor (ASP300, Leica, Germany) overnight to dehydrate and paraffin wax-embed the samples. Scaffold sections of 10 μm were obtained using a microtome (Leica RM 2255, Leica) and

mounted on Polysine®-coated glass slides (Fisher Scientific, Dublin, Ireland) for staining. The slides were deparaffinised with xylene and rehydrated in descending grades of alcohol (100% to 50%). Following a wash step in tap water, samples were incubated with a solution of 1% alcian blue 8GX (Sigma) in 3% acetic acid for 20 minutes to stain acidic mucins, followed by incubation with a solution of 0.2% safranin-O in 1% acetic acid for 2 minutes to counterstain cells. A wash step with tap water was performed between each stain. The slides were subsequently dehydrated using ascending grades of ethanol and xylene before they were mounted using DPX (Sigma). Images were captured analysed using an Eclipse 90i microscope and DS Ri1 digital camera with NIS Elements software (Nikon, Japan).

2.2.4.2. Tight junction formation

Immunofluorescent analysis of cell-seeded CCS scaffolds was carried out to detect the presence of tight junction protein 1 (zonula occludens-1; ZO-1), a regulator of paracellular epithelial permeability and marker of a protective barrier formation [53, 282]. Samples were washed three times with DPBS and fixed for 30 minutes in 10% neutral buffered formalin. Subsequently, they were processed using an automated tissue processor overnight to dehydrate and paraffin wax-embed the samples. Scaffold sections of 10µm were obtained using a microtome and mounted on Polysine®-coated glass slides for staining. The slides were deparaffinised with xylene and rehydrated in descending grades of alcohol (100% to 50%). After 2 washes in DPBS, samples were isolated using a PAP marking pen (Sigma), transferred to a humidified chamber and an antigen retrieval step was performed by incubation with 20µg/ml proteinase K (Sigma) in TE buffer (pH 8) at 37°C for 10 minutes. The sections were subsequently permeabilised with 0.1% triton x-100 (Sigma) in DPBS for 10 minutes. Non-specific binding of primary antibody was inhibited by incubation with 1% bovine serum albumin (BSA; Sigma) in DPBS for 30 minutes at room temperature before the samples were incubated with 1/100 rabbit anti-ZO-1 polyclonal antibody (Invitrogen) in 1% BSA in DPBS in a humidified chamber at 4°C overnight. On the following day, the samples were incubated with 1/100 FITC-labelled anti-rabbit IgG (Medical Supply Company Ltd., Dublin, Ireland) in 1% BSA in DPBS for one hour at room temperature. Slides were counterstained with 4', 6-diamidino-2-phenylindole (DAPI, Sigma), mounted in ibidi mounting medium (ibidi, Planegg, Germany) and analysed using an Eclipse

90i microscope and DS Ri1 digital camera with NIS Elements software. Two DPBS washes were performed between each step.

2.2.4.3. Epithelial ciliation

The detection of Calu-3 ciliation on CCS scaffolds, a hallmark of the pseudostratified columnar tracheobronchial epithelium and critical component of mucociliary clearance [285], was examined by scanning electron microscopy (SEM). This was also performed to examine epithelial cell morphology and monolayer formation. Cell-seeded samples were washed three times with DPBS and fixed in 3% glutaraldehyde (Sigma) for 1 hour at room temperature. They were then dehydrated in ascending grades of ethanol and dried using supercritical CO₂ in a critical point dryer. The samples were subsequently mounted on aluminium stubs, sputter-coated and imaged using a Tescan Mira XMU scanning electron microscope. Images were captured at 5kV using secondary electron mode, taken at a working distance between 12-18mm.

2.2.4.4. Expression of genetic markers of epithelial differentiation

The ability of CCS scaffolds to support the differentiation of the Calu-3 cell line was further analysed by quantitative relative gene expression of MUC5AC, ZO-1, and FOXJ1, genetic markers for mucus production, epithelial tight junction formation and ciliation, respectively [282, 285, 286]. RNA was isolated from cell lysates (Section 2.2.3) using an RNeasy kit (Qiagen) and quantified using a NanoDrop 2000 spectrophotometer (Thermo Scientific, Dublin, Ireland), with absorption read at 260nm. 200ng of total RNA was reverse transcribed to cDNA using a QuantiTect reverse transcription kit (Qiagen). RT-polymerase chain reactions were run on 7500 real-time PCR System (Applied Biosystems, UK) using a QuantiTect SYBR Green PCR Kit (Qiagen) with QuantiTect primers (Qiagen). The expression of mRNA was calculated by the delta-delta Ct ($2^{-\Delta\Delta C_t}$) method relative to the housekeeping gene 18S [287] and gene expression in CCS culture was compared to that in cell insert culture at each respective time point.

2.2.5. Cell morphology and migration on CCS scaffolds

Cell-seeded scaffolds were stained with haematoxylin and eosin and fast green (H&E&FG) to observe cell distribution and migration into the scaffold away from the ALI. Samples were prepared for staining as described in Section 2.2.4.1.

Following rehydration of the scaffold sections, the slides were incubated with Harris haematoxylin (Sigma) for 5 minutes and washed in tap water for 5 minutes to “blue” the stain. Differentiation of the samples was then performed with acidified 70% ethanol before they were further stained with 0.1% eosin Y (Sigma) in 95% ethanol. Finally, the sections were incubated with 0.05% fast green FCF (Sigma) to counterstain the scaffold prior to dehydration and mounting with DPX. Images were captured using a microscope as described in Section 2.2.4.1.

2.2.6. Data analysis

Analysis of microscopy images, including the estimation of mucus layer thickness, was performed using the ImageJ processing software. Quantitative data obtained were analysed using Microsoft Excel and GraphPad Prism 4.0 Software (GraphPad Software, San Diego, CA). In cases of analysis between two groups, statistical difference was assessed by two-tailed Student t-test. In cases of analysis between multiple groups, statistical difference between groups was assessed by 2-way ANOVA with Bonferroni *post hoc* analysis. Each cell-based experiment was performed a minimum of three times (n=3; three biological replicates); the number of technical replicates performed within each experiment is specified under the relevant figures.

2.3. Results

2.3.1. Epithelial cell growth on CCS scaffolds

The ability of CCS scaffolds to support the growth of the Calu-3 bronchial epithelial cell line was assessed by dsDNA quantification. Scaffolds with mean pore diameters of 120 μ m and 325 μ m were analysed under both ALI and LLI conditions. The cells were cultured successfully on the scaffolds and showed significantly increased growth when cultured at an ALI (Fig. 2.2). Culture of Calu-3 cells on scaffolds in this environment showed enhanced cell numbers on scaffolds with both mean pore sizes relative to those submerged in media at a LLI from day 7 to day 28. Additionally, at days 21 and 28, significantly higher cell numbers were recorded with culture on 325 μ m pore scaffolds at an ALI compared to those on 120 μ m pore scaffolds ($p < 0.001$ and $p < 0.05$, respectively). In all cases, the CCS scaffolds acted as a viable substrate for culture of the Calu-3 airway cell line.

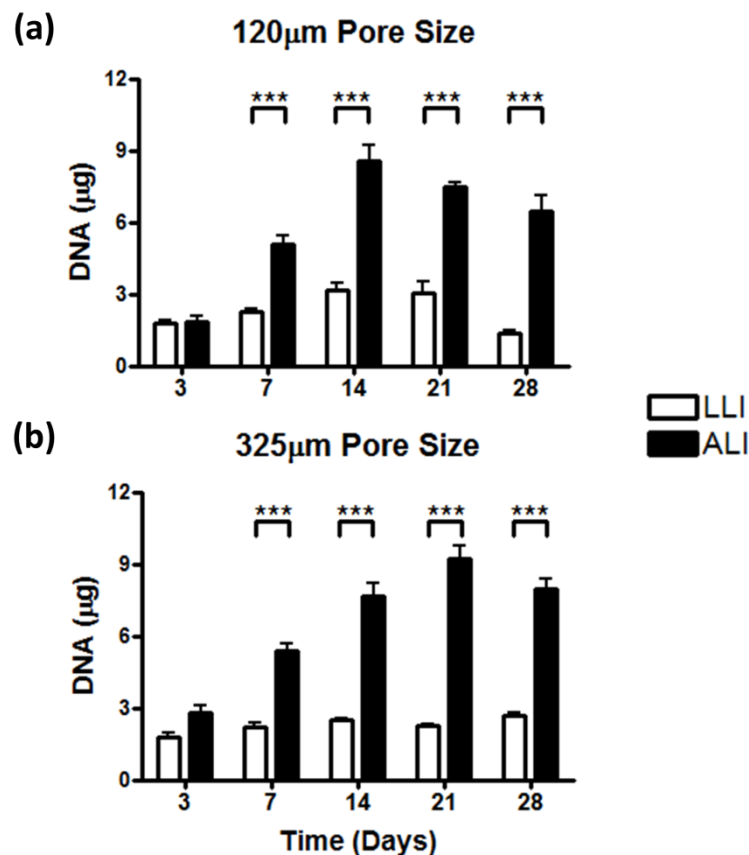


Figure 2.2: Calu-3 cell growth on collagen-chondroitin-6-sulphate scaffolds. Cells were cultured on scaffolds with a mean pore diameter of (a) 120 μ m or (b) 325 μ m at either an air-liquid interface (ALI) or liquid-liquid interface (LLI). Scaffolds were seeded with 2×10^5 cells. Results displayed as mean \pm SEM. $n=3$; *** $p < 0.001$.

2.3.2. Mucin expression on CCS scaffolds

CCS scaffolds with mean pore diameters of 120 μ m and 325 μ m were assessed for their ability to support the differentiation of Calu-3 cells cultured under ALI and LLI conditions by examination of mucin glycoprotein expression. Alcian blue and safranin-O staining revealed that cells cultured on the scaffolds expressed mucin at an ALI after 14 days in culture, regardless of mean pore size (Fig. 2.3). Large amounts of both secreted mucus and mucin bound to cellular surfaces were visualised, indicating differentiation of the epithelial cell line; notably, this level of secretion was absent in LLI conditions.

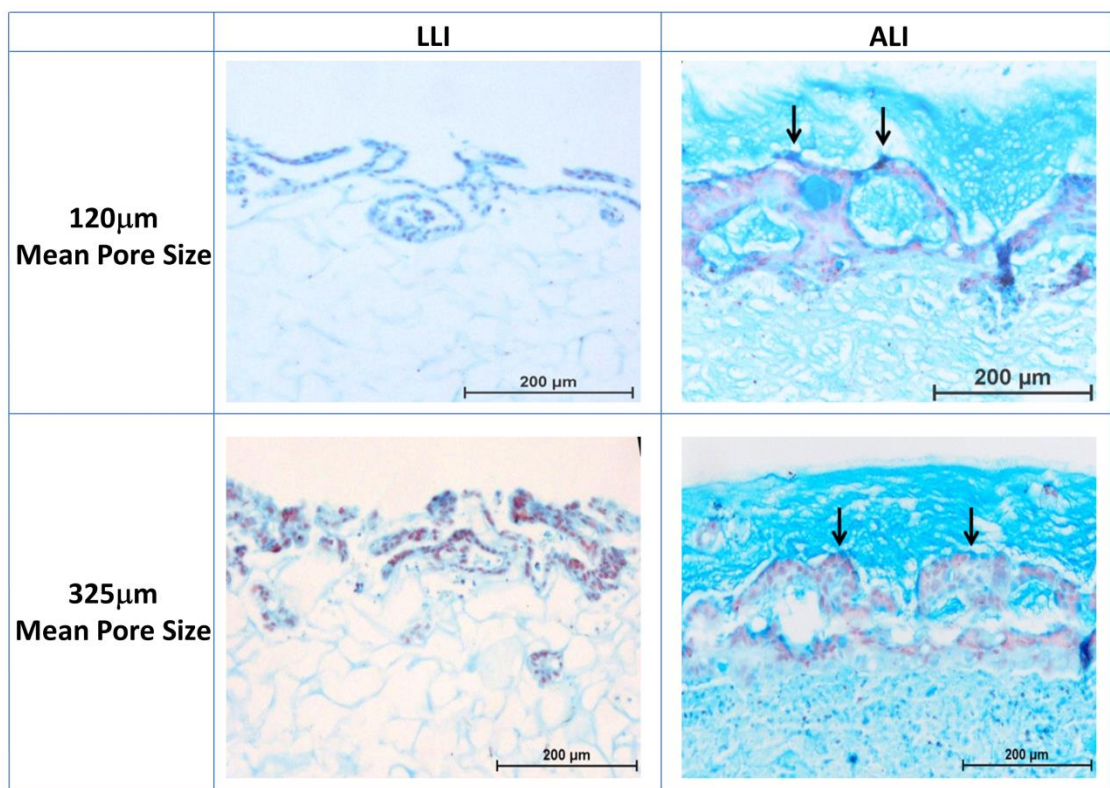


Figure 2.3: Mucin expression by Calu-3 cells cultured on collagen-chondroitin-6-sulphate scaffolds. Cells were cultured on scaffolds with a mean pore diameter of 120 μ m or 325 μ m at either an air-liquid interface (ALI) or liquid-liquid interface (LLI). Alcian blue staining at day 14 visualised cell-tethered acidic mucin (black arrows) and mucus as a blue-dark blue colour and scaffolds as blue with a fibrous appearance. Safranin-O visualised cells as a light pink colour. n=3 (performed in duplicate).

2.3.3. Tight junction formation on CCS scaffolds

The ability of CCS scaffolds with mean pore diameters of 120 μ m and 325 μ m to support the differentiation of Calu-3 cells cultured under ALI and LLI conditions was also assessed by detection of the tight junction protein ZO-1. Cells expressed ZO-1 protein in all 3D cultures by day 14, regardless of mean pore size or culture conditions (Fig. 2.4). Although the cellular distribution was different upon scaffolds when compared to the cell insert ALI control due to the porous nature of the former, the staining of ZO-1 intercellular bands between adjacent cells along the struts of the scaffold matched that observed in the cell insert ALI control. This indicated the formation of tight junctions between Calu-3 cells cultured on CCS scaffolds.

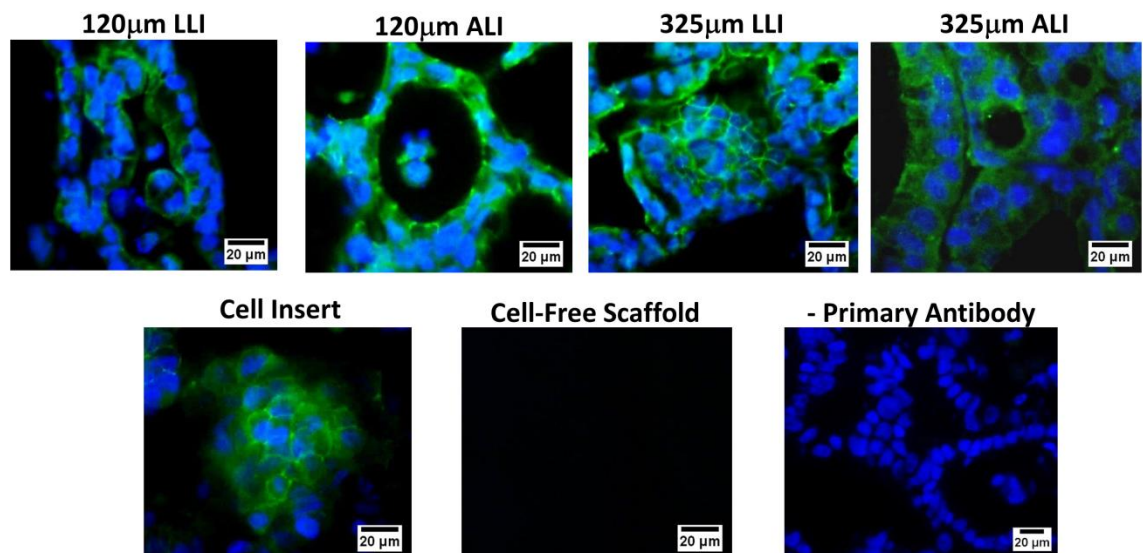


Figure 2.4: Zonula occludens-1 (ZO-1) expression by Calu-3 cells cultured on collagen-chondroitin-6-sulphate scaffolds. Cells were cultured on scaffolds with a mean pore diameter of 120 μ m or 325 μ m at either an air-liquid interface (ALI) or liquid-liquid interface (LLI). Expression of ZO-1 protein at day 14 is indicated by green fluorescence around blue cell nuclei. n=3 (performed in duplicate).

2.3.4. Ciliation on CCS scaffolds

The ability of CCS scaffolds with mean pore diameters of 120 μ m and 325 μ m to support the differentiation of Calu-3 cells cultured under ALI conditions was examined with SEM to assess epithelial cell morphology and cilia formation in 3D culture. Irrespective of the mean pore diameter, Calu-3 cells lined the struts of the CCS scaffold and grew into the porous structure (Fig. 2.5). The cells adopted either a flattened shape or formed rounded clusters of cells, with no evidence of ciliation or a confluent monolayer formation. This was in contrast to the cell insert culture at an ALI, where such a monolayer of epithelial cells expressing small microvilli extensions from their apical surface was observed. This indicated that the porous scaffolds did not support the differentiation of Calu-3 cells to form a ciliated cell monolayer at an ALI.

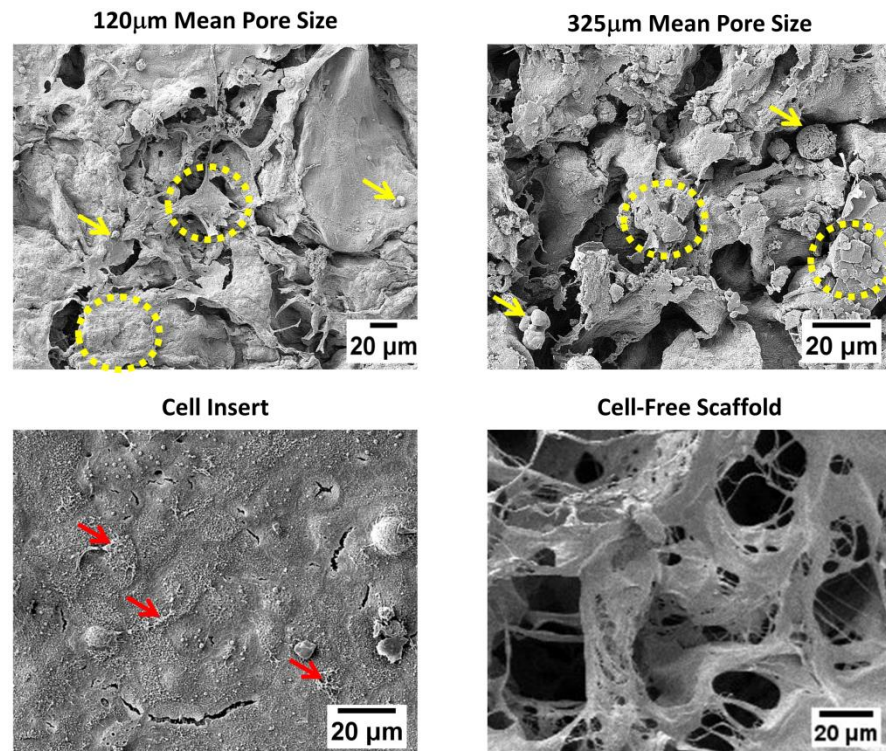


Figure 2.5: Scanning electron micrographs of Calu-3 cells cultured on collagen-chondroitin-6-sulphate scaffolds. Cells were cultured on scaffolds with a mean pore diameter of 120 μ m or 325 μ m at an air-liquid interface (ALI). Cells were also cultured on cell inserts at an ALI as a comparison. Upon scaffolds, cells adopted either a flattened morphology (circles) or were rounded in structure (yellow arrows). On cell inserts, cells formed a monolayer with small microvilli structures (red arrows). n=1; the image of the cell-free scaffold was provided by Dr Amos Matsiko, RCSI.

2.3.5. Expression of genetic markers of cellular differentiation on CCS scaffolds

2.3.5.1. Expression of MUC5AC on CCS scaffolds

Analysis of the expression of MUC5AC, a canonical gene indicating mucus expression [286], was performed on cells cultured on CCS scaffolds with mean pore diameters of 120 μ m and 325 μ m under ALI and LLI conditions. A significant upregulation of MUC5AC was detected when cells were cultured on CCS scaffolds at an ALI compared to both scaffold LLI culture and conventional cell insert ALI culture (Fig. 2.6). This effect was time-dependent, occurring at days 7, 14, and 21 before returning to similar expression levels in all groups by day 28. A similar pattern of expression was seen in scaffolds with mean pore diameters of both 120 μ m (Fig. 2.6a) and 325 μ m (Fig.2.6b). LLI culture had similar levels of expression to cell insert groups at all time points with the exception of day 7, where the 120 μ m scaffold had almost a 6-fold increase in relative expression ($p < 0.001$). Furthermore, significantly higher MUC5AC expression for scaffolds with a mean pore size of 325 μ m at an ALI than for 120 μ m scaffolds at an ALI was observed on day 14 ($p < 0.05$).

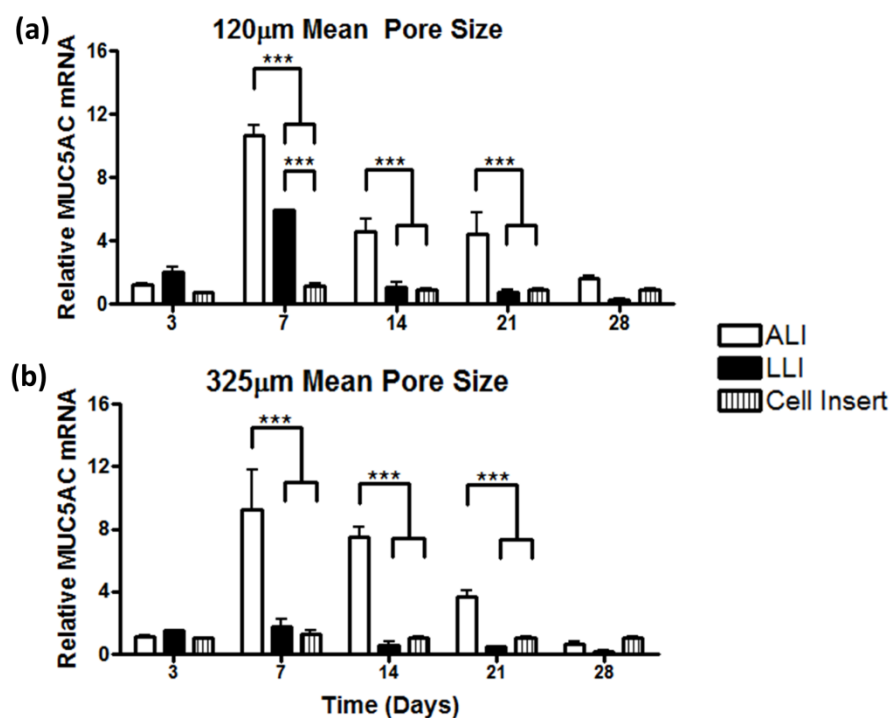


Figure 2.6: MUC5AC mRNA expression by Calu-3 cells on collagen-chondroitin-6-sulphate scaffolds. Cells were cultured on scaffolds with a mean pore diameter of (a) 120µm or (b) 325µm at either an air-liquid interface (ALI) or liquid-liquid interface (LLI). Cells were also cultured on cell inserts at an ALI as a comparison. Quantification of MUC5AC mRNA expression is displayed as mean \pm SEM with expression relative to the cell insert group at each respective time point. n=3; ***p<0.001.

2.3.5.2. Expression of ZO-1 on CCS scaffolds

Analysis of the expression of ZO-1, the gene encoding for ZO-1 tight junction protein [282], was performed on cells cultured on CCS scaffolds with mean pore diameters of 120µm and 325µm under ALI and LLI conditions. Expression remained consistently at similar levels for the culture period between all culture groups, with the exception of day 3 (Fig. 2.7). At this time point, ZO-1 expression appeared greater in LLI scaffold culture than in ALI conditions for both CCS scaffold culture and for cell insert culture, with a statistically significant increase for cells cultured on 120µm scaffolds (Fig. 2.7a; p<0.001) and a non-significant increase in 325µm scaffolds (Fig. 2.7b; p>0.05). This higher level of expression, however, had decreased by day 7. Overall, expression of ZO-1 on CCS scaffolds matched that of conventional cell insert ALI culture.

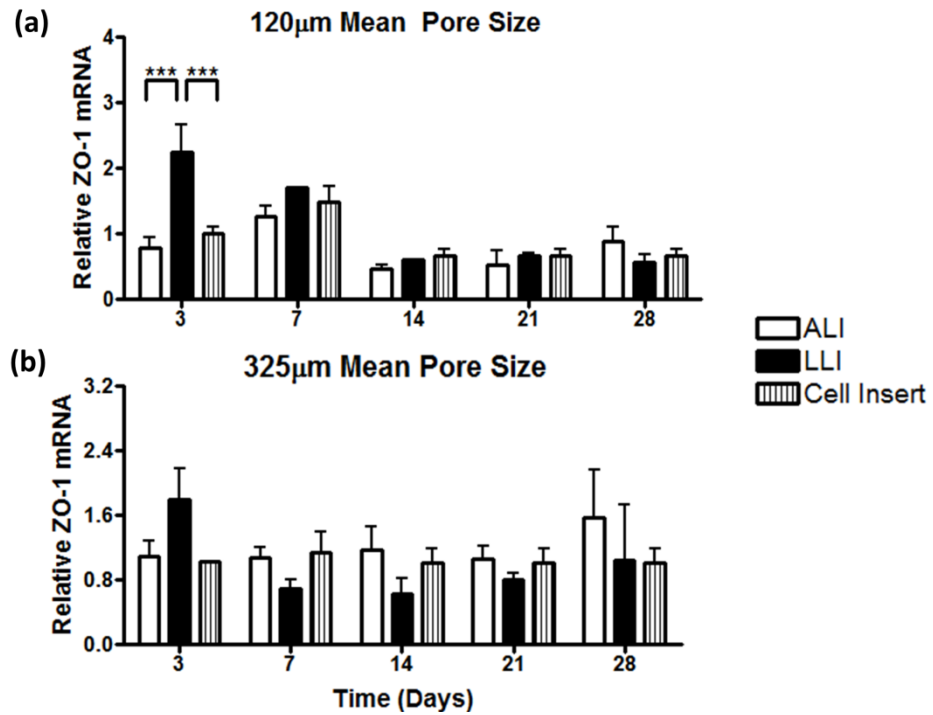


Figure 2.7: ZO-1 mRNA expression by Calu-3 cells on collagen-chondroitin-6-sulphate scaffolds. Cells were cultured on scaffolds with a mean pore diameter of (a) 120µm or (b) 325µm at either an air-liquid interface (ALI) or liquid-liquid interface (LLI). Cells were also cultured on cell inserts at an ALI as a comparison. Quantification of ZO-1 mRNA expression is displayed as mean \pm SEM with expression relative to the cell insert group at each respective time point. n=3; ***p<0.001.

2.3.5.3. Expression of FOXJ1 on CCS scaffolds

Analysis of the expression of FOXJ1, a key gene regulating motile cilia expression [285], was performed on cells cultured on CCS scaffolds with mean pore diameters of 120µm and 325µm under ALI and LLI conditions. Expression remained low and variable for the culture period for both scaffolds in both culture conditions (Fig. 2.8). Overall, genetic expression of FOXJ1 in 3D matched that of the cell insert positive control that was cultured at an ALI.

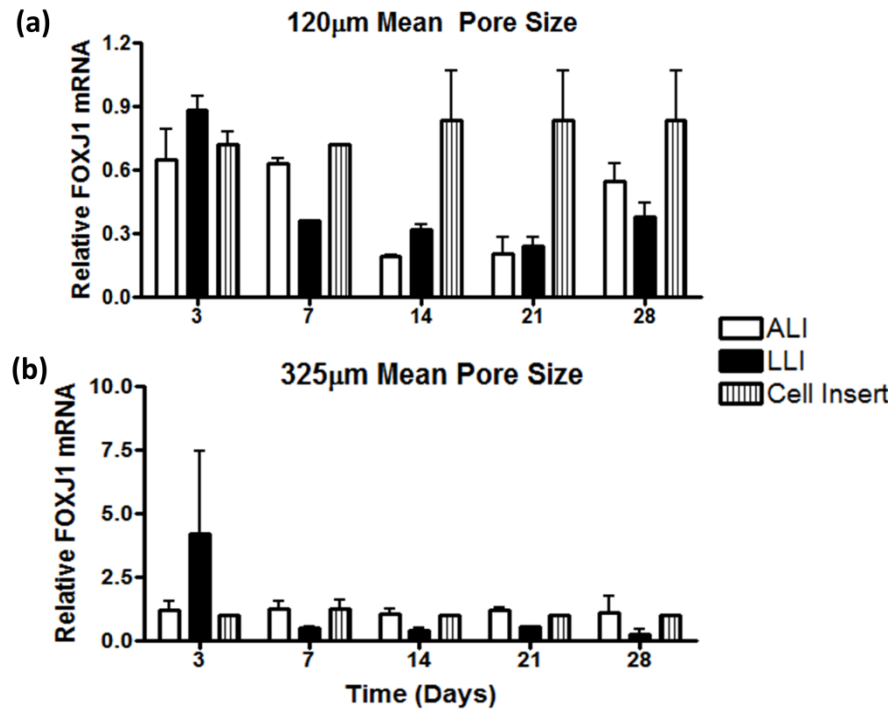


Figure 2.8: FOXJ1 mRNA expression by Calu-3 cells on collagen-chondroitin-6-sulphate scaffolds. Cells were cultured on scaffolds with a mean pore diameter of (a) 120µm or (b) 325µm at either an air-liquid interface (ALI) or liquid-liquid interface (LLI). Cells were also cultured on cell inserts at an ALI as a comparison. Quantification of FOXJ1 mRNA expression is displayed as mean \pm SEM with expression relative to the cell insert group at each respective time point. n=3.

2.3.6. Cell morphology and migration on CCS scaffolds

Cell-seeded scaffolds of both mean pore sizes were stained with H&E&FG to observe cell distribution and migration into the scaffold under ALI conditions. Cells migrated into scaffolds of both mean pore sizes over time, preventing the formation of a single epithelial layer on the apical surface exposed to the atmosphere at the ALI (Fig. 2.9). Histological stains showed that reducing the mean pore size of the scaffold from 325 μ m to 120 μ m decreased migration but did not halt the process. Further modification of the substrate properties by chemical crosslinking using EDAC also reduced the extent of inward migration, but not completely. The stiffer scaffolds (+EDAC) had less clusters of cells in its core for each scaffold pore size, relative to its less stiff counterpart (-EDAC), but isolated cells could still be observed within the scaffold. Ultimately, although the porous CCS scaffolds supported the growth and mucus secretion of the respiratory cell line, they could not fully support the formation of an epithelial monolayer at an ALI.

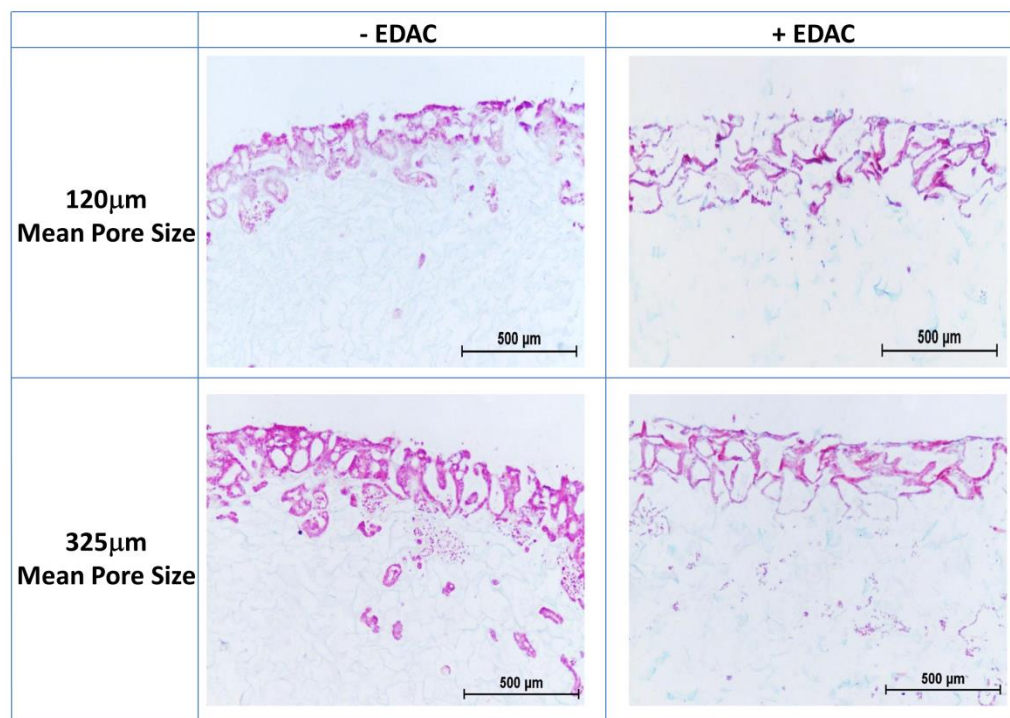


Figure 2.9: Migration of Calu-3 cells into collagen-chondroitin-6-sulphate scaffolds. Cells were cultured on scaffolds with a mean pore diameter of 120 μ m or 325 μ m at an air-liquid interface at day 14 with or without crosslinking using 1-ethyl-3-(3-dimethylaminopropyl)carbodiimide hydrochloride (EDAC). Haematoxylin & eosin and fast-green staining visualised scaffolds as a light-blue colour and cells appeared as pink-purple with darker nuclei. n=3 (performed in triplicate).

2.4. Discussion

The major objective of this chapter was to assess the potential of CG scaffolds as a 3D substrate for the growth and differentiation of a bronchial epithelial cell line with a view to develop a novel *in vitro* platform for respiratory drug delivery and tissue regenerative applications. Specifically, two major goals were pursued: firstly, to analyse Calu-3 growth and differentiation on CG scaffolds under ALI and LLI culture conditions and secondly, to examine the effect of mean pore size on cell growth, differentiation and monolayer formation. The results demonstrated that the Calu-3 bronchial epithelial cell line proliferated successfully on CCS scaffolds of mean pore diameters of both 120µm and 325µm and that ALI culture conditions significantly increased cell proliferation on scaffolds. Furthermore, ALI culture on CCS scaffolds induced mucin expression within the seeded cells that was superior to LLI scaffold culture and to ALI cell insert culture. Calu-3 cells also formed intercellular tight junctions along the struts of CCS scaffolds. However, while these results are encouraging, it was noticeable that cilia formation was not observed within the cell-seeded scaffolds and Calu-3 cells did not form a confluent epithelial monolayer across the apical side due to the porous nature of the scaffold. Scaffolds with smaller mean pore sizes reduced the extent of cellular migration away from the ALI but could not entirely halt inward flux of cells. Taken together, these data validate the CG scaffolds as a 3D substrate for the growth and differentiation of a bronchial epithelial cell line, and with further scaffold modification to improve cell monolayer retention at the ALI, suggest that these scaffolds can function as suitable substrates for a novel *in vitro* tracheobronchial model.

The Calu-3 bronchial epithelial cell line was cultured successfully on the CCS scaffolds and showed significantly increased growth when cultured at an ALI (Fig 2.2). ALI culture is recognised as a useful technique to promote airway cell differentiation in cell insert culture by mimicking the cell's natural environment [288], and this characteristic was observed in airway epithelial culture on the CCS scaffolds as well. The highly porous nature of the scaffold provided a large surface area for the cells to adhere to and grow with the result that the cells had sufficient space to achieve almost a 4-fold increase in cell number by day 21, as indicated by the significant increase in dsDNA content. The increase in cell number between

325 μ m and 120 μ m scaffolds at an ALI recorded at days 21 and 28 was likely due to the larger pores facilitating cell migration (Fig. 2.9), nutrient uptake and waste removal, as has been seen with a pre-osteoblastic cell line cultured on CCS scaffolds [276]. This analysis confirmed that CCS scaffolds of both mean pore diameters support the growth of the bronchial epithelial cell line in both ALI and LLI conditions.

In addition to augmenting cell number, ALI conditions had a pronounced effect on Calu-3 differentiation in 3D culture, as evident from increased mucin expression (Fig 2.3). Alcian blue staining of cell-seeded scaffolds confirmed the presence of mucin glycoproteins from day 14 with ALI culture that was not present with LLI. The height of the mucus border observed with ALI conditions was approximately 150-200 μ m; this was much greater than 15 μ m in Calu-3 cells grown on cell inserts and the physiological height of airway surface liquid which has been estimated to range from 5-58 μ m, depending on the method of measurement [289, 290]. Interestingly, the levels of mucus achieved in CG scaffolds might provide a closer approximation to that in diseased lungs, where certain hypersecretory conditions like chronic bronchitis, cystic fibrosis and asthma have a thicker mucus barrier [9, 11, 291]. On this matter, the ability to generate such thick levels of mucus using CCS scaffolds could provide a useful *in vitro* disease model. Regardless, CCS scaffolds clearly induced mucus secretion from Calu-3 cells when cultured at an ALI and this indicates that they modulate the differentiation of the bronchial epithelial cell line to exhibit an important feature of a differentiated tracheobronchial epithelium.

Further analysis of the mechanism by which the CCS scaffolds induced mucus secretion from Calu-3 cells revealed that transcription of MUC5AC, a principal component of airway mucus [284, 286], increased significantly when cells were cultured on scaffolds at an ALI at days 7, 14, and 21 (Fig. 2.6). Calu-3 cells are known to initiate expression of mucins and secretion of mucus from day 10-14 when exposed to an ALI from day 2 and this expression has been sustained beyond 21 days in cell insert culture [53, 292, 293]; thus, this temporal pattern of MUC5AC mRNA expression could represent the transcriptional upregulation that occurs during this time period. The importance of ALI culture with this 3D model was clearly demonstrated by comparison between scaffolds elevated to an ALI

and those kept submerged at an LLI, whereby significantly higher expression of MUC5AC was found with cells grown at an ALI on the CCS scaffolds.

It might not be altogether surprising that ALI culture conditions increases Calu-3 MUC5AC transcription and translation in 3D culture as it reflects the requirement of an ALI for mucin expression in conventional cell insert culture; however, given that an ALI environment was also used in the cell insert culture group to which expression was normalised, it is very interesting to note that cells cultured on CCS scaffolds of both mean pore diameters had elevated MUC5AC mRNA levels relative to the cell insert culture. This large rise in mRNA expression could be attributed to the synergistic presence of an extracellular matrix (ECM) component in the system; indeed, even when in LLI culture in 3D at day 7, 120µm scaffolds had significantly higher MUC5AC expression than cell insert ALI culture, adding credence to this theory (Fig. 2.6a). Furthermore, elevated MUC5AC transcription in the presence of ECM constituents has been noted elsewhere in the case of primary human respiratory epithelial cells cultured on collagen [73] and the GAG hyaluronate [167, 294], though no reports on chondroitin-6-sulphate were reported to date. Thus, while the exact mechanism has not been delineated in this study, we propose that the CCS scaffold composition induces enhanced MUC5AC transcription and mucin expression through a yet to be determined ECM-cell receptor-mediated signalling pathway.

Calu-3 cells cultured on CCS scaffolds expressed the tight junction protein ZO-1, regardless of the scaffold mean pore diameter or culture conditions (Fig. 2.4). The formation of such intercellular junctions between adjacent cells lining the struts of the porous scaffolds indicated that a protective epithelial layer can potentially form on these biomaterials where suitable substrate surface is available to do so. The presence of an ALI was not found to be crucial here, but this is not altogether surprising, given that Calu-3 cells form epithelial barriers in submerged liquid-covered conditions that can be of a stronger integrity than at an ALI [53, 295]. Of course, due to the porous nature of the CCS scaffolds, the cell distribution was different upon scaffolds when compared to the cell insert ALI control. Thus, unlike the cell insert culture groups, the formation of a single, confluent, interconnected epithelial barrier along the entire interface between scaffold and the apical environment was not achieved, which was a limitation of the CCS scaffold as a

fully-porous substrate. This observation was confirmed by scanning electron micrographs of cell-seeded scaffolds of both mean pore diameters (Fig. 2.5).

Analysis of ZO-1 gene expression indicated that the CCS scaffold substrate induced a significant upregulation of transcription for 120 μ m scaffolds at day 3 under LLI culture conditions (Fig. 2.7; $p < 0.001$). However, the impact of this expression was unclear, given that mRNA expression had returned to similar levels between all groups by day 7 and that no major difference between scaffold groups was observed from immunofluorescent detection of the protein. Of course, due to the transient nature of the early peak in ZO-1 gene expression, altered expression of ZO-1 protein could have been missed by day 14. Ultimately, quantitative reverse transcriptase-polymerase chain reaction (qRT-PCR) analysis and positive ZO-1 immunofluorescence indicate that the CCS scaffold can support the differentiation of a bronchial epithelial cell line to form intercellular junctions that regulate paracellular transport across epithelia and have the potential to facilitate the formation of a functional epithelial barrier with modification of the porous scaffold surface.

While two important indicators of bronchial epithelial cell differentiation, mucus secretion and tight junction formations, were present in the 3D CCS culture model, the third hallmark of a pseudostratified columnar tracheobronchial epithelium and critical component of mucociliary clearance- cilia [285] - was not detected. Calu-3 cells lining the surface of the scaffold had no visible microvilli extensions to suggest ciliogenesis within the cells (Fig. 2.5), in spite of the presence of the crucial ALI environment [288]. This was in contrast to cell insert culture, where numerous extensions were visible on top of the epithelial monolayer. Mucociliary clearance removes particulates and excess mucus from the respiratory tract via the coordinated metachronal beating of cilia and so their absence from CCS scaffold culture was unfavourable. Furthermore, qRT-PCR data detected low or variable levels of FOXJ1 expression in Calu-3 cells cultured on CCS scaffolds when compared to cell insert culture (Fig. 2.8; $p > 0.05$), indicating a trend of reduced expression of the putative master regulator of ciliogenesis in primary airway cells [285, 296].

Ciliation of primary tracheobronchial epithelial cells cultured *in vitro* on cell inserts typically occurs after 21-28 days [60, 194]; the appearance of microvilli on Calu-3 cells in ALI culture, however, has been reported from as early as day 11 [53], and so examination of ciliation was undertaken at day 14 in this study for comparative purposes with the literature. The microvilli structures formed on Calu-3 cells at this time point are widely referred to as immature cilia and their presence or absence can still indicate the potential for ciliation in a shorter timeframe. It is very possible that the fully-porous nature of the CCS scaffold contributed to the lack of microvilli formation observed in Calu-3 cells seeded onto the biomaterial due to the absence of a complete and confluent epithelial barrier along the scaffold surface. The development of such a barrier determines the resultant cell shape, apical-basolateral polarisation, and junctional protein connections between epithelial cells [297]; as reviewed by Paz and colleagues, the occurrence of tight junction formation and cell-basement membrane tethering are followed by cilia formation in respiratory cells. Moreover, the mechanisms of lateral planar polarization that proceed as a confluent monolayer forms assist in the alignment and organisation of cilia to facilitate coordinated beating. Thus, with this in mind, it can be postulated that this lack of a single epithelial barrier along the scaffold surface has contributed as a negative regulator of ciliation of Calu-3 cells cultured on CCS scaffolds. Tight junctions can form between adjacent cells along the struts of the scaffold (Fig. 2.4) and therefore, the modification of CCS scaffold architecture to incorporate a continuous flat topography on the apical side of the scaffold could encourage a resultant monolayer formation and potentially, the expression of microvilli structures.

Histological analysis of scaffold cross-sections further emphasised the need for this modification of scaffold structure to permit epithelial cell retention in a monolayer at the ALI. Although the CCS scaffolds supported the growth of Calu-3 cells on a 3D substrate and their expression of two biomarkers of differentiation in ALI culture conditions, H&E&FG staining showed that as time progressed, greater numbers of cells grew into the centre of the scaffold over time (Fig. 2.9). This reflects the highly porous design of these scaffolds for other tissue engineering applications where cell influx into the scaffold is desired [255-258, 273], though in the case of a tracheobronchial model, epithelial cell retention at the ALI with little

scaffold infiltration is favoured. Inward cellular migration was reduced by decreasing mean pore size and EDAC crosslinking to a certain extent, but this was not sufficient to prevent Calu-3 cells travelling inwards and proliferating away from the ALI.

Given that one of the specific objectives of the thesis is to create a model that resembles the tissue architecture of the tracheobronchial region of the respiratory tract, this finding reinforced the limitation highlighted by analyses of ZO-1 staining and SEM: the 3D porous CCS scaffold cannot act as a tissue-engineered submucosal analogue for the culture of fully-functional tracheobronchial epithelium due to its highly porous surface. Therefore, these findings suggest that in order to address this limitation and utilise the favourable properties of freeze-dried CG scaffolds proven above with a concomitant epithelial monolayer formation, adaptation of CCS scaffold structure is required. This requirement will form a central objective in Chapter 3, whereby a CG scaffold is redesigned into a bilayered form in order to introduce a dense film layer amenable for Calu-3 monolayer formation while still retaining the favourable porous character for 3D co-culture of lung fibroblasts. Nevertheless, this chapter has served to validate the use of the scaffold as a substrate for the development of a 3D tissue-engineered model of the tracheobronchial region of the respiratory tract and provides the opportunity to utilise the biomaterial's beneficial composition along with the advantages of its porous nature for co-culture, once modification of the apical surface has been performed.

2.5. Conclusion

In conclusion, this chapter demonstrates that CG scaffolds support the growth and differentiation of the Calu-3 bronchial epithelial cell line and are a suitable substrate for a novel *in vitro* model, particularly when used with airway culture-enhancing ALI conditions. With modification of CG scaffold structure to facilitate a continuous cell monolayer formation to tailor it towards a better representation of the tracheobronchial tissue architecture, these models can be potentially utilised for drug delivery and respiratory tissue regenerative applications.

Chapter 3: The development of a bilayered CG scaffold as a substrate for a bronchial epithelial cell line 3D *in vitro* culture model

This chapter has been published as O’Leary et al., The development of a tissue-engineered tracheobronchial epithelial model using a bilayered collagen-hyaluronate scaffold, 2016, *Biomaterials*, 85: 111-127.

3.1.	Introduction	98
3.2.	Materials and Methods	100
3.2.1.	<i>Bilayered collagen-hyaluronate (CHyA-B) scaffold manufacture</i>	100
3.2.1.1.	<i>Collagen-hyaluronate (CHyA) film layer fabrication</i>	100
3.2.1.2.	<i>Bilayered scaffold manufacture</i>	100
3.2.1.3.	<i>Chemical crosslinking</i>	101
3.2.2.	<i>CHyA-B scaffold characterisation</i>	101
3.2.2.1.	<i>Scaffold ultrastructure</i>	101
3.2.2.2.	<i>Interfacial adhesion strength</i>	101
3.2.2.3.	<i>Mechanical testing</i>	102
3.2.2.4.	<i>Pore size analysis</i>	102
3.2.3.	<i>Calu-3 epithelial cell culture on CHyA-B scaffolds</i>	103
3.2.3.1.	<i>Cell source and culture medium</i>	103
3.2.3.2.	<i>Epithelial cell monoculture</i>	104
3.2.3.3.	<i>Epithelial cell co-culture with fibroblasts</i>	105
3.2.4.	<i>Cell morphology and migration</i>	106
3.2.4.1.	<i>Histology</i>	106
3.2.4.2.	<i>Scanning electron microscopy (SEM)</i>	106
3.2.5.	<i>Calu-3 epithelial cell differentiation on CHyA-B scaffolds</i>	107
3.2.5.1.	<i>Immunofluorescence</i>	107
3.2.5.2.	<i>Transmission electron microscopy (TEM)</i>	107
3.2.5.3.	<i>Expression of genetic markers of epithelial cell differentiation</i>	108
3.2.6.	<i>Evaluation of Calu-3 epithelial cell barrier integrity</i>	108
3.2.6.1.	<i>Transepithelial electrical resistance (TEER) measurement</i>	108
3.2.6.2.	<i>Fluorescein isothiocyanate (FITC)-labelled dextran permeability assay</i>	109
3.2.7.	<i>Data analysis</i>	109
3.3.	Results	111
3.3.1.	<i>CHyA-B scaffold characterisation</i>	111

3.3.1.1. Scaffold ultrastructure	111
3.3.1.2. Interfacial adhesion strength	112
3.3.1.3. Mechanical testing	112
3.3.1.4. Pore size analysis	114
3.3.2. Calu-3 epithelial cell monoculture on CHyA-B scaffolds	116
3.3.2.1. Cell morphology and migration	116
3.3.2.2. Mucin expression	118
3.3.2.3. Tight junction formation	119
3.3.2.4. Epithelial ciliation	121
3.3.3. Expression of genetic markers of epithelial cell differentiation	122
3.3.3.1. The effect of CHyA-B scaffolds on epithelial cell gene expression	122
3.3.3.2. The effect of time on epithelial cell gene expression	124
3.3.4. Calu-3 epithelial cell co-culture with fibroblasts on CHyA-B scaffolds	126
3.3.4.1. Cell morphology and migration	126
3.3.4.2. Mucin expression	128
3.3.4.3. Tight junction formation	129
3.3.4.4. Epithelial ciliation	130
3.3.5. Evaluation of Calu-3 epithelial cell barrier integrity	131
3.3.5.1. TEER measurement	131
3.3.5.2. FITC-labelled dextran permeability assay	131
3.4. Discussion	133
3.5. Conclusion	141

3.1. Introduction

Collagen-glycosaminoglycan (CG) scaffolds have been verified as a suitable substrate for the growth and differentiation of a bronchial epithelial cell line in three-dimensional (3D) culture, but the results in Chapter 2 demonstrated that scaffold structure should be optimised for tracheobronchial modelling. CG scaffolds are highly porous due to their freeze-dry manufacture process and this high porosity, coupled with excellent biocompatibility and cell adhesion properties, can facilitate 3D culture of a variety of connective tissue and stromal cell types within the structure for bone tissue engineering and *in vitro* vascularisation applications [258, 280]. For respiratory epithelium, however, it is desired that cells do not migrate into the core of the scaffold and maintain their presence instead entirely on the scaffold surface at the air-liquid interface (ALI) as a continuous cell layer. Retention of epithelial cells at this site would then allow the possibility of using the highly porous core of the CG scaffold for co-culture with mesenchymal cells to enhance the physiological representation of tracheobronchial tissue within the *in vitro* model.

In order to tailor the CG scaffold to resemble the anatomical architecture of tracheobronchial tissue more closely, two central modifications were proposed from that described in Chapter 2. Firstly, using the same CG suspension for both components, a bilayered scaffold structure would be manufactured that consisted of a thin film top-layer and porous sub-layer. In this manner, the scaffold structure would facilitate the culture of both bronchial epithelium on a two-dimensional (2D) surface to form a confluent monolayer and also the 3D co-culture of fibroblasts in a porous layer beneath the epithelium. Secondly, the GAG in the scaffold copolymer was changed from chondroitin-6-sulphate to hyaluronate (HyA). Collagen membranes and hyaluronan-derivative films have shown promise for respiratory epithelial culture [99, 294] but they have not yet been investigated as a co-polymer film to combine the benefits of each macromolecule alone. Regarding the sub-layer, porous collagen-hyaluronate scaffolds, previously designed by our group for cartilage regeneration, have been shown to facilitate cell growth and chondrogenic differentiation with mesenchymal stem cells (MSCs; [298-300]). Accordingly, these scaffolds were incorporated as the sub-layer of our epithelial *in vitro* substrate for co-culture of fibroblasts and representation of a fibrocartilaginous submucosa.

Finally, type I collagen and hyaluronate are the predominant extracellular constituents of the tracheobronchial respiratory tract [17], and therefore the bilayered collagen-hyaluronate scaffold can further recapitulate the ECM of the tissue that is being modelled.

The inclusion of the film layer has the potential to alter the physical and mechanical properties of the porous CHyA scaffold. As mentioned in Chapter 2, the mean pore size of the scaffold and scaffold stiffness play a significant role in modulating cell adhesion, viability and phenotype when cultured on the biomaterial [276, 277]. Thus, one focus of the research presented in this chapter was to quantify these properties in the bilayered scaffold in order to evaluate the effect of the film layer on the lyophilisation and crosslinking procedures standardised by our group for CG scaffolds. Additionally, these characteristics were also analysed to relate them to resultant epithelial cell behaviour and to identify the optimal properties for 3D tracheobronchial tissue culture.

In order to build on the initial *in vitro* studies from Chapter 2, the Calu-3 bronchial cell line was once again selected as the respiratory epithelial cell type of choice in this chapter. ALI culture conditions were used in all experiments, in line with the findings from Chapter 2. This chapter also introduced another cell line for co-culture experiments- the Wi38 fibroblast [301]. This fibroblast type has been previously investigated in tracheobronchial cell insert co-culture systems [60] and the cell is derived from lung tissue, an important factor that affects epithelial cell phenotype [100, 202]. While fibroblasts have previously been shown to adhere to and remain viable in CG scaffolds [302], the Wi38 fibroblast has not been used in CG scaffold culture to date.

Thus, the major objective of Chapter 3 was to engineer a bilayered collagen-hyaluronate (CHyA-B) scaffold as a tissue-engineered template for the development of a physiologically-representative 3D *in vitro* tracheobronchial epithelial co-culture model. Specifically, three aims were pursued:

1. To develop a reproducible manufacture process for the CHyA-B scaffold with analysis of the effect of lyophilisation freezing temperature and chemical crosslinking on scaffold ultrastructure, porosity and mechanical properties.

2. To assess the feasibility of the resultant lead scaffold to act as a 3D substrate for the growth and differentiation of the Calu-3 bronchial epithelial cell line.
3. To develop a co-culture system of Calu-3 epithelial cells and Wi38 lung fibroblasts and validate this system by analysis of markers of differentiation and epithelial barrier strength.

3.2. Materials and Methods

3.2.1. Bilayered collagen-hyaluronate (CHyA-B) scaffold manufacture

3.2.1.1. Collagen-hyaluronate (CHyA) film layer fabrication

CHyA films were fabricated using a modification of a method to dehydrate a suspension of collagen and hyaluronate under airflow [303]. A suspension of 0.5% microfibrillar bovine tendon collagen (Integra Life Sciences, Plainsboro, NJ) and 0.044% hyaluronate sodium salt derived from *Streptococcus equi* (Sigma-Aldrich, Arklow, Ireland) in 0.5M acetic acid was blended at 15,000rpm and 4°C for 3.5 hours using an Ultra Turrax T18 Overhead blender (IKA Works Inc., Wilmington, NC) and subsequently degassed under a vacuum to remove all air bubbles created from the homogenising process, as described in Section 2.2.1.1. 50ml of the slurry suspension was pipetted onto a 12.5x12.5cm² polytetrafluoroethylene (PTFE) plate and left overnight under an air current in a fume hood to increase dehydration of the solvent. This process produced a thin transparent CHyA copolymer film.

3.2.1.2. Bilayered scaffold manufacture

A process was developed where CHyA-B scaffolds were fabricated by freeze-drying CHyA films in combination with an overlying CHyA slurry. CHyA films were rehydrated in 0.5M acetic acid for 2 hours and cut to fit onto the base of a 6x6cm² stainless steel grade 304 SS pan. 4ml or 16ml of CHyA slurry was then pipetted over the hydrated film layer to give an approximate scaffold thickness of 1mm or 4mm, respectively, and the combination was subsequently freeze-dried using two lyophilisation methods designed by our group [255, 275]. In the first method, the slurry-film combination was frozen at a constant cooling rate of 1°C/minute to a final temperature of -10°C prior to sublimation, as outlined in Section 2.2.1.1. The

second method utilised a customised anneal cycle where the slurry-film combination was initially frozen to a temperature of -20°C before being heated to -10°C and held at this temperature for 24 hours prior to sublimation [275]. For characterisation studies, a comparative single-layer fully porous CHyA scaffold was also fabricated using the anneal cycle (i.e. with no film layer present). After freeze-drying, the scaffolds were crosslinked and sterilised using a dehydrothermal (DHT) process at 105°C for 24 hours in a vacuum oven at 50mTorr (VacuCell 22, MMM, Germany) as described in Section 2.2.1.1 [283].

3.2.1.3. Chemical crosslinking

DHT-crosslinked CHyA-B scaffolds were chemically crosslinked using 1-ethyl-3-(3-dimethylaminopropyl)carbodiimide hydrochloride (EDAC; Sigma) as described in Section 2.2.1.2. Scaffolds were cut into discs and pre-hydrated for 30 minutes in Dulbecco's Phosphate Buffered Saline (DPBS; Sigma) before they were added to a mixture of 6mM EDAC per gram of CHyA-B scaffold for 2 hours [274]. N-hydroxysuccinimide (NHS; Sigma) was included as a catalyst at a molar ratio of 2.5M EDAC:1M NHS [278]. The scaffolds were then washed three times with DPBS to remove any residual cytotoxic product and stored in DPBS at 4°C until use. All steps were performed under sterile conditions.

3.2.2. CHyA-B scaffold characterisation

3.2.2.1. Scaffold ultrastructure

CHyA-B scaffolds were examined using scanning electron microscopy (SEM) in order to evaluate their bilayered architecture and to estimate film thickness. Samples were mounted to an aluminium stub using a carbon paste and sputter-coated with gold. Imaging of the scaffolds was performed using a Tescan Mira XMU scanning electron microscope (Tescan, Czech Republic). Images were captured at 5kV using secondary electron mode, taken at a working distance between 12-18mm. Two batches of CHyA-B scaffolds were used for analysis.

3.2.2.2. Interfacial adhesion strength

Interfacial adhesion strength between the film and porous layers of the CHyA-B scaffolds was determined using a custom-designed interfacial strength test rig fitted to a mechanical testing machine (Z050, Zwick-Roell, Ulm, Germany) as previously described [300]. Using an Araldite® high-viscosity adhesive (Radionics,

Dublin, Ireland), 9.5mm diameter samples were glued to aluminium test stubs and inserted into the test rig. They were then hydrated in DPBS *in situ* in the rig prior to testing to failure using a 5N load cell under a tensile load applied at a strain rate of 10% per minute. Failure was expected to occur either at the ultimate tensile strength of one of the component layers of the scaffold or as a result of delamination at the layer interface. Two batches of CHyA-B scaffolds were used for analysis.

3.2.2.3. Mechanical testing

Uni-axial, unconfined compressive testing was carried out to determine the bulk compressive elastic modulus of CHyA-B and CHyA scaffolds, a property that affects cellular growth and differentiation [274, 299]. Scaffolds were cut into 9.5mm discs with a height of 4mm and chemically crosslinked with EDAC where appropriate. DHT-crosslinked scaffolds were pre-hydrated in DPBS for 30 minutes prior to testing. A Z050 mechanical testing machine was fitted with a 5N load cell and used in the procedure. The pre-hydrated samples were immersed in PBS throughout the tests. The tests were conducted at a strain rate of 10% per minute and each sample was tested three times. Stress was calculated from scaffold surface area and applied force, whilst strain was calculated from displacement of the scaffolds in relation to the original thickness. The compressive modulus was defined based on the slope of a linear fit to the stress-strain curve over 2-5% strain. Two batches of each scaffold were used for analysis.

3.2.2.4. Pore size analysis

Scaffold pore size analysis was performed to assess the effect of the lyophilisation cycle on the mean pore diameter and porosity of CHyA-B scaffolds, two important properties for cell adhesion and growth [276]. To calculate the mean pore size, scaffold samples were cut from random locations on fabricated scaffold sheets from two manufacturing batches and analysed using a technique described previously [256, 275]. The samples were embedded in JB-4® glycolmethacrylate (Polysciences Europe, Eppelheim, Germany). 10µm sections were stained for 4 minutes in a 0.5% toluidine blue solution (Sigma). Digital images were captured at 10x magnification using an optical microscope and digital camera (Section 2.2.4.1). Mean pore size analysis of captured images was carried out on MATLAB (MathWorks Inc, MA, USA) using a pore topology analyser developed by our

group in conjunction with the Sigmedia Research Group in the Electrical Engineering Department at Trinity College Dublin, Ireland [275]. The programme transformed the images into binary form and calculated the average pore radii based on best-fit elliptical lengths. For each sample, a minimum of eighteen sections spanning the entire cross-section of the scaffold were analysed, resulting in the calculation of diameter of more than one thousand pores from each scaffold group. Two batches of each scaffold were used for analysis.

Scaffold porosity was quantified through analysis of the relative density of the scaffold (f_{scaffold}) to its theoretical dry solid composite (f_{solid} ; Equation 1). The density of punched scaffold discs was calculated by measuring their mass, diameter and height using a mass balance (Mettler Toledo MX5; Mason Technology, Dublin) and digital Vernier callipers (Krunstoffwerke; Radionics). The solid composite scaffold density was calculated using the known density of collagen ($f = 1.3\text{g/cm}^3$). The density of hyaluronate was assumed to be negligible. A minimum of ten samples across four manufacturing batches was analysed for each group.

$$\text{Porosity (\%)} = \left(1 - \frac{\rho_{\text{scaffold}}}{\rho_{\text{solid}}}\right) \times 100 \quad (1)$$

3.2.3. Calu-3 epithelial cell culture on CHyA-B scaffolds

3.2.3.1. Cell source and culture medium

The Calu-3 bronchial epithelium cell line (ATCC, Middlesex, UK) was used for monoculture and co-culture experiments. The cells were cultured in a 1:1 mixture of Dulbecco's modified Eagle's medium (DMEM; Sigma) and Ham's F12 medium (Sigma) supplemented with 10% foetal bovine serum (Biosera, Ringmer, UK), 2mM L-glutamine (Sigma), 14mM sodium bicarbonate (Sigma) and 100U/ml penicillin/streptomycin (Sigma). This was referred to as Calu-3 medium. Cells were used between passages 20-50. The Wi38 human embryonic lung fibroblast cell line (ATCC) was used for co-culture experiments. These cells were cultured in Eagle's minimal essential medium (Sigma) supplemented with 10% foetal bovine serum, 2mM L-glutamine, 26mM sodium bicarbonate, 100U/ml penicillin/streptomycin and 1mM sodium pyruvate (Sigma). This was referred to as Wi38 medium. Cells were used between passages 21-26 and cultured at 37°C and

5% CO₂ in a humidified atmosphere. Unless otherwise stated, all cell culture incubation steps were also performed in these conditions. A summary of the monoculture and co-culture groups outlined below (Sections 3.2.3.2 and 3.2.3.3) is provided in Figure 3.1.

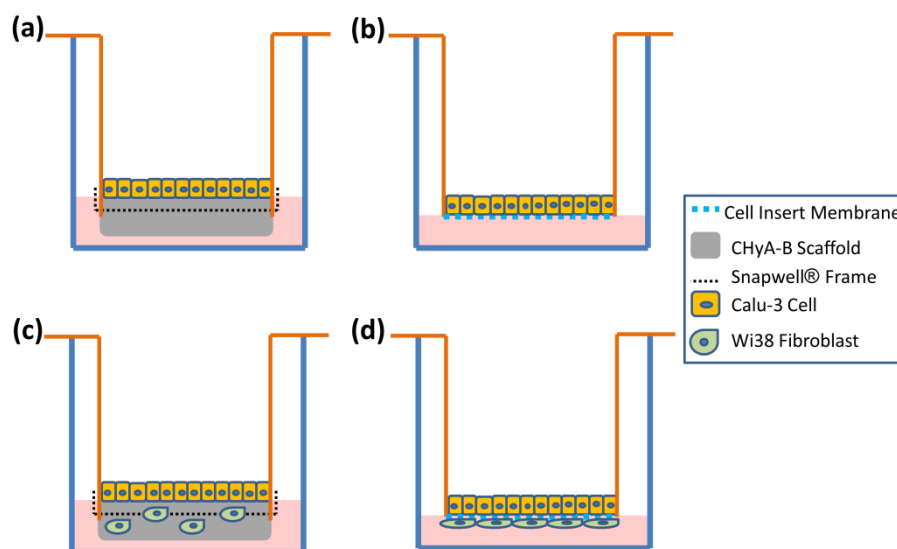


Figure 3.1: Calu-3 epithelial cell and Wi38 fibroblast air-liquid interface (ALI) culture models examined for in vitro experiments. In all cases, Calu-3 cells are grown at the ALI. (a) Epithelial cell monoculture on a bilayered collagen-hyaluronate (CHyA-B) scaffold. The polymeric membrane is removed from a Snapwell® cell insert and replaced with a CHyA-B scaffold fastened using the plastic frame prior to Calu-3 seeding. (b) Epithelial cell monoculture on a cell insert polymeric membrane. (c) Epithelial cell-fibroblast co-culture on a CHyA-B scaffold. The three-dimensional porous sub-layer of the scaffolds is seeded with Wi38 fibroblasts prior to fastening the scaffold in the Snapwell® frame and Calu-3 seeding. (d) Epithelial cell-fibroblast co-culture on a cell insert. Wi38 fibroblasts are seeded onto the underside of the cell insert prior to Calu-3 seeding.

3.2.3.2. Epithelial cell monoculture

The ability of CHyA-B scaffolds to support the growth and differentiation of the Calu-3 cell line in monoculture was assessed under ALI culture conditions. In order to facilitate ALI culture on the scaffold, a customised cell culture system was developed using the plastic frame of a Snapwell® cell insert (Corning Costar, NY). 15.6mm-diameter cut scaffolds were pre-hydrated in DPBS or chemically crosslinked as appropriate (Section 3.2.1.3) and preconditioned in Wi38 medium at 37°C. The polymeric membranes of the Snapwell® inserts were removed and the plastic frame was used to pin the scaffold into place with the film top-layer forming an apical compartment with an effective area of 12mm in diameter for

epithelial cell seeding (Fig. 3.1a). The basolateral compartment was filled with 2ml of Wi38 medium and the apical compartment with 400µl of Calu-3 medium. The film top-layer was seeded with 5×10^5 Calu-3 cells/cm² into the apical compartment; this equated to 100µl of a suspension that contained 5.6×10^5 cells. The media was removed from the apical compartment 3 days later to introduce an ALI and the cells were fed via the basolateral compartment for the remainder of the culture period using a 1:1 mixture of Calu-3:Wi38 media. Media replaced every 2-3 days for the duration of the experiments.

Calu-3 epithelial cells were also seeded onto 12mm Transwell® cell inserts (Corning Costar) for comparison with scaffold culture (Fig. 3.1b). The cell inserts were initially preconditioned by filling the basal compartment with 1ml of Wi38 medium and the apical compartment with 400µl of Calu-3 medium. The apical compartment was seeded with 5.6×10^5 Calu-3 cells in 100µl of a suspension and incubated for 3 days, similar to scaffold culture. Thereafter, the media was removed from the apical compartment to introduce an ALI and the cells were fed via the basolateral compartment for the remainder of the culture period using a 1:1 mixture of Calu-3:Wi38 media. Media replaced every 2-3 days for the duration of the experiments.

3.2.3.3. Epithelial cell co-culture with fibroblasts

The ability of CHyA-B scaffolds to support the growth and differentiation of the Calu-3 epithelial cell line in co-culture with Wi38 lung fibroblasts was assessed under ALI culture conditions (Fig. 3.1c). CHyA-B scaffolds were seeded using a modification of a previously described method [304]. 15.6mm-diameter scaffolds were chemically crosslinked (Section 3.2.1.3) and preconditioned in Wi38 medium at 37°C. The porous sublayer of each scaffold sample was then seeded with 50µl of a cell suspension that contained 6×10^5 Wi38 cells and incubated for 2 hours to allow for cell attachment. Thereafter, the scaffolds were covered in 2ml of Wi38 medium and grown for 3 days to allow for cell acclimatisation to the scaffold environment. Subsequently, they were then inserted into the Snapwell® system and the scaffold top-layer was seeded with Calu-3 cells as described in Section 3.2.3.2.

Calu-3-Wi38 co-culture was also established on 12mm Transwell® cell inserts for comparison with scaffold culture (Fig. 3.1d). Following the preconditioning step, the cell inserts were inverted, seeded with fibroblasts at a density of 3×10^4 cells/cm² and incubated for 2 hours to allow for fibroblast attachment; this equated to 33,600 cells that were added in 50µl of a cell suspension. Afterwards, the samples were returned to wells containing 1ml of Wi38 medium and grown for 3 days prior to Calu-3 seeding as outlined in Section 3.2.3.2.

3.2.4. Cell morphology and migration

3.2.4.1. Histology

Cell-seeded scaffolds were stained with haematoxylin and eosin and fast green (H&E&FG) to observe Calu-3 epithelial cell distribution on the CHyA-B top-layer and migration of Wi38 into the scaffold sublayer. Scaffold and cell insert samples were washed three times with DPBS and fixed for 30 minutes in 10% neutral buffered formalin (Sigma). The scaffolds were removed from the Snapwell® system and processed using an automated tissue processor (ASP300, Leica, Germany) overnight to dehydrate and paraffin wax-embed the samples. The samples were then sectioned, stained and analysed as outlined in Section 2.2.5.

3.2.4.2. Scanning electron microscopy (SEM)

Calu-3 cells were examined by SEM to further analyse epithelial cell distribution on the CHyA-B top-layer in monoculture. Cell-seeded samples were washed with DPBS and fixed in 3% glutaraldehyde (Sigma) for 1 hour at room temperature. They were then dehydrated in ascending grades of ethanol and dried using supercritical carbon dioxide in a critical point dryer. The samples were subsequently mounted on aluminium stubs, sputter-coated and imaged using a Tescan Mira XMU scanning electron microscope. Images were captured at 5kV using secondary electron mode, taken at a working distance between 12-18mm.

3.2.5. Calu-3 epithelial cell differentiation on CHyA-B scaffolds

3.2.5.1. Immunofluorescence

Immunofluorescent staining was carried out to detect the presence of two markers of tracheobronchial epithelial differentiation and functionality- MUC5AC and zonula-occludens-1 (ZO-1). These markers represented mucus production by Calu-3 cells and the formation of tight junctions, respectively [282, 286]. Cell-seeded scaffolds and cell inserts were washed in DPBS and fixed in 10% neutral buffered formalin for 20 minutes. The samples were permeabilised with 0.1% triton x-100 (Sigma) and non-specific binding of primary antibody was inhibited by incubation with 1% bovine serum albumin (BSA; Sigma) in DPBS. They were then incubated with either 1/100 mouse anti-MUC5AC monoclonal antibody (Abcam, Cambridge, UK) or 1/100 rabbit anti-ZO-1 polyclonal antibody (Molecular Probes, Invitrogen, UK). All antibodies were prepared in 1% BSA in DPBS and incubated for 2 hours at room temperature. A 1/500 goat anti-mouse Alexafluor®-594 or 1/500 goat anti-rabbit Alexafluor®-488 secondary antibody (Molecular Probes) in 1% BSA in DPBS was added for 1 hour at room temperature followed by counterstaining with 1/500 Alexafluor®-488- or 1/500 TRITC-labelled phalloidin (Sigma) for F-actin, as appropriate. Finally, the samples were mounted in Fluoroshield® with 4', 6-diamidino-2-phenylindole (DAPI; Sigma). Images were captured and analysed using an Axio Examiner.Z1 confocal microscope (Carl Zeiss, Cambridge, UK).

3.2.5.2. Transmission electron microscopy (TEM)

Cell-seeded samples were analysed by TEM to identify the presence of cilia on Calu-3 epithelial cells and to observe cell morphology. Scaffold and cell insert samples were washed in DPBS and fixed in 10% neutral buffered formalin for 20 minutes prior to treatment. The samples were then stained with 1% osmium tetroxide for 1 hour, followed by dehydration using descending grades of methanol. They were subsequently immersed in a 1:1 100% Methanol/London resin (LR) white and finally in pure LR white for 1 hour at room temperature. The samples were then embedded in LR white and ultrathin sections were generated using an EM UC6 ultramicrotome (Leica, Germany) and mounted on copper grids prior to examination in a Hitachi H-7650 electron microscope (Hitachi, Leixlip, Ireland) operating at 100kV.

3.2.5.3. Expression of genetic markers of epithelial cell differentiation

Relative gene expression of Calu-3 cells seeded on scaffolds in monoculture was quantified using quantitative reverse transcriptase-polymerase chain reaction (qRT-PCR) as previously described [258]. Cell-seeded scaffolds were flash frozen in liquid nitrogen and lysed in a solution containing 0.01% β -mercaptoethanol (Sigma) in RLT lysis buffer (Qiagen, Crawley, UK) for 20 minutes. Subsequently, they were homogenised using an Ultra Turrax T18 Overhead blender and homogeniser spin columns (Omega Biotek, Norcross, GA) to remove any residual scaffold. RNA was isolated from cell lysates using an RNeasy kit (Qiagen) and quantified using a NanoDrop 2000 spectrophotometer (Thermo Scientific, Cheshire, UK) with absorption read at 260nm. 200ng of total RNA was reverse transcribed to cDNA using a QuantiTect reverse transcription kit (Qiagen). RT-polymerase chain reactions were run on 7500 real-time PCR System (Applied Biosystems, UK) using a QuantiTect SYBR Green PCR Kit (Qiagen) with QuantiTect primers (Qiagen). The expression of mRNA was calculated by the delta-delta Ct ($2^{-\Delta\Delta C_t}$) method relative to the housekeeping gene 18S [40]. Expression of three genetic markers was analysed: MUC5AC as a marker for mucus production, ZO-1 as a marker for tight junctions, and FOXJ1 as a marker of epithelial cell ciliation [282, 285, 286].

3.2.6. Evaluation of Calu-3 epithelial cell barrier integrity

3.2.6.1. Transepithelial electrical resistance (TEER) measurement

The integrity of the epithelial barrier formed by Calu-3 cells cultured on CHyA-B scaffolds was quantified by the measurement of TEER in monoculture and co-culture systems. Prior to measurement of TEER using an EVOM voltohmmeter (World Precision Instruments, Stevenage, UK), cell culture medium was initially added to the apical compartment of the ALI cultures and samples were incubated for 1 hour. Electrical resistance was measured using STX-2 chopstick electrodes (World Precision Instruments) immediately upon removal of cells from the incubator. TEER was calculated by subtracting the resistance of a cell-free scaffold or insert and correcting for the surface area available for epithelial cell growth (1.12cm^2). To compare TEER values between groups following a plateau of the measurements [305], the average TEER values from day 11-14 were taken for each group and compared.

3.2.6.2. Fluorescein isothiocyanate (FITC)-labelled dextran permeability assay

The integrity of the epithelial barrier formed by Calu-3 cells on CHyA-B scaffolds was further assessed through analysis of paracellular transport through the cell layer [53]. The samples were initially washed and incubated with Hank's buffered salt solution (HBSS; Sigma) in both the apical and basolateral compartments for 1 hour. Subsequently, the HBSS in the apical compartment was replaced with a 500µg/ml solution of FITC-labelled dextran of an average molecular weight of 70kDa (FD70). Sampling from the basolateral compartment was performed every 30 minutes for 2 hours to quantify transported drug, with an equal volume of HBSS used to replace the removed volume of basolateral solution at each time point. Additionally, a sample of the initial apical FD70 content was taken for analysis and TEER measurements were performed before and after the experiment to confirm that the barrier integrity was unaltered during the transport assay. The fluorescence of sampled time points was quantified by measuring excitation at 485nm and emission at 535nm.

Fluorescence values were converted to concentration of FD70 using a standard curve and the apparent permeability coefficient (P_{app}) of FD70 was calculated using Equation 2, where F is flux (rate of change in cumulative mass transported), A is the surface area available for epithelial cell growth, and C_0 is the initial FD70 concentration in donor chamber.

$$P_{app} = F \times \left(\frac{1}{A \times C_0} \right) \quad (2)$$

3.2.7. Data analysis

Analysis of histological, confocal and electron microscopy images were performed using the Fiji processing software, including the measurement of length of ciliary structures. Quantitative data obtained were analysed using Microsoft Excel and GraphPad Prism 4.0 Software (GraphPad Software, San Diego, CA). In cases of analysis between two groups, statistical difference was assessed by two-tailed Student t test. In cases of analysis between multiple groups, statistical difference between groups was assessed by 2-way ANOVA with Bonferroni *post hoc* analysis. Scaffold characterisation experiments were performed using technical replicates, with the number of batches outlined in the relevant Materials and

Methods section above. Each cell-based experiment was performed a minimum of three times (n=3; three biological replicates); the number of technical replicates performed within each experiment is specified under the relevant figures.

3.3. Results

3.3.1. CHyA-B scaffold characterisation

3.3.1.1. Scaffold ultrastructure

CHyA-B scaffolds were examined using SEM in order to evaluate their architecture and to estimate film thickness (Fig. 3.2). The freeze-dry protocol was successfully modified to facilitate the integration of the film component into the CHyA slurry to yield a bilayered porous CHyA-B scaffold. The initial dehydration process reproducibly produced a transparent co-polymer film that was incorporated following rehydration and lyophilisation, irrespective of the freeze-dry cycle. From analysis of the scanning electron micrographs, the film was approximately 20µm in thickness with a smooth and uniform appearance. Below the film layer, an integrated network of pores could be seen with high interconnectivity that constituted the scaffold sub-layer.

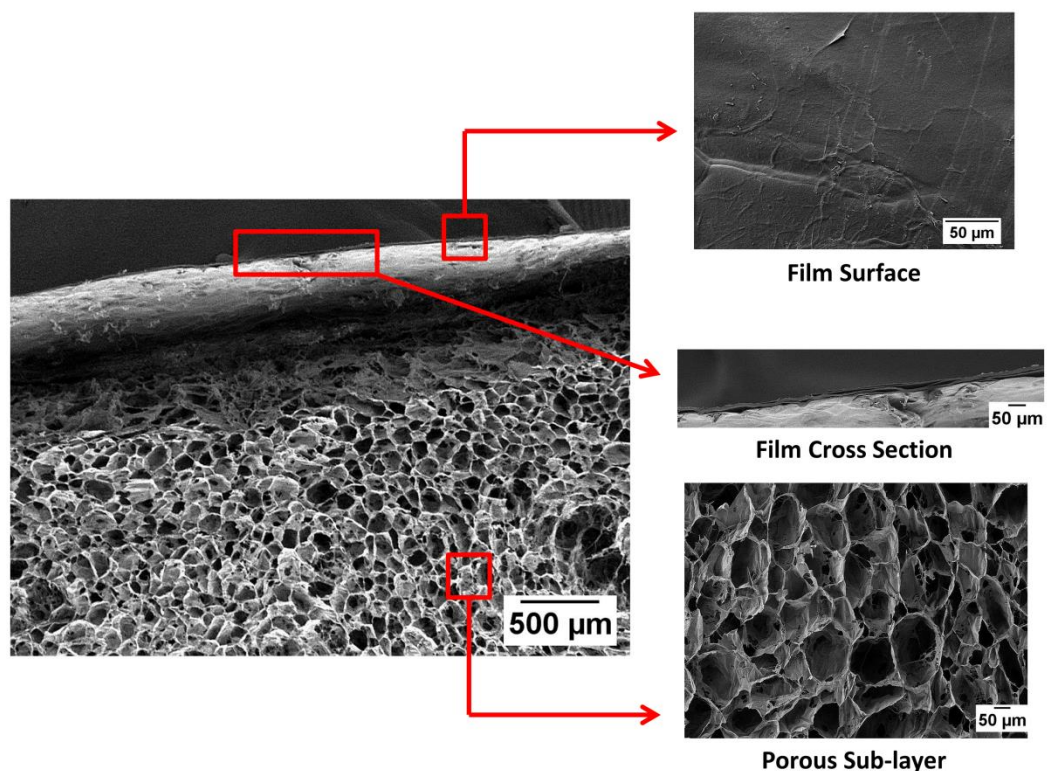


Figure 3.2: Bilayered collagen-hyaluronate scaffold ultrastructure. Representative scanning electron micrograph images of a scaffold freeze-dried to a final temperature of -10°C show the scaffold's ultrastructure, film surface and thickness, and interconnected porous sub-layer. n=3.

3.3.1.2. Interfacial adhesion strength

The interfacial adhesion strength between the film and porous layers of the CHyA-B scaffolds was determined to quantify the degree of integration between the two layers. In all cases, strain failure occurred as a result of delamination of the film and porous layers, indicating that the strength of adhesion between layers was weaker than that of the tensile strength of the individual layers (Fig. 3.3a). Overall, EDAC crosslinking did not significantly weaken the maximum adhesive strength of CHyA-B scaffolds prior to failure, despite observation of an apparent reduction ($p=0.07$).

3.3.1.3. Mechanical testing

Uni-axial, unconfined compressive testing of CHyA-B scaffolds was carried out to determine the bulk compressive elastic modulus, a property known to affect cellular growth and differentiation [274, 299]. The inclusion of the film layer onto porous CHyA scaffolds was found to increase substrate stiffness, particularly in combination with EDAC crosslinking (Fig. 3.3b). When chemically crosslinked, CHyA-B scaffolds had a significantly greater compressive modulus, irrespective of the freeze-dry cycle. Furthermore, in the case of the scaffolds freeze-dried using an anneal step, the inclusion of the film layer in the scaffold significantly raised the compressive modulus in both the absence and presence of chemical crosslinking, changing from 0.4kPa to 0.8kPa in the DHT-crosslinked group ($p<0.05$) and from 1.2kPa to 1.9kPa with additional EDAC crosslinking ($p<0.001$). Overall, the chemical crosslinking with EDAC significantly increased the compressive modulus relative to DHT crosslinking alone in all groups, as expected ($p<0.001$), and these data demonstrated that the inclusion of a film layer resulted in a stiffer scaffold.

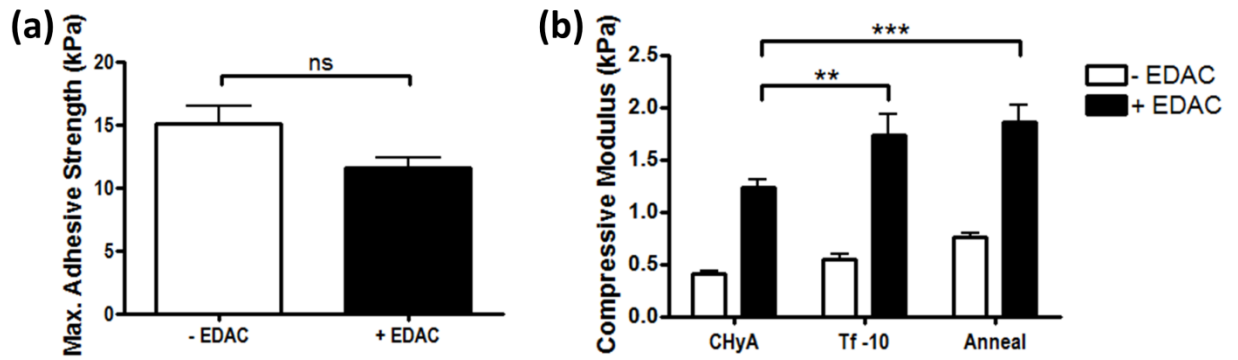


Figure 3.3: Mechanical properties of bilayered collagen-hyaluronate scaffolds. (a) Layer adhesive strength of bilayered scaffolds with or without crosslinking using 1-ethyl-3-(3-dimethylaminopropyl)carbodiimide hydrochloride (EDAC). $n=4$; $^{ns}p>0.05$. (b) Compressive moduli of scaffolds manufactured using an anneal cycle (Anneal) or a final freezing temperature of -10°C ($T_f -10$) with or without EDAC crosslinking. A single-layered fully porous collagen-hyaluronate scaffold (CHyA) is included for comparison. $n=6$; $**p<0.01$; $***p<0.001$. Results of both graphs displayed as mean \pm SEM.

3.3.1.4. Pore size analysis

Scaffold pore size analysis was performed to assess the effect of the film layer and lyophilisation cycle on the mean pore diameter and porosity of the porous sub-layer of CHyA-B scaffolds, two important properties for cell adhesion and growth [276] (Fig. 3.4). CHyA-B scaffolds manufactured using an anneal cycle had a mean pore size diameter of 80 μ m, compared to 70 μ m when lyophilised using a final freezing temperature of -10°C (Fig. 3.4a; $p>0.05$). The inclusion of a film layer did not influence the scaffold pore size, with no significant difference observed between bilayered scaffolds and fully-porous scaffolds manufactured using the same anneal cycle. Regarding the porosity of the CHyA-B sub-layer, both fabrication processes produced highly porous materials, with a percentage porosity of greater than 98% in both scaffold groups (Fig. 3.4b). The anneal cycle, however, produced a porous biomaterial that was more homogenous in its pore size distribution (Fig. 3.4c-3.4f). Ultimately, the manufacture of CHyA-B with an anneal cycle resulted in a more uniformly porous scaffold with a larger pore size.

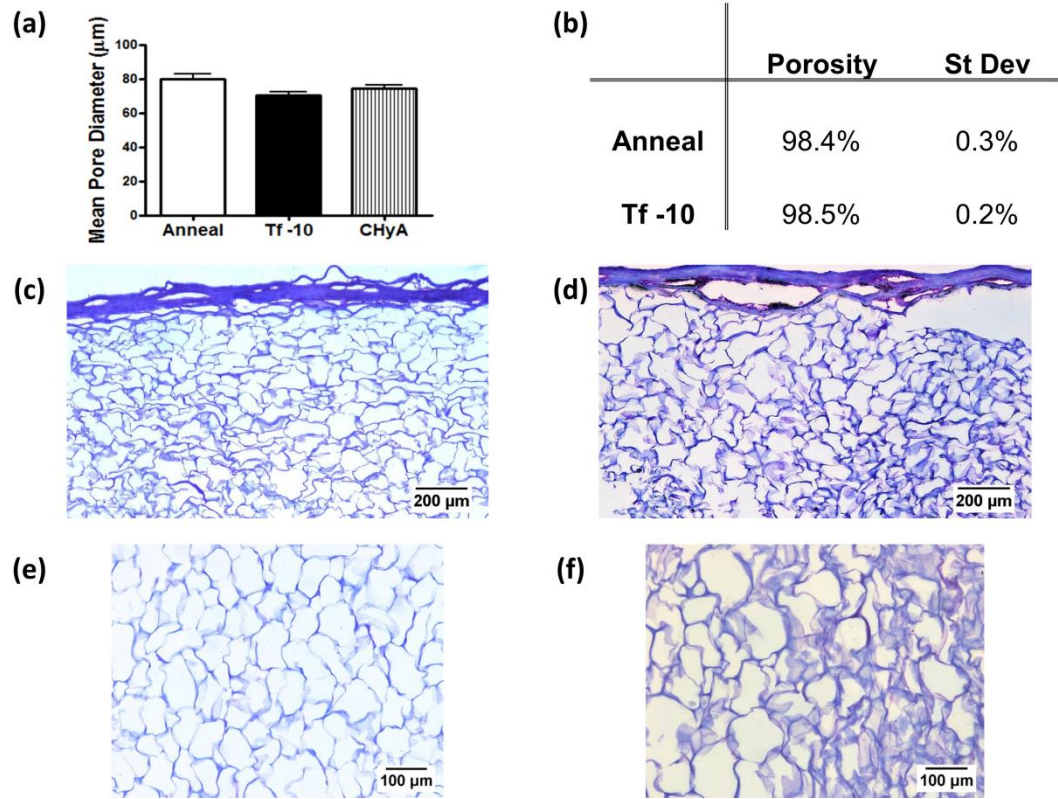


Figure 3.4: Pore size analysis of bilayered collagen-hyaluronate scaffolds. Scaffolds were manufactured using an anneal cycle (Anneal) or a final freezing temperature of -10°C ($T_f -10$). (a) Mean pore diameter of scaffold sub-layer. A single-layered fully porous collagen-hyaluronate scaffold (CHyA) is included for comparison. $n=3$. (b) Percentage porosity of scaffold sub-layer. $n=10$. (c-f) Sample toluidine blue sections of (c, e) anneal and (d, f) $T_f -10$ scaffolds used for software analysis. Representative images visualise scaffolds as a dark blue colour. $n=3$.

3.3.2. Calu-3 epithelial cell monoculture on CHyA-B scaffolds

3.3.2.1. Cell morphology and migration

Histological analysis and SEM were undertaken to examine Calu-3 morphology and monolayer formation on the CHyA-B apical film layer. H&E&FG staining revealed that Calu-3 cells cultured on EDAC-crosslinked CHyA-B scaffolds formed an epithelial monolayer that was maintained over the culture period of 21 days (Fig. 3.5). This was in contrast to cells cultured on scaffolds without EDAC crosslinking, where the samples failed to maintain their structural integrity to the extent that they had shrank and/or collapsed by day 21. Within this group, cells formed clusters of cells on the scaffold surface instead of a monolayer (Fig. 3.5a). On day 28, a confluent monolayer was seen on the film surface of EDAC-crosslinked CHyA-B scaffolds using SEM, confirming the histological findings (Fig. 3.5b). A coating of small microvilli and clusters of cilia-like structures were also observed in SEM images. Overall, these data indicated that EDAC-crosslinked CHyA-B scaffolds are suitable for Calu-3 epithelial cell monolayer culture on a 3D substrate that was still maintained after 4 weeks in culture; these scaffolds were accordingly selected for cell culture studies.

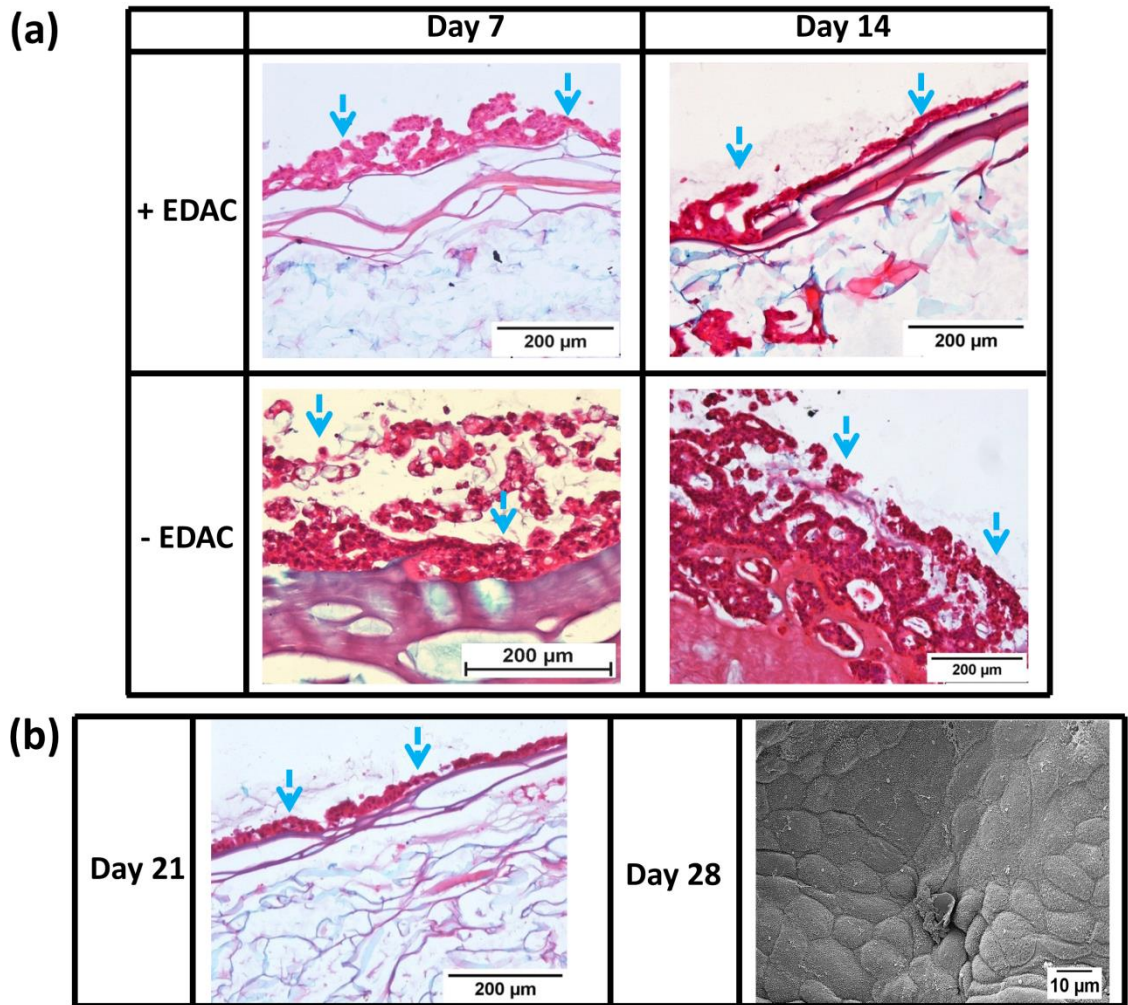


Figure 3.5: Calu-3 cell monoculture on bilayered collagen-hyaluronate scaffolds. (a) Scaffolds were fabricated with or without crosslinking using 1-ethyl-3-(3-dimethylaminopropyl)carbodiimide hydrochloride (EDAC). n=9. (b) Long-term Calu-3 culture on EDAC-crosslinked scaffolds. Only EDAC-crosslinked scaffolds maintained their structure in cell culture beyond day 14. Representative haematoxylin & eosin and fast green images visualised scaffolds as a light-blue colour with a pink-purple film layer and cells appeared as pink-purple with darker nuclei (blue arrows). n=9. Representative scanning electron micrographs at day 28 visualised a confluent monolayer with cobblestone morphology on EDAC-crosslinked scaffolds. n=3.

3.3.2.2. Mucin expression

The ability of the CHyA-B scaffolds to support Calu-3 cell differentiation in monoculture was assessed by analysis of MUC5AC mucin expression. Immunofluorescent staining of Calu-3 cells cultured on scaffolds showed a notable increase in MUC5AC glycoprotein secretion when compared to conventional cell insert culture (Fig.3.6). Z-stack images detected the presence of MUC5AC on the apical side of the Calu-3 cells at day 14 (Fig. 3.6a, 3.6b) with greater glycoprotein fluorescence present in the scaffold cultures than in the cell insert cultures (Fig 3.6c, 3.6d). This finding suggests that the CHyA-B scaffold stimulated mucus secretion from the Calu-3 bronchial epithelial cell line.

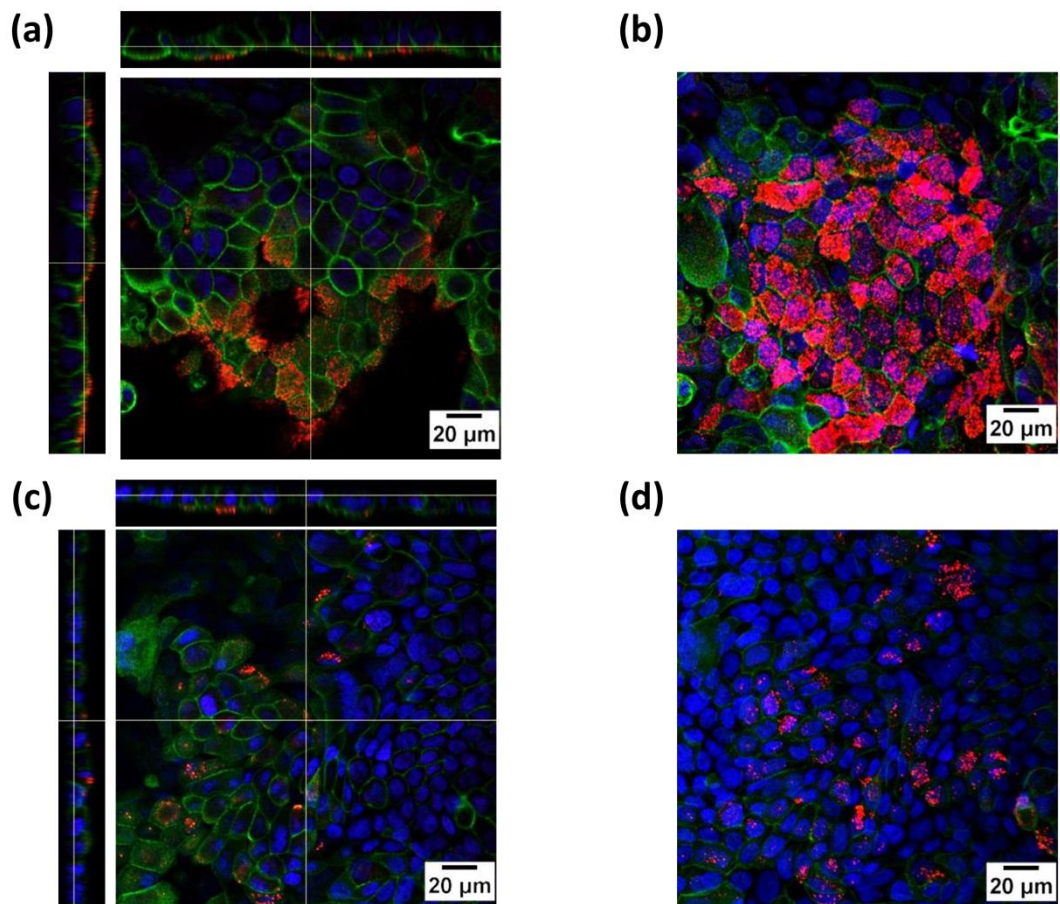


Figure 3.6: MUC5AC expression by Calu-3 cells in monoculture on bilayered collagen-hyaluronate (CHyA-B) scaffolds. Calu-3 epithelial cells were cultured either on (a, b) CHyA-B scaffolds or on (c, d) cell inserts at an air-liquid interface for 14 days. (a, c) Representative z-stack images display apical MUC5AC secretion (red) on top of cells counterstained for nuclei (blue) and F-actin (green). (b, d) Maximum intensity projections of MUC5AC expression reconstructed from z-stacks. n=3 (performed in duplicate).

3.3.2.3. Tight junction formation

The ability of CHyA-B scaffolds to support the differentiation of Calu-3 cells in monoculture was further assessed by analysis of ZO-1 as a marker of bronchial epithelial tight junction formation. ZO-1 protein was detected in CHyA-B scaffolds, with immunofluorescent images capturing the presence of the tight junction protein between epithelial cells at days 14 on the CHyA-B film top-layer (Fig. 3.7). This was characteristic of tight intercellular junctions that restrict paracellular transport across the epithelium (Fig. 3.7a, 3.7c). Additionally, z-stack orthogonal views highlighted that these junctional bands were concentrated on the apical side of epithelial cells which further reflected epithelial polarisation and the typical intracellular localisation of ZO-1 (Fig. 3.7a). CHyA-B and cell insert culture systems displayed equivalence, with the presence and classical distribution of ZO-1 also present in monoculture on Transwell® inserts (Fig. 3.7c, 3.7d). Overall, these results indicate the Calu-3 cells formed tight intercellular junctions on the apical side of CHyA-B scaffolds cultured at an ALI.

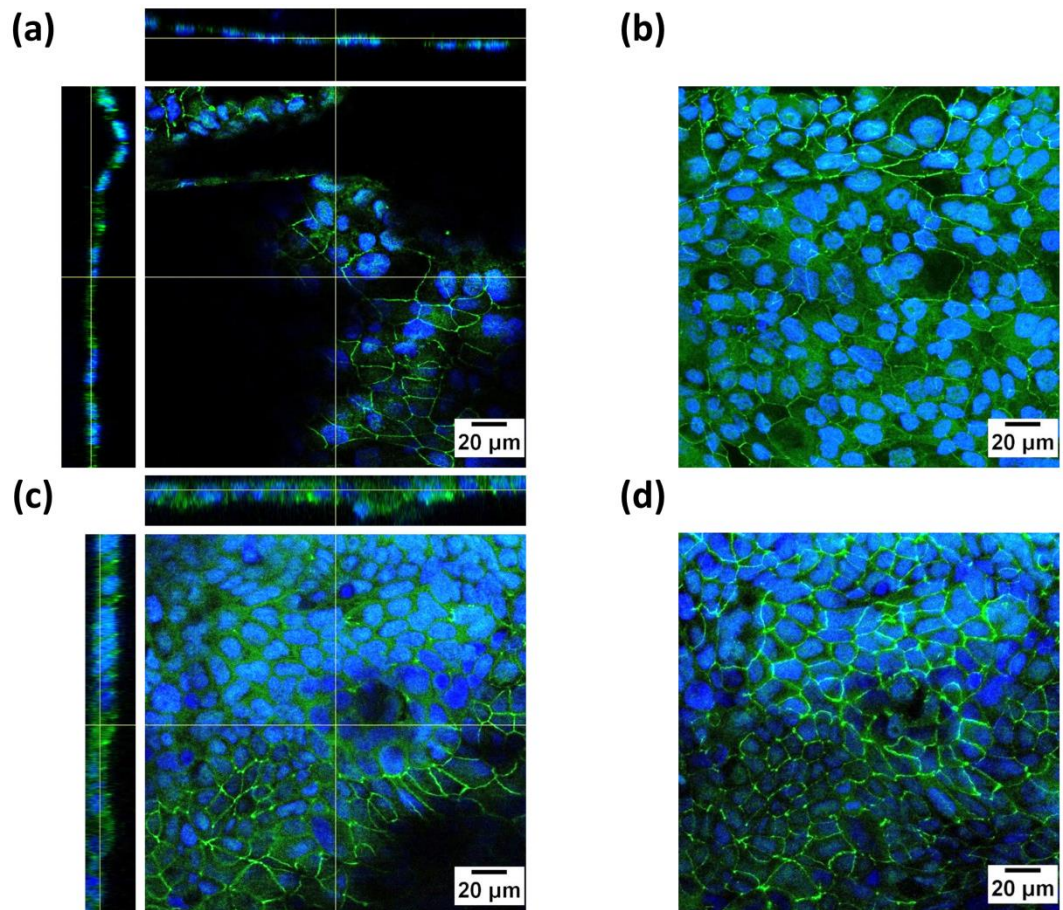


Figure 3.7: ZO-1 expression by Calu-3 cells in monoculture on bilayered collagen-hyaluronate (CHyA-B) scaffolds. Calu-3 epithelial cells were cultured either on (a, b) CHyA-B scaffolds or on (c, d) cell inserts at an air-liquid interface for 14 days. (a, c) Representative z-stack images display ZO-1 bands (green) with punctate apical concentrations at the borders of cells counterstained for nuclei (blue). (b, d) Maximum intensity projections of ZO-1 expression reconstructed from z-stacks. n=3 (performed in duplicate).

3.3.2.4. Epithelial ciliation

The third assessment of the ability of CHyA-B scaffolds to support the differentiation of Calu-3 cells in monoculture examined the formation of motile cilia by TEM imaging. TEM analysis detected the presence of microvilli-like premature cilia on the apical side of Calu-3 cells in both samples at day 14 of culture (Fig. 3.8). Notably, the ciliary structures formed in cells cultured on CHyA-B were longer than those observed in cell insert culture (Fig. 3.8b, 3.8d). Additionally, the cells on scaffolds adopted a pseudostratified columnar morphology along the film layer that was not observed in culture on polymeric cell inserts (Fig. 3.8a, 3.8c). Thus, these data suggested that the CHyA-B induced a more organotypic respiratory epithelium with ciliation within Calu-3 cells.

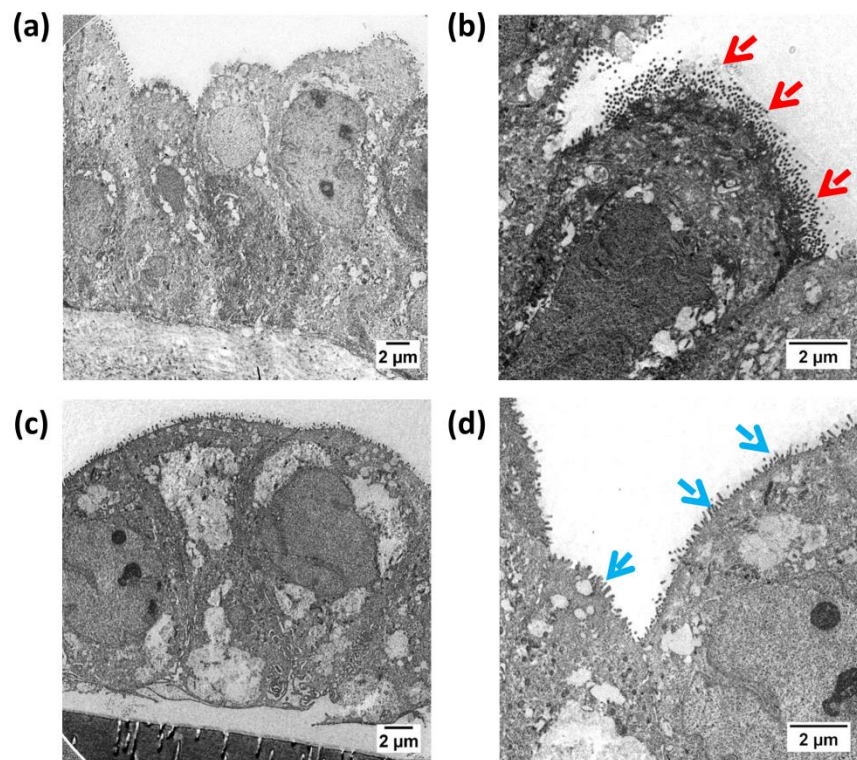


Figure 3.8: Transmission electron microscopy images of Calu-3 cells in monoculture on bilayered collagen-hyaluronate (CHyA-B) scaffolds. Calu-3 epithelial cells were cultured either on (a, b) CHyA-B scaffolds or on (c, d) cell inserts for 14 days at an air-liquid interface. (a, b) Cells cultured on scaffolds adopted a pseudostratified columnar morphology with expression of cilia along the epithelial layer (red arrows). (c, d) Cells cultured on cell inserts adopted a cuboidal morphology with expression of shorter cilia (blue arrows). n=1; representative images were captured by Mr. Brenton Cavanagh, RCSI.

3.3.3. Expression of genetic markers of epithelial cell differentiation

3.3.3.1. The effect of CHyA-B scaffolds on epithelial cell gene expression

The effect of CHyA-B scaffold culture on the transcription of genes that support the differentiation of Calu-3 cells in monoculture was analysed by quantitative relative gene expression of MUC5AC, ZO-1, and FOXJ1 to represent mucus production, epithelial barrier formation and ciliation, respectively [282, 285, 286]. It was revealed that the presence of the CHyA-B scaffold induced the upregulation of two of these genes, MUC5AC and FOXJ1 (Fig. 3.9). Calu-3 cells cultured on scaffolds showed a significant upregulation of MUC5AC gene expression compared to that of conventional cell insert culture at days 7, 14, and 21 (Fig. 3.9a). A significant upregulation of FOXJ1 was also observed when compared to that of cell insert culture at day 7 (Fig. 3.9c; $p < 0.01$), though equivalent expression levels were detected between the culture systems at later time points. Regarding ZO-1 gene expression, Calu-3 cells cultured on scaffolds exhibited a marginal upregulation compared to those of the cell insert groups at days 7 and 14, though this trend was non-significant (Fig. 3.9c; $p = 0.21$ and $p = 0.25$, respectively), confirming that ZO-1 expression on CHyA-B scaffolds matched that of conventional cell insert ALI culture. Overall, these data emphasised the ability of the CHyA-B scaffold to influence the phenotype of the bronchial epithelial cell line at the transcriptional level and promote differentiation of the Calu-3 cells to secrete mucus and express cilia.

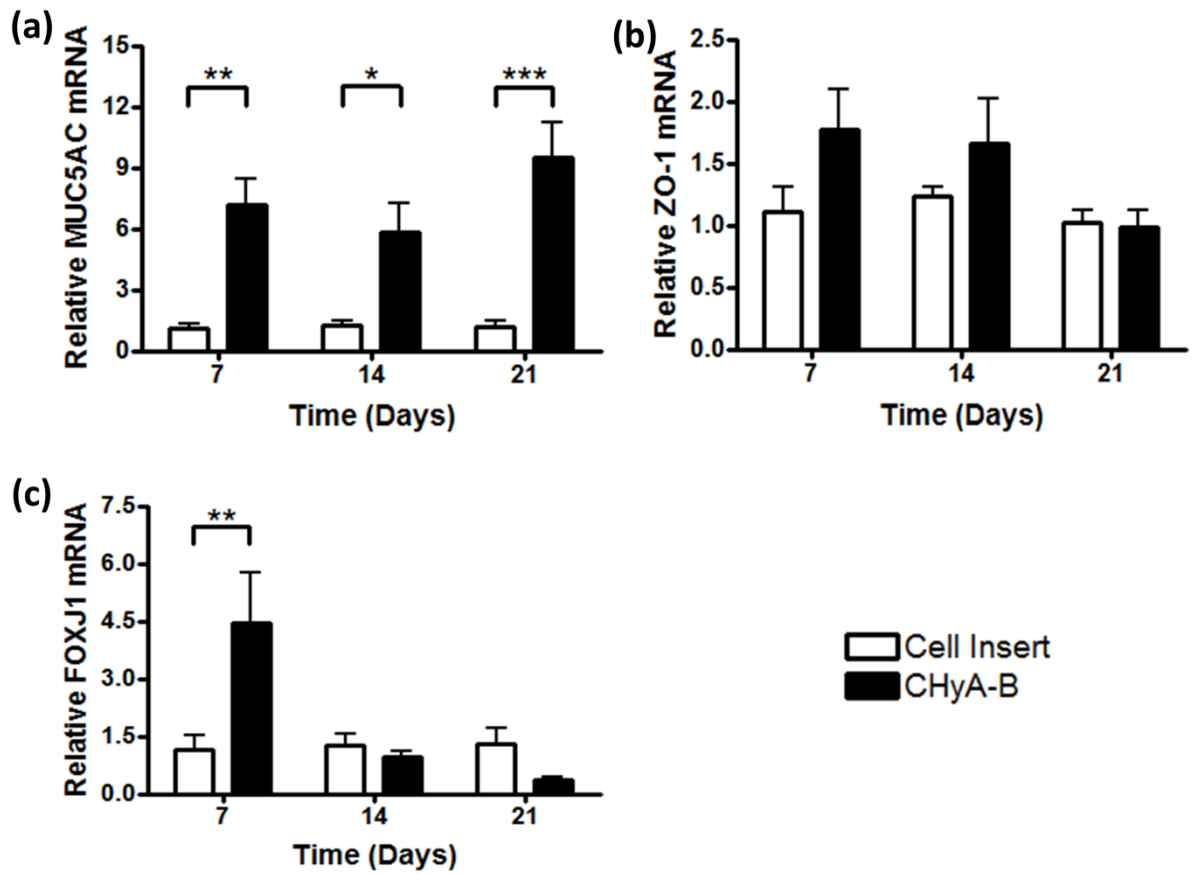


Figure 3.9: The effect of bilayered collagen-hyaluronate (CHyA-B) scaffolds on the relative mRNA expression of Calu-3 cells in monoculture. Calu-3 epithelial cells were cultured on either scaffolds or on cell inserts an air-liquid interface for 21 days. Quantification of (a) MUC5AC, (b) ZO-1 and (c) FOXJ1 mRNA expression is displayed as mean \pm SEM with expression relative to the cell insert group at the respective time point. $n=3$ (performed in duplicate for two experiments and with single samples for one experiment); * $p<0.05$; ** $p<0.01$; *** $p<0.001$.

3.3.3.2. The effect of time on epithelial cell gene expression

The influence of the culture time period on the transcription of Calu-3 genes in scaffold and cell insert monoculture models was also analysed by quantitative relative gene expression of MUC5AC, ZO-1 and FOXJ1 (Fig. 3.10). MUC5AC expression was observed to increase in cells cultured on CHyA-B scaffolds over time ($p < 0.05$), unlike in cells that were cultured on the polymeric cell inserts (Fig. 3.10a). In a similar pattern to the effect of the CHyA-B biomaterial on ZO-1 expression, prolonged time in culture over 21 days did not affect mRNA levels in both cell culture systems either. Interestingly, Calu-3 cells cultured on cell inserts showed a significant upregulation of FOXJ1 at days 14 and 21 relative to day 7 that did not occur in CHyA-B culture (Fig. 3.10c); when considered with the previous FOXJ1 analysis in Fig. 3.9c, this indicated that FOXJ1 expression in cell insert culture matched that of scaffold culture at later time points due to a time-dependent increase in expression. Therefore, CHyA-B scaffold induced a magnitude of FOXJ1 expression comparable to cell insert culture in half the amount of time to the current standard. To summarise, this analysis demonstrated that the CHyA-B scaffold promoted a sustained mucus-secreting epithelial phenotype and more rapid ciliation that did not occur with conventional cell insert culture.

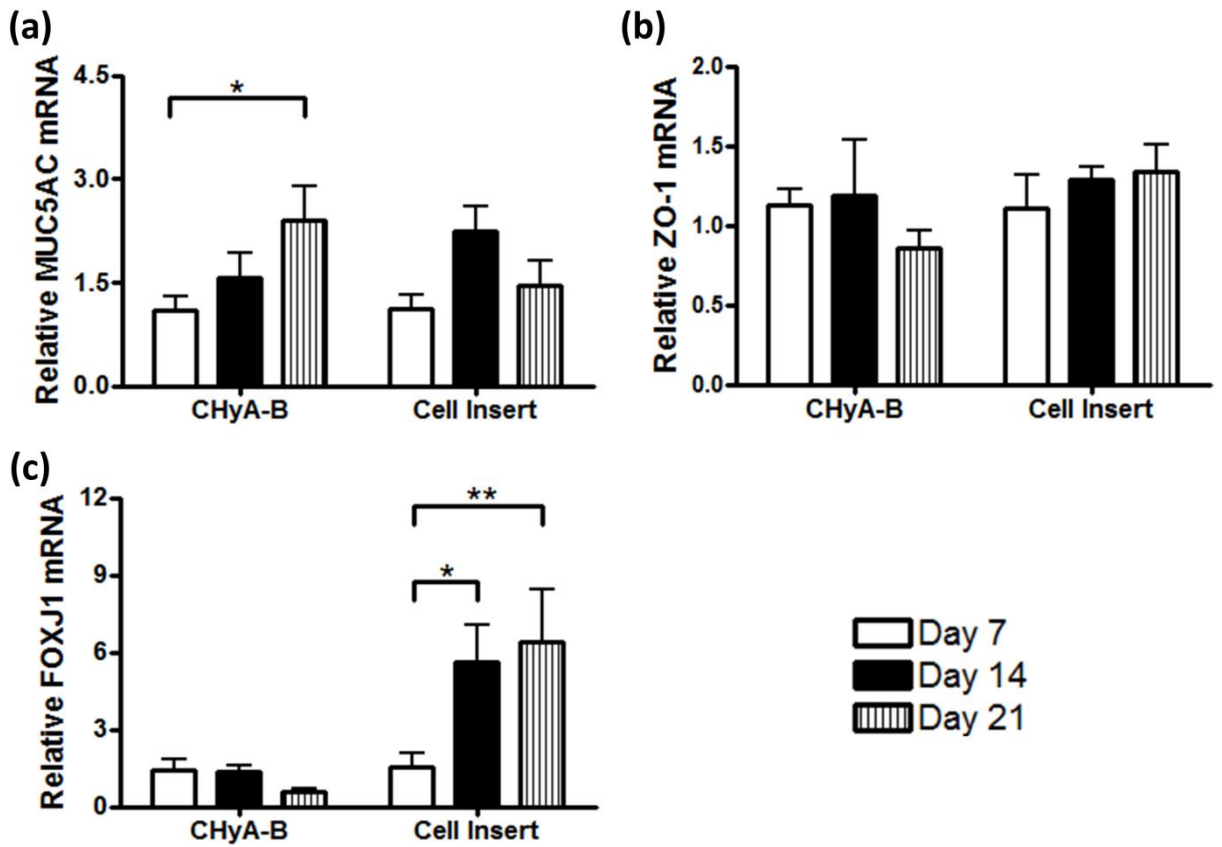


Figure 3.10: The effect of time on the relative mRNA expression of Calu-3 cells in monoculture. Calu-3 epithelial cells were cultured on either bilayered collagen-hyaluronate (CHyA-B) scaffolds or on cell inserts an air-liquid interface for 21 days. Quantification of (a) MUC5AC, (b) ZO-1 and (c) FOXJ1 expression is displayed as mean \pm SEM with expression relative to the day 7 time point for each respective culture model. $n=3$ (performed in duplicate for two experiments and with single samples for one experiment); * $p<0.05$; ** $p<0.01$.

3.3.4. Calu-3 epithelial cell co-culture with fibroblasts on CHyA-B scaffolds

3.3.4.1. Cell morphology and migration

Following the successful formation of a confluent and differentiated Calu-3 epithelial cell barrier on EDAC-crosslinked CHyA-B scaffolds in monoculture, a co-culture system of Calu-3 epithelial cells and Wi38 lung fibroblasts was examined in order to assess the scaffold's capacity to act as a substrate for 3D *in vitro* co-culture models (Fig. 3.11). Histological staining at day 14 confirmed that in addition to the presence of the Calu-3 cell monolayer on CHyA-B scaffolds, Wi38 cells populated the porous sub-layer, with evidence of inward cellular migration (Fig. 3.11a). Parallel monoculture of Calu-3 cells on CHyA-B scaffolds in tandem with co-cultured samples displayed an absence of any cells in the porous scaffold sub-layer but still exhibited retention of the epithelial cell barrier on the scaffold film layer (Fig. 3.11b), indicating that any cells observed in the porous layer of co-cultures were fibroblasts. Furthermore, these cells adopted a different morphology in the 3D porous structure to that observed when Calu-3 cells are cultured in such an environment (Chapter 2). Overall, bilayered CHyA-B scaffolds facilitated a bronchial epithelial-fibroblast co-culture with distinct cellular localisation and organisation of each cell type at the desired region on the 3D substrate.

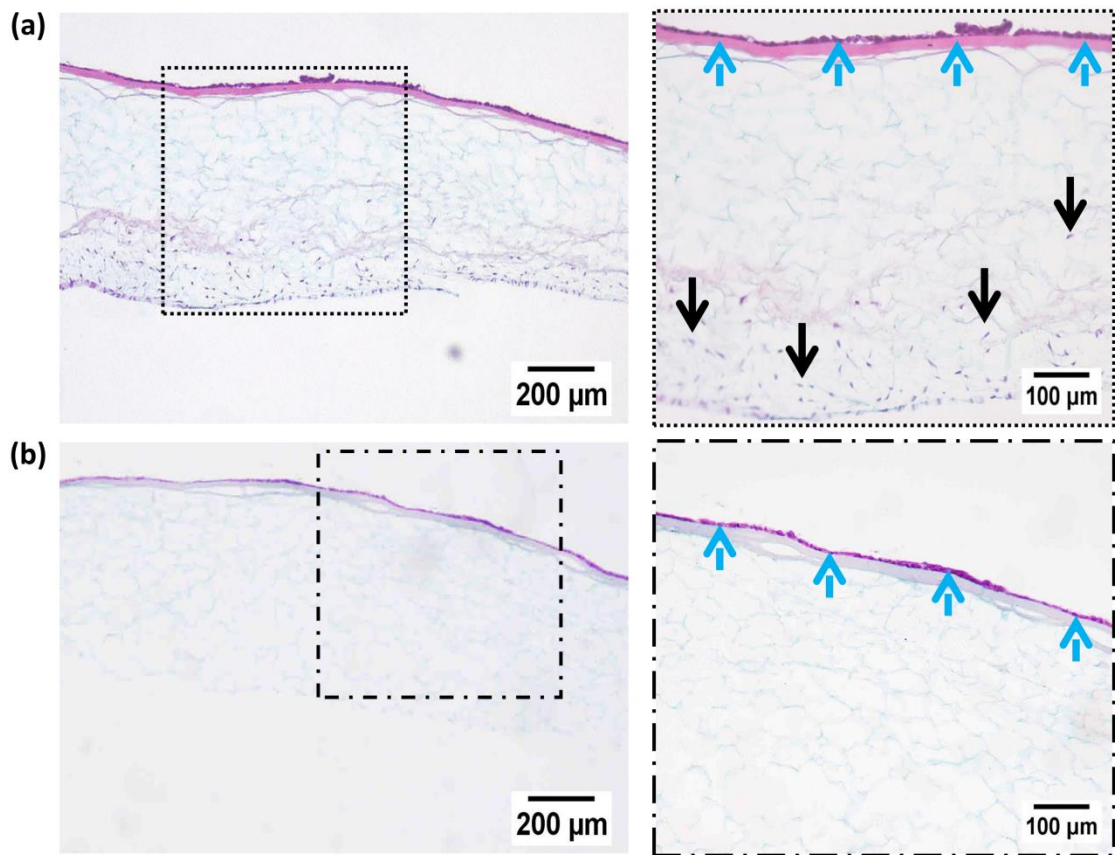


Figure 3.11: Co-culture on bilayered collagen-hyaluronate scaffolds. (a) Calu-3 cells and Wi38 fibroblasts cultured together were imaged at 14 days. Higher magnification images (boxes) showed Calu-3 cells forming a monolayer along the film top-layer (blue arrows) and Wi38 fibroblasts migrating into the porous sub-layer (black arrows). (b) Monoculture of Calu-3 cells on scaffolds showed the formation of a matching epithelial cell monolayer to that on co-cultured scaffolds but a notable absence of cells in the porous sub-layer. Representative haematoxylin & eosin and fast green staining visualised scaffolds as a light-blue colour with a pink-purple film layer and cells appeared as pink-purple with darker nuclei. $n=3$ (performed in triplicate).

3.3.4.2. Mucin expression

The influence of Wi38 fibroblasts on the differentiation of Calu-3 epithelial cells to secrete mucus was analysed by immunofluorescence of MUC5AC glycoprotein. MUC5AC was detected in Calu-3 scaffold co-cultures (Fig. 3.12), as seen previously with scaffold monoculture samples. Notably, less MUC5AC was secreted from epithelial cells on CHyA-B scaffolds in co-culture than in monoculture (Fig. 3.12b) but fluorescence was still greater than that observed from cell insert co-culture samples (Fig. 3.12d). Thus, the stimulation of enhanced mucus secretion by CHyA-B scaffolds was maintained in co-culture with lung fibroblasts.

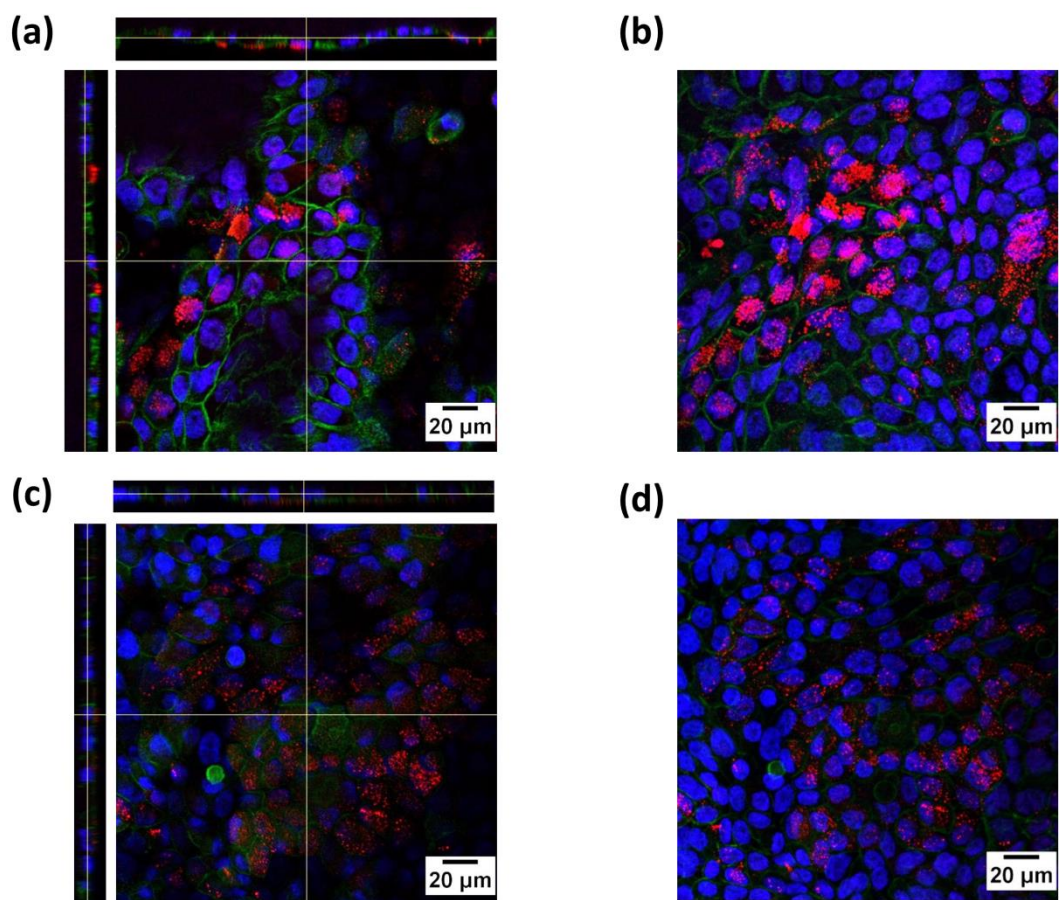


Figure 3.12: MUC5AC expression by Calu-3 cells in co-culture on bilayered collagen-hyaluronate (CHyA-B) scaffolds. Calu-3 epithelial cells were cultured with Wi38 fibroblasts either on (a, b) CHyA-B scaffolds or on (c, d) cell inserts at an air-liquid interface for 14 days. (a, c) Representative z-stack images display apical MUC5AC secretion (red) on top of cells counterstained for nuclei (blue) and F-actin (green). (b, d) Maximum intensity projections of MUC5AC expression reconstructed from Z-stacks. $n=3$ (performed in duplicate). Co-culture experiments were performed concurrently with monoculture experiments (Fig. 3.6).

3.3.4.3. Tight junction formation

The influence of Wi38 fibroblasts on the ability of Calu-3 epithelial cells to form tight junctions was analysed by immunofluorescence of ZO-1. The protein was detected in Calu-3 scaffold co-cultures as seen previously with scaffold monoculture samples (Fig. 3.13). Clear bands were present in cell insert co-culture as well as in CHyA-B samples (Fig. 3.13c, 3.13d). Therefore, the formation of an epithelial barrier on the CHyA-B scaffold occurred in co-culture as well as in monoculture.

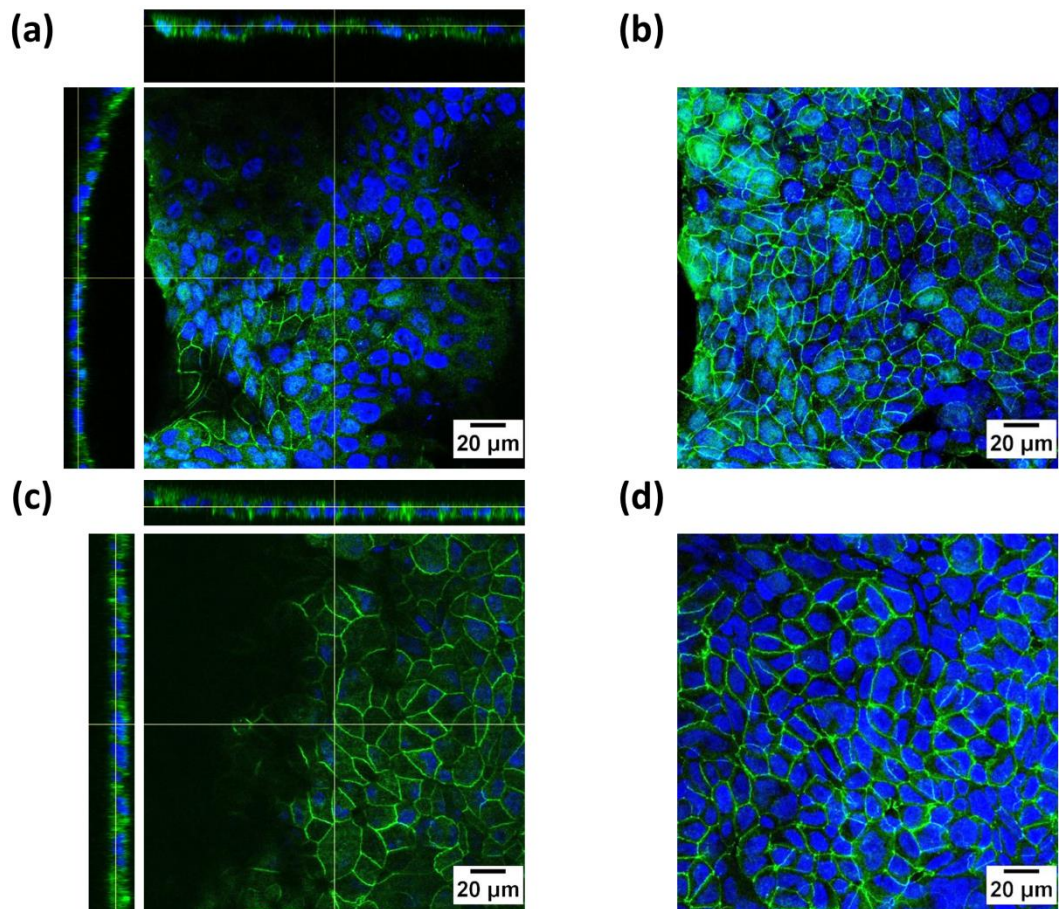


Figure 3.13: ZO-1 expression by Calu-3 cells in co-culture on bilayered collagen-hyaluronate (CHyA-B) scaffolds. Calu-3 epithelial cells were cultured with Wi38 fibroblasts either on (a, b) CHyA-B scaffolds or on (c, d) cell inserts at an air-liquid interface for 14 days. (a, c) Representative z-stack images display ZO-1 bands (green) with punctate apical concentrations at the borders of cells counterstained for nuclei (blue). (b, d) Maximum intensity projections of ZO-1 expression reconstructed from z-stacks. $n=3$ (performed in duplicate). Co-culture experiments were performed concurrently with monoculture experiments (Fig. 3.7).

3.3.4.4. Epithelial ciliation

The influence of Wi38 fibroblasts on the ability of Calu-3 epithelial cells to express cilia was analysed by TEM (Fig. 3.14). Calu-3 cells were less pseudostratified in appearance on CHyA-B scaffolds in co-culture when compared to monoculture on scaffolds (Fig. 3.14a). In spite of this observation, longer cilia were once again present on cells cultured on CHyA-B relative to cell insert culture, as was the case with epithelial cell monoculture. Accordingly, Calu-3 and Wi38 co-culture on CHyA-B scaffolds maintained the principal feature of a ciliated tracheobronchial epithelium.

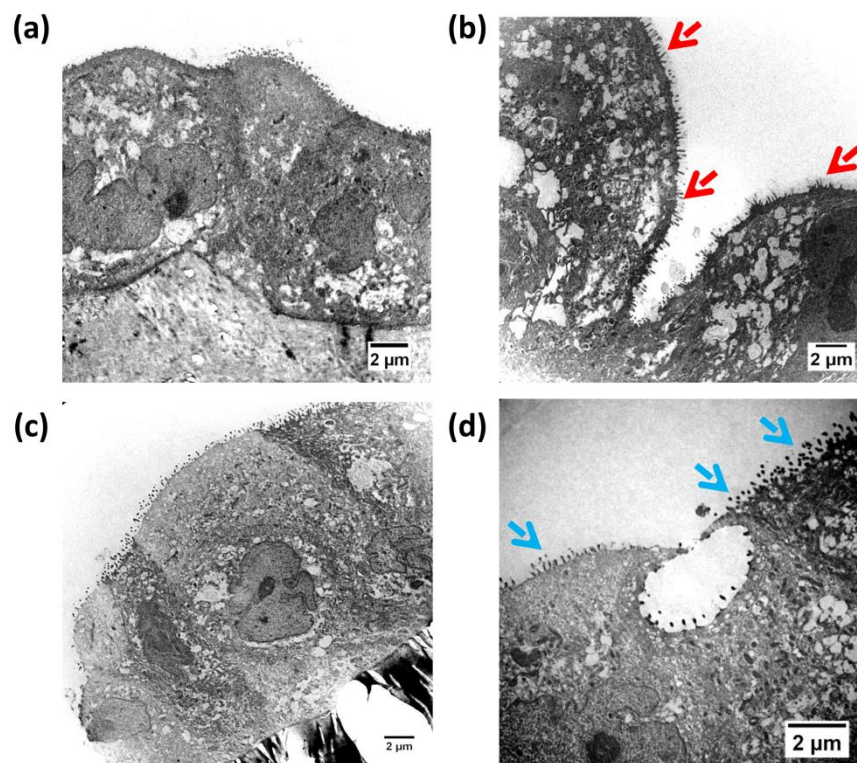


Figure 3.14: Transmission electron microscopy (TEM) images of Calu-3 cells in co-culture on bilayered collagen-hyaluronate (CHyA-B) scaffolds. Calu-3 epithelial cells were cultured with Wi38 fibroblasts either on (a, b) CHyA-B scaffolds or on (c, d) cell inserts for 14 days at an air-liquid interface. (a, b) Cells cultured on scaffolds adopted a cuboidal morphology with expression of cilia along the epithelial layer (red arrows). (c, d) Cells cultured on cell inserts adopted a cuboidal morphology with expression of shorter cilia (blue arrows). n=1; representative TEM images were captured by Mr. Brenton Cavanagh, RCSI. Co-culture experiments were performed concurrently with monoculture experiments (Fig. 3.8).

3.3.5. Evaluation of Calu-3 epithelial cell barrier integrity

3.3.5.1. TEER measurement

In order to confirm that the differentiated epithelial layer formed upon CHyA-B scaffolds displayed an effective barrier function in both monoculture and co-culture, the integrity of the epithelial barrier was quantified by the measurement of TEER (Fig. 3.15). In both monoculture and co-culture systems, Calu-3 cells cultured on scaffolds formed a barrier that was $>500\Omega\text{cm}^2$ with mean TEER values on day 14 of $681\Omega\text{cm}^2$ and $691\Omega\text{cm}^2$, respectively (Fig 3.15a). TEER values within scaffold cultures were lower on average than those obtained from cell insert cultures. This was evident when the average TEER values of each group following day 11 were compared (Fig. 3.15b), where an increasing trend from CHyA-B monoculture to cell insert co-culture was recorded. In both culture systems, the inclusion of Wi38 fibroblasts increased TEER, although this trend was non-significant ($p>0.05$). Fibroblasts seeded alone onto scaffolds or cell inserts did not develop a functional TEER value, in line with previous studies [60].

3.3.5.2. FITC-labelled dextran permeability assay

Finally, in order to fully confirm that the differentiated epithelial layer formed upon CHyA-B scaffolds displayed an effective barrier function in both monoculture and co-culture, the integrity of the epithelial barrier was quantified by the assessment of permeability to the large molecular weight compound FD70 (Fig. 3.15). The ability of the epithelial barrier to impede the paracellular transport of FD70 was observed in all samples, with low P_{app} values recorded in scaffold cultures and no transport detected in cell insert culture (Fig. 3.15c). Taken together with the TEER data, these results collectively highlighted the presence of a functional epithelial barrier in scaffold culture.

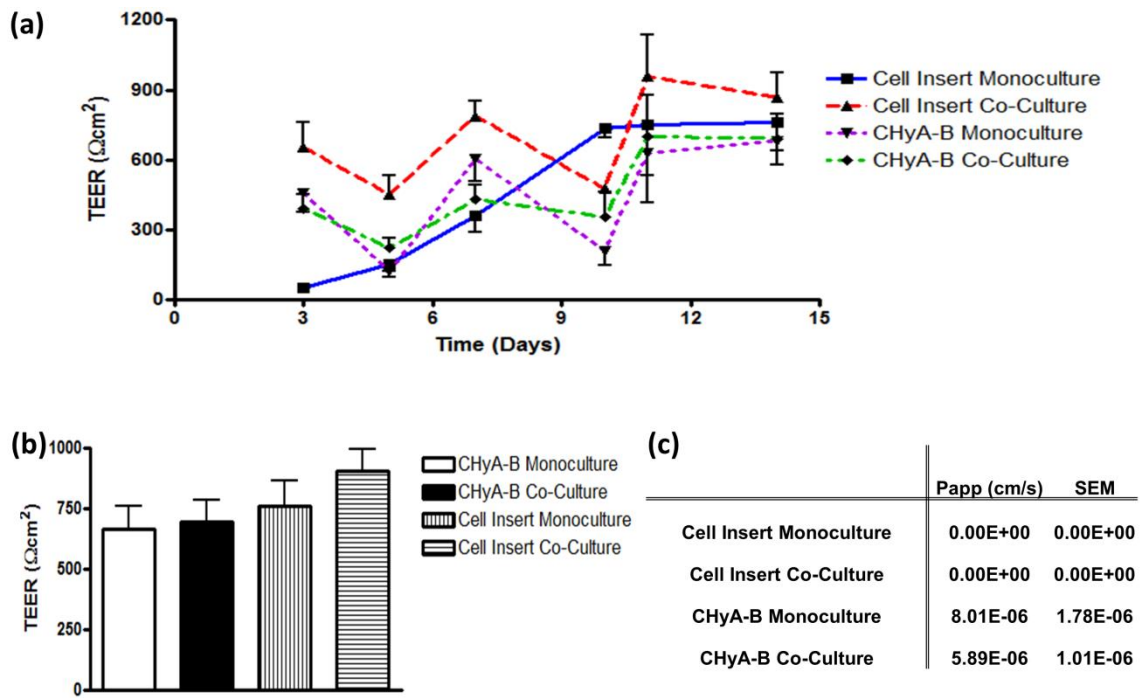


Figure 3.15: Calu-3 epithelial cell barrier integrity in monoculture and co-culture on bilayered collagen-hyaluronate (CHyA-B) scaffolds. Calu-3 cells were either cultured in monoculture or in co-culture with Wi38 fibroblasts for 14 days at an air-liquid interface. Cells were also cultured on cell inserts in monoculture and in co-culture. (a) Transepithelial electrical resistance (TEER) of Calu-3 cells. Results displayed as mean \pm SEM. $n=5$ (performed in triplicate). (b) Average TEER values of Calu-3 epithelial cell barriers following plateau of electrical resistance ($>$ day 10). Results displayed as mean \pm SEM. (c) Apparent permeability coefficient (P_{app}) of fluorescein isothiocyanate-labelled dextran 70 (FITC-dextran) through the Calu-3 cell barrier at Day 14. $n=3$ (performed in triplicate).

3.4. Discussion

In order to tailor the CG scaffold to facilitate epithelial cell culture on a more physiologically-representative alternative to current synthetic respiratory epithelial cell insert culture systems, the major objective of this study was to manufacture a tissue-engineered bilayered collagen-hyaluronate (CHyA-B) scaffold as a template for a 3D tracheobronchial *in vitro* epithelial co-culture model. Specifically, we sought to: (i) fabricate and characterise a CHyA-B scaffold, incorporating film and porous layers for epithelial and fibroblast culture, respectively; (ii) assess Calu-3 bronchial epithelial cell growth and differentiation on the film layer; and (iii) investigate whether the scaffold could support an epithelial-fibroblast co-culture model with physiologically relevant tissue architecture in order to validate the scaffold as a substrate for 3D tracheobronchial epithelial *in vitro* culture systems. The results led to the development of a novel freeze-dried CHyA-B scaffold consisting of a thin 2D film fused to a porous 3D scaffold on which Calu-3 cells were able to grow, express mucin, cilia, and form an epithelial barrier with cell retention at the ALI. Notably, EDAC crosslinking was found to be crucial for maintenance of scaffold structure and epithelial monolayer formation. Finally, co-culture of Calu-3 cells with Wi38 lung fibroblasts was achieved on the CHyA-B scaffold, with fibroblast migration into the porous core to provide a submucosal tissue analogue of the upper respiratory tract and potential for epithelial-fibroblast crosstalk. Taken together, these data demonstrate the potential of the bilayered CHyA-B scaffold as a suitable substrate for a 3D *in vitro* tracheobronchial epithelial model that can be employed for drug discovery and disease-modelling purposes to advance the successful development of novel therapies for the treatment of chronic respiratory disease.

The CHyA-B scaffold was successfully constructed through modification of a lyophilisation technique [255, 275], whereby a CHyA film was manufactured separately, rehydrated and lyophilised with an overlying CHyA suspension to create fusion of the film layer with an interconnected porous 3D sub-layer. This process was reproducible for two different freeze-dry cycles involving a final freezing temperature of -10°C and a custom anneal cycle. The use of different freezing temperatures is known to influence the final pore size in scaffolds [255, 275] and thus the scaffolds were manufactured with two different freezing

temperatures to verify the reproducibility of the fusion process for a range of temperatures. Successful fabrication with both cycles confirmed this reproducibility and highlighted the versatility of the manufacture process to make bilayered scaffolds using different freezing parameters. Ultrastructural analysis of the scaffold confirmed the bilayered architecture, complete with an intact film top-layer spread across a porous sublayer (Fig. 3.2). The two layers of the scaffold adhered to each other during lyophilisation and maintained this connection during physical manipulation and handling in experiments, although analysis of interfacial adhesion strength highlighted that this junction was the weakest structural point within the scaffold (Fig. 3.3a). Regardless, the manufacture process successfully yielded a bilayered scaffold of adequate durability that could act as a blueprint to produce a 3D iteration of the tracheobronchial tissue structure.

Further analysis of the mechanical properties of the CHyA-B scaffold showed that the inclusion of the film layer increased substrate stiffness, particularly in combination with EDAC crosslinking (Fig. 3.3b). Uni-axial, unconfined compressive analysis of CHyA-B and single-layer fully porous CHyA scaffolds revealed that the presence of the film layer increased the compressive modulus from 1.2kPa in CHyA scaffolds to 1.7-1.9kPa in CHyA-B scaffolds, with non-significant variations seen between the methods of CHyA-B freeze-drying. Previous studies have indicated that compressive mechanical properties modulate cellular responses and lineage specification in stem cells through mechanical feedback [274, 277], and research within our own group has indicated that the scaffold stiffness can influence the osteogenic and chondrogenic potential of rat MSCs cultured on CHyA scaffolds [299]. In the case of this study, however, fibroblasts were used as the secondary cell type for co-culture as opposed to a multipotent stem cell population, due to their prominent use in other respiratory models [60, 100]; thus, the risk of osteogenic induction as a result of a significantly stiffer scaffold was not relevant. Indeed, given the contractile behaviour of fibroblasts in CG matrices [302], stiffer scaffolds could be of greater benefit as they are more resistant to cell-mediated contraction [306].

The third phase of CHyA-B scaffold characterisation analysed the mean pore size and porosity of the porous sub-layer (Fig. 3.4). Two lyophilisation cycles were performed in CHyA-B manufacture to examine the effect, if any, of the film layer on

pore size and porosity. The results indicated that the sub-layer had a homogenous porous structure that was amenable as a framework for 3D co-culture with epithelia. Inclusion of the film layer gave mean pore diameters of 80µm and 70µm with anneal and -10°C cycles, respectively (Fig. 3.4a). The inclusion of a film layer did not significantly alter the scaffold pore size, with no significant difference observed between bilayered scaffolds and fully-porous scaffolds manufactured using the same anneal cycle. Previous work carried out by our group has indicated that the optimal mean pore size of a porous biomaterial depends on a compromise between sufficiently small enough pores to increase the surface area for cell attachment [256] and sufficiently large enough pores to allow for cell migration and nutrient flow [276]. This ideal pore size can vary from one cell type to another, and the optimal pore diameter for this fibroblast cell line has not been reported to date. Therefore, the anneal cycle was selected as the fabrication method for CHyA-B co-culture studies as data with a pre-osteoblast cell line indicated that larger pores increase cell viability and migration as culture time periods progress [276]. Moreover, while both cycles produced highly porous materials (Fig. 3.4b), the anneal cycle gave a more homogenous distribution of pores (Fig. 3.4c-3.4f), reinforcing the decision to manufacture scaffolds by this method for co-culture experiments with fibroblasts.

Following the characterisation of the CHyA-B scaffold and the identification of suitable fabrication parameters, the second objective of this study focused on the analysis of the ability of the scaffold to support the growth and differentiation of the Calu-3 bronchial epithelial cell line. Histological analysis showed that EDAC crosslinking of CHyA-B scaffolds was necessary for epithelial monolayer formation and cell retention at the ALI. The formation of an epithelial monolayer was only observed in the stiffer scaffolds. In the absence of EDAC crosslinking, cells tended to stay in clusters on the film layer (Fig. 3.5a). The Calu-3 monolayer observed at day 14 on stiffer CHyA-B scaffolds persisted through longer culture periods of 21 and 28 days (Fig. 3.5b), complete with a cobblestone morphology at the latter time point that is the hallmark of a confluent epithelial monolayer. It has been previously shown that EDAC crosslinking improves osteoblast cell numbers and distribution within collagen-GAG scaffolds [274], though at present, the cellular mechanism behind why a stiffer film facilitates epithelial monolayer formation is unknown. On

the other hand, in the absence of EDAC crosslinking, the porous underside of CHyA-B samples contracted following prolonged incubation in cell culture medium, leading to gradual dissociation from the film layer and loss of biomaterial integrity by day 21. EDAC crosslinking did not increase the strength of connection between the two scaffold layers, as indicated by interfacial adhesion strength analysis (Fig. 3.3a); on the contrary, the stiffer scaffold appeared to exhibit lower adhesion strength prior to failure than in non-EDAC-crosslinked CHyA-B scaffolds, although this was non-significant ($p=0.07$). Therefore, this finding suggests that the EDAC crosslinking step maintains CHyA-B scaffold integrity by reducing contraction of the porous layer, rather than by increasing the strength of interaction between scaffold layers. Taken together, these data collectively show that EDAC crosslinking is pivotal for the maintenance of the bilayered structure of CHyA-B in cell culture and contributes to epithelial monolayer formation, validating the EDAC-crosslinked CHyA-B scaffold as an effective substrate for the culture of a viable bronchial cell line as part of an *in vitro* model.

Having established EDAC-crosslinked CHyA-B scaffolds as the substrate of choice for Calu-3 epithelial culture, the study subsequently assessed Calu-3 differentiation prior to co-culture. The first differentiation marker analysed was the glycoprotein MUC5AC, a substantial component of the respiratory mucus coating and an important indicator of mucociliary epithelial cell differentiation [286, 307]. Culture on the CHyA-B scaffold had a direct effect in increasing and maintaining elevated MUC5AC gene transcription at days 7, 14 and 21 relative to the standard cell insert culture (Fig. 3.9a). Importantly, the CHyA-B scaffold directly increased MUC5AC gene expression relative to the standard cell insert culture that is normally used to induce mucus secretion from Calu-3 cells, highlighting the effect of ECM components on epithelial cell response. In line with findings from Calu-3 culture on CG scaffolds in Chapter 2, this increase in expression in MUC5AC was also observed to increase over time on CHyA-B scaffolds between days 7 and 21 (Fig. 3.10a). The presence of hyaluronate might be responsible for these effects, as has been observed elsewhere with culture on hyaluronan-derivative films [167]. Of course, collagen also increases mucus secretion from tracheobronchial epithelial cells [73] and thus the CHyA co-polymer scaffold is a useful substrate for such airway epithelial cultures.

The increased expression of MUC5AC mRNA translated through to greater secretion of the glycoprotein in scaffold monoculture at day 14 than that from cell insert monoculture (Fig. 3.6). Respiratory mucus has a prominent role in forming a defensive barrier in the respiratory tract and can hinder the delivery of aerosolised therapeutics to both the tracheobronchial epithelium itself and their transit down the airways to the alveolar region for systemic drug delivery [308]. Indeed, the effect of secreted mucins on efficacious respiratory drug delivery has become even more pertinent in chronic disorders that have a hypersecretory phenotype like asthma, bronchitis and CF [9, 11, 291]. In this regard, the ability of CHyA-B scaffolds to induce greater mucus secretion could therefore be of great value for drug transport assays and disease modelling. Overall, CHyA-B scaffolds were validated as a substrate to support functional mucus expression from an airway epithelium.

Calu-3 cells cultured on CHyA-B scaffolds also expressed the tight junction protein ZO-1, indicating the formation of an epithelial barrier layer on the scaffold substrate and differentiation of the Calu-3 cells. Scaffold culture exhibited a non-significant upregulation of ZO-1 gene expression compared to that of the conventional cell insert culture at days 7 and 14, suggesting a trend of increased expression of this barrier protein (Fig. 3.9b). Immunofluorescent detection of ZO-1 visualised the intercellular mesh-like network of the protein that is characteristic of its distribution in epithelial monolayers (Fig. 3.7; [53]). Furthermore, the distribution of the F-actin counterstain observed on the cell's circumference reinforced the hypothesis of an epithelial barrier formation (Fig. 3.6a); such localisation to the cell periphery and affiliation with ZO-1 is recognised as a core component of barrier integrity [309]. These data, coupled with the SEM images of the confluent monolayer (Fig. 3.5b), emphasise the ability of the CHyA-B scaffolds to facilitate the expression of tight junctions typical of a functional tracheobronchial epithelial barrier and contribute to its validation as a model containing an organotypic epithelium.

In addition to displaying a propensity for the induction of mucus secretion and formation of intercellular barrier junctions, the CHyA-B scaffold also had a beneficial effect on the expression of cilia in Calu-3 cells. Cilia are an integral component of the mucociliary escalator in the respiratory tract, extending from the

apical epithelial surface to beat in a metachronal pattern and remove particulates and debris from the airways [285], and are thus an important feature of a fully-functional tracheobronchial epithelium. Analysis of expression of FOXJ1, a master regulator of motile ciliogenesis [285, 296], revealed that CHyA-B scaffolds upregulated this gene by a similar order of magnitude to that in Calu-3 cells on cell inserts, but in half the amount of time (Fig. 3.9c, 3.10c). Ciliogenesis is one feature of respiratory epithelial cell culture that typically takes between 21-28 days [60] and so the finding of an early upregulation of FOXJ1 is noteworthy. The upregulation suggests an earlier promotion of ciliogenesis in bronchial epithelial cells cultured on CHyA-B scaffolds and therefore, more rapid development of an *in vitro* model for subsequent toxicity testing or disease studies. In the case of Calu-3 cells, the ciliation was assessed after 14 days in culture in line with the literature [53] and at this time point, the microvilli structures observed in scaffold monoculture were longer than those in cell insert monoculture (1µm vs 0.5µm) and thinner in shape (Fig. 3.8). Neither culture system produced fully-elongated cilia, though this might be due in part to the inherent limited ciliary potential of the Calu-3 cell line. Discrepancies between primary tracheobronchial and Calu-3 transcriptional profiles have been reported [310] which could culminate in the absence of other co-factors needed for complete ciliation. Nevertheless, in this chapter, the improved inductive effect provided by CHyA-B scaffolds in comparison to cell insert culture was clearly demonstrated.

This chapter sought to not only investigate whether the scaffold could support a bronchial epithelial cell line in monoculture, but also to develop an epithelial-fibroblast co-culture model with improved physiological tissue architecture and validate the scaffold as a substrate for 3D airway epithelial *in vitro* culture. To this end, Calu-3 cells were cultured together with Wi38 fibroblasts on CHyA-B scaffolds in order to establish whether the fibroblasts could migrate into the porous scaffold towards the epithelial monolayer. Histological analysis provided evidence of Wi38 attachment and cellular migration into the scaffold towards the epithelial monolayer (Fig. 3.11). While the native ECM of the trachea and bronchi is more densely packed than the submucosal framework present in CHyA-B in its cell-free form, the CHyA-B scaffold provides an improved 3D representation of the native ECM for 3D co-culture than the flat 2D nature of cell inserts and holds greater

potential for recapitulation of the native tissue. CG scaffolds have consistently demonstrated their ability to support the attachment, proliferation and functionalisation of such cells in a 3D environment [276, 298-300, 302], combined with suitable porosity to allow for cellular migration into the scaffold and nutrient flow [276]. Moreover, the porous nature can provide suitable void space for fibroblasts to fill with their own deposited ECM matrix following anchorage to the scaffold struts [311]. In summary, the CHyA-B scaffold's architecture can potentially facilitate epithelial-fibroblast crosstalk in addition to mimicking the *in vivo* tracheobronchial arrangement of mesenchymal cells embedded in the ECM beneath the epithelial monolayer.

Having developed an epithelial-fibroblast co-culture model using CHyA-B scaffolds with favourable cell distribution, analysis of the three markers of Calu-3 differentiation was also performed in scaffold co-cultures to validate the maintenance, or potentially the improvement, of expression of functional biomarkers. This analysis demonstrated that the three principal hallmarks of a functional tracheobronchial barrier- mucus secretion, barrier formation and ciliation- continued to be exhibited by Calu-3 cells (Fig. 3.12-3.14). Of particular note, MUC5AC glycoprotein expression was lower than that observed in scaffold monoculture (Fig. 3.12), although still greater in intensity than that observed in cell insert mono-culture and co-culture. This result indicates that both the scaffold biomaterial and the Wi38 fibroblasts modulate epithelial mucin expression in the CHyA-B co-culture system, with the resultant MUC5AC levels representing a culmination of signalling events regulated by material and cell factors. The addition of fibroblasts to cell insert culture, on the other hand, did not alter MUC5AC expression by Calu-3 cells. A recent study by Harrington et al. reported that the inclusion of lung fibroblasts to Calu-3 culture on an electrospun polyethylene terephthalate scaffold (PET) scaffold induced apical MUC5AC expression [231]. Interestingly, no MUC5AC secretion was detected in Calu-3 monoculture on electrospun PET which contrasts with the data presented here of PET cell inserts (Fig. 3.6c, 3.12c). This difference could be a result of the substrate topography of the electrospun material. Nevertheless, the CHyA-B data show that both the natural polymeric scaffold and fibroblast factors influence mucus secretion in our model.

Immunofluorescent staining of ZO-1 did not discern any difference in ZO-1 staining in CHyA-B mono- and co-culture systems (Fig. 3.13). This was reflected in the quantitative barrier analysis using TEER (Fig. 3.15a, 3.15b). Scaffold TEER values were lower than those obtained for cell insert cultures, albeit non-significantly. Co-culture increased the TEER with scaffolds and cell inserts relative to monoculture, as has been regularly observed in the literature [60, 231, 305]. Data on TEER values from *ex vivo* human lung tissue have not been reported to date but analysis of rabbit tissue and human primary epithelial cell cultures indicate a range of 300-650 Ωcm^2 (reviewed in [54]). Thus, the lower TEER values obtained from cell barriers following plateau on CHyA-B in mono-culture and co-culture (662 Ωcm^2 and 694 Ωcm^2 , respectively) offer a closer physiological reflection than those from cell insert mono- and co-culture (756 Ωcm^2 and 902 Ωcm^2 , respectively). In all cases, analysis of paracellular permeability using FD70 confirmed that all epithelial barriers formed were suitably robust (Fig. 3.15c) and further justified the hypothesis that CHyA-B scaffolds displayed a positive effect on the organotypic culture of a physiologically relevant *in vitro* tracheobronchial epithelium.

While this chapter has successfully achieved its objectives and developed a novel scaffold and co-culture system for 3D *in vitro* modelling of the upper respiratory tract, it suffers from one principal limitation- the use of a bronchial epithelial cell line instead of primary human tracheobronchial epithelial cells. It is well-known that current bronchial cell lines do not exhibit the exact phenotypic traits to that of pseudostratified columnar epithelium *in vivo* [54]. Differences have also been noted between cell line and primary cell cultures in toxicological response to known carcinogens [55]. Accordingly, Chapter 4 investigates the development of a primary tracheobronchial cell co-culture system with the CHyA-B scaffold to further recapitulate the *in vivo* anatomy and physiology in this 3D model. Nevertheless, it is advantageous to use a standardised cell line for the development of a novel tissue-engineered scaffold design with a new application. Firstly, the risk of confounding results related to donor variability is avoided at the early stages of development; this recommendation is in line with guidance for the development of novel assays with respiratory cells [52]. Secondly, respiratory cell lines such as Calu-3 cells remain of great interest for respiratory drug development [54, 312] and have previously been investigated for other synthetic constructs [231]. It is

therefore of interest as the choice of epithelial cell in its own right and this study has added to our understanding by evaluating the positive influence of a naturally-derived polymeric scaffold on the differentiation of the Calu-3 cell line towards a more pseudostratified tracheobronchial epithelium with the associated hallmark *in vivo* functional features.

3.5. Conclusion

In conclusion, this chapter has developed a bilayered collagen-hyaluronate scaffold as a 3D *in vitro* model of the tracheobronchial region of the respiratory tract. This scaffold combines a film layer for epithelial cell culture and a porous 3D sub-layer for co-culture with other cell types. The scaffold demonstrated the ability to support the growth and differentiation of a bronchial cell line in addition to epithelial-fibroblast co-culture. This biomaterial can act as a customisable platform technology to generate a physiologically-representative 3D system and will be utilised for the development of a primary tracheobronchial epithelial-fibroblast *in vitro* model in Chapter 4. Overall, CHyA-B scaffolds are a promising tool that can open new avenues to advance our understanding of airway epithelial regulation, dysregulation in disease and subsequent drug discovery and delivery for effective treatment.

Chapter 4: The development of a 3D primary tracheobronchial epithelial cell-derived co-culture system for applications in respiratory *J b j* modelling

4.1.	Introduction	144
4.2.	Materials and Methods	146
4.2.1.	<i>Bilayered collagen-hyaluronate (CHyA-B) scaffold fabrication</i>	146
4.2.1.1.	<i>CHyA-B scaffold manufacture</i>	146
4.2.1.2.	<i>Chemical crosslinking</i>	146
4.2.2.	<i>Primary tracheobronchial epithelial cell culture on CHyA-B scaffolds</i>	147
4.2.2.1.	<i>Cell source and culture medium</i>	147
4.2.2.2.	<i>Epithelial cell monoculture</i>	147
4.2.2.3.	<i>Epithelial cell co-culture with fibroblasts</i>	148
4.2.3.	<i>Cell morphology and migration</i>	148
4.2.4.	<i>Primary tracheobronchial epithelial cell differentiation on CHyA-B scaffolds</i>	149
4.2.4.1.	<i>Immunofluorescence</i>	149
4.2.4.2.	<i>Scanning electron microscopy (SEM)</i>	149
4.2.4.3.	<i>Transmission electron microscopy (TEM)</i>	149
4.2.4.4.	<i>Expression of genetic markers of epithelial differentiation</i>	150
4.2.5.	<i>Evaluation of primary tracheobronchial epithelial cell barrier integrity</i>	150
4.2.5.1.	<i>Transepithelial electrical resistance (TEER) measurement</i>	150
4.2.5.2.	<i>Fluorescein isothiocyanate (FITC)-labelled dextran permeability assay</i>	150
4.2.6.	<i>Data analysis</i>	151
4.3.	Results	152
4.3.1.	<i>Primary tracheobronchial epithelial cell monoculture on CHyA-B scaffolds</i> ..	152
4.3.1.1.	<i>Cell morphology and migration</i>	152
4.3.1.2.	<i>Mucin expression</i>	153
4.3.1.3.	<i>Tight junction formation</i>	154
4.3.1.4.	<i>Epithelial ciliation</i>	155
4.3.1.5.	<i>Epithelial ultrastructure- SEM</i>	156
4.3.1.6.	<i>Epithelial ultrastructure- TEM</i>	157
4.3.2.	<i>Primary tracheobronchial epithelial cell co-culture with fibroblasts on CHyA-B scaffolds</i>	158
4.3.2.1.	<i>Cell morphology and migration</i>	158
4.3.2.2.	<i>Mucin expression</i>	160

4.3.2.3. <i>Tight junction formation</i>	161
4.3.2.4. <i>Epithelial ciliation</i>	163
4.3.2.5. <i>Epithelial ultrastructure- SEM</i>	164
4.3.2.6. <i>Epithelial ultrastructure- TEM</i>	166
4.3.3. <i>Expression of genetic markers of epithelial differentiation</i>	167
4.3.4. <i>Evaluation of primary tracheobronchial epithelial cell barrier integrity</i>	168
4.3.4.1. <i>TEER measurement</i>	168
4.3.4.2. <i>FITC-labelled dextran permeability assay</i>	168
4.4. <i>Discussion</i>	170
4.5. <i>Conclusion</i>	177

4.1. Introduction

A bilayered collagen-hyaluronate (CHyA-B) scaffold has been successfully developed as a three-dimensional (3D) substrate for an *in vitro* co-culture model using a bronchial epithelial cell line (Chapter 3). However, in order to provide a more complete physiological iteration of the tracheobronchial region of the respiratory tract, primary epithelial cells should ideally be utilised in scaffold culture [313]. Calu-3 cells were a useful cell line to analyse on CHyA-B scaffolds in the first instance due to their wide use in pharmaceutical industry and academia for respiratory drug development, as well as their similarity to the *in vivo* upper respiratory epithelium [54, 312], but inherent differences inevitably exist between these immortalised cells and primary cells. For example, Pezzulo et al. have reported differences in Calu-3 cell transcriptional profiles compared to *in vivo* airway epithelium, while another toxicological study by Balharry and colleagues has highlighted discrepancies between cell line and primary cell cultures in toxicological response to known carcinogens [55, 310]. Accordingly, the inclusion of primary tracheobronchial epithelial cells on CHyA-B scaffolds in combination with co-cultured lung fibroblasts has the potential to provide the most organotypic *in vitro* model.

The native tracheobronchial epithelium is a pseudostratified cell layer of three main cell types- ciliated epithelial cells, goblet cells and basal cells [15]. Columnar ciliated cells account for greater than 50% of the epithelial cells and are the most predominant cell type [6]. In addition to contributing to the protective epithelial barrier in the respiratory tract, these cells are responsible for the clearance of mucus secretions towards the throat by the metachronal beating of cilia [285]. The mucus secretions are provided primarily by the goblet cells and submucosal glands; they serve to provide an extra physical, diffusional and antibacterial layer of protection to the airways [307, 314]. The function of the basal cell has conventionally been to facilitate anchorage of the columnar epithelial cells to the basement membrane [115], though more recent research has characterised it as a major progenitor cell of the tracheobronchial region of the airways [109, 110, 315]. From the perspective of developing an organotypic *in vitro* model of the conducting region of the respiratory tract, the presence of these three cell types would be ideal for representation of the physiological *milieu*. Of course, as highlighted in

previous chapters with the Calu-3 cell line, the generation of a robust epithelial barrier of suitable integrity is essential from a respiratory drug development or disease modelling perspective and must also be considered with primary tracheobronchial epithelial cell culture.

In this study, normal human bronchial epithelial (NHBE) cells were selected as the primary tracheobronchial epithelial cell for evaluation of 3D culture on CHyA-B scaffolds. Primary airway cells are typically isolated from lung tissue [70, 316] or nasal turbinates [246, 317]. The cells sourced from a commercial supplier in this chapter were obtained from the epithelial lining of airways above the bifurcation of the trachea. These cells can provide a mixed ciliated and goblet cell culture model of the airway (reviewed in [54]) and as such are a suitable choice of primary cell to investigate the principal features of the pseudostratified epithelium in monoculture on CHyA-B scaffolds.

This chapter also investigated an epithelial-fibroblast co-culture model on CHyA-B scaffolds. Several respiratory co-culture methods have been established using cell inserts that have demonstrated a more organotypic epithelial phenotype [60, 68, 318]. However, there is an overall consensus in the literature that the introduction of an extracellular matrix (ECM) analogue into the co-culture environment could further enhance cell culture, cell-cell signalling and functionality [83]. Tissue-engineered co-culture models of primary tracheobronchial epithelial cells with fibroblasts have almost exclusively focused on the use of type I collagen hydrogels as the ECM mimic [100, 192, 193, 198, 199, 202]. CHyA-B scaffolds, on the other hand, are a co-polymer of type I collagen and hyaluronate- two components that have been shown to individually boost primary respiratory epithelial differentiation [73, 294]- and the bilayered structure demonstrates more robust mechanical and handling properties than relatively weak hydrogels (Chapter 3; [207]). Therefore, this substrate has the potential to improve upon the current cell insert and tissue-engineered standards for *in vitro* models.

Thus, the overall objective of Chapter 4 was to develop a 3D primary tracheobronchial epithelial cell-derived co-culture system for application in respiratory *in vitro* modelling using CHyA-B scaffolds. Specifically, two aims were pursued:

1. To assess the feasibility of the CHyA-B scaffold to act as a 3D substrate for the growth and differentiation of NHBE primary respiratory epithelial cells in monoculture.
2. To develop a 3D co-culture system of NHBE epithelial cells and Wi38 lung fibroblasts and to validate this system by analysis of markers of differentiation and epithelial barrier integrity.

4.2. Materials and Methods

4.2.1. Bilayered collagen-hyaluronate (CHyA-B) scaffold fabrication

4.2.1.1. CHyA-B scaffold manufacture

CHyA-B scaffolds were fabricated by freeze-drying CHyA films in combination with a CHyA suspension as described in Section 3.2.1. [255]. A suspension of 0.5% microfibrillar bovine tendon collagen (Integra Life Sciences, Plainsboro, NJ) and 0.044% hyaluronate sodium salt derived from *Streptococcus equi* (Sigma-Aldrich, Arklow, Ireland) in 0.5M acetic acid was blended, degassed and cast onto a 12.5x12.5cm² polytetrafluoroethylene (PTFE) plate overnight to produce a thin transparent CHyA copolymer film. The film was subsequently rehydrated in 0.5M acetic acid for two hours, cut to fit onto the base of a 6x6cm² stainless steel grade 304 SS pan and covered with 4ml of CHyA slurry before the combination was freeze-dried using a customised lyophilisation method [275]. After freeze-drying, the scaffolds were crosslinked and sterilised using a dehydrothermal (DHT) process at 105°C for 24 hours in a vacuum oven at 50mTorr (VacuCell 22, MMM, Germany) [283].

4.2.1.2. Chemical crosslinking

DHT-crosslinked CHyA-B scaffolds were chemically crosslinked using 1-ethyl-3-(3-dimethylaminopropyl)carbodiimide hydrochloride (EDAC; Sigma) in combination with N-hydroxysuccinimide (NHS; Sigma) as described in Section 2.2.1.2 [274, 278]. The scaffolds were then washed three times with Dulbecco's phosphate buffered saline (DPBS; Sigma) to remove any residual cytotoxic product and stored in DPBS at 4°C until use. All steps were performed under sterile conditions.

4.2.2. Primary tracheobronchial epithelial cell culture on CHyA-B scaffolds

4.2.2.1. Cell source and culture medium

NHBE cells were used as the source of primary tracheobronchial epithelial cells (Lonza, Basel, Switzerland). The cells were cultured in bronchial epithelial growth medium (BEGM; Lonza) which consisted of bronchial epithelial basal medium (BEBM) supplemented with bovine pituitary extract (BPE), hydrocortisone, epidermal growth factor (EGF), adrenaline, transferrin, insulin, all-*trans* retinoic acid (atRA), triiodothyronine (T₃), gentamicin and amphotericin-B. Concentrations of the supplements in the supplement were withheld by Lonza. NHBE cells were sourced from two donors for experiments (Lot numbers 0000312626 and 0000326160) except for the electron microscopy experiments, where donor 0000326160 was used only. Cells were used at passage 3. The Wi38 human embryonic lung fibroblast cell line (ATCC, Middlesex, UK) was used for co-culture experiments. These cells were cultured in Eagle's minimal essential medium (Sigma) supplemented with 10% foetal bovine serum (Biosera, Ringmer, UK), 2mM L-glutamine (Sigma), 26mM sodium bicarbonate (Sigma), 100U/ml penicillin/streptomycin (Sigma) and 1mM sodium pyruvate (Sigma). This was referred to as Wi38 medium. Cells were used between passages 21-26. All cells were cultured at 37°C and 5% CO₂ under a humidified atmosphere. Unless otherwise stated, all cell culture incubation steps were also performed in these conditions.

4.2.2.2. Epithelial cell monoculture

The ability of CHyA-B scaffolds to support the growth and differentiation of the NHBE primary cells in monoculture was assessed under air-liquid interface (ALI) culture conditions. A customised cell culture system was developed using the frame of a Snapwell® cell insert (Corning Costar, NY) as described in Section 3.2.3.2. The scaffold samples were seeded with 2.5×10^5 NHBE cells/cm² into the apical compartment and an ALI was introduced 3 days later with subsequent basolateral feeding for the remainder of the culture period using a 1:1 mixture of BEGM:Wi38 media.

NHBE primary cells were also seeded onto 12mm Transwell® cell inserts (Corning Costar) for comparison with scaffold culture. On the day before NHBE cell

seeding, the cell inserts were coated with rat-tail type I collagen (Sigma) at a density of $10\mu\text{g}/\text{cm}^2$. On the following day, the cell inserts were seeded with 2.5×10^5 NHBE cells/ cm^2 as outlined in Section 3.2.3.2 using a 1:1 mixture of BEGM:Wi38 media.

4.2.2.3. Epithelial cell co-culture with fibroblasts

The ability of CHyA-B scaffolds to support the growth and differentiation of the NHBE primary cells in co-culture with Wi38 lung fibroblasts was assessed under ALI culture conditions. CHyA-B scaffolds were seeded using a modification of a previously described method [304], as described in Section 3.2.3.3. The porous sublayer of each scaffold sample was seeded with 6×10^5 Wi38 cells followed by insertion into the Snapwell® system and subsequent seeding with NHBE cells as described in Section 4.2.2.2.

NHBE-Wi38 co-culture was also established on 12mm Transwell® cell inserts for comparison with scaffold culture. Following the collagen-coating of the apical side of the cell insert, they were seeded on the basolateral and apical sides with fibroblasts at a density of 3×10^4 cells/ cm^2 and NHBE cells at a density of 2×10^5 cells/ cm^2 , respectively, as outlined in Section 3.2.3.3.

4.2.3. Cell morphology and migration

Cell-seeded scaffolds were stained with haematoxylin and eosin and fast green (H&E&FG) to observe NHBE epithelial cell distribution on the CHyA-B top-layer and migration of Wi38 into the scaffold sublayer. This was performed as described in Section 3.2.4.1. Briefly, the samples were fixed, processed overnight using an automated tissue processor (ASP300, Leica, Germany) and sectioned using a microtome (Leica RM 2255, Leica). The sections were deparaffinised and stained with H&E&FG prior to dehydration and mounting with DPX (Sigma). Images were captured using an Eclipse 90i microscope and DSRI1 digital camera with NIS Elements Software (Nikon, Japan).

4.2.4. Primary tracheobronchial epithelial cell differentiation on CHyA-B scaffolds

4.2.4.1. Immunofluorescence

Immunofluorescent staining was carried out to detect the presence of three markers of tracheobronchial epithelial differentiation and functionality- MUC5AC, zonula occludens-1 (ZO-1), and β -tubulin IV (BIV). These markers represented mucus production by goblet cells, the formation of tight junctions and ciliation of the epithelial cells, respectively [282, 286, 319]. Immunofluorescence was performed as outlined in Section 3.2.5.1. Briefly, cell-seeded samples were fixed, permeabilised and incubated with 1% bovine serum albumin (BSA; Sigma) in DPBS to preclude non-specific binding of primary antibody. They were then incubated with either 1/100 mouse anti-MUC5AC monoclonal antibody (Abcam, Cambridge, UK), 1/100 rabbit anti-ZO-1 polyclonal antibody (Molecular Probes, Invitrogen, UK), or 1/400 mouse anti-BIV monoclonal antibody (Sigma), followed by incubation with a 1/500 goat anti-mouse Alexafluor®-594 or 1/500 goat anti-rabbit Alexafluor® 488 secondary antibody (Molecular Probes) and counterstaining with 1/500 Alexafluor®-488-labelled or 1/500 TRITC-labelled phalloidin (Sigma) for F-actin, as appropriate. Finally, the samples were mounted in Fluoroshield® with 4', 6-diamidino-2-phenylindole (DAPI; Sigma). Images were captured and analysed using an Axio Examiner.Z1 confocal microscope (Carl Zeiss, Cambridge, UK).

4.2.4.2. Scanning electron microscopy (SEM)

NHBE cells were examined by SEM to analyse the effects of CHyA-B scaffolds and Wi38 co-culture on epithelial barrier formation and ciliation. Cell-seeded scaffolds were fixed in 3% glutaraldehyde, dehydrated in ascending grades of ethanol and dried using supercritical CO₂ in a critical point dryer as outlined in Section 2.2.4.3. The samples were subsequently mounted on aluminium stubs, sputter-coated and imaged using a Tescan Mira XMU scanning electron microscope at 5kV using secondary electron mode, taken at a working distance between 12-18mm.

4.2.4.3. Transmission electron microscopy (TEM)

Analysis of NHBE ciliation on CHyA-B scaffolds was performed by TEM. This was also performed to examine pseudostratification of the epithelial cell layer. Scaffold

samples were fixed, dehydrated, embedded in London Resin (LR) white and sectioned as outlined in Section 3.2.5.2. Images were captured with a Hitachi H-7650 electron microscope (Hitachi, Leixlip, Ireland) operating at 100kV.

4.2.4.4. Expression of genetic markers of epithelial differentiation

The ability of CHyA-B scaffolds to support the differentiation of NHBE primary cells was analysed by quantitative relative gene expression of MUC5AC, ZO-1, and FOXJ1, genetic markers for mucus production, epithelial tight junction formation and ciliation, respectively [282, 285, 286]. Cell-seeded samples were washed with DPBS and the cells in the apical compartment (i.e. the NHBE cells) were lysed in 550 μ l of 0.01% β -mercaptoethanol (Sigma) in RLT lysis buffer (Qiagen, Crawley, UK). 200ng of isolated RNA was reverse transcribed to cDNA and RT-polymerase chain reactions were run as described in Section 2.2.4.4. The expression of mRNA was calculated by the delta-delta Ct ($2^{-\Delta\Delta C_t}$) method relative to the housekeeping gene GAPDH [287].

4.2.5. Evaluation of primary tracheobronchial epithelial cell barrier integrity

4.2.5.1. Transepithelial electrical resistance (TEER) measurement

The integrity of the epithelial barrier formed by NHBE cells cultured on CHyA-B scaffolds was quantified by the measurement of TEER in monoculture and co-culture systems. TEER measurement was performed as described in Section 3.2.6.1. To compare TEER values between groups following a plateau of the measurements [305], the average TEER values from day 11-21 were taken for each group and compared.

4.2.5.2. Fluorescein isothiocyanate (FITC)-labelled dextran permeability assay

The integrity of the epithelial barrier formed by NHBE cells on CHyA-B scaffolds was further assessed through analysis of paracellular transport through the cell layer [53], as outlined in Section 3.2.6.2. Briefly, the samples were incubated with a 500 μ g/ml solution of FITC-labelled dextran of an average molecular weight of 70kDa (FD70) and the apparent permeability coefficient (P_{app}) was calculated using Equation 2, where F is flux (rate of change in cumulative mass transported), A is the surface area available for epithelial cell growth, and C_0 is the initial FD70 concentration in the donor chamber.

$$P_{app} = F \times \left(\frac{1}{A \times Co} \right) \quad (2)$$

4.2.6. Data analysis

Analysis of histological and electron microscopy images, including the measurement of the length of ciliary structures, was performed using the Fiji processing software. Quantitative data obtained were analysed using Microsoft Excel and GraphPad Prism 4.0 Software (GraphPad Software, San Diego, CA). Statistical difference between groups was assessed by 2-way ANOVA with Bonferroni *post hoc* analysis. Each cell-based experiment was performed a minimum of three times (n=3; three biological replicates); the number of technical replicates performed within each experiment is specified under the relevant figures.

4.3. Results

4.3.1. Primary tracheobronchial epithelial cell monoculture on CHyA-B scaffolds

4.3.1.1. Cell morphology and migration

CHyA-B scaffolds and cell inserts were seeded with NHBE cells, cultured for 28 days and subsequently stained with H&E&FG to observe NHBE cell distribution. Histological analysis revealed that NHBE cells formed an epithelial layer along the film top-layer that was maintained over the culture period, with no cellular migration into the porous sublayer (Fig. 4.1a). Cell morphology was the same as that of NHBE cells cultured on cell inserts (Fig. 4.1b), with all cells adopting a flat, spread and squamoid morphology on both substrates. These data indicated that CHyA-B scaffolds supported NHBE adhesion and growth in monoculture over the culture period, albeit with the absence of a pseudostratified columnar morphology.

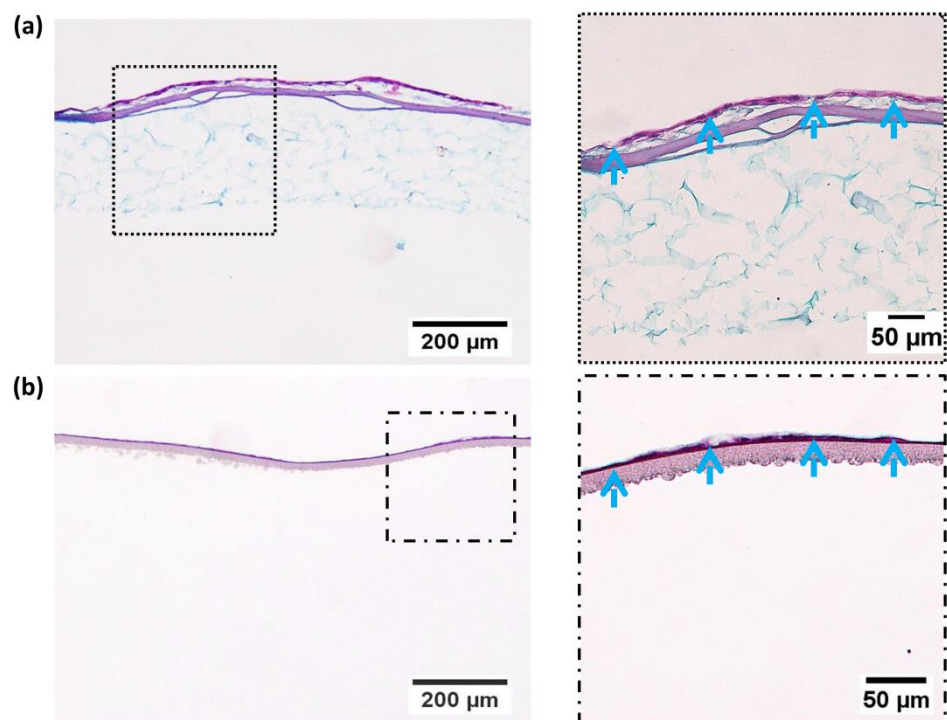


Figure 4.1: Primary tracheobronchial epithelial cell monoculture on bilayered collagen-hyaluronate (CHyA-B) scaffolds. NHBE cells were cultured either on (a) CHyA-B scaffolds or on (b) cell inserts at an air-liquid interface for 28 days. Higher magnification images (boxes) showed the formation of a squamous monolayer along the film top-layer or cell insert membrane (blue arrows). Representative haematoxylin and eosin and fast green staining visualised scaffolds as a light-blue colour with a pink-purple film layer and cells appeared as pink-purple with darker nuclei. n=3.

4.3.1.2. Mucin expression

The ability of the CHyA-B scaffolds to support primary tracheobronchial epithelial cell differentiation was assessed by analysis of MUC5AC glycoprotein expression, a marker of mucus-secreting goblet cells [320]. Immunofluorescent z-stack images detected the presence of MUC5AC on the apical side of the NHBE cells at day 28 in both scaffold and cell insert monoculture (Fig. 4.2). MUC5AC distribution was patchy across the epithelial layer in both groups (Fig. 4.2a, Fig. 4.2c) with no discernible increase in the presence of glycoprotein between them, as emphasised by maximum intensity projection analysis (Fig. 4.2b, 4.2d). These data indicated that a sub-population of NHBE cells matured into goblet cells on CHyA-B scaffolds and that the degree of differentiation was equivalent to conventional cell insert culture.

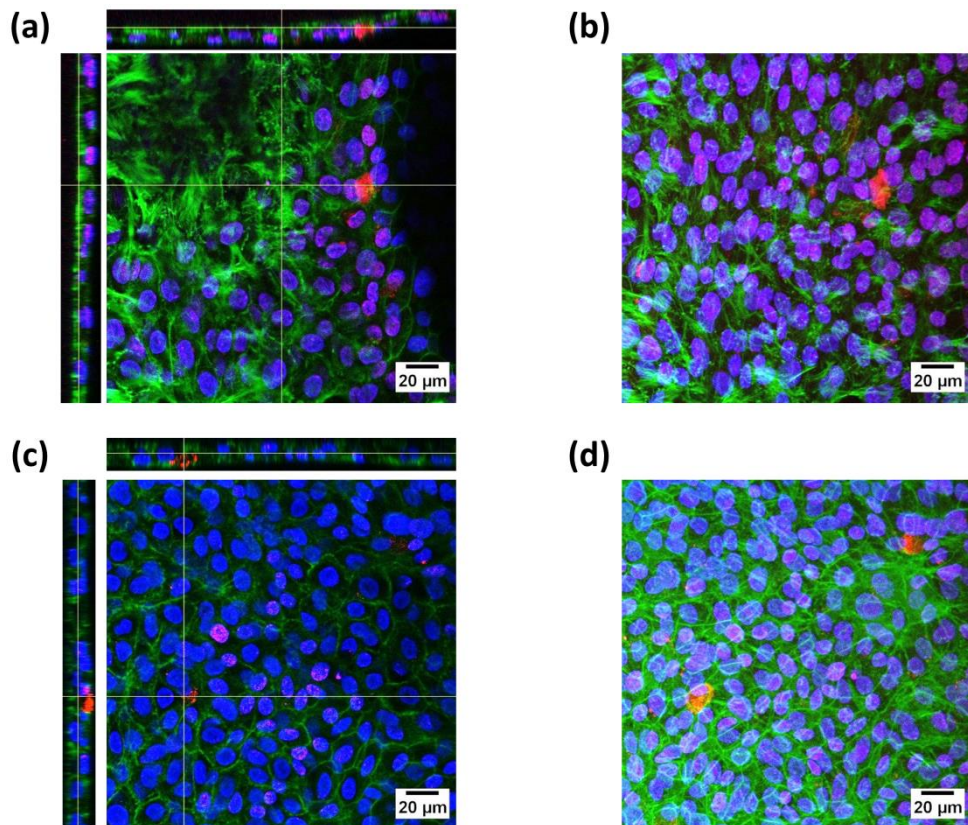


Figure 4.2: MUC5AC expression on primary tracheobronchial epithelial cells in monoculture on bilayered collagen-hyaluronate (CHyA-B) scaffolds. NHBE cells were cultured either on (a, b) CHyA-B scaffolds or on (c, d) cell inserts at an air-liquid interface for 28 days. (a, c) Representative z-stack images display apical MUC5AC secretion (red) on top of cells counterstained for nuclei (blue) and F-actin (green). (b, d) Maximum intensity projections of MUC5AC expression reconstructed from z-stacks. n=3.

4.3.1.3. Tight junction formation

The ability of the CHyA-B scaffolds to support primary tracheobronchial epithelial cell tight junction formation was assessed by analysis of ZO-1 expression, a protein regulating paracellular permeability in epithelia [282]. Bands of ZO-1 were detected across the entire cell layer on CHyA-B scaffolds that were concentrated on the apical side of epithelial cells, reflecting epithelial polarisation and correct intracellular localisation (Fig. 4.3a). ZO-1 expression on CHyA-B scaffolds matched that of cell insert culture (Fig. 4.3b, 4.3d); interestingly, the more widely distributed ZO-1 borders on CHyA-B scaffolds indicated that the adhered NHBE cells were stretched on the film top-layer more than on the collagen-coated polymeric membrane. Nevertheless, the positive detection of ZO-1 suggested that CHyA-B facilitated the formation of tight junctions between primary NHBE cells.

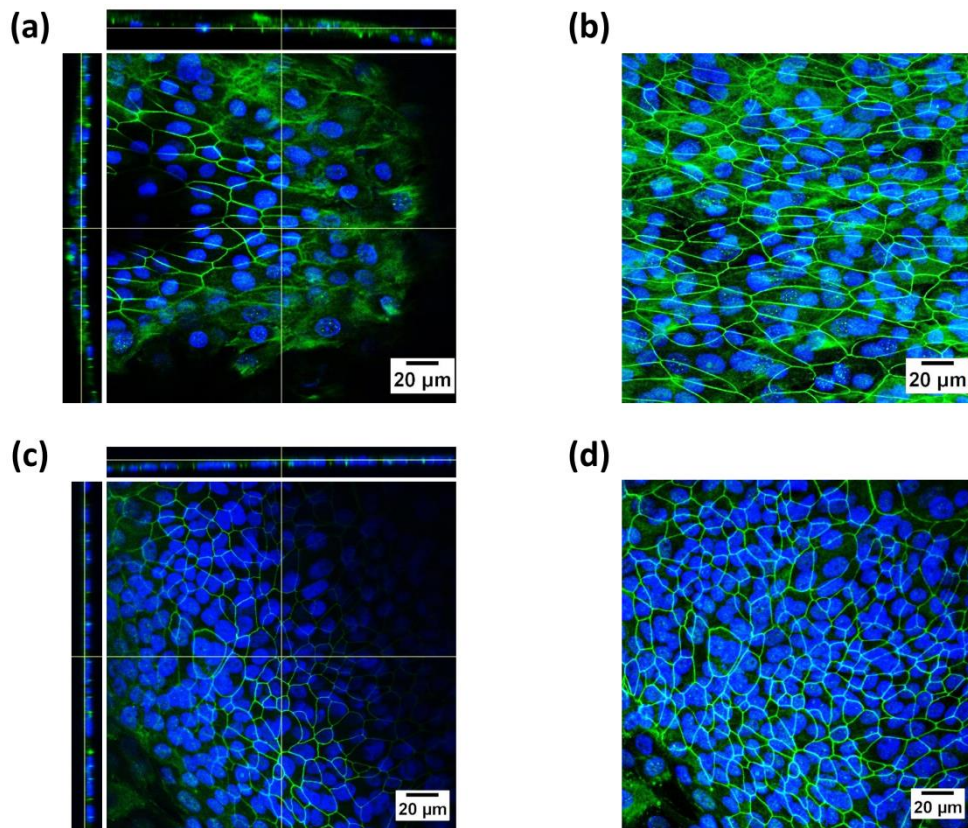


Figure 4.3: ZO-1 expression on primary tracheobronchial epithelial cells in monoculture on bilayered collagen-hyaluronate (CHyA-B) scaffolds. NHBE cells were cultured either on (a, b) CHyA-B scaffolds or on (c, d) cell inserts at an air-liquid interface for 28 days. (a, c) Representative z-stack images display ZO-1 bands (green) with punctate apical concentrations around the borders of cells counterstained for nuclei (blue). (b, d) Maximum intensity projections of ZO-1 expression reconstructed from z-stacks. n=3.

4.3.1.4. Epithelial ciliation

The third assessment of primary tracheobronchial epithelial cell differentiation on CHyA-B scaffolds examined the expression of BIV, a cytoskeletal protein present in motile cilia [60]. Immunofluorescent analysis did not detect BIV in NHBE cells on either CHyA-B scaffolds or cell inserts, indicating the absence of ciliation (Fig. 4.4). Faint punctate expression of yellow fluorescence was rarely observed in cell insert culture (Fig. 4.4.c), though these spots were very small to represent cilia and were not located on the apical side of cells. The phalloidin counterstain for F-actin microfilaments revealed that the epithelial cells were stretched across both substrates, suggesting that they did not adopt a columnar morphology that is typical of ciliated cells. In summary, these data indicate that NHBE differentiation towards a pseudostratified ciliated phenotype did not occur in monoculture.

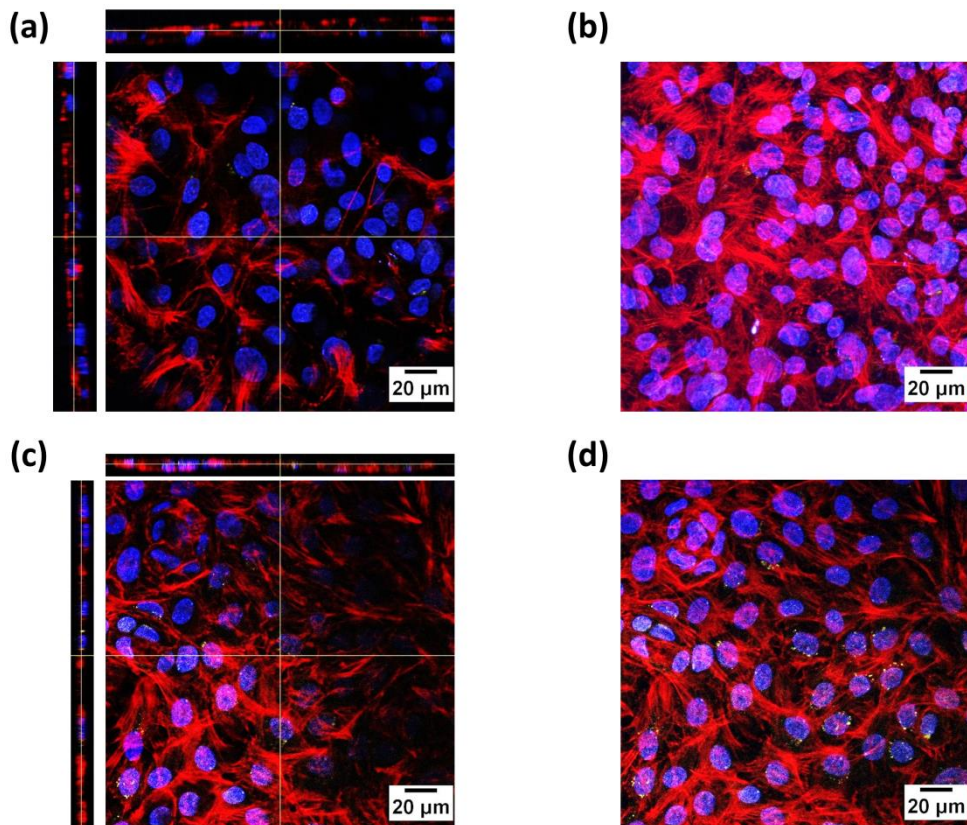


Figure 4.4: β -tubulin IV (BIV) expression on primary tracheobronchial epithelial cells in monoculture on bilayered collagen-hyaluronate (CHyA-B) scaffolds. NHBE cells were cultured either on (a, b) CHyA-B scaffolds or on (c, d) cell inserts at an air-liquid interface for 28 days. (a, c) Representative z-stack images display an absence of apical expression of BIV (yellow) on top of cells counterstained for nuclei (blue) and F-actin (red). (b, d) Maximum intensity projections of BIV expression reconstructed from z-stacks. n=3.

4.3.1.5. Epithelial ultrastructure- SEM

NHBE cells were examined by SEM to capture epithelial barrier formation and ciliation, if present, at high magnification. Image analysis confirmed that the primary epithelial cell layer did not adopt a cobblestone conformation typical of the *in vivo* tracheobronchial region (Fig. 4.5). Instead, NHBE cells were widely spread across the CHyA-B scaffold with occasional overlapping of the confluent epithelial layer (Fig. 4.5a). While intercellular connections had formed, the cell surfaces were smooth with no ciliation (Fig.4.5b). A similar cell shape and distribution was seen with cell insert culture (Fig. 4.5c, 4.5d). This analysis indicated that NHBE cell commitment to a pseudostratified ciliated lineage did not occur in monoculture.

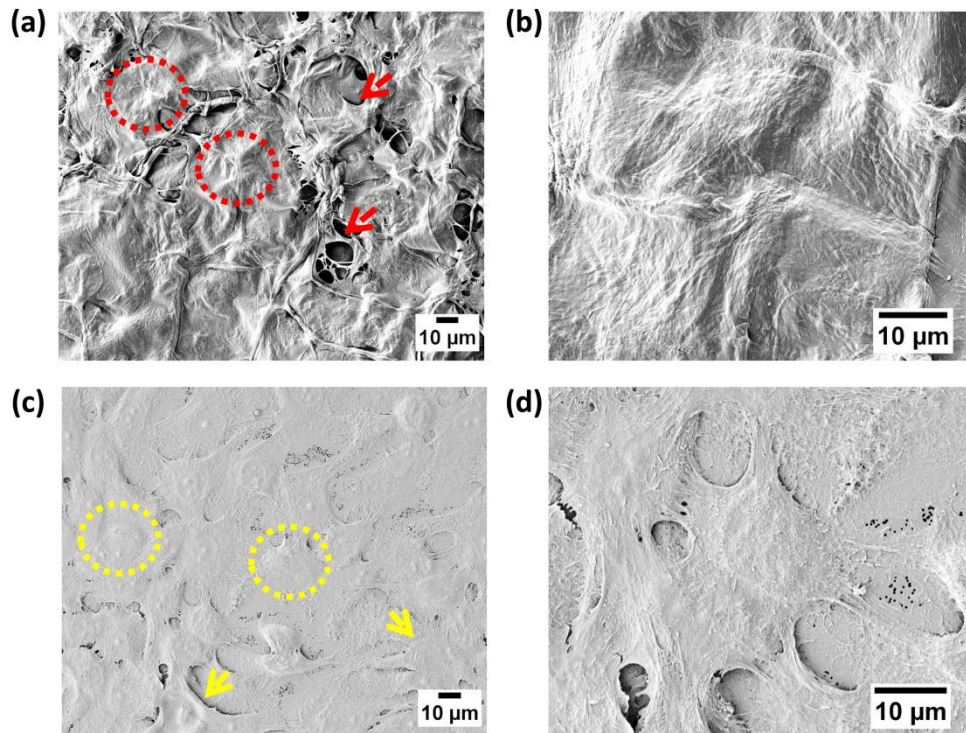


Figure 4.5: Ultrastructural analysis of primary tracheobronchial epithelial cells in monoculture on bilayered collagen-hyaluronate (CHyA-B) scaffolds using scanning electron microscopy. NHBE cells were cultured for 28 days at an air-liquid interface. (a, b) On CHyA-B scaffolds, representative images visualised cells as squamous and extended (red circles) in a confluent layer with occasional overlapping (red arrows). (c, d) On cell inserts, cells were also visualised as squamous and extended in shape (yellow circles) in a confluent layer. Overlapping of cells (yellow arrows) was less than that observed on CHyA-B scaffolds. n=1.

4.3.1.6. Epithelial ultrastructure- TEM

The final assessment of pseudostratification and ciliation of NHBE cells in monoculture on CHyA-B scaffolds and cell inserts was performed by TEM. In a similar result to BIV immunofluorescence and SEM, cilia were notably absent in both culture models and no pseudostratification of the epithelia was observed (Fig. 4.6). Ultimately, these findings confirmed that monoculture of NHBE cells was insufficient for full differentiation of the primary tracheobronchial epithelial cells in both of these *in vitro* models and that further addition of other stimulators of differentiation, such as signalling factors from co-cultured fibroblasts, were warranted.

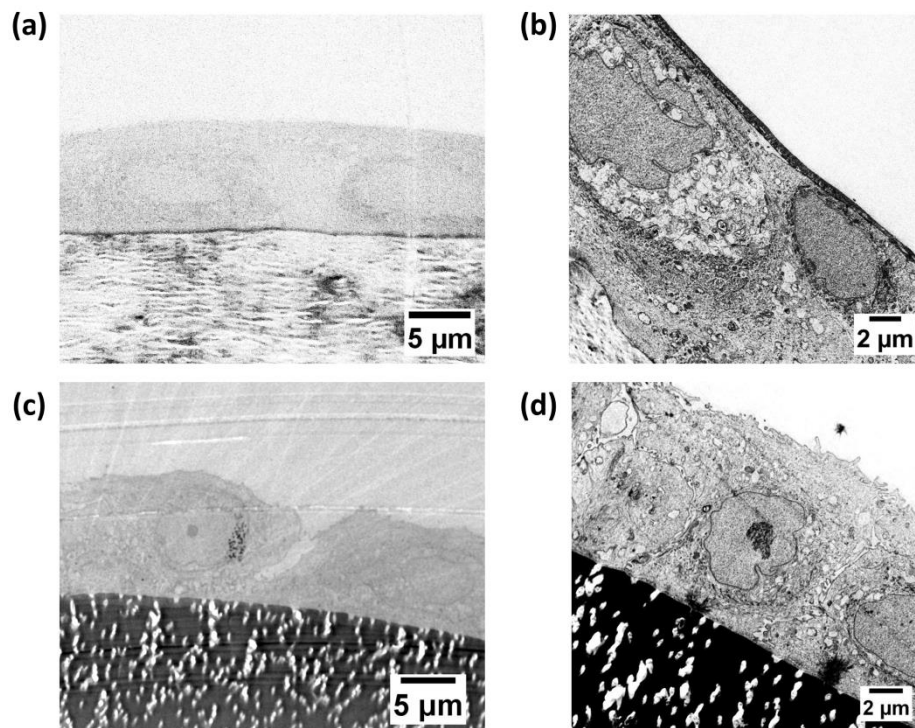


Figure 4.6: Ultrastructural analysis of primary tracheobronchial epithelial cells in monoculture on bilayered collagen-hyaluronate (CHyA-B) scaffolds using transmission electron microscopy. NHBE cells were cultured for 28 days at an air-liquid interface. (a, b) Cells cultured on scaffolds adopted a flattened morphology with no expression of cilia. (c, d) Cells cultured on cell inserts adopted a flattened morphology and with no expression of cilia. n=1; representative images were captured by Mr. Brenton Cavanagh, RCSI.

4.3.2. Primary tracheobronchial epithelial cell co-culture with fibroblasts on CHyA-B scaffolds

4.3.2.1. Cell morphology and migration

Having completed the assessment of NHBE primary cell monoculture on CHyA-B scaffolds, the epithelial cells were next evaluated in co-culture with Wi38 fibroblasts. In comparison to monoculture (Fig. 4.1), H&E&FG staining showed that the inclusion of Wi38 cells into the culture systems resulted in the generation of a thicker respiratory epithelium (Fig. 4.7). Notably, on CHyA-B scaffolds, NHBE cells were visualised as layered in structure, complete with an orientation reminiscent of pseudostratified epithelium (Fig. 4.7a). Fibroblasts migrated into the porous sublayer of CHyA-B and populated the submucosal region in close proximity to the epithelial cell layer. The epithelial layer on cell inserts was also thicker and more columnar than that observed in monoculture, but less stratification of epithelia was observed than in scaffold culture (Fig.4.7b); fibroblasts were thinly stretched in a two-dimensional (2D) conformation along the underside of the polymeric membrane. Overall, histological analysis showed that a more physiologically-representative tracheobronchial epithelium was present in co-culture groups, particularly on CHyA-B scaffolds.

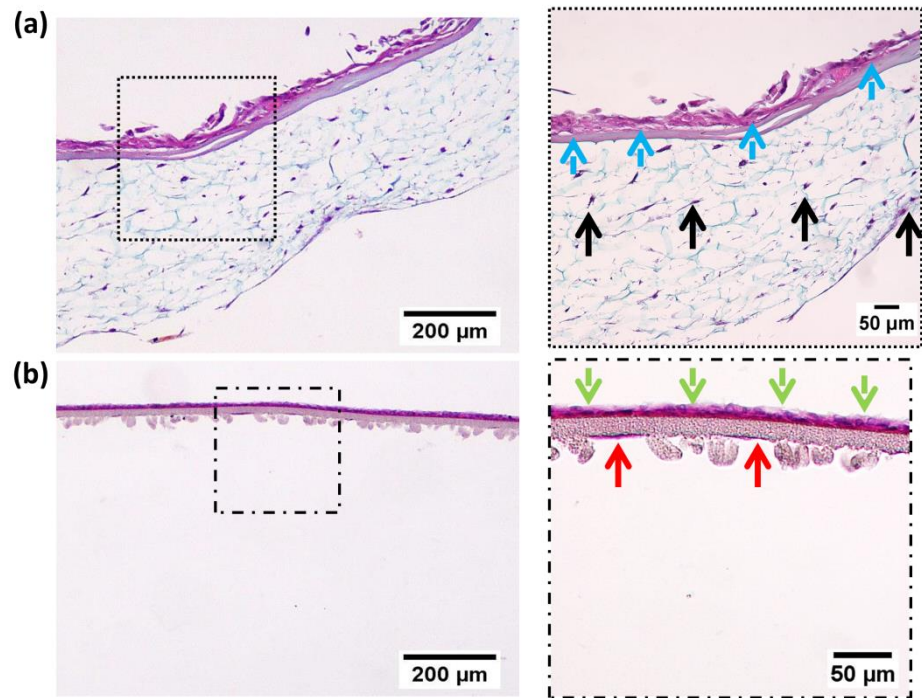


Figure 4.7: Primary tracheobronchial epithelial cell co-culture on bilayered collagen-hyaluronate scaffolds. NHBE cells were co-cultured with Wi38 fibroblasts either on (a) CHyA-B scaffolds or on (b) cell inserts at an air-liquid interface for 28 days. (a) NHBE cells and Wi38 fibroblasts populated the CHyA-B scaffold. Higher magnification images (dotted box) showed the formation of a stratified NHBE cell layer along the film top-layer (blue arrows) and Wi38 fibroblasts migrating into the porous sublayer (black arrows). (b) NHBE cells formed a thinner layer on cell inserts (dashed box; green arrows) with fibroblasts thinly spread on the underside of the insert (red arrows). Representative haematoxylin & eosin and fast green staining visualised scaffolds as a light-blue colour with a pink-purple film layer and cells appeared as pink-purple with darker nuclei. n=3.

4.3.2.2. Mucin expression

The influence of Wi38 fibroblasts on the ability of NHBE epithelial cells to differentiate into mucus-secreting goblet cells was also analysed by MUC5AC immunofluorescence. The presence of fibroblasts in co-culture did not appear to alter the expression levels of MUC5AC, irrespective of the choice of cell substrate (Fig. 4.8). Apical secretions reflecting a patchy distribution of goblet cells were visualised in both CHyA-B (Fig. 4.8a, 4.8b) and cell insert (Fig. 4.8c, 4.8d) cultures; this distribution was the same as that observed in monoculture (Fig. 4.2). Therefore, the presence of goblet cells in the primary tracheobronchial epithelial layer was maintained in the CHyA-B 3D co-culture *in vitro* model.

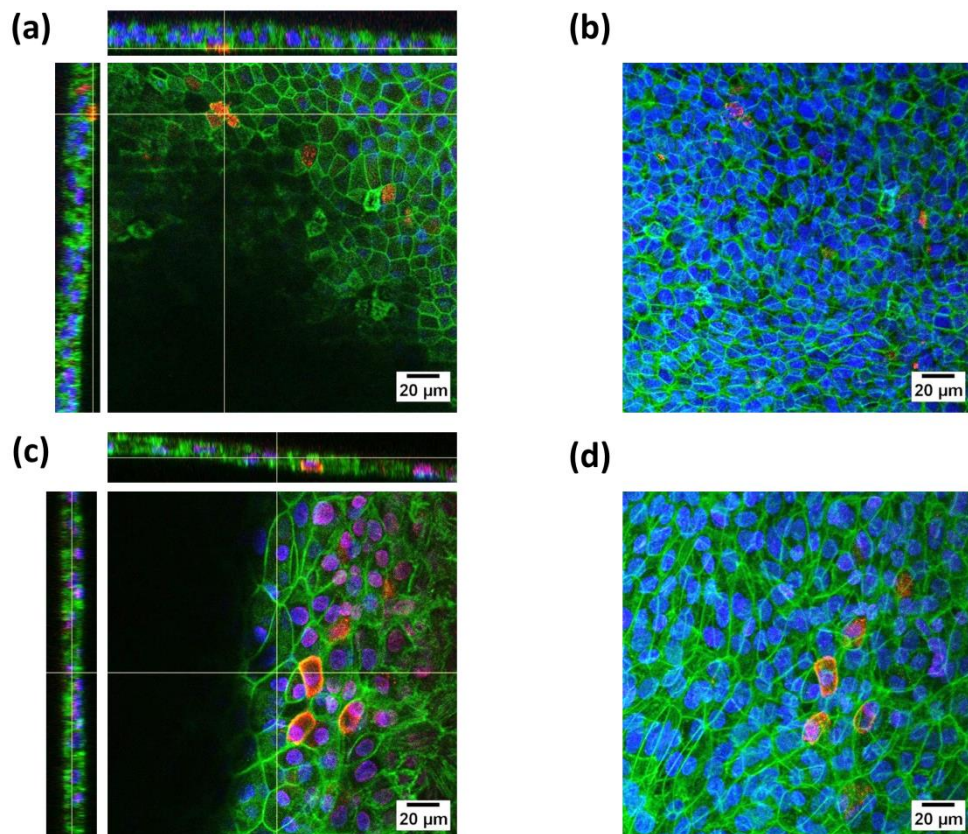


Figure 4.8: MUC5AC expression on primary tracheobronchial epithelial cells in co-culture on bilayered collagen-hyaluronate (CHyA-B) scaffolds. NHBE cells were co-cultured with Wi38 fibroblasts either on (a, b) CHyA-B scaffolds or on (c, d) cell inserts at an air-liquid interface for 28 days. (a, c) Representative z-stack images display apical MUC5AC secretion (red) on top of cells counterstained for nuclei (blue) and F-actin (green). (b, d) Maximum intensity projections of MUC5AC expression reconstructed from z-stacks. n=3. Co-culture experiments were performed concurrently with monoculture experiments (Fig. 4.2).

4.3.2.3. Tight junction formation

The effect of Wi38 fibroblasts on the expression of ZO-1 in NHBE cells was also performed. The inclusion of Wi38 cells resulted in a clearer expression of ZO-1 bands in both CHyA-B scaffolds and cell insert culture groups (Fig. 4.9) than those detected in monoculture (Fig. 4.3). Notably, clearer polarisation of the protein towards the apical side of cell-cell junctions occurred in CHyA-B co-culture than that observed in scaffold monoculture and the cells were not as widely spread on the film surface, suggesting a more columnar morphology (Fig. 4.9a, Fig. 4.9b). ZO-1 expression was similarly present in cell insert co-culture, though z-stack images indicated that the cell layer was thinner (Fig. 4.9c, 4.9d). These data indicated that the CHyA-B scaffold supported the formation of a thick, polarised epithelial barrier by facilitating 3D co-culture of lung fibroblasts.

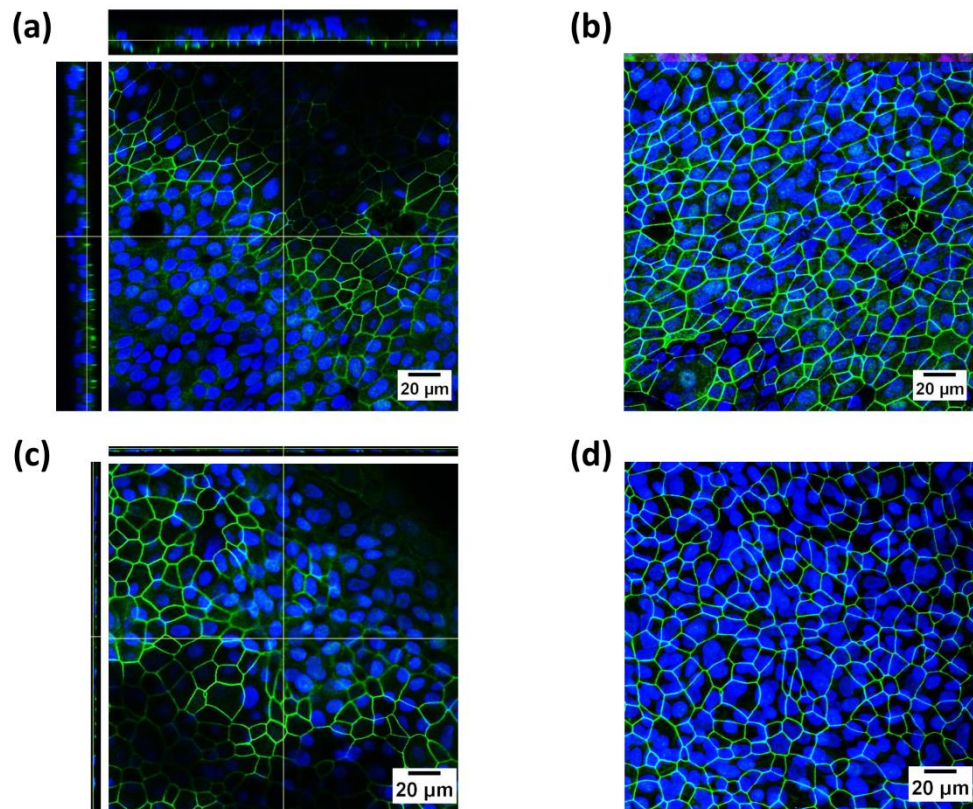


Figure 4.9: ZO-1 expression on primary tracheobronchial epithelial cells in co-culture on bilayered collagen-hyaluronate (CHyA-B) scaffolds. NHBE cells were co-cultured with Wi38 fibroblasts either on (a, b) CHyA-B scaffolds or on (c, d) cell inserts at an air-liquid interface for 28 days. (a, c) Representative z-stack images display ZO-1 bands (green) on the periphery of cells counterstained for nuclei (blue). (b, d) Maximum intensity projections of ZO-1 expression reconstructed from Z-stacks. $n=3$. Co-culture experiments were performed concurrently with monoculture experiments (Fig. 4.3).

4.3.2.4. Epithelial ciliation

The influence of Wi38 fibroblasts on the expression of BIV by NHBE cells was also examined (Fig. 4.10). Positive detection of BIV only occurred in NHBE-Wi38 co-culture on CHyA-B scaffolds (Fig. 4.10a, 4.10b). Clusters of BIV were observed on the apical surface of NHBE cells at the ALI that were distributed along the cell layer of a thick, polarised epithelium. Of critical note, apical expression of BIV was not detected in either cell insert co-culture (Fig. 4.10c, 4.10d) or any monoculture systems (Fig. 4.4). Thus, only the CHyA-B scaffold 3D co-culture model supported the ciliation of NHBE cells and resultantly, their differentiation into a physiologically-representative tracheobronchial epithelium.

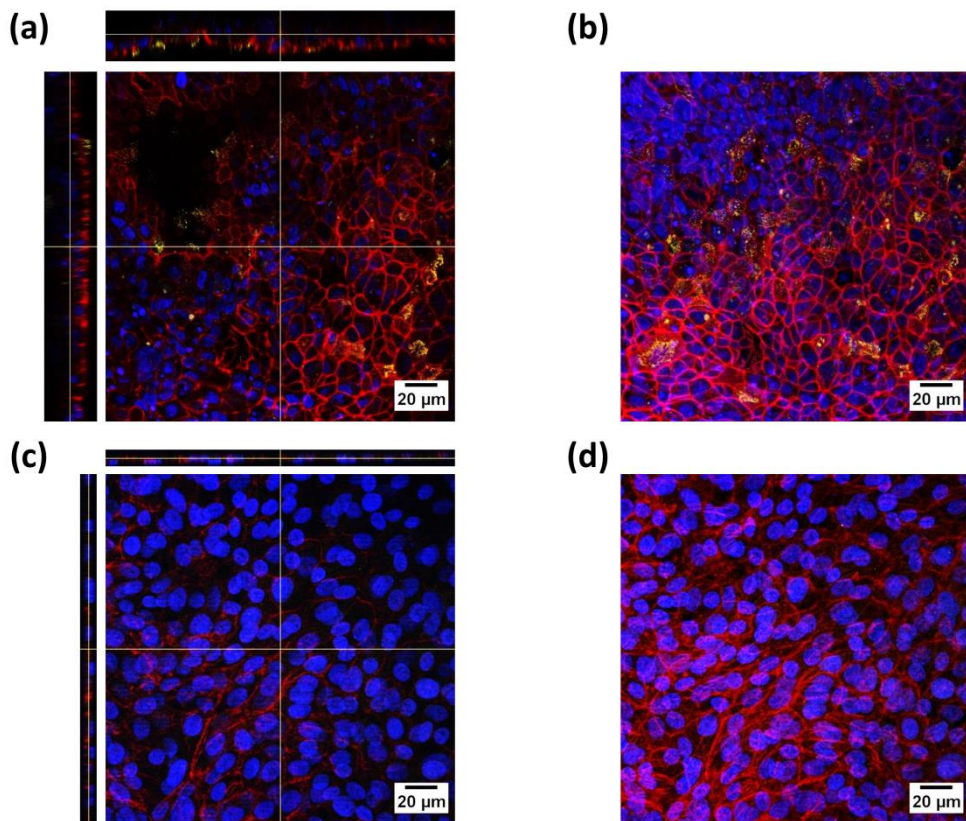


Figure 4.10: β -tubulin IV (BIV) expression on primary tracheobronchial epithelial cells in co-culture on bilayered collagen-hyaluronate (CHyA-B) scaffolds. NHBE cells were co-cultured with Wi38 fibroblasts either on (a, b) CHyA-B scaffolds or on (c, d) cell inserts at an air-liquid interface for 28 days. (a, c) Representative z-stack images display apical expression of BIV (yellow) on top of cells counterstained for nuclei (blue) and F-actin (red). (b, d) Maximum intensity projections of BIV expression reconstructed from z-stacks. $n=3$. Co-culture experiments were performed concurrently with monoculture experiments (Fig. 4.4).

4.3.2.5. Epithelial ultrastructure- SEM

Further examination of NHBE cells in co-culture on CHyA-B scaffolds was conducted using SEM to investigate epithelial ciliation and tight junction formation. The analysis confirmed that primary cells formed a ciliated columnar cell layer with the presence of a cobblestone morphology that reflected tight cell-cell junctions (Fig. 4.11). Specifically, ciliary extensions were seen along the confluent cobblestone layer and higher magnification images captured the presence of visible connections between adjacent NHBE cells (Fig. 4.11a, 4.11b). Although the NHBE-Wi38 co-culture with cell inserts provided a similar cell barrier with tight cellular connections, ciliation was far less prominent, with only very small elevations observed on the apical surface (Fig. 4.11c, 4.11d). Thus, the presence of a more organotypic tracheobronchial epithelium with CHyA-B co-culture was reaffirmed.

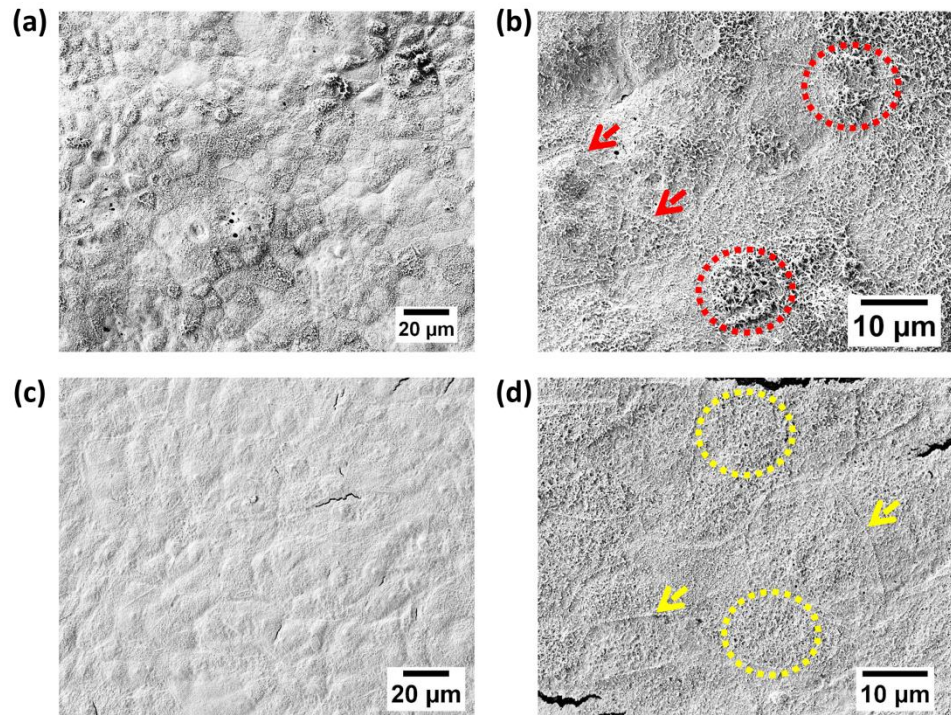


Figure 4.11: Ultrastructural analysis of primary tracheobronchial epithelial cells in co-culture on bilayered collagen-hyaluronate (CHyA-B) scaffolds using scanning electron microscopy. NHBE cells were co-cultured with Wi38 fibroblasts for 28 days at an air-liquid interface. (a, b) On scaffolds, representative images visualised cells as a confluent, cobblestone monolayer with cell-cell junctions (red arrows) and ciliated cells (red circles) present. (c, d) On cell inserts, the confluent, cobblestone cell monolayer with cell-cell junctions (yellow arrows) had limited expression of small microvilli (yellow circles). n=1. Co-culture experiments were performed concurrently with monoculture experiments (Fig. 4.5).

4.3.2.6. Epithelial ultrastructure- TEM

In order to fully investigate the formation of a pseudostratified tracheobronchial epithelium on CHyA-B scaffolds in co-culture, TEM imaging of sample cross-sections was undertaken. In accordance with histology, immunofluorescence and SEM data, the epithelial barrier visualised was thicker, pseudostratified and ciliated in morphology (Fig. 4.12a). A thicker cell layer was also seen in cell insert co-culture (Fig. 4.12c) compared to those present in monoculture groups (Fig. 4.6), but this layer was more multi-layered in structure and lacked the clear, protruding clusters of cilia observed in scaffold co-culture (Fig. 4.12b, 4.12d). In summary, TEM analysis once again illustrated the ability of the CHyA-B 3D co-culture model to provide the most organotypic *in vitro* iteration of the *in vivo* respiratory epithelium.

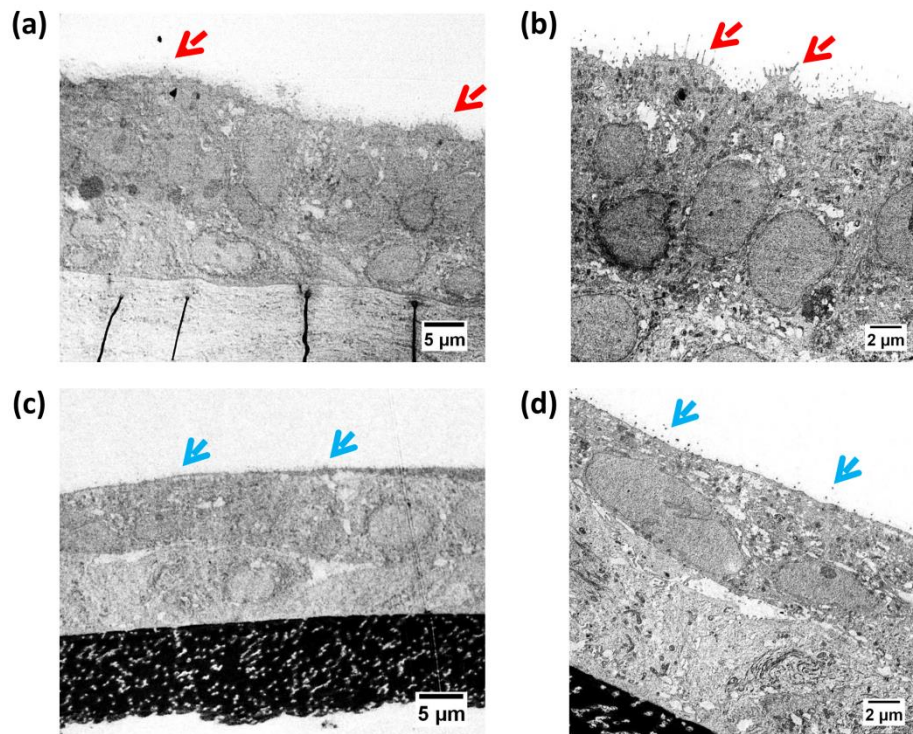


Figure 4.12: Ultrastructural analysis of primary tracheobronchial epithelial cells in co-culture on bilayered collagen-hyaluronate (CHyA-B) scaffolds using transmission electron microscopy. NHBE cells were co-cultured with Wi38 fibroblasts for 28 days at an air-liquid interface. (a, b) Cells cultured on scaffolds adopted a pseudostratified columnar morphology with expression of cilia along the epithelial layer (red arrows). (c, d) Cells cultured on cell inserts adopted a multi-layered morphology and expression of cilia was either absent or limited in shape and height (blue arrows). n=1; representative images were captured by Mr. Brenton Cavanagh, RCSI. Co-culture experiments were performed concurrently with monoculture experiments (Fig. 4.6).

4.3.3. Expression of genetic markers of epithelial differentiation

The effect of CHyA-B scaffolds and Wi38 fibroblasts on NHBE primary cell gene expression of MUC5AC, ZO-1 and FOXJ1 was analysed to evaluate transcriptional regulation of mucus production, tight junction formation and ciliation, respectively [282, 285, 286]. While neither factor significantly altered the expression of MUC5AC (Fig. 4.13a), the presence of the CHyA-B scaffold and fibroblasts significantly upregulated the expression of FOXJ1 compared to that in conventional cell insert co-culture, with an approximate 35-fold increase in gene expression (Fig. 4.13c; $p < 0.05$). Furthermore, CHyA-B scaffolds were also a positive regulator of ZO-1 transcription in co-culture, although this finding was non-significant (Fig. 4.13b; $p > 0.05$). Of note, the stimulatory effects of the scaffold substrate did not occur in NHBE monoculture groups. Therefore, it was observed that a combination of the biomaterial and culture of lung fibroblasts in the porous sublayer was required to increase the transcription of genes regulating barrier formation and ciliation of NHBE primary cells.

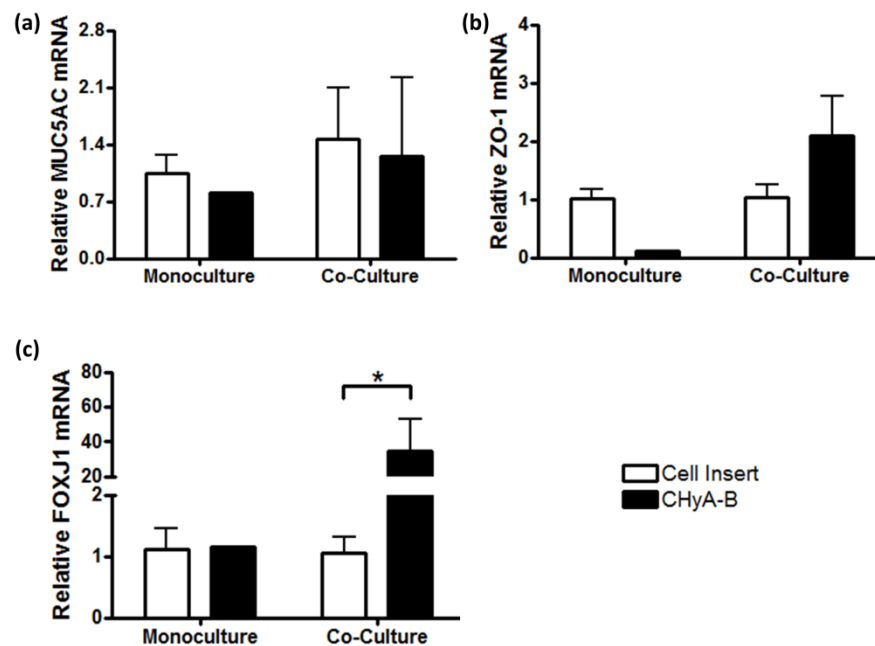


Figure 4.13: Expression of genetic markers of primary tracheobronchial epithelial differentiation in co-culture on bilayered collagen-hyaluronate (CHyA-B) scaffolds. NHBE cells were co-cultured with Wi38 fibroblasts on either scaffolds or cell inserts at an air-liquid interface for 21 days. Quantification of (a) MUC5AC, (b) ZO-1 and (c) FOXJ1 mRNA expression is displayed as mean \pm SEM with expression relative to the cell insert group grown in monoculture or co-culture, as appropriate. $n=2$; * $p < 0.05$.

4.3.4. Evaluation of primary tracheobronchial epithelial cell barrier integrity

4.3.4.1. TEER measurement

In order to confirm that the differentiated epithelial barrier formed upon CHyA-B scaffolds was of sufficient integrity, TEER measurement was assessed in all monoculture and co-culture groups (Fig. 4.14). The TEER values for NHBE cells depended on both the use of CHyA-B scaffold as the culture substrate and also on the inclusion of Wi38 in co-culture (Fig. 4.14a). This was particularly evident when the average peak TEER values of each group (day 11-21) were compared (Fig. 4.14b), where an increasing trend from cell insert and scaffold monoculture to scaffold and cell insert co-culture was recorded. At peak values, cell insert co-culture had a mean TEER of $1829\Omega\text{cm}^2$, which was significantly larger than all other groups, including the mean TEER of $858\Omega\text{cm}^2$ detected in scaffold co-culture ($p < 0.001$). Notably, by day 28, the TEER of the CHyA-B co-culture model was maintained at $423\Omega\text{cm}^2$, compared to values of $46\Omega\text{cm}^2$, $80\Omega\text{cm}^2$, and $1239\Omega\text{cm}^2$ recorded with cell insert monoculture, scaffold monoculture, and cell insert co-culture, respectively. Physiological TEER values of the tracheobronchial region are reported to be in the range of $300\text{-}650\Omega\text{cm}^2$ (reviewed in [54]) and therefore, only the scaffold co-culture group was in the physiological range at this time point. Fibroblasts seeded alone onto scaffolds or cell inserts did not develop a functional TEER value, in line with previous studies [60].

4.3.4.2. FITC-labelled dextran permeability assay

Finally, in order to fully confirm that the differentiated epithelial barrier formed upon CHyA-B scaffolds was of sufficient integrity, paracellular permeability was assessed in all monoculture and co-culture groups (Fig. 4.14). The ability of the NHBE cell barrier to impede the paracellular transport of FD70 at day 21 was observed in both monoculture and co-culture on CHyA-B scaffold culture models, with low P_{app} values recorded (Fig. 4.15c). In conjunction with the TEER data, these results collectively highlighted the presence of a functional epithelial barrier in scaffold culture that is of suitable integrity for physiological modelling.

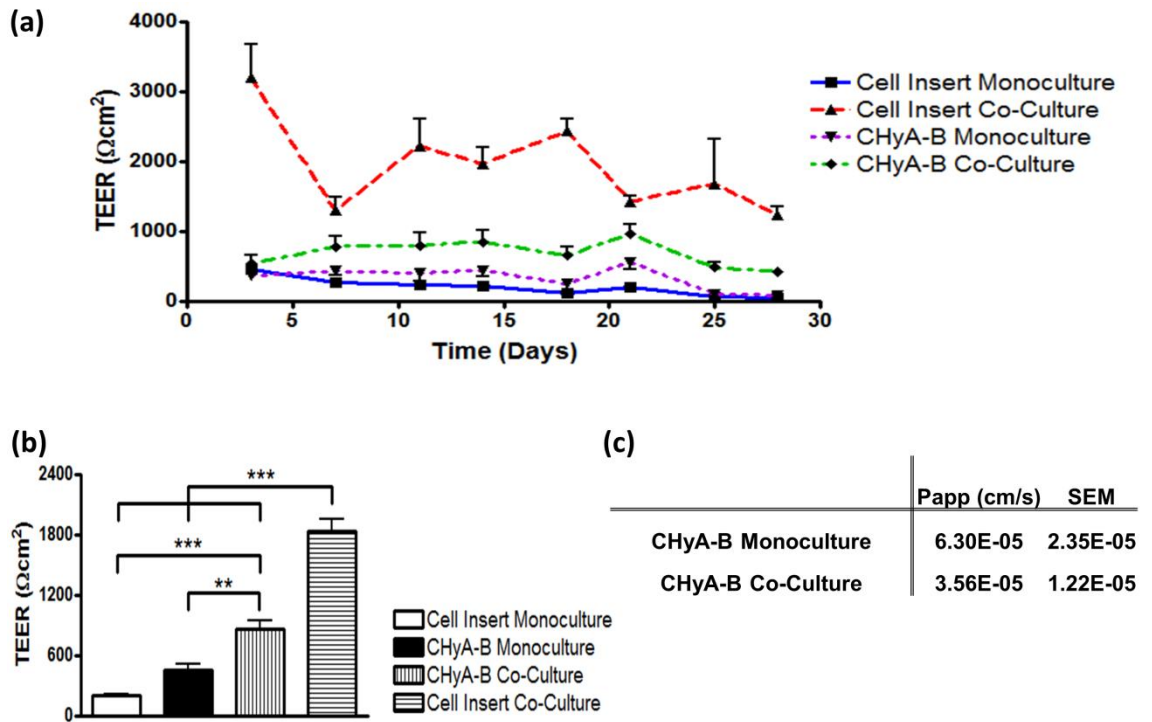


Figure 4.14: Primary tracheobronchial epithelial cell barrier integrity in monoculture and co-culture on bilayered collagen-hyaluronate (CHyA-B) scaffolds. NHBE cells were cultured on either CHyA-B scaffolds or cell inserts at an air-liquid interface for 21-28 days. (a) Transepithelial electrical resistance (TEER) of NHBE cells. $n=1-8$ (performed in triplicate). (b) Average TEER values of NHBE epithelial cell barriers following plateau of electrical resistance (days 11-21). Results displayed as mean \pm SEM. $**p<0.01$; $***p<0.001$. (c) Apparent permeability coefficient (P_{app}) of fluorescein isothiocyanate-labelled dextran 70 (FITC-dextran) through the NHBE cell barrier on CHyA-B scaffolds at Day 21. $n=3$.

4.4. Discussion

In order to provide a more complete *in vitro* physiological representation of the conducting region of the respiratory tract, the major objective of Chapter 4 was to develop a 3D primary tracheobronchial epithelial cell-derived co-culture system for application in respiratory *in vitro* modelling using CHyA-B scaffolds. Specifically, we sought to: (i) assess the feasibility of the CHyA-B scaffold to act as a 3D substrate for the growth and differentiation of NHBE primary respiratory epithelial cells in monoculture, and (ii) develop a 3D co-culture system of NHBE epithelial cells and Wi38 lung fibroblasts and validate this system by analysis of markers of differentiation and epithelial barrier function. The results demonstrated that the NHBE cells attached to and grew on CHyA-B scaffolds over the 28 day culture period. They expressed two markers of epithelial differentiation, though the adoption of a flattened squamous morphology and lack of ciliation indicated that full differentiation of the primary cells did not occur in monoculture on CHyA-B scaffolds. However, the inclusion of Wi38 fibroblasts in a 3D scaffold co-culture induced pseudostratification of the epithelium and the expression of additional biomarkers that were absent in monoculture. Notably, the presence of cilia only occurred in co-culture on CHyA-B scaffolds, suggesting that the synergistic effect of lung fibroblasts and a 3D CHyA-B scaffold substrate contributed to differentiation, which was corroborated by analysis of gene expression. Finally, analysis of epithelial barrier integrity revealed that the TEER in scaffold co-culture was closest to physiological reference levels. Taken together, these data confirm that the CHyA-B scaffold co-culture system is an improved iteration of the tracheobronchial region with primary epithelial culture and this organotypic model can be brought forward in the future as a physiologically-relevant platform tool to evaluate novel therapies or disease pathophysiology.

The examination of NHBE epithelial cell morphology revealed that the cells did not exhibit the phenotype of a native tracheobronchial epithelium in monoculture, despite maintenance of a viable cell layer on the CHyA-B scaffold over the 28 day culture period. Instead of a pseudostratified columnar epithelial conformation, NHBE cells flattened and spread along the CHyA-B film top-layer to coat the scaffold in a squamous-like epithelium (Fig. 4.1). This morphology was seen repeatedly in histological analysis, immunofluorescent z-stack images of F-actin

counterstaining (Fig. 4.2, 4.4) and, most notably, in scanning and transmission electron micrographs (Fig. 4.5, 4.6). Of course, squamous epithelium still performs a barrier function in other tubular organs such as the oesophagus [321], but in the respiratory tract, squamoid metaplasia is associated with the loss of ciliary function in the tracheobronchial region, impaired clearance of mucus, and the exacerbation of chronic diseases such as chronic obstructive pulmonary disease (COPD) and pulmonary carcinoma [322]. Therefore, while serendipitous in nature, this finding could be of interest for pursuing an *in vitro* disease model of squamous metaplasia in combination with a 3D ECM analogue [323]. For the purposes of this study, however, the presence of such morphology was not in line with the objectives hitherto outlined. It is important to note, however, that the NHBE morphology on CHyA-B scaffolds matched that of cells cultured on collagen-coated inserts, indicating that the scaffold itself was not responsible for the induction of this cell morphology. Furthermore, NHBE cells also remained viable in scaffold culture over the period of 28 days; this positive finding highlighted that, at a minimum, CHyA-B scaffolds had the capacity to support viable primary tracheobronchial epithelial cell growth in monoculture.

In addition to supporting their viability, the CHyA-B scaffold also facilitated the culture of a mucin-secreting goblet cell population and tight junction formation between epithelial cells in monoculture (Fig 4.2, 4.3). The detection of MUC5AC, a biomarker for goblet cells [307, 324], confirmed their presence and highlighted that one important aspect of epithelial mucociliary differentiation had occurred (Fig. 4.2). In the Calu-3 cell line, MUC5AC secretions were dramatically increased by scaffold monoculture (Chapter 3; see Fig. 3.6), while an inductive effect was not observed in the case of NHBEs. This might be due to the fact that primary tracheobronchial epithelial cells encompass a more heterogeneous population of cell subtypes than the Calu-3 cell line, where all of the epithelial cells do not serve a secretory function *in vivo*; indeed most tracheobronchial epithelial cells *in vivo* are ciliated columnar epithelial cells [6]. Conversely, Calu-3 cells are derived from a cancerous submucosal gland [56] and secrete mucins, including MUC5AC; accordingly, this would result in greater detection levels. The presence of ZO-1 protein bands along the cell monolayer on CHyA-B scaffolds indicated that the cell layer had the potential to create a continuous epithelial barrier at the ALI (Fig. 4.4).

With a similar distribution to that observed in Calu-3 cell culture on CHyA-B scaffolds (Chapter 3), the mesh-like chain of junctions between the cells is characteristic of a well-differentiated epithelial monolayer and indicates functionalisation of the NHBE cells [53, 60]. It is worth noting that this network was stretched in appearance in NHBE scaffold monoculture, reflecting wider cellular spreading across the CHyA film layer (Fig. 4.4a); this observation is in line with the evidence of a flat, squamous cell morphology previously discussed. In addition, z-stack images validated these data through the visualisation of a thin cell layer in the 3D projections. Nevertheless, the very presence of ZO-1 and its localisation to the apical region of cell junctions is advantageous for a 3D *in vitro* epithelial model because it is the hallmark of tight junction formation. Irrespective of cell morphology, these results show the NHBE cells expressed two important features of an *in vivo* tracheobronchial epithelium when in an *in vitro* CHyA-B scaffold monoculture model.

One important physiological feature of the tracheobronchial epithelium that was absent in CHyA-B scaffold monoculture, however, were ciliated cells. BIV, a cytoskeletal protein present in the axoneme of the ciliary apparatus [319], is localised to the apical side of epithelial cells and is visualised in respiratory epithelia as thin extensions that gather in clusters of cilia [60]. Such extensions were absent from NHBE cells that were cultured alone upon both CHyA-B scaffolds and cell inserts (Fig. 4.4). Ultrastructural analysis corroborated the immunofluorescence data with a clear absence of ciliary structures observed on cultured cells (Fig. 4.5, 4.6). Accordingly, the completion of the first study objective confirmed that the CHyA-B scaffold could feasibly support NHBE cell growth, goblet cell differentiation and tight junction formation in monoculture, but not the full commitment to a mucociliary phenotype. In order to achieve such ciliation within *in vitro* primary tracheobronchial epithelial culture systems, a multitude of culture conditions (e.g. ALI; [99]), ECM components (e.g. collagen, hyaluronate [73, 99, 294]), and media supplements (e.g. atRA [69]) have been reported. Fibroblast factors provided from co-culture, however, have also been shown to induce ciliation in primary tracheobronchial epithelial cells [60, 100, 198]. Therefore, in line with the potential for lung fibroblasts to stimulate the expression of this third marker of epithelial differentiation and also with the objective to

develop a co-culture model with physiologically-relevant tissue architecture and composition, this Chapter proceeded to investigate a CHyA-B scaffold NHBE-Wi38 co-culture model as a means of fully recapitulating the ciliated epithelium in a 3D *in vitro* model.

The inclusion of Wi38 fibroblasts into the porous sublayer of the CHyA-B scaffold was found to have a major effect on the differentiation of NHBE cells into a pseudostratified ciliated epithelium. Histological analysis revealed that both scaffold and cell insert co-cultures experienced thickening of the epithelial layer when compared to the corresponding monoculture (Fig. 4.7). This thickening was more prominent in peripheral regions with the CHyA-B co-culture model than in the cell insert co-culture. While some areas on the scaffold were multi-layered in appearance, subsequent TEM imaging indicated that the epithelial layer was pseudostratified in structure along the majority of the film layer (Fig 4.12). The NHBE cells in cell insert co-culture, on the other hand, did not adopt this morphology, despite exhibiting a similar epithelial thickness in TEM sections. The greatest advantage of the scaffold co-culture, however, was the detection of cilia that was not present in any of the other three *in vitro* models in this chapter, including the cell insert co-culture model. Immunofluorescent analysis of BIV revealed characteristic clusters of cilia on the apical side of the scaffold that were diffusively spread across the primary tracheobronchial epithelial layer (Fig. 4.10). Cilia-like microvilli were also observed along the pseudostratified layer captured by TEM (Fig. 4.12), while ultrastructural analysis with SEM served to re-emphasise the ubiquitous coating of cells with ciliary extensions (Fig. 4.11). Taken together, these data demonstrate that the 3D CHyA-B substrate holds a clear advantage over the conventional co-culture cell insert substrate and can enhance the recapitulation of a pseudostratified epithelium with production of an integral component of the mucociliary clearance mechanism within the upper respiratory tract, in conjunction with fibroblasts in the submucosal porous layer [285].

Of course, as well as stimulating ciliogenesis within the novel 3D *in vitro* model, it was important that the Wi38 fibroblasts also maintained the two other characteristics of native tracheobronchial epithelium in scaffold co-culture-specifically, the differentiation into goblet cells and the formation of tight junctions. Immunofluorescent analysis of MUC5AC and ZO-1 confirmed that these

biomarkers were also present in co-culture groups (Fig. 4.8, 4.9). The presence of Wi38 fibroblasts in culture did not alter the sparse distribution of goblet cells, regardless of the use of a scaffold or cell insert substrate (Fig. 4.8). The fibroblasts did influence the pattern of ZO-1 staining on CHyA-B scaffolds, however. A narrowing of the distance between the protein bands on the periphery was observed in co-culture when compared to monoculture (Fig. 4.9a). This resulted in a more refined cobblestone pattern between ZO-1 that was less stretched and more reminiscent of previous observations of cell line and primary culture [53, 60]. This pattern also reflected the adoption of a columnar morphology by the NHBE cells, particularly when examined with the corresponding confocal z-stack images that depicted a thicker epithelium and localisation of nuclei along the xz and yz axes that was typical of pseudostratification. Cell insert co-culture, by contrast, exhibited the same distribution of tight junction protein, but the cell layer was much thinner (Fig. 4.9c). SEM of scaffold co-culture samples also corroborated the presence of tight junctions between cobblestone-shaped cells (Fig. 4.11b). In summary, these results confirm that NHBE mature into goblet cells and there is extensive cobblestone patterning of ZO-1 expression in CHyA-B co-cultures, in addition to the previous findings of epithelial layer thickening and pseudostratification observed on the scaffold from histological and ultrastructural analyses and co-cultures.

Thus, having developed a primary epithelial-fibroblast scaffold co-culture model with favourable cell distribution that expressed key markers of tracheobronchial differentiation, analysis of epithelial gene expression was subsequently undertaken in order to examine the effect of the CHyA-B scaffold and Wi38 fibroblasts on key genes that contribute to the regulation of NHBE differentiation (Fig. 4.13). The expression of two genes, ZO-1 and FOXJ1, were upregulated through a combination of the presence of fibroblasts and the 3D culture conditions provided by the CHyA-B scaffold. The introduction of fibroblasts *per se* was insufficient to bring about gene upregulation, as indicated by the comparison of cell insert monoculture to cell insert co-culture samples, while the relative comparison of CHyA-B scaffolds to cell inserts in monoculture highlighted that the scaffold substrate did not upregulate these genes by direct interaction with the NHBE cell. Biomechanical cues from 3D matrices can trigger different signalling

cues and molecular pathways in fibroblasts [101, 325], and a recent study has identified hepatocyte growth factor (HGF) secretion from lung fibroblasts as an important paracrine factor for bronchial epithelial growth [326]. With this in mind, we postulate that the 3D microenvironment of the CHyA-B porous sublayer promotes the inductive effect of Wi38 lung fibroblasts on the co-cultured NHBE cells through the secretion of growth factors and other signalling molecules.

CHyA-B scaffolds have previously exhibited different effects on the upregulation of MUC5AC and FOXJ1 genes in Calu-3 cells (Chapter 3; see Fig. 3.9 and 3.10). Calu-3 cell populations exhibit a predominantly mucus-secreting phenotype when cultured at an ALI [53]; accordingly, stimulation by scaffolds to increase mucus secretion would be observed in the majority of seeded cells. In contrast, any possible stimulation of MUC5AC expression by CHyA-B scaffolds in the goblet cell sub-population of the primary epithelial cell layer might have been masked by the presence of greater numbers of ciliated cells. CHyA-B scaffolds also induced FOXJ1 gene transcription at a faster rate in Calu-3 cells than cell insert substrates. In this chapter, however, such effects on the rate of transcription are unknown. Relative mRNA expression was analysed at day 21 alone for comparison with a previously published study that demonstrated the ability of a hyaluronan-derivative membrane to increase mucociliary gene expression in a similar manner to CHyA-B scaffolds [294]. Moreover, a single time point was also chosen because a primary focus of the study was the influence of co-culture, rather than time, on NHBE mRNA expression.

The final stage of the validation of the CHyA-B 3D co-culture model involved the assessment of primary epithelial barrier integrity (Fig. 4.14). The TEER values for NHBE cells depended on both the use of CHyA-B as the culture substrate and also on the inclusion of Wi38 co-culture. Peak TEER values of both scaffold and cell insert co-culture systems were significantly higher than both monoculture systems, in agreement with the literature [60, 231, 305]. Additionally, peak values of the cell insert co-culture ($1829\Omega\text{cm}^2$) were double those of the scaffold co-culture groups ($858\Omega\text{cm}^2$), indicating that the strongest barrier formed in the case of the former. However, while the presence of a higher TEER might initially appear advantageous for modelling an epithelial barrier, it is important to have a magnitude of barrier integrity that is reflective of the target tissue when performing

drug permeation and transport studies. Different delivery routes of drugs will involve different levels of barrier permeability, ranging from the relatively permeable capillaries in the peripheral circulation (3-30 Ωcm^2) to the strong barrier of the skin (9703 Ωcm^2 ; [327]); while TEER values from *ex vivo* human lung tissue have not been reported to date, analysis of rabbit tissue and human primary epithelial cell cultures indicate a range of 300-650 Ωcm^2 (reviewed in [54]). Thus, while still greater than 650 Ωcm^2 , the peak TEER obtained by the CHyA-B scaffold co-culture might offer a suitable compromise between the presence of a physiologically-relevant composition and the achievement of a TEER that is closer to the physiological range than cell insert co-culture. Indeed, by day 28, the TEER in the CHyA-B scaffold co-culture had reduced to 423 Ωcm^2 , rendering it the only culture group that was within the physiological range at this time point. Analysis of paracellular permeability using FD70 confirmed that the primary epithelial barrier was less robust in scaffold monoculture than in scaffold co-culture, with an average P_{app} value that was ten times lower in the case of the latter. The transport of a range of other molecules and FITC-dextran of other molecular weights has been described in other studies [328-331], but although information on FD70 is not abundant, a P_{app} value in the range of 10^{-6} to 10^{-7} indicates minimal paracellular transport. To summarise, the CHyA-B scaffold co-culture model provided the most organotypic quantitation of functional epithelial barrier integrity after 28 days of culture.

Despite the achievement of the objective to develop a 3D primary tracheobronchial epithelial cell-derived co-culture system for application in respiratory *in vitro* modelling using CHyA-B scaffolds, this chapter is not without its limitations. The principal limitation within this chapter was the absence of confirmation of basal cell presence to complete the complement of primary tracheobronchial epithelial cell types within the CHyA-B 3D *in vitro* model. Immunofluorescent detection using an anti-cytokeratin 14 antibody is planned for future work but it can be hypothesised at present that the cell sub-type is likely to be present in the scaffold co-culture to safeguard ciliated cell adherence to the substrate [6]. Additionally, the data in this chapter could also be further enriched with quantitative data of the relative proportions of ciliated cells and goblet cells that were identified in CHyA-B co-culture; such histomorphometric or flow cytometric data for native tracheobronchial

tissue, however, is scant at present and no current study of tissue-engineered models of the upper respiratory tract has reported such detailed data for comparison. Finally, while it was clear that NHBE cell differentiation towards ciliated columnar cells required a combination of the novel CHyA-B scaffold and the presence of co-cultured fibroblasts, it can be argued that the cilia formed were not fully mature in structure. Motile cilia in the respiratory tract are typically 7µm in length [332] and longer cilia have been visualised in other studies than the cilia observed here [60, 100, 294]. Future optimisation of the co-culture media composition- in particular, the concentration of atRA [69, 333]- has the potential to even further enhance ciliation within the 3D CHyA-B co-culture model. Nevertheless, the beneficial effect of inducing ciliation in NHBE epithelial cells through a combination of fibroblasts and the scaffold was clearly demonstrated in this study and validated the CHyA-B scaffold as an effective tracheobronchial model for the development of novel translational therapeutics and disease modelling.

4.5. Conclusion

In conclusion, this chapter has successfully developed a 3D primary tracheobronchial epithelial cell-derived co-culture system using CHyA-B scaffolds previously optimised with Calu-3 epithelial cells. This organotypic *in vitro* model contains the phenotypic features of the native pseudostratified epithelium and co-cultured submucosal fibroblasts that are all arranged in an ECM architecture composed of natural polymers found in abundance in the upper region of the airways. This scaffold co-culture has great potential to be brought forward as an innovative and physiologically-representative platform to develop novel therapeutics, perform toxicological analysis of inhalable formulations and generate more sophisticated disease models.

Chapter 5: The manufacture of an all-*h f* *Ur*retinoic acid-eluting bilayered scaffold as a platform technology for airway tissue regeneration

5.1.	Introduction	180
5.2.	Materials and Methods	182
5.2.1.	<i>All-trans retinoic acid-loaded bilayered collagen-hyaluronate (atRA-CHyA-B) scaffold fabrication</i>	182
5.2.1.1.	<i>All-trans retinoic acid-loaded collagen-hyaluronate (atRA-CHyA) film manufacture</i>	182
5.2.1.2.	<i>atRA-CHyA-B scaffold manufacture</i>	182
5.2.1.3.	<i>Chemical crosslinking</i>	182
5.2.2.	<i>atRA-CHyA film and atRA-CHyA-B scaffold characterisation</i>	183
5.2.2.1.	<i>Fourier transform infrared spectroscopy (FTIR)</i>	183
5.2.2.2.	<i>atRA encapsulation efficiency</i>	183
5.2.2.3.	<i>atRA in vitro release</i>	184
5.2.2.4.	<i>High performance liquid chromatographic (HPLC) analysis</i>	185
5.2.3.	<i>Primary tracheobronchial epithelial cell culture</i>	185
5.2.3.1.	<i>Cell source and culture medium</i>	185
5.2.3.2.	<i>Primary tracheobronchial epithelial cell culture on atRA-CHyA films</i>	186
5.2.3.3.	<i>Primary tracheobronchial epithelial cell culture on atRA-CHyA-B scaffolds</i>	187
5.2.4.	<i>Epithelial cell viability on atRA-CHyA films and atRA-CHyA-B scaffolds</i>	187
5.2.4.1.	<i>Cell growth on atRA-CHyA films and atRA-CHyA-B scaffolds</i>	187
5.2.4.2.	<i>Cell morphology and migration on atRA-CHyA-B scaffolds</i>	187
5.2.5.	<i>Primary tracheobronchial epithelial cell differentiation on atRA-CHyA films and atRA-CHyA-B scaffolds</i>	188
5.2.5.1.	<i>Immunofluorescence</i>	188
5.2.5.2.	<i>Expression of genetic markers of epithelial differentiation</i>	188
5.2.5.3.	<i>Scanning electron microscopy (SEM)</i>	189
5.2.5.4.	<i>Transmission electron microscopy (TEM)</i>	189
5.2.6.	<i>Data analysis</i>	189
5.3.	Results	190
5.3.1.	<i>atRA-CHyA film characterisation</i>	190
5.3.1.1.	<i>atRA-CHyA film manufacture and stability</i>	190
5.3.1.2.	<i>atRA-CHyA film encapsulation efficiency</i>	192
5.3.1.3.	<i>In vitro release of atRA from atRA-CHyA films</i>	194

5.3.2.	<i>Primary tracheobronchial epithelial cell culture on atRA-CHyA films</i>	196
5.3.2.1.	<i>Epithelial cell growth</i>	196
5.3.2.2.	<i>Mucin expression</i>	197
5.3.2.3.	<i>Epithelial ciliation</i>	198
5.3.2.4.	<i>Expression of genetic markers of epithelial differentiation</i>	199
5.3.3.	<i>atRA-CHyA-B scaffold characterisation</i>	200
5.3.3.1.	<i>atRA-CHyA-B scaffold manufacture and atRA encapsulation efficiency</i>	200
5.3.3.2.	<i>In vitro release of atRA from atRA-CHyA-B scaffolds</i>	200
5.3.4.	<i>Primary tracheobronchial epithelial cell culture on atRA-CHyA-B scaffolds</i>	202
5.3.4.1.	<i>Epithelial cell growth</i>	202
5.3.4.2.	<i>Cell morphology and migration</i>	202
5.3.4.3.	<i>Mucin expression</i>	204
5.3.4.4.	<i>Epithelial ciliation</i>	206
5.3.4.5.	<i>Epithelial ultrastructure- SEM</i>	208
5.3.4.6.	<i>Epithelial ultrastructure- TEM</i>	210
5.3.4.7.	<i>Expression of genetic markers of epithelial differentiation</i>	211
5.4.	<i>Discussion</i>	212
5.5.	<i>Conclusion</i>	219

5.1. Introduction

Bilayered collagen-hyaluronate (CHyA-B) scaffolds have been successfully developed as a three-dimensional (3D) substrate for an *in vitro* co-culture model using both a bronchial epithelial cell line (Chapter 3) and primary tracheobronchial epithelial cells (Chapter 4), but their potential for tissue regeneration has not been investigated. As reviewed in Chapter 1, the treatment of extensive tracheobronchial injury through resection of the damaged tissue with primary anastomosis is restricted by the size of the segment. When lesions caused by cancer, stenosis, infections or congenital abnormalities are greater than half the length of the adult trachea or one third the length in children, allografts or prosthetic devices are required. Unfortunately, allograft transplantation is severely limited by the complications of immunosuppressive treatment such as cardiovascular and renal toxicity, while artificial prosthesis is associated with numerous issues, including device migration and dislodgement, material degradation and failure, tissue granulation and tracheal stenosis [41]. While the much-publicised tissue engineering approach to develop biocompatible alternatives using decellularised (DC) tracheae has shown potential as a novel intervention [97, 98, 251], an overall high patient mortality rate has provoked calls for additional *in vitro* studies before widespread clinical trials are initiated [334]. Moreover, the true clinical benefit of bioengineered synthetic scaffolds has been cast in doubt following recent investigations into potential misconduct and negligence [235-239]. With this in mind, as well as the general supply and compatibility issues of DC tissue (Section 1.3.5.2), investigation into the development of a natural polymeric implant using CHyA-B scaffolds as a different strategy is certainly warranted. It is paramount, however, that rapid epithelialisation of the film top-layer with mucociliary function occurs for efficacious tissue regeneration.

In this chapter, we hypothesise that all-*trans* retinoic acid (atRA) has the potential to improve the epithelialisation of CHyA-B scaffolds with enhanced mucociliary function. atRA, a small molecule drug, is often added to primary airway epithelial cell cultures as a supplement to enhance mucociliary differentiation [69]. Indeed, atRA has been identified as a putative therapeutic for lung regeneration, albeit with mixed outcomes in human and animal trials for the reversal of alveolar injury due

to pulmonary emphysema [78, 161-165]. The drug increases mucus secretion and cilia expression in tracheobronchial epithelium through interaction with retinoid receptors and the receptor for hyaluronan-mediated motility (RHAMM; [166, 167]). As discussed in Chapter 4, increasing the exposure of primary tracheobronchial epithelial cells seeded onto CHyA-B scaffolds to atRA could increase the formation of longer, more mature motile cilia. From a tracheal tissue regeneration perspective, an atRA-loaded CHyA-B scaffold could enhance epithelial repair to restore an epithelium that both provides a mucus defensive barrier and ciliary clearance to prevent plugging of the airways.

The incorporation of atRA into a hydrophilic polymeric material such as the CHyA-B scaffold, however, presents a challenge from a manufacturing perspective. atRA is very hydrophobic in nature (LogP 6.3; [335]) and labile to heat, light and oxygen-mediated degradation [336]. Accordingly, most studies involving atRA-loaded particles and scaffolds have used synthetic polymers or modified glycosaminoglycans to accommodate the molecule's poor aqueous solubility [337-341]. It is currently unknown if it is possible to blend such a molecule into a collagen-based scaffold.

Therefore, the overall objective of Chapter 5 was to manufacture an atRA-loaded bilayered collagen-hyaluronate (atRA-CHyA-B) scaffold as a platform technology for tracheal tissue regeneration. Specifically, three aims were pursued:

1. To fabricate and characterise an atRA-loaded collagen-hyaluronate (atRA-CHyA) film layer as a novel drug-eluting biomaterial.
2. To assess the potential of atRA to enhance the differentiation of primary tracheobronchial epithelial cells cultured on the atRA-CHyA films.
3. To incorporate the atRA-loaded film layer into the CHyA-B scaffold to fabricate an atRA-CHyA-B scaffold and to evaluate its potential as a biomaterial to enhance functional epithelialisation of the scaffold.

5.2. Materials and Methods

5.2.1. All-trans retinoic acid-loaded bilayered collagen-hyaluronate (atRA-CHyA-B) scaffold fabrication

5.2.1.1. All-trans retinoic acid-loaded collagen-hyaluronate (atRA-CHyA) film manufacture

atRA-CHyA films were manufactured by a modification of the CHyA film fabrication process outlined in Section 3.2.1.1. A suspension of 0.5% microfibrillar bovine tendon collagen (Integra Life Sciences, Plainsboro, NJ) and 0.044% hyaluronate sodium salt derived from *Streptococcus equi* (Sigma-Aldrich, Arklow, Ireland) in 0.5M acetic acid was blended at 15,000rpm and 4°C for 3.5 hours using an Ultra Turrax T18 Overhead blender (IKA Works Inc., Wilmington, NC) and subsequently degassed under a vacuum to remove all air bubbles created from the homogenising process. A 2mg/ml stock solution of atRA (Sigma) in dimethylsulphoxide (DMSO) was prepared and a sufficient volume was blended into the degassed CHyA suspension at 15,000rpm for 15 minutes to produce a final concentration of atRA of 0.1µg/ml, 1µg/ml or 10µg/ml. The atRA-CHyA suspension was degassed and 50ml of the slurry suspension was pipetted onto a 12.5x12.5cm² polytetrafluoroethylene (PTFE) plate and left overnight under an air current in a fume hood to produce a thin atRA-CHyA copolymer film. Due to the light-sensitive nature of atRA, all steps following its addition were performed in the dark.

5.2.1.2. atRA-CHyA-B scaffold manufacture

atRA-CHyA-B scaffolds were manufactured by freeze-drying atRA-CHyA films in combination with CHyA slurry as outlined in Section 3.2.1.2. atRA-CHyA films fabricated from a CHyA suspension containing 10µg/ml atRA were rehydrated in 0.5M acetic acid for 2 hours and lyophilised using a customised anneal cycle [275]. After freeze-drying, the scaffolds were crosslinked and sterilised using a dehydrothermal (DHT) process at 105°C for 24 hours in a vacuum oven at 50mTorr (VacuCell 22, MMM, Germany) [283].

5.2.1.3. Chemical crosslinking

DHT-crosslinked atRA-CHyA-B scaffolds were chemically crosslinked using 1-ethyl-3-(3-dimethylaminopropyl)carbodiimide hydrochloride (EDAC; Sigma) in

combination with N-hydroxysuccinimide (NHS; Sigma) as described in Section 2.2.1.2 [274, 278]. The scaffolds were then washed three times with Dulbecco's phosphate buffered saline (DPBS; Sigma) to remove any residual cytotoxic product and used immediately afterwards for cell culture experiments. All steps were performed under sterile conditions.

5.2.2. atRA-CHyA film and atRA-CHyA-B scaffold characterisation

5.2.2.1. Fourier transform infrared spectroscopy (FTIR)

The effect of the incorporation of atRA on the macromolecular structure of CHyA films was determined by Fourier transform infrared spectroscopy (FTIR). 1x1cm² pieces of films fabricated from suspensions containing 0µg/ml, 10µg/ml or 10µg/ml with DHT crosslinking were milled with potassium bromide to create a homogenous solid dispersion that was subsequently compressed into a transparent disc. FTIR analysis was carried out using a Tensor II FTIR instrument (Bruker, Coventry, UK) and Opus Software. The spectra were collected over a wavenumber range of 400–4000cm⁻¹ with a correction for background run before each reading. Two separate batches of atRA-CHyA films were used for the analysis.

5.2.2.2. atRA encapsulation efficiency

The quantity of atRA in atRA-CHyA films was assessed to determine both the encapsulation efficiency of atRA in the co-polymer film and also the effect of the DHT process on atRA stability. atRA-CHyA films fabricated from suspensions containing 0.1µg/ml, 1µg/ml or 10µg/ml atRA were cut into 36cm² sections and digested using a bacterial collagenase from *Clostridium histolyticum* (Sigma). The film pieces were hydrated in a buffer containing 0.1M Tris-HCL and 0.05M CaCl₂ at pH 7.4 and 37°C. They were then incubated for 2 hours at 37°C with a collagenase solution with an activity of 100U/ml. Following film digestion, the enzymatic reaction was stopped by adding 0.25M EDTA (pH 9) at a ratio of 1:6 EDTA:buffer and placing the samples on ice for 10 minutes. Blank atRA-free CHyA films and a 1µg/ml atRA solution were also included as negative and positive controls in the digestion assay, respectively. The samples were diluted 1:1 in methanol and analysed for atRA content using high-performance liquid chromatographic (HPLC) analysis (Section 5.2.2.4), with atRA concentration

normalised to mass per cm^2 . A minimum of two separate batches of atRA-CHyA films at each concentration were used for the analysis.

The quantification of atRA in atRA-CHyA-B scaffolds was assessed to determine both the encapsulation efficiency of atRA in the bilayered scaffold and also the effect of the lyophilisation process on atRA stability. $6 \times 6 \text{cm}^2$ scaffolds were cut into pieces with each containing 7.5cm^2 of the film layer. The sample pieces were subsequently hydrated, digested and analysed with HPLC as outlined above. Two batches of atRA-CHyA-B scaffolds were used for analysis.

5.2.2.3. atRA *in vitro* release

The *in vitro* release profile of atRA from atRA-CHyA films was determined to both ascertain the kinetics of drug elution from the biomaterial and also to determine the effect of the DHT process on the release kinetics. A release buffer of a 1:1 mixture of Dulbecco's Modified Eagle's Medium (DMEM; Sigma) and Ham's F12 medium (Sigma) containing 100U/ml penicillin/streptomycin (Sigma) was prepared for the study. atRA-CHyA films were cut into equal pieces of 12cm^2 and incubated in 5ml of release buffer at 37°C within a 15ml falcon tube with gentle agitation to facilitate sink conditions. The release medium was removed for analysis over the course of 48 hours and replaced with fresh, pre-warmed release buffer. Sampling was performed every 2 hours for the first 10 hours, every 2 hours from 24-34 hours inclusive, and at 48 hours. The removed samples were diluted 1:1 in methanol and analysed for atRA content using HPLC analysis (Section 5.2.2.4), with atRA concentration normalised to mass per cm^2 . After 48 hours, the films were digested using a collagenase solution as described in Section 5.2.2.1 to assess the remaining atRA within the film. Two batches of atRA-CHyA films were used for analysis.

The *in vitro* release of atRA from atRA-CHyA-B scaffolds was determined to both ascertain the kinetic profile of drug elution from the biomaterial and also to determine the effect of EDAC crosslinking on the release kinetics. $6 \times 6 \text{cm}^2$ scaffolds were cut into equal pieces containing 6.75cm^2 of the film layer and crosslinked using EDAC as outlined in Section 5.2.1.3 following the calculation of their mass, where appropriate. The samples were then incubated in release buffer and sampled as outlined above for atRA-CHyA films.

5.2.2.4. High performance liquid chromatographic (HPLC) analysis

HPLC analysis was performed using an Agilent Technologies 1120 Compact LC with a Kinetex 5u C18 100Å (250 x 4.6mm) column (Phenomenex, Cheshire, UK). The mobile phase used in the analysis consisted of methanol:acetonitrile:water:acetic acid (8:1:1:0.05) and was set to a flow rate of 1ml/min, as adapted from Cirpanli et al. [338]. UV detection carried out at 356nm. The concentration of atRA in each sample was determined using an atRA calibration curve which was constructed using standard solutions ranging from 10µg/ml to 0.00056µg/ml (Appendix 1).

5.2.3. Primary tracheobronchial epithelial cell culture

5.2.3.1. Cell source and culture medium

Human primary bronchial/tracheal epithelial cells (ATCC, Middlesex, UK) that were not previously exposed to atRA were used for scaffold culture experiments. The cells were cultured in airway epithelial cell basal medium (ATCC) supplemented with a bronchial epithelial cell growth kit (ATCC), 10U/ml penicillin/streptomycin (Sigma), and 33µM phenol red (Sigma), as per the manufacturer's guidelines. Fully-supplemented medium contained 500µg/ml human serum albumin, 0.6µM linoleic acid, 0.6µg/ml lecithin, 6mM L-glutamine, 0.4% extract P, 1µM adrenaline, 5µg/ml transferrin, 10nM triiodothyronine, 5µg/ml hydrocortisone, 5ng/ml recombinant human epidermal growth factor and 5µg/ml recombinant human insulin. Primary cells were sourced from one donor for experiments (Lot number 58704922) and they were used at passage 4. All cells were cultured at 37°C and 5% CO₂ under a humidified atmosphere. Unless otherwise stated, all cell culture incubation steps were also performed in these conditions. A summary of the cell culture systems outlined below (Sections 5.2.3.2 and 5.2.3.3) is provided in Figure 5.1.

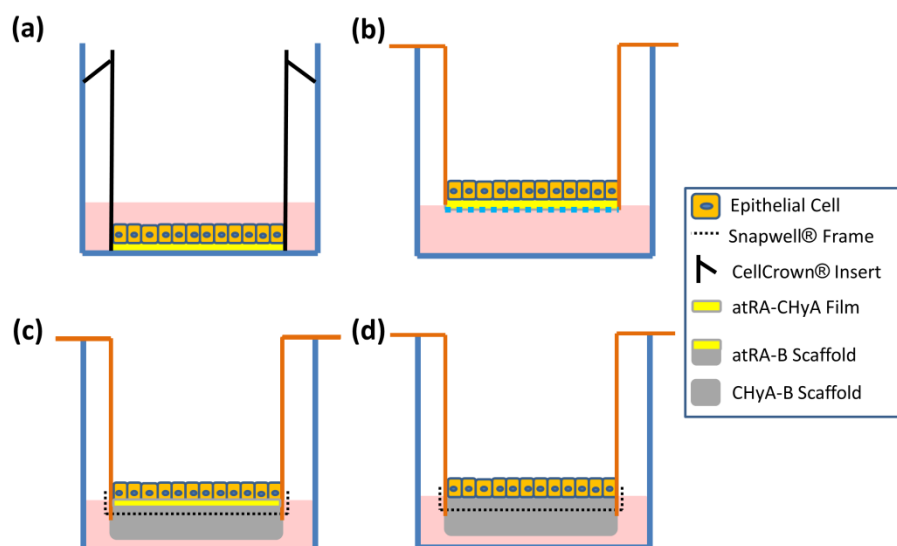


Figure 5.1: Primary tracheobronchial epithelial cell air-liquid interface (ALI) culture models examined for in vitro experiments. (a, b) Cell culture on all-*trans* retinoic acid-loaded collagen-hyaluronate (atRA-CHyA) films. The film was initially fastened in submerged culture using a CellCrown® insert and later transferred onto a cell insert membrane for culture at an ALI. (c) Cell culture on all-*trans* retinoic acid-loaded bilayered collagen-hyaluronate (atRA-CHyA-B) scaffolds. The polymeric membrane is removed from a Snapwell® cell insert and replaced with an atRA-CHyA-B scaffold that is fastened using the plastic frame prior to cell seeding. (d) Cell culture on an atRA-free bilayered collagen-hyaluronate (CHyA-B) scaffold.

5.2.3.2. Primary tracheobronchial epithelial cell culture on atRA-CHyA films

The effect of atRA incorporation on the growth and differentiation of primary tracheobronchial epithelial cells on CHyA films was assessed under air-liquid interface (ALI) conditions. Films fabricated from CHyA suspensions containing 0.1 µg/ml, 1 µg/ml and 10 µg/ml atRA were prepared, DHT-crosslinked and pre-hydrated in DPBS. 12mm discs were punched from each film and transferred to a 24-well plate for an initial period of submerged culture (Fig. 5.1a), during which the films were immobilised at the bottom of the well plates using CellCrown® inserts (Scaffdex, Tampere, Finland). The wells were filled with 900 µl of media and the films were seeded with 2.5×10^5 cells/cm², equating to 100 µl of a suspension that contained 2.8×10^5 cells. The films were carefully transferred into Transwell® inserts (Corning Costar, NY) 3 days later for ALI culture (Fig. 5.1b). The basolateral compartment was filled with 600 µl of media for the remainder of the culture period, with media replaced every 2-3 days. CHyA films containing no atRA were also included in experiments, with cell-seeded films cultured in airway

medium with or without 0.3µg/ml atRA (equivalent to 1×10^{-7} M) as a supplement; these represented positive and negative controls, respectively.

5.2.3.3. Primary tracheobronchial epithelial cell culture on atRA-CHyA-B scaffolds

The ability of atRA-CHyA-B scaffolds to support the growth and differentiation of the primary tracheobronchial epithelial cells was assessed under ALI culture conditions. A customised cell culture system was developed using the frame of a Snapwell® cell insert (Corning Costar, NY) as described in Section 3.2.3.2. The scaffold samples were seeded with 2.5×10^5 primary tracheobronchial cells/cm² into the apical compartment and an ALI was introduced 3 days later with subsequent basolateral feeding for the remainder of the culture period. CHyA-B scaffolds containing no atRA were also included as a negative control.

5.2.4. Epithelial cell viability on atRA-CHyA films and atRA-CHyA-B scaffolds

5.2.4.1. Cell growth on atRA-CHyA films and atRA-CHyA-B scaffolds

Cellular growth was quantified using a Quant-IT Picogreen® dsDNA assay kit (Molecular Probes, Invitrogen, UK) as outlined in Section 2.2.3. Cell-seeded biomaterials were flash frozen in liquid nitrogen, incubated in lysis buffer and homogenised to extract nucleic acids. 50µl of the lysate was assayed for double-stranded DNA (dsDNA) content as a measure of cell viability and the remaining volume was stored at -80°C for analysis of gene expression (Section 5.2.5.2).

5.2.4.2. Cell morphology and migration on atRA-CHyA-B scaffolds

Cell-seeded scaffolds were stained with haematoxylin and eosin and fast green (H&E&FG) to observe primary epithelial cell distribution on the atRA-CHyA-B scaffold top-layer. Scaffold samples were prepared as outlined in Section 3.2.4.1. Briefly, the samples were fixed, processed overnight using an automated tissue processor (ASP300, Leica, Germany) and sectioned using a microtome (Leica RM 2255, Leica). The sections were deparaffinised and stained with H&E&FG prior to dehydration and mounting with DPX (Sigma). Images were captured using an Eclipse 90i microscope and DSRi1 digital camera with NIS Elements Software (Nikon, Japan).

5.2.5. Primary tracheobronchial epithelial cell differentiation on atRA-CHyA films and atRA-CHyA-B scaffolds

5.2.5.1. Immunofluorescence

Immunofluorescent staining of MUC5AC and β -tubulin IV (BIV) was carried out to assess the effect of atRA on inducing and maintaining mucociliary differentiation in primary tracheobronchial epithelial cells cultured on atRA-CHyA films and atRA-CHyA-B scaffolds. These markers represented mucus production by goblet cells and ciliation of the epithelial cells, respectively [60, 284]. Immunofluorescence was performed as outlined in Section 3.2.5.1. Briefly, cell-seeded biomaterials were fixed, permeabilised and incubated with 1% bovine serum albumin (BSA; Sigma) in DPBS to preclude non-specific binding of primary antibody. They were then incubated with either 1/100 mouse anti-MUC5AC monoclonal antibody (Abcam, Cambridge, UK) or 1/400 mouse anti-BIV monoclonal antibody (Sigma) followed by incubation with a 1/500 goat anti-mouse Alexafluor®-594 secondary antibody (Molecular Probes). In the case of atRA-CHyA-B scaffold samples, an additional counterstain with 1/500 Alexafluor®-488-phalloidin for F-actin was performed. Finally, the samples were mounted in Fluoroshield® with 4', 6-diamidino-2-phenylindole (DAPI; Sigma). Images were captured and analysed using an Axio Examiner.Z1 confocal microscope (Carl Zeiss, Cambridge, UK).

5.2.5.2. Expression of genetic markers of epithelial differentiation

The ability of atRA-CHyA films and atRA-CHyA-B scaffolds to support the differentiation of primary tracheobronchial epithelial cells was analysed by quantitative relative gene expression of MUC5AC and FOXJ1, genetic markers for mucus production and ciliation, respectively [285, 286]. Quantitative reverse transcriptase-polymerase chain reaction (qRT-PCR) was performed as outlined in Section 2.2.4.4. 200ng of isolated RNA (Section 5.2.4.1) was reverse transcribed to cDNA and RT-polymerase chain reactions were run on 7500 real-time PCR System (Applied Biosystems, UK) using a QuantiTect SYBR Green PCR Kit (Qiagen) with QuantiTect primers (Qiagen). The expression of mRNA was calculated by the delta-delta Ct ($2^{-\Delta\Delta C_t}$) method relative to the housekeeping gene 18S [287], with gene expression compared to that on atRA-free CHyA films or CHyA-B scaffolds, as appropriate.

5.2.5.3. Scanning electron microscopy (SEM)

The ability of atRA-CHyA-B scaffolds to support the ciliation of primary tracheobronchial epithelial cells was examined by scanning electron microscopy (SEM). Cell-seeded scaffolds were fixed in 3% glutaraldehyde, dehydrated in ascending grades of ethanol and dried using supercritical CO₂ in a critical point dryer as outlined in Section 2.2.4.3. The samples were subsequently mounted on aluminium stubs, sputter-coated and imaged using a Tescan Mira XMU scanning electron microscope at 5kV using secondary electron mode, taken at a working distance between 12-18mm.

5.2.5.4. Transmission electron microscopy (TEM)

Analysis of primary tracheobronchial epithelial ciliation on atRA-CHyA-B scaffolds was also performed by transmission electron microscopy (TEM). Scaffold samples were fixed, dehydrated, embedded in London Resin (LR) white and sectioned as outlined in Section 3.2.5.2. Images were captured with a Hitachi H-7650 electron microscope operating at 100kV.

5.2.6. Data analysis

Analysis of microscopy images was performed using the Fiji processing software. Quantitative data obtained were analysed using Microsoft Excel and GraphPad Prism 4.0 Software (GraphPad Software, San Diego, CA). In cases of analysis between two groups, statistical difference was assessed by two-tailed Student t-test. For multiple groups, statistical difference between groups was assessed by 1-way ANOVA at one time point or 2-way ANOVA for multiple time points, as appropriate. Bonferroni *post hoc* analysis was performed in all ANOVA assessments. Scaffold characterisation experiments were performed using technical replicates, with the number of batches outlined in the relevant Materials and Methods section. Each cell-based experiment was performed a minimum of three times (n=3; three biological replicates); the number of technical replicates performed within each experiment is specified under the relevant figures.

5.3. Results

5.3.1. atRA-CHyA film characterisation

5.3.1.1. atRA-CHyA film manufacture and stability

The incorporation of atRA into CHyA films was successfully achieved for a range of concentrations. A biofabrication process was designed that reproducibly yielded atRA-CHyA films that were stable in structure (Fig. 5.2). The addition of the hydrophobic drug to an aqueous suspension through the use of a blender granted immediate dispersal into a large aqueous volume with constant agitation, preventing precipitation following the initial addition. The dehydration process produced co-polymer films loaded with several concentrations of atRA, between which a clear emergence of a canary yellow hue was observed as the suspension concentration increased from 0µg/ml to 10µg/ml (Fig. 5.2a). Thus, this manufacturing process appeared to successfully incorporate the highly hydrophobic molecule into a natural biomaterial for a range of concentrations in a consistent and repeatable manner.

The effect of the incorporation of atRA on the macromolecular structure of CHyA films was determined by FTIR to assess the stability of the co-polymer film. Spectral data confirmed that the presence of atRA at the higher concentration of 10µg/ml did not alter the distribution or shape of the characteristic amide bands of collagen [342-344]; the amide A band at 3418cm⁻¹, amide I band at ~1645cm⁻¹ and amide II band at ~1250cm⁻¹ were all unaffected by both the presence of atRA (Fig. 5.2c) and by the presence of atRA with DHT crosslinking (Fig. 5.2d). These data indicated that the biocompatible CHyA co-polymer secondary and tertiary structure had been unchanged by the presence of the hydrophobic atRA molecule and thus reflected macromolecular stability in the atRA-CHyA film.

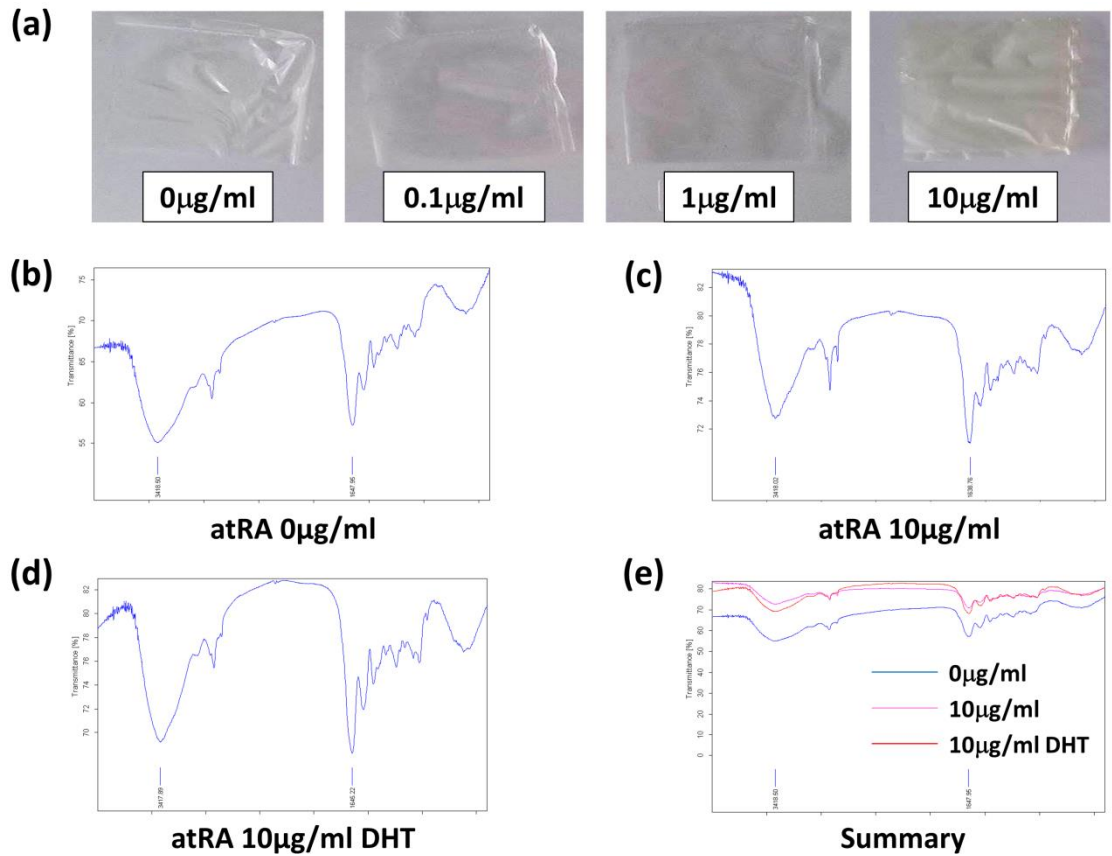


Figure 5.2: The manufacture of stable all-*trans* retinoic acid-loaded collagen-hyaluronate (atRA-CHyA) films for a range of concentrations. (a) atRA-CHyA films fabricated from suspensions of CHyA containing 0 µg/ml, 1 µg/ml or 10 µg/ml atRA. (b-d) Representative Fourier transform infrared spectrometric (FTIR) analysis of (b) 0 µg/ml CHyA films and (c) 10 µg/ml atRA-CHyA films without or (d) with dehydrothermal crosslinking (DHT). (e) A summary of the three FTIR spectra. Y-axis, absorbance; X-axis, wavenumber (cm⁻¹); n=3.

5.3.1.2. atRA-CHyA film encapsulation efficiency

The quantity of atRA in atRA-CHyA films was assessed to determine both its encapsulation efficiency of in the co-polymer film and also the effect of the DHT process on atRA stability. HPLC analysis revealed that the encapsulation efficiency was generally low and that both the initial loading concentration of atRA and the DHT process influenced the quantity of atRA entrapped in the CHyA co-polymer matrix (Table 5.1). The atRA-CHyA films fabricated from a 10µg/ml suspension increased the encapsulation efficiency by 6% when compared to films prepared from CHyA suspensions containing 1µg/ml atRA (Table 5.2). In films fabricated from a CHyA suspension containing 0.1µg/ml atRA, however, no atRA could be detected before or after DHT crosslinking, suggesting that the atRA was lost during the homogenisation and drying processes in manufacture. As a result, no further examination of 0.1µg/ml films was performed.

DHT crosslinking reduced the concentration of atRA in all films by approximately 0.35µg/cm², irrespective of the loading concentration. As a result, greater variability was detected in the final concentration of atRA per cm² within DHT-crosslinked 1µg/ml samples than within 10µg/ml films due to different amounts of drug loading. This was seen most clearly by expression of the data as percentage encapsulation efficiency (Table 5.2), where the DHT-crosslinked 10µg/ml films had a standard deviation ± 4.3% compared to a deviation of ± 11.4% in the 1µg/ml films. Overall, for films that were DHT-crosslinked to ensure sterility, the 10µg/ml atRA-CHyA film had the highest levels and least variable degree of atRA encapsulation, albeit 13.2% of the initial loading concentration.

Table 5.1: Concentration of all-*trans* retinoic acid (atRA) loading in collagen-hyaluronate (CHyA) films. The films were fabricated from CHyA suspensions containing atRA at concentrations of 0.1µg/ml, 1µg/ml or 10µg/ml with or without dehydrothermal (DHT) crosslinking. Results displayed as mean ± standard deviation. n=6-11.

Film [atRA]	<u>atRA (µg/cm²)</u>	
	- DHT	+ DHT
0.1µg/ml	0	0
1µg/ml	0.07 (± 0.01)	0.07 (± 0.04)
10µg/ml	0.82 (± 0.30)	0.46 (± 0.15)

Table 5.2: Encapsulation efficiency of all-*trans* retinoic acid (atRA) loading in collagen-hyaluronate (CHyA) films. The films were fabricated from CHyA suspensions containing atRA at concentrations of 0.1µg/ml, 1µg/ml or 10µg/ml with or without dehydrothermal (DHT) crosslinking. Results displayed as mean ± standard deviation. n=6-11.

Film [atRA]	<u>Encapsulation Efficiency (%)</u>	
	- DHT	+ DHT
0.1µg/ml	0	0
1µg/ml	14.1 (± 2.3)	18.8 (± 11.4)
10µg/ml	20.1 (± 4.4)	13.2 (± 4.3)

5.3.1.3. *In vitro* release of atRA from atRA-CHyA films

The *in vitro* release profile of atRA from atRA-CHyA films was determined to both ascertain the kinetics of drug elution from the biomaterial and also to determine the effect of the DHT process on the release kinetics. In the case of films prepared from both 1µg/ml and 10µg/ml atRA-CHyA suspensions, an early release peak was recorded after which a reduction in detected atRA occurred (Fig. 5.3). The release of atRA peaked at 2 hours from 1µg/ml films and no further atRA could be detected thereafter, irrespective of DHT crosslinking (Fig.5.3a). For 10µg/ml films, peak atRA levels were reached at 6 hours without DHT crosslinking and at 4 hours with DHT, followed by a gradual decline in detection over the course of 30 hours (Fig. 5.3b). While the resultant cumulative release ranged from 4-11% and 52-53% for 1µg/ml (Fig. 5.3c) and 10µg/ml (Fig. 5.3d) formulations, respectively, no residual atRA was detected in the films after the 48 hour period; this indicated that the atRA had degraded over time at 37°C following film hydration. Regardless, the 10µg/ml atRA-CHyA film provided both a higher quantity of atRA release and a longer duration of release than the 1µg/ml atRA-CHyA film.

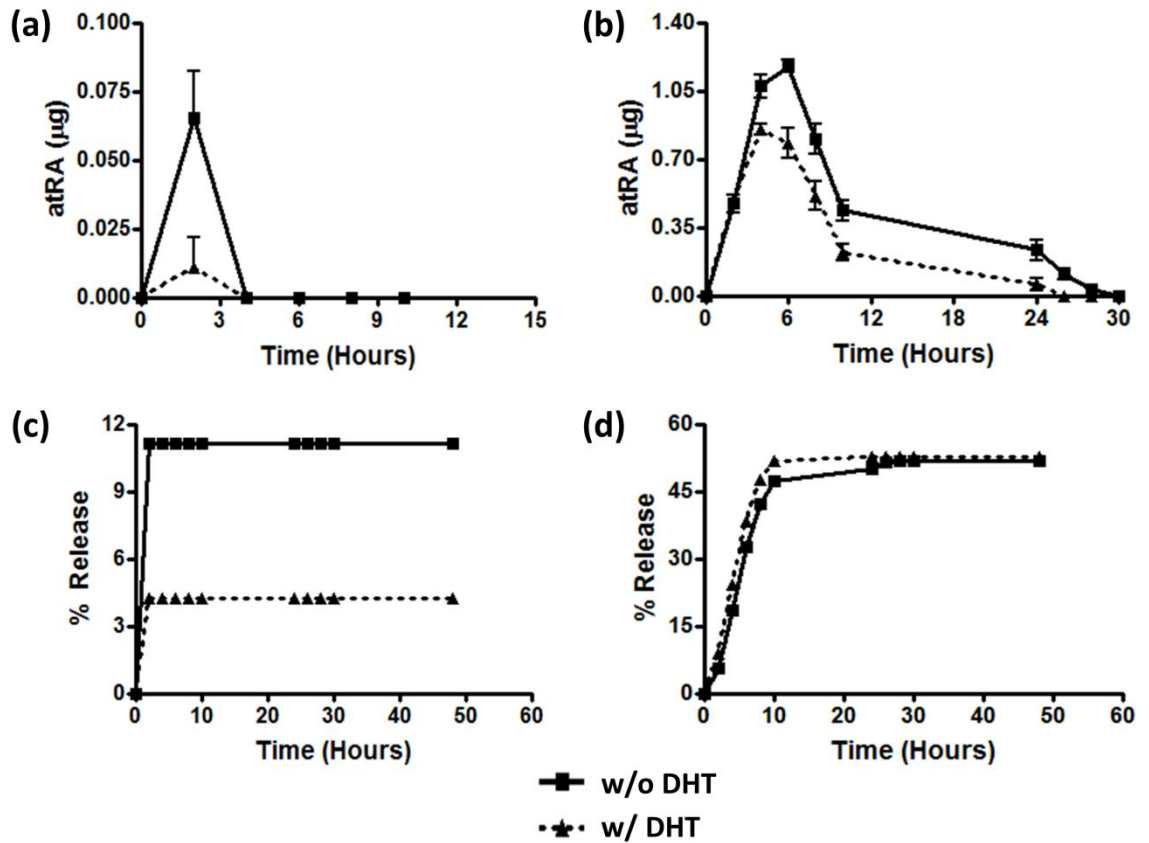


Figure 5.3: All-*trans* retinoic acid (atRA) release from atRA-loaded collagen-hyaluronate (atRA-CHyA) films. Films were fabricated from CHyA suspensions containing 1 µg/ml or 10 µg/ml atRA. (a, b) atRA release (µg) over time from (a) 1 µg/ml or (b) 10 µg/ml atRA-CHyA films with or without dehydrothermal (DHT) crosslinking. Results displayed as mean ± SEM. n=3. (c, d) Cumulative percentage release of atRA from (c) 1 µg/ml or (d) 10 µg/ml films with or without DHT crosslinking. Results displayed as a mean percentage of original atRA quantity present in the film. n=3.

5.3.2. Primary tracheobronchial epithelial cell culture on atRA-CHyA films

5.3.2.1. Epithelial cell growth

Analysis of cellular growth on atRA-CHyA films was performed in order to determine whether the quantity of atRA incorporation into the biomaterial did not inhibit the growth of seeded primary tracheobronchial epithelial cells.

Quantification of dsDNA showed that there was no significant difference in the number of cells present on atRA-CHyA films and atRA-free CHyA films (Fig. 5.4). Indeed, the lowest dsDNA content was observed in the atRA media positive control, where the primary cells were cultured on CHyA films in media that was supplemented with a commonly reported concentration of 0.3 μ g/ml atRA. Overall, the incorporation of atRA did not inhibit primary tracheobronchial epithelial cell growth and therefore did not adversely affect the biocompatible nature of the CHyA copolymer.

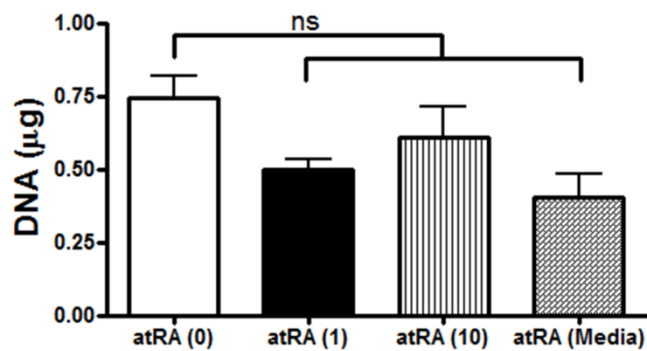


Figure 5.4: Primary tracheobronchial epithelial cell viability on all-*trans* retinoic acid-loaded collagen-hyaluronate (atRA-CHyA) films. Cells were cultured on atRA-CHyA films fabricated from CHyA suspensions containing 0 μ g/ml (atRA (0)), 1 μ g/ml (atRA (1)) or 10 μ g/ml (atRA (10)) atRA for 21 days at an air-liquid interface. 0 μ g/ml CHyA films were also cultured in airway medium containing 0.3 μ g/ml atRA (atRA (Media)). Results displayed as mean \pm SEM. n=3; ^{ns}p>0.05.

5.3.2.2. Mucin expression

Immunofluorescent staining of MUC5AC was carried out to assess the effect of the incorporation of atRA into CHyA films on inducing and maintaining primary tracheobronchial epithelial cell differentiation into mucus-secreting goblet cells [284]. Positive staining was observed for cells cultured on atRA-free CHyA and atRA-CHyA films, with no apparent difference seen in the fluorescence intensity between the two different concentrations of atRA (Fig. 5.5b, 5.5c). The distribution of the red fluorescence, however, was different in appearance on the 10 μ g/ml atRA-CHyA film samples, with larger clusters of MUC5AC (Fig. 5.5c). Overall, the observed staining pattern indicated that atRA-CHyA films facilitated primary epithelial cell functionalisation into MUC5AC-secreting goblet cells.

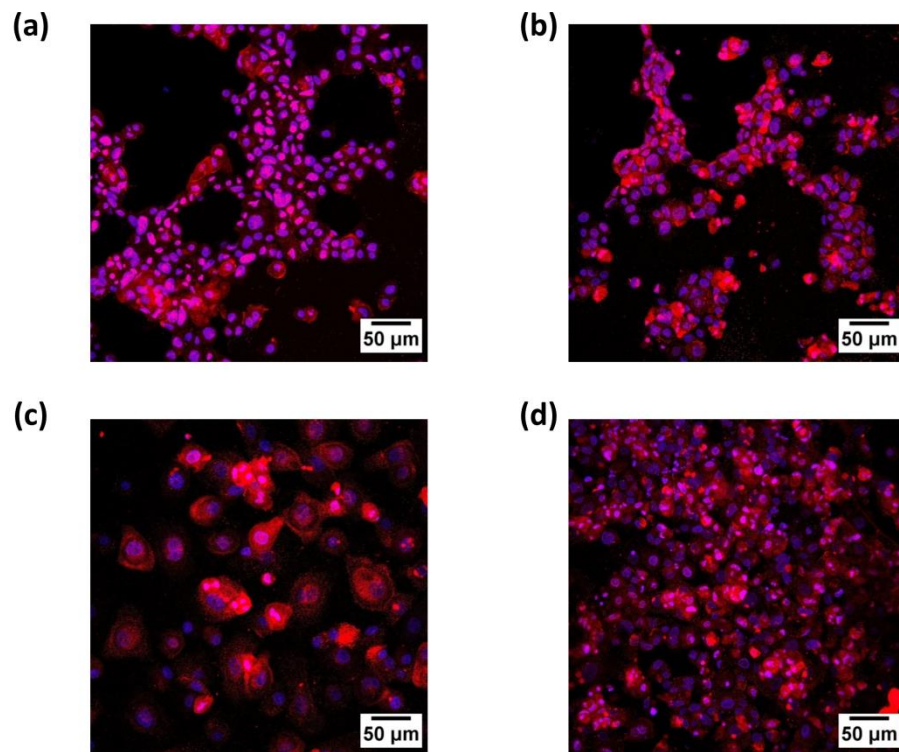


Figure 5.5: MUC5AC expression in primary tracheobronchial epithelial cells on all-*trans* retinoic acid-loaded collagen-hyaluronate (atRA-CHyA) films. Cells were cultured on films fabricated from suspensions containing (a) 0 μ g/ml, (b) 1 μ g/ml or (c) 10 μ g/ml atRA for 21 days at an air-liquid interface. (d) 0 μ g/ml CHyA films were also cultured in airway medium containing 0.3 μ g/ml atRA. Representative maximum intensity projections reconstructed from z-stacks display expression of MUC5AC (red) with cells counterstained for nuclei (blue). n=3.

5.3.2.3. Epithelial ciliation

Immunofluorescent staining of BIV was carried out to assess the effect of the incorporation of atRA into CHyA films on inducing and maintaining the ciliation of primary tracheobronchial epithelial cells [60]. Positive staining was observed for cells cultured on atRA-free and atRA-CHyA films (Fig. 5.6), with an increase in BIV fluorescence detected in cells cultured on atRA-CHyA films made using 10 μ g/ml atRA-CHyA suspensions (Fig. 5.6c). This level closely matched that of cell-seeded CHyA films supplemented with atRA throughout the culture period (Fig. 5.6d). Although the cytoskeletal protein was not concentrated on the apical side of the cell at the ALI, it was clear overall that inclusion of atRA at a concentration of 10 μ g/ml into CHyA films induced a greater production of the structural protein of motile cilia in primary tracheobronchial epithelial cells.

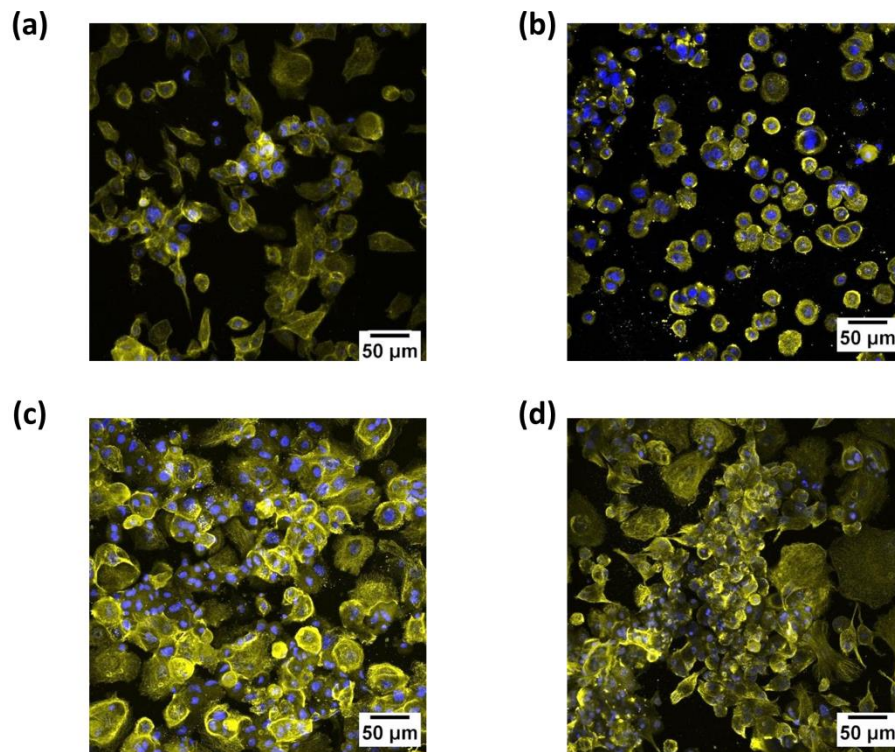


Figure 5.6: β -tubulin IV (BIV) expression in primary tracheobronchial epithelial cells on all-*trans* retinoic acid-loaded collagen-hyaluronate (atRA-CHyA) films. Cells were cultured on films fabricated from suspensions containing (a) 0 μ g/ml, (b) 1 μ g/ml or (c) 10 μ g/ml atRA for 21 days at an air-liquid interface. (d) 0 μ g/ml CHyA films were also cultured in airway medium containing 0.3 μ g/ml atRA. Representative maximum intensity projections reconstructed from z-stacks display expression of BIV (yellow) with cells counterstained for nuclei (blue). n=3.

5.3.2.4. Expression of genetic markers of epithelial differentiation

qRT-PCR analysis was undertaken to examine the ability of incorporated atRA to induce the upregulation of two genes of mucociliary differentiation within primary tracheobronchial epithelial cells cultured on films- MUC5AC and FOXJ1 [285, 286]. Overall, the incorporation of atRA was found to upregulate the expression of both genes within cultured cells (Fig. 5.7). Increased levels of expression were detected with higher concentrations of atRA incorporation, indicating a dose-response effect.

In particular, the cells cultured on 10 μ g/ml atRA-CHyA films experienced a statistically significant increase in expression. An approximate 17-fold increase was detected in MUC5AC mRNA expression over cells cultured on CHyA films in atRA-free conditions (Fig. 5.7a; $p < 0.05$), in addition to an approximate 60-fold increase in FOXJ1 mRNA over 0 μ g/ml CHyA films ($p < 0.001$) and 1 μ g/ml atRA-CHyA films ($p < 0.05$; Fig. 5.7b). Taken together with the immunofluorescent analysis, these data suggested that atRA orchestrated the induction of mucociliary differentiation through upregulation of MUC5AC and FOXJ1 genes.

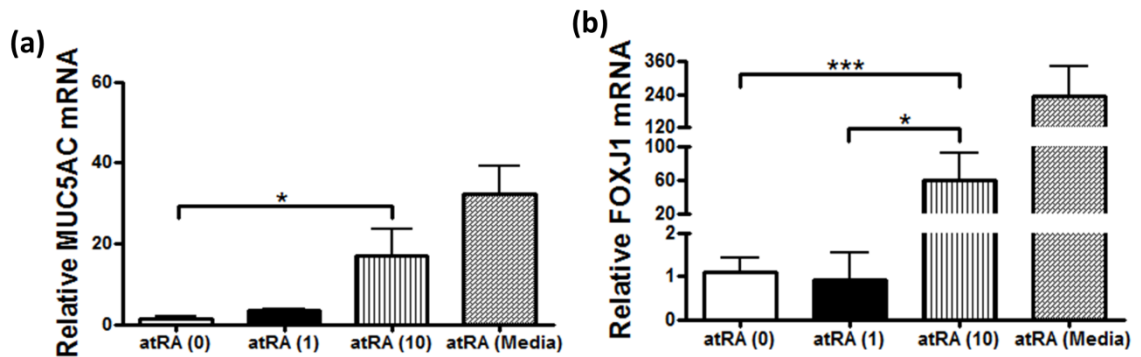


Figure 5.7: The effect of all-*trans* retinoic acid (atRA) incorporation into CHyA films on the relative mRNA expression of primary tracheobronchial epithelial cells. Cells were cultured on films fabricated from collagen-hyaluronate (CHyA) suspensions containing 0 μ g/ml (atRA (0)), 1 μ g/ml (atRA (1)) or 10 μ g/ml (atRA (10)) atRA for 21 days at an air-liquid interface. 0 μ g/ml CHyA films were also cultured in airway medium containing 0.3 μ g/ml atRA (atRA (Media)). Quantification of (a) MUC5AC and (b) FOXJ1 mRNA expression is displayed as mean \pm SEM with expression relative to culture on 0 μ g/ml CHyA films. $n=3$; * $p < 0.05$; *** $p < 0.001$.

5.3.3. atRA-CHyA-B scaffold characterisation

5.3.3.1. atRA-CHyA-B scaffold manufacture and atRA encapsulation efficiency

Therefore, based on the pharmaceutical and *in vitro* analyses of the manufactured atRA-CHyA films, the atRA-CHyA film formulated from a 10µg/ml stock suspension was selected as the film of choice to bring forward for incorporation into a bilayered CHyA scaffold. The films were successfully incorporated into the previously optimised freeze-dry process (Chapter 3) to yield a bilayered atRA-CHyA-B scaffold with a visible yellow film top-layer that indicated the presence of the loaded drug (Fig. 5.8a). This was confirmed by analysis of the encapsulation efficiency of atRA within the atRA-CHyA-B scaffold. This demonstrated that there was no further loss in atRA as a result of the lyophilisation process required for scaffold manufacture, with no significant difference between the DHT-crosslinked 10µg/ml atRA-CHyA films (Table 5.2) and the DHT-crosslinked atRA-CHyA-B scaffolds (Fig 5.8b; 13.2% vs 11.0%, $p=0.3$). Furthermore, HPLC analysis of the 0.5M acetic acid solvent used to hydrate the atRA-CHyA film prior to freeze-drying did not contain any traces of atRA (not shown). Taken together, these results indicated that the atRA-CHyA-B scaffold fabrication procedure consistently produced a bilayered material with stable retention of the hydrophobic compound.

5.3.3.2. In vitro release of atRA from atRA-CHyA-B scaffolds

The release of atRA from atRA-CHyA-B scaffolds was determined to both ascertain the kinetics of drug elution from the biomaterial and also to determine the effect of EDAC crosslinking on the release kinetics. HPLC analysis of the sampled time points revealed a peak release of atRA at 4 hours, followed by a rapid reduction in atRA released over the following 6 hours with none detected by 24 hours (Fig. 5.8c). Thus, the pattern of atRA release from the bilayered scaffold mirrored that of atRA-CHyA films, indicating that the lyophilisation process did not alter the mechanism of atRA incorporation into the thin co-polymer biomaterial. The cumulative release of atRA, however, was greater from atRA-CHyA-B scaffold samples, with approximately 72% of the incorporated atRA released by 24 hours (Fig. 5.8d) compared to 52% from atRA-CHyA films (Fig. 5.3d). EDAC crosslinking reduced the cumulative release from atRA-CHyA-B scaffolds to 64%. As in the case of atRA-CHyA films, digestion of the atRA-CHyA-B scaffold samples after the release detected no residual atRA, indicating that atRA degradation occurred

following hydration at 37°C. Overall, the atRA-CHyA-B scaffold provided a local elution of the airway epithelial mucociliary factor for 24 hours following hydration in physiological media.

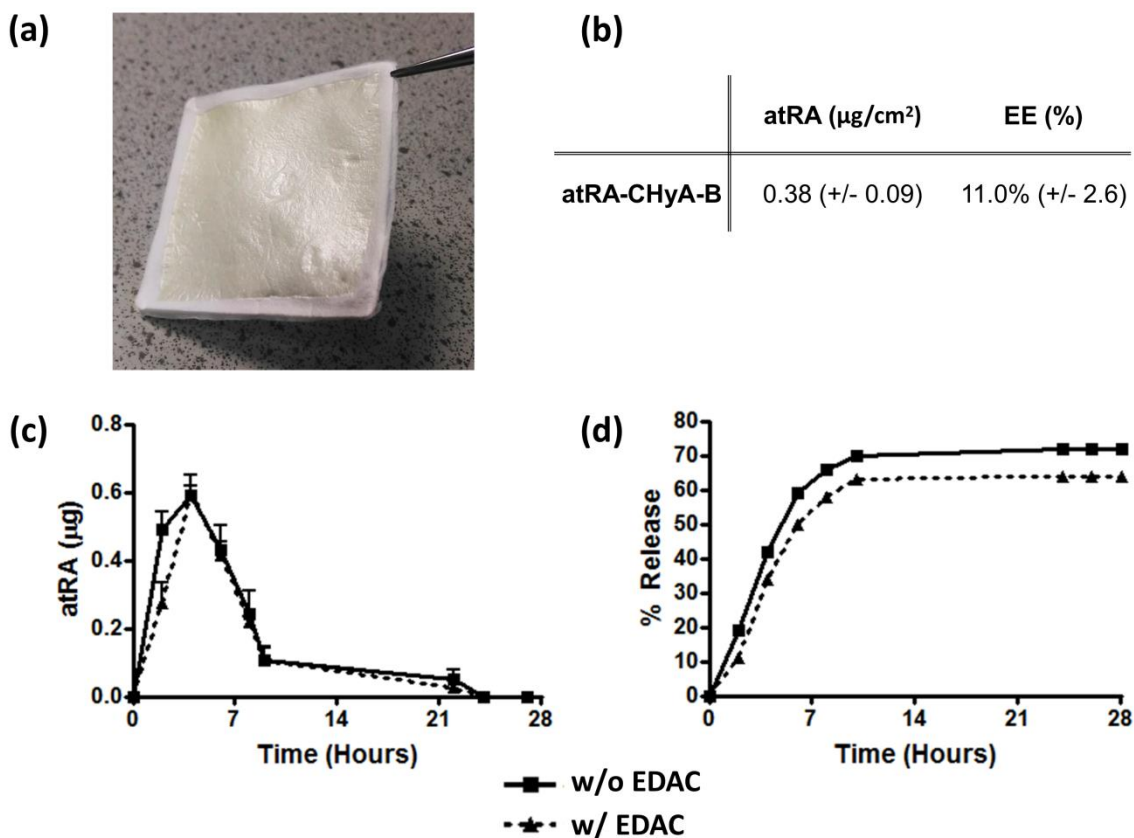


Figure 5.8: Bilayered all-*trans* retinoic acid-loaded collagen-hyaluronate (atRA-CHyA-B) scaffold characterisation. (a) Macroscopic image of atRA-CHyA-B scaffold. A CHyA film prepared from a CHyA suspension containing 10 $\mu\text{g}/\text{ml}$ atRA (yellow) is incorporated into a porous CHyA layer. (b) Encapsulation efficiency of dehydrothermal-crosslinked atRA-CHyA-B scaffolds. Results displayed as mean \pm standard deviation. $n=6$. (c) atRA release (μg) over time from atRA-CHyA-B scaffolds with or without crosslinking using 1-ethyl-3-(3-dimethylaminopropyl)carbodiimide hydrochloride (EDAC). Results displayed as mean \pm SEM. $n=3$. (d) Cumulative percentage release of atRA over time. Results displayed as a mean percentage of original atRA quantity present in the scaffold film layer. $n=3$.

5.3.4. Primary tracheobronchial epithelial cell culture on atRA-CHyA-B scaffolds

5.3.4.1. Epithelial cell growth

Analysis of cellular growth on atRA-CHyA-B scaffolds was performed in order to initially determine the scaffold's ability to support primary tracheobronchial epithelial cell growth. Quantification of dsDNA revealed that the cellular viability on atRA-CHyA-B scaffold samples was significantly lower than that on CHyA-B scaffolds at day 7 (Fig. 5.9a; $p < 0.01$), but by the end of the culture period, no significant difference in dsDNA quantity was observed between the two groups. At day 7, the dsDNA content on CHyA-B (atRA-free) scaffolds was twice the amount present on atRA-CHyA-B scaffolds, reflecting a lower cell number when atRA was present in the film. By day 21, however, the dsDNA content had dropped from $1.13\mu\text{g}$ to $0.31\mu\text{g}$ on CHyA-B scaffolds ($p < 0.01$), while a reduction from $0.54\mu\text{g}$ to $0.29\mu\text{g}$ occurred on atRA-CHyA-B scaffolds ($p > 0.05$); this finding highlighted that from day 7 onwards, the cells remaining on the atRA-CHyA-B scaffolds were still viable over the culture period. Moreover, the difference in dsDNA content at day 21 was not statistically significant between CHyA-B and atRA-CHyA-B groups ($p > 0.05$). Overall, following an initial period of reduced cellular growth on the atRA-CHyA-B scaffold, the biomaterial was a viable substrate for the remaining primary epithelial cells in culture.

5.3.4.2. Cell morphology and migration

In conjunction with the quantification of dsDNA content on atRA-CHyA-B scaffolds, cell-seeded scaffolds were stained with H&E&FG to observe primary tracheobronchial epithelial cell growth and distribution on the scaffold top-layer. Histological analysis highlighted that the cells present on the atRA-CHyA-B scaffolds exhibited a more organotypic morphology than those grown on CHyA-B (atRA-free) scaffolds, although an epithelial monolayer was not present in either sample groups (Fig. 5.9b, 5.9c). Cells upon atRA-CHyA-B scaffolds adopted a multi-layered columnar morphology and were arranged in clusters interspersed with squamous cells (Fig. 5.9b). On CHyA-B scaffolds, by contrast, only collections of squamoid epithelial cells were visible (Fig. 5.9c). Overall, the data corroborated the reduced dsDNA content detected in both samples at day 21, with a sparse presence of cells visualised in all groups. In summary, in spite of the general reduced numbers of cells, the morphology on atRA-CHyA-B scaffolds highlighted

their potential to prevent squamous metaplasia and support a pseudostratified epithelium.

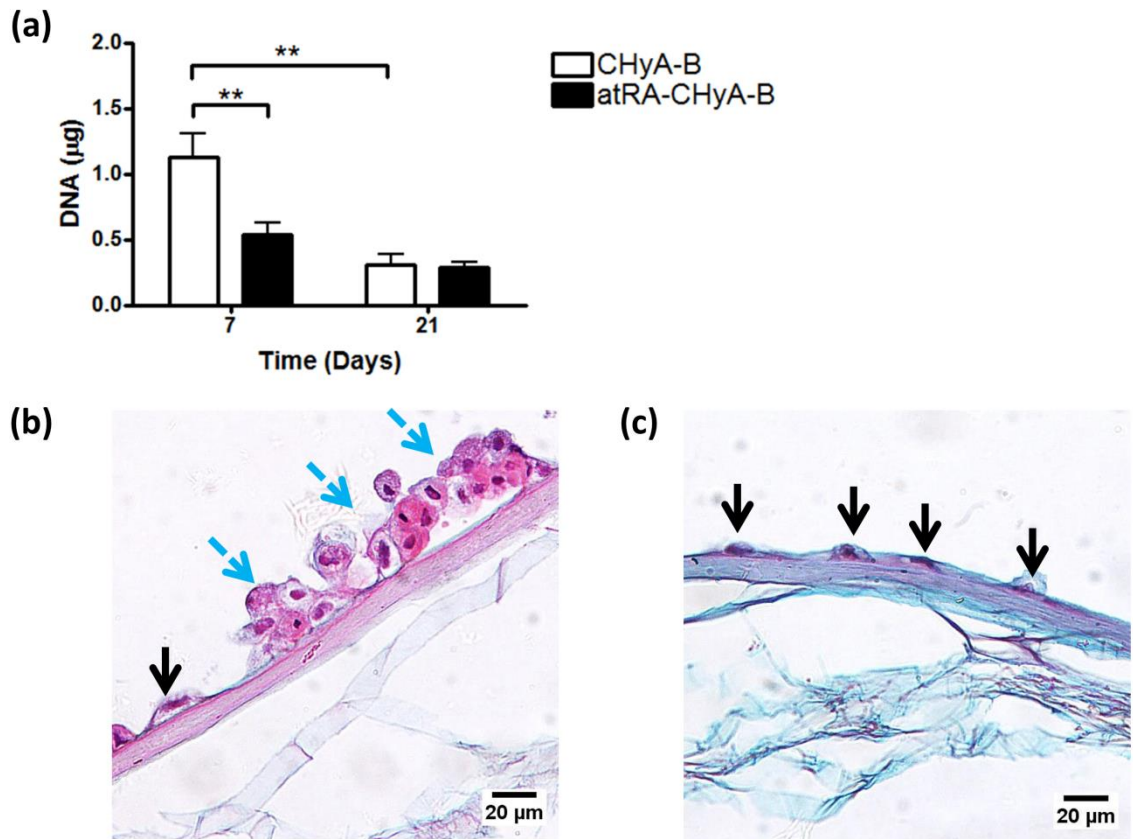


Figure 5.9: Primary tracheobronchial epithelial cell viability on bilayered all-*trans* retinoic acid-loaded collagen-hyaluronate (atRA-CHyA-B) scaffolds. Epithelial cells were cultured either on atRA-CHyA-B scaffolds or on atRA-free CHyA-B scaffolds at an air-liquid interface for 21 days. (a) DNA content on atRA-CHyA-B scaffolds. Results displayed as mean \pm SEM. $n=3$; $**p<0.01$. (b) On atRA-loaded scaffolds, epithelial cells formed clusters of columnar cells (blue arrows) with interspersed squamous cells (black arrows). (c) On atRA-free scaffolds, cells adopted a squamous morphology only (black arrows). Representative haematoxylin & eosin and fast green staining visualised scaffolds as a light-blue colour with a pink-purple film layer and cells appeared as pink-purple with darker nuclei. $n=1$.

5.3.4.3. Mucin expression

Having observed a sparse but viable population of primary tracheobronchial epithelial cells on atRA-CHyA-B scaffolds, immunofluorescent staining of MUC5AC was carried out to assess the effect of the incorporation of atRA on inducing and maintaining cell differentiation into mucus-secreting goblet cells [284]. Positive detection of MUC5AC was observed within the clusters of layered cells on atRA-CHyA-B scaffolds, with apical localisation of the mucin observed from analysis of z-stack constructions (Fig. 5.10a). While maximum intensity projections of the confocal images did not discern any greater levels of red fluorescence between groups (Fig. 5.10b, 5.10d), this apical localisation was not apparent within the CHyA-B (atRA-free) culture groups (Fig. 5.10c). A small degree of red fluorescence overlapping with the nuclear DAPI stain was observed in one image, but this observation was not synonymous with the typical staining pattern of MUC5AC and the faint pink colour most likely represented interference with the blue fluorescent emission. Thus, the atRA-CHyA-B scaffold enhanced the differentiation of the primary tracheobronchial epithelial cells into goblet cells when compared to the culture of the same cells on atRA-free CHyA-B scaffolds.

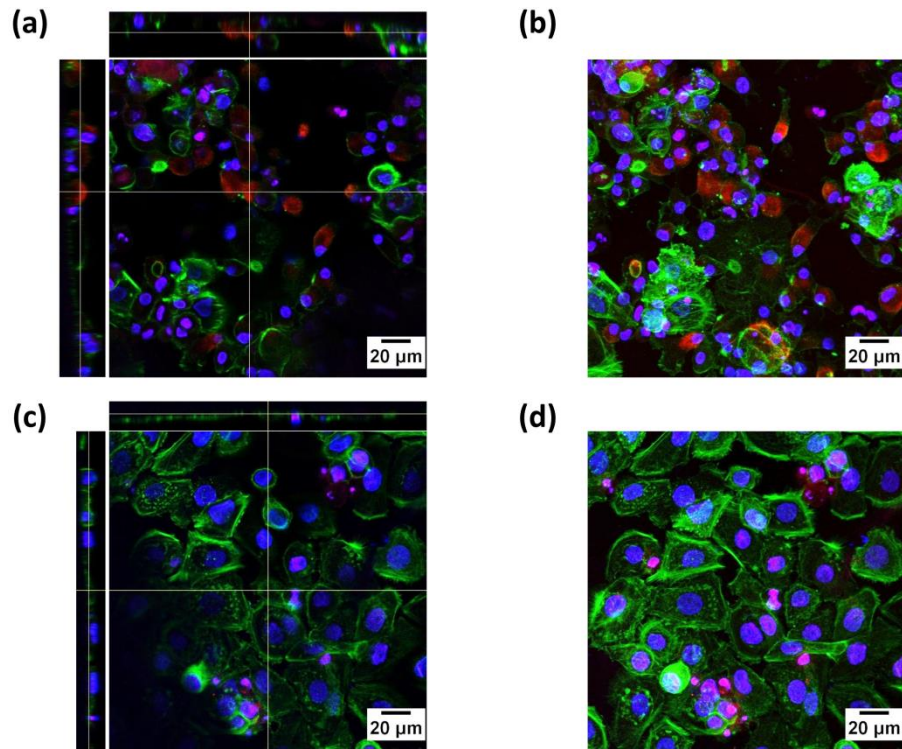


Figure 5.10: MUC5AC expression in primary tracheobronchial epithelial cells on bilayered all-*trans* retinoic acid-loaded collagen-hyaluronate (atRA-CHyA-B) scaffolds. Epithelial cells were cultured either on (a, b) atRA-CHyA-B scaffolds or on (c, d) atRA-free CHyA-B scaffolds at an air-liquid interface for 21 days. (a, c) Representative z-stack images display apical MUC5AC secretion (red) on top of cells counterstained for nuclei (blue) and F-actin (green). (b, d) Maximum intensity projections of MUC5AC expression reconstructed from z-stacks. n=3.

5.3.4.4. Epithelial ciliation

The ability of atRA-CHyA-B scaffolds to support the ciliation of primary tracheobronchial epithelial cells in addition to mucus secretion was examined by immunofluorescent staining of BIV, a cytoskeletal protein within the axoneme of cilia [60]. Confocal microscopic analysis revealed an absence of BIV in the primary cells cultured on scaffolds, irrespective of whether atRA was loaded or not into the film top-layer (Fig. 5.11). The localisation of BIV clusters to the apical region of the cells that is representative of mature motile cilia was not visible (Fig. 5.11a, 5.11c), although the maximum intensity projection of atRA-CHyA-B scaffold samples visualised a faint signal of BIV fluorescence within the cytoskeletal framework of the epithelial cells that was not visible within cells on CHyA-B (atRA-free) scaffolds (Fig. 5.11b, 5.11d). Nevertheless, the prevailing finding from these data was that ciliation did not occur within the primary tracheobronchial epithelial cells in atRA-CHyA-B scaffold culture.

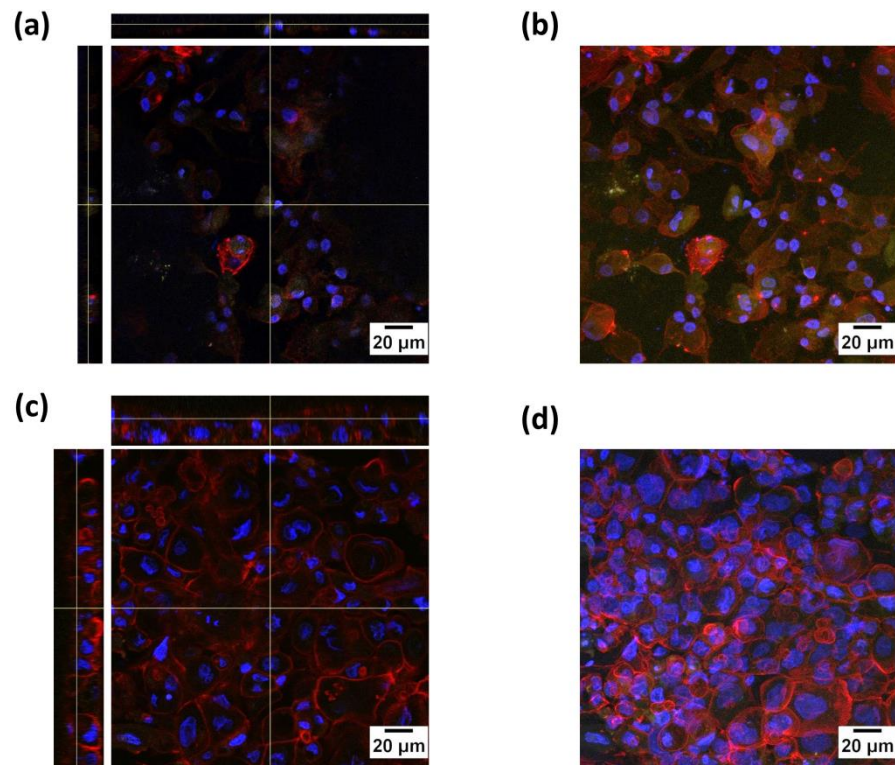


Figure 5.11: β -tubulin IV (BIV) expression in primary tracheobronchial epithelial cells on bilayered all-*trans* retinoic acid-loaded collagen-hyaluronate (atRA-CHyA-B) scaffolds. Epithelial cells were cultured either on (a, b) atRA-CHyA-B scaffolds or on (c, d) atRA-free CHyA-B scaffolds at an air-liquid interface for 21 days. (a, c) Representative z-stack images display apical BIV expression (yellow) on top of cells counterstained for nuclei (blue) and F-actin (red). (b, d) Maximum intensity projections of BIV expression reconstructed from z-stacks. n=3.

5.3.4.5. Epithelial ultrastructure- SEM

Primary tracheobronchial epithelial cells on atRA-CHyA-B scaffolds were also examined by SEM to detect epithelial barrier formation and ciliation. The analysis confirmed that the cells formed clusters of cells without evidence of ciliation (Fig.5.12). In accordance with the histological data (Fig. 5.9b), cells on atRA-CHyA-B scaffolds were raised and multi-layered in morphology with interspersed flattened cells of a squamous nature (Fig. 5.12a); neither ciliated structures on the cell surface nor intercellular barrier junctions were present (Fig. 5.12b). Of course, the cobblestone conformation typical of the *in vivo* tracheobronchial region was also absent from the atRA-free CHyA-B scaffold samples, upon which isolated regions of spread cells were detected on a film top-layer that was largely barren of a respiratory epithelium (Fig. 5.12c, 5.12d). Overall, the tracheobronchial cells did not adopt an organotypic epithelium with mucociliary differentiation on both types of scaffold assessed.

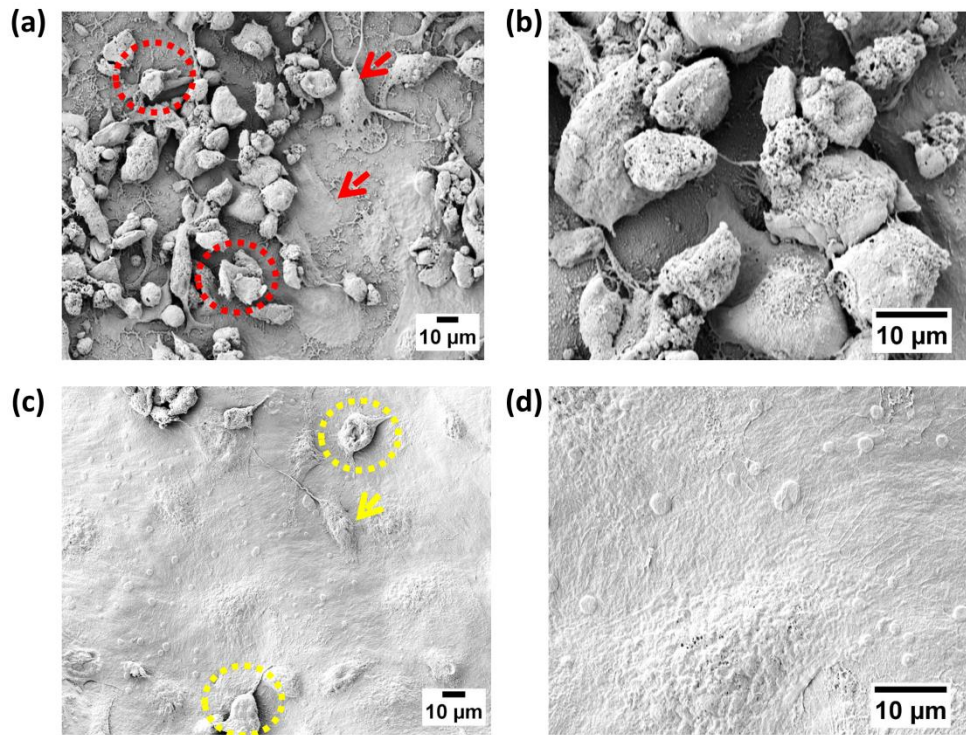


Figure 5.12: Ultrastructural analysis of primary tracheobronchial epithelial cells on bilayered all-*trans* retinoic acid-loaded collagen-hyaluronate (atRA-CHyA-B) scaffolds using scanning electron microscopy. Epithelial cells were cultured at an air-liquid interface for 21 days. (a) On atRA-CHyA-B scaffolds, representative images visualised cells as clusters of cells (red circles) with interspersed flattened cells (red arrows). (b) Higher magnification images of cells displayed an absence of cilia. (c) On atRA-free CHyA scaffolds, cells were sparser across the film layer and were visualised as raised and extended in shape (yellow circles) and with flattened morphology (yellow arrows). (d) A confluent cell layer and evidence of cilia were absent. n=1.

5.3.4.6. Epithelial ultrastructure- TEM

The final assessment of the effect of atRA-CHyA-B scaffolds on the ciliation of primary tracheobronchial epithelial cells was performed by TEM. In a similar result to BIV immunofluorescence and SEM, cilia were notably absent in both culture models (Fig. 5.13). Multi-layered cell clusters were again visible on atRA-CHyA-B scaffolds (Fig. 5.13a) while cells on CHyA-B scaffolds were more isolated and squamous (Fig. 5.13b). Ultimately, these findings confirmed that ciliated epithelial cells of the upper respiratory tract were absent on atRA-CHyA-B and CHyA-B samples.

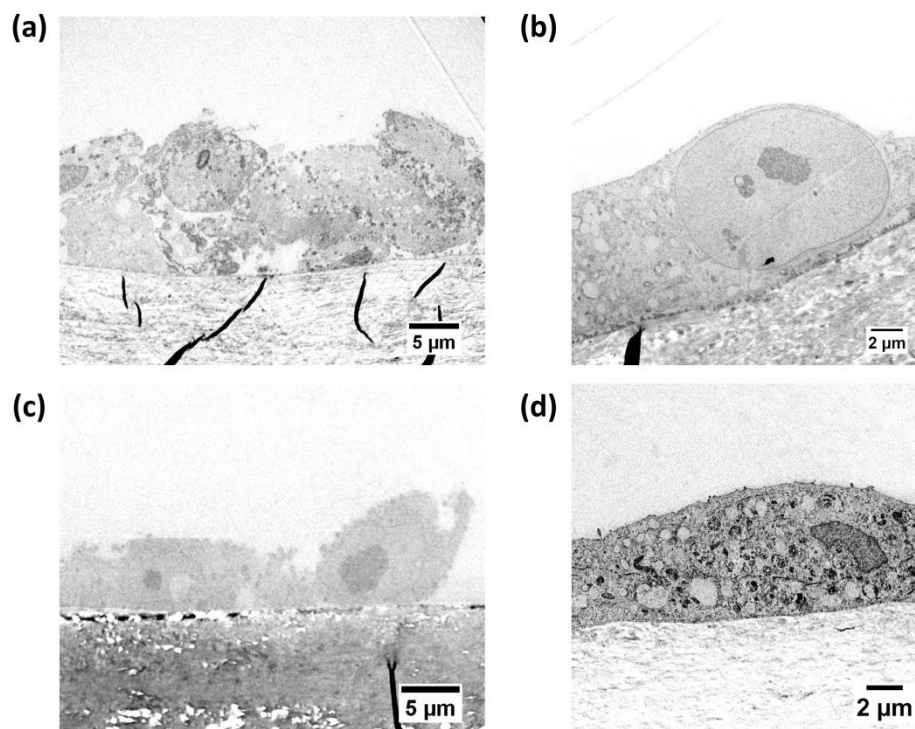


Figure 5.13: Ultrastructural analysis of primary tracheobronchial epithelial cells on bilayered all-*trans* retinoic acid-loaded collagen-hyaluronate (atRA-CHyA-B) scaffolds using transmission electron microscopy. Epithelial cells were cultured at an air-liquid interface for 21 days. (a, b) On atRA-CHyA-B scaffolds, cells grew in clusters with no expression of cilia. (c, d) On atRA-free CHyA-B scaffolds, cells adopted a squamous morphology and with no expression of cilia. n=1; representative images were captured by Mr. Brenton Cavanagh, RCSI.

5.3.4.7. Expression of genetic markers of epithelial differentiation

Despite the evident lack of differentiation of the cultured primary tracheobronchial epithelial cells towards a fully functional epithelium with ciliated cells, qRT-PCR analysis of MUC5AC and FOXJ1 was performed in order to ascertain the ability of atRA-CHyA-B scaffolds to modulate the expression of genetic markers that were previously upregulated on atRA-CHyA films. Interestingly, a large increase in relative mRNA expression was detected for both MUC5AC and FOXJ1 in cells cultured on atRA-CHyA-B scaffolds when compared to atRA-free scaffolds (Fig. 5.14). Expression of MUC5AC, a canonical gene for mucus expression [286], exhibited an approximate 43-fold increase in transcription, and FOXJ1, a critical gene for ciliogenesis [285] (Fig. 5.14a; $p < 0.05$), exhibited a significant 605-fold increase in the atRA-CHyA-B scaffold model (Fig. 5.14b; $p < 0.01$). Thus, in spite of the lack of translation of the ciliary protein BIV observed in *in vitro* culture, the incorporation of atRA significantly upregulated the expression of a key ciliary gene in primary tracheobronchial epithelial cells. Accordingly, these data suggest that the atRA-CHyA-B scaffolds have the potential to enhance the ciliation of the respiratory epithelium under certain conditions.

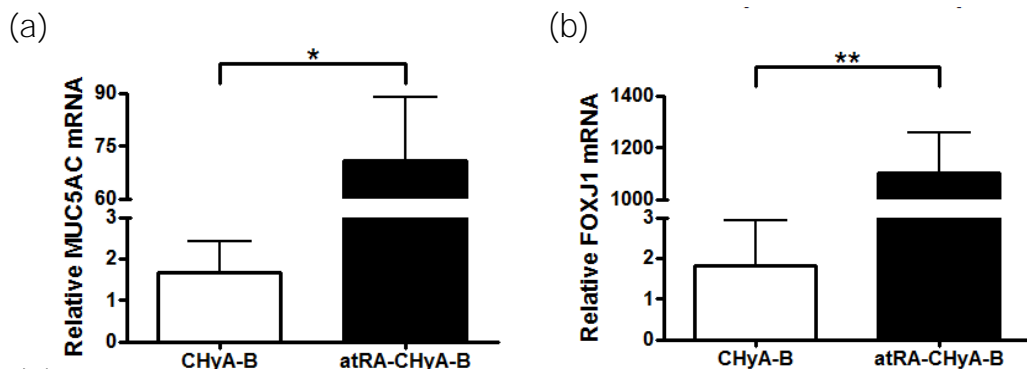


Figure 5.14: The effect of bilayered all-*trans* retinoic acid-loaded collagen-hyaluronate (atRA-CHyA-B) scaffolds on the relative mRNA expression of primary tracheobronchial epithelial cells. Epithelial cells were cultured either on atRA-CHyA-B scaffolds or on atRA-free CHyA-B scaffolds at an air-liquid interface for 21 days. Quantification of (a) MUC5AC mRNA expression and (b) FOXJ1 mRNA expression is displayed as mean \pm SEM with expression relative to culture on CHyA-B scaffolds. $n=3$; * $p < 0.05$; ** $p < 0.01$.

5.4. Discussion

In order to develop the CHyA-B scaffold as an implant with the potential to support functional epithelialisation for tissue regeneration, the major objective of this chapter was to manufacture an atRA-CHyA-B scaffold as a platform technology for tracheal tissue regeneration. Specifically, we sought to: (i) fabricate and characterise an atRA-CHyA film layer as a novel drug-eluting biomaterial; (ii) assess the potential of atRA to enhance the differentiation of primary tracheobronchial epithelial cells cultured on the atRA-CHyA films; and (iii) incorporate the atRA-loaded film layer into the CHyA-B scaffold to successfully develop the atRA-CHyA-B scaffold and to evaluate its potential as a biomaterial to enhance functional epithelialisation of the scaffold. The results led to the development of a reproducible process that successfully incorporated the hydrophobic drug into CHyA films for a range of concentrations without disruption of the copolymer structure. While the encapsulation efficiency of atRA was generally low in the atRA-CHyA films and the rate of *in vitro* release was rapid, a film fabricated from a stock CHyA suspension containing 10µg/ml atRA was identified as the lead biomaterial. The film had the highest and most consistent level of atRA incorporation, in addition to a favourable release pattern that induced the expression of mucus and BIV protein expression in primary tracheobronchial epithelial cells cultured upon it. This atRA-CHyA film was integrated into the bilayered scaffold fabrication process (Chapter 3) to yield an atRA-CHyA-B scaffold without any loss of atRA-loading from the film manufacture procedure. Despite limited cell attachment and a lack of ciliation on the atRA-CHyA-B scaffold, the presence of the drug significantly upregulated the expression of two genetic markers of mucociliary differentiation within cultured epithelial cells. Taken together, these data demonstrate the feasibility of manufacture of an atRA-CHyA-B scaffold and its potential for functional epithelialisation and tracheal tissue regeneration.

atRA was successfully integrated into the CHyA film fabrication process through the use of a homogenising blender prior to solvent casting (Fig. 5.2). The physicochemical properties of atRA presented a challenge for integration into a hydrophilic natural polymer scaffold. Firstly, the aqueous solubility of atRA is reported to be less than 1mg/ml at 25°C [335], which could even be further

reduced at the colder 4°C temperature used during slurry preparation. Additionally, the pKa of atRA is an estimated 4.2 (reported in [335]), meaning that the drug would be primarily unionised at the pH of the CHyA slurry (pH 3.2) and as a result, less soluble. Therefore, the blender was utilised to rapidly disperse atRA through a large volume of aqueous vehicle following its addition to prevent both precipitation and agglomeration. Most pharmaceutical suspensions require the use of a suspending agent to stabilise less-soluble drugs in the disperse phase of the formulation [345], and thus it is possible that the collagen and hyaluronate co-polymer suspension similarly stabilises the atRA dispersion through a combination of steric hindrance and its viscous nature. Upon the formation of the atRA-CHyA films by solvent casting, no residual atRA or evidence of crystallisation was observed, suggesting integration of the hydrophobic molecule into the co-polymeric structure (Fig. 5.2a). The mechanism by which atRA associates with the CHyA co-polymer has not been investigated, but as no chemical coupling agent was used in atRA-CHyA film formation, non-covalent hydrophobic interactions could predominate between atRA and the CHyA copolymer. The inclusion of a hydrophobic drug did not destabilise the macromolecular structure of the film, as confirmed by the characteristic FTIR amide bands of the collagen macromolecule and linkage to hyaluronate observed even at the at the higher atRA concentration of 10µg/ml [298, 342-344]. This qualitative analysis of secondary and tertiary structure served to reaffirm the stable incorporation of atRA into the biocompatible CHyA substrate.

Although the fabrication process appeared to produce atRA-CHyA films in a reproducible and homogenous manner, HPLC analysis revealed that the encapsulation efficiency of atRA was generally low and the DHT process further reduced the quantity of atRA entrapped in the CHyA co-polymer matrix (Tables 5.1, 5.2). atRA is labile to heat, light and oxygen-mediated degradation [336], and as a result, losses during the blending and dehydration steps were very likely. Indeed, even prior to DHT sterilisation, no atRA was detected in films fabricated from 0.1µg/ml atRA-CHyA stock suspensions, leading to its early exclusion from the study. In spite of these drug losses, however, the resultant concentration of atRA in the DHT-sterilised 10µg/ml atRA-CHyA formulation was approximately 0.46µg/cm², a concentration proximate to that of an atRA-loaded hyaluronan-

derivative membrane that acted as a substrate for improved ciliation and mucus secretion of respiratory epithelial cells [341]. Through derivation from the experimental steps of the published protocol within this report, the atRA present in the hyaluronan-derivative film was calculated to be $0.45\mu\text{g}/\text{cm}^2$. Consequently, the concentration of atRA remaining within the atRA-CHyA film in this study contains an absolute quantity of the drug in the concentration range amenable for differentiation of respiratory epithelial cells, irrespective of low percentage encapsulation efficiency relative to the original loading concentration.

The elution of atRA from atRA-CHyA films was rapid. Following film hydration, a burst release of atRA was observed from the $1\mu\text{g}/\text{ml}$ and $10\mu\text{g}/\text{ml}$ films within the first 2-8 hours, followed by a rapid decline in atRA concentration in the release buffer (Fig. 5.3). Indeed, within the $1\mu\text{g}/\text{ml}$ atRA-CHyA film samples, only the early time point sample of 2 hours contained atRA (Fig. 5.3a). Although only 11% of the incorporated atRA was cumulatively detected in release buffer at this time point (Fig. 5.3c), no further atRA was found within the film sample at 48 hours; this indicated that the atRA present had degraded. In a similar trend, the rapid release from the $10\mu\text{g}/\text{ml}$ atRA-CHyA films tailed off after 8 hours (Fig. 5.3b); notably, the quantity of atRA released over this time period was much higher for the $10\mu\text{g}/\text{ml}$ atRA-CHyA films. Unlike the other reported delivery systems for atRA that encase the drug within a synthetic polymeric shell or matrix to regulate exposure to media, dissolution and sustained release [337-341], atRA would quickly be exposed to the aqueous environment in the atRA-CHyA film following rehydration and polymer swelling in the physiological buffer. This in turn could trigger the loss of hydrophobic interactions in a polar environment and dissociation of the atRA molecule, resulting in its burst release. On the other hand, atRA degradation in this environment at 37°C would reduce the high atRA concentrations so that if the quantity of atRA loading is insufficient, any released drug would be cleared in a short period of time. Therefore, the $10\mu\text{g}/\text{ml}$ atRA-CHyA film provides the necessary level of atRA-loading to provide the adequate temporal and spatial control of atRA release to facilitate a short exposure period for epithelial cells cultured thereon.

When primary respiratory epithelial cells were cultured on the atRA-CHyA films, this early release of atRA from the $10\mu\text{g}/\text{ml}$ atRA-CHyA films was found to induce

the expression of two markers of mucociliary differentiation within cultured primary tracheobronchial epithelial cells with no undesired cytotoxic effect. Quantification of dsDNA confirmed that drug incorporation into CHyA films did not adversely affect the viability of seeded cells for both concentrations of atRA-CHyA films (Fig. 5.4), negating concerns about the growth-suppressive effect of atRA that is utilised in other therapies as an oncologic therapeutic [159]. Indeed, the lowest number of cells was detected in the 0.3µg/ml atRA-supplemented media positive control, a concentration conventionally used to increase ciliation in primary airway culture and to prevent squamous epithelium formation *in vitro* [69, 341], although this decrease was non-significant ($p>0.05$). Immunofluorescent analysis of primary respiratory epithelial cells cultured on the atRA-CHyA films showed that the expression of BIV, a structural protein present in motile cilia [60, 319], matched that of cells cultured in the presence of 0.3µg/ml atRA-supplemented media (Fig. 5.6). This finding was reflected in the significant increase in FOXJ1 gene expression detected in cells cultured on the 10µg/ml atRA-CHyA films, indicating that atRA released from the film stimulated the transcription of the key regulator of ciliation within primary cells (Fig. 5.7a). While the incorporation of atRA did not appear to have a major effect on MUC5AC glycoprotein expression within cells cultured on CHyA films despite the significant increase in MUC5AC mRNA expression in 10µg/ml atRA-CHyA culture (Fig. 5.7), mucin was present in all *in vitro* culture samples (Fig. 5.5). Earlier studies have demonstrated that the CHyA material can induce mucin secretion in its own capacity in the Calu-3 cell line (Chapter 3) and support goblet cell differentiation in primary culture (Chapter 4). The effect of atRA on MUC5AC expression might therefore be partially masked by the stimulatory effect of the biomaterial, as has been noted with ciliation of cells on other hyaluronan-containing materials [167]. Regardless, the combination of the CHyA film and atRA at a loading concentration of 10µg/ml primary epithelial cells enhance the functionalisation of tracheobronchial epithelial cells into a mucociliary phenotype compared to atRA-free CHyA films without any atRA supplementation.

When these results were considered in combination with the characterisation of the atRA-CHyA film encapsulation and release, the decision was subsequently made to select the 10µg/ml atRA-CHyA film as the lead film formulation for the modification of the CHyA-B scaffold fabrication process to produce a bilayered

atRA-CHyA-B scaffold. These films were successfully incorporated into porous scaffolds using the previously optimised freeze-dry process (Chapter 3) to yield a bilayered atRA-CHyA-B scaffold with a visible yellow film top-layer, indicating the presence of the loaded drug (Fig. 5.8a). The freeze-drying process did not reduce the concentration of atRA loaded in the film layer significantly ($0.46\mu\text{g}/\text{cm}^2$ prior to lyophilisation versus $0.38\mu\text{g}/\text{cm}^2$ afterwards; $p>0.05$) and HPLC analysis of the acetic acid solvent used to re-hydrate the atRA-CHyA films prior to lyophilisation showed that it did not contain any atRA. As mentioned above, the atRA molecule exists in a primarily unionised form at a pH of 3.2 and thus, this probably contributed to its association with the CHyA copolymer matrix. Given that lyophilisation is a suitable manufacturing process for preserving sensitive drugs [345], no detrimental effects on atRA were expected. The freeze-drying process also did not alter the drug release kinetics from the film layer in atRA-CHyA-B samples, as inferred from the early burst release of $>50\%$ of encapsulated atRA (Fig. 5.8c, 5.8d). EDAC crosslinking has previously been shown to dramatically reduce the rate of release of an osteogenic peptide from other collagen-based scaffolds designed by our group [269], but while an 8% reduction in cumulative release was seen in the atRA-CHyA-B scaffold following the chemical crosslinking step, the temporal pattern of rapid release indicates that EDAC-mediated covalent linkage of atRA to the amine residues in the film was negligible. Instead, it is likely that the chemical crosslinking step reduced the layer of polymer swelling and infiltration of release buffer into the scaffold top-layer which in turn lowered the rate of release. Regardless, the release profile of $10\mu\text{g}/\text{ml}$ atRA-CHyA films that induced the mucociliary differentiation of seeded cells was mirrored by atRA-CHyA-B scaffolds, highlighting its promise to induce similar functionalisation of epithelium.

Despite the presence of similar atRA-loading and release kinetics between $10\mu\text{g}/\text{ml}$ atRA-CHyA films and atRA-CHyA-B scaffolds, analysis of cellular growth and distribution on the scaffold culture group revealed that the growth of cells had decreased (Fig. 5.9). The quantities of dsDNA in both atRA-free CHyA-B scaffolds and atRA-CHyA-B scaffolds was lower at day 21 (Fig. 5.9a) than on corresponding films (Fig. 5.4), with recorded reductions from $0.74\mu\text{g}$ to $0.31\mu\text{g}$ ($p<0.05$) for atRA-free samples and from $0.61\mu\text{g}$ to $0.29\mu\text{g}$ ($p>0.05$) in atRA-loaded biomaterials.

This drop was confirmed by H&E&FG imaging (Fig. 5.9b, Fig. 5.9c) and SEM (Fig. 5.12), whereby a sparse distribution of cells was seen along the film layer.

Examination of an earlier time point at day 7, however, showed that a statistically significant drop in cell numbers occurred on the CHyA-B scaffolds over time while the level of viability on atRA-CHyA-B scaffolds was consistent at days 7 and 21.

This finding is noteworthy as it suggests that the low dsDNA content on the atRA-CHyA-B scaffolds might be due to reduced cell attachment to the scaffold rather than due to a toxicological effect of atRA. Furthermore, the morphology of cells on atRA-CHyA-B scaffolds was less squamous than that on CHyA-B scaffolds, with interspersed clusters that were columnar in appearance (Fig. 5.9b). This suggests that the atRA-CHyA-B scaffolds have the potential to induce a physiologically-relevant cell shape and orientation in primary tracheobronchial epithelial cells that attach to the film layer.

In addition to adopting a more columnar morphology, the clusters of cells seen on atRA-CHyA-B scaffolds also displayed an increase in apical secretion of MUC5AC, when compared to the cells on CHyA-B (atRA-free) scaffolds (Fig. 5.10). The lack of red fluorescence in the CHyA-B scaffold culture group, coupled with the visualisation of squamous morphology, confirmed that a subpopulation of the seeded primary tracheobronchial epithelial cells only differentiated into mucus-secreting goblet cells when atRA was present in the bilayered scaffold. This finding was also confirmed by the dramatic increase in MUC5AC gene expression within the cell-seeded atRA-CHyA-B samples (Fig. 5.14a; $p < 0.05$), highlighting an intracellular target gene by which atRA brings about increased mucin expression and epithelial functionalisation on atRA-CHyA-B scaffolds.

On the other hand, the expression of the other marker of mucociliary differentiation studied, cilia, was absent in both atRA-CHyA-B and CHyA-B scaffold culture.

Confocal and electron microscopy failed to detect a ciliated epithelial cell phenotype in either group (Fig. 5.11-5.13). This was in contrast to the upregulation of FOXJ1 transcription within atRA-CHyA-B scaffold culture that was quantified by RT-PCR analysis at day 21 (Fig. 5.14b; $p < 0.01$). As described in Chapter 2, the absence of a complete and confluent epithelial barrier along the scaffold surface could have contributed to the lack of visible microvilli or cilia. The development of such a barrier determines the resultant cell shape, apical-basolateral polarisation,

and junctional protein connections between epithelial cells [297]; as reviewed by Paz and colleagues, the occurrence of tight junction formation and cell-basement membrane tethering are followed by cilia formation in respiratory cells. Moreover, the mechanisms of lateral planar polarization that proceed as a confluent monolayer forms assist in the alignment and organisation of cilia to facilitate coordinated beating. Accordingly, additional signalling events in addition to FOXJ1 upregulation could be required for full cellular commitment to a ciliary phenotype, which would explain these paradoxical results. In summary, improved cellular attachment to the atRA-CHyA-B scaffold could subsequently synergise with atRA to enhance the ciliogenesis of primary tracheobronchial epithelial cells in addition to the enhancement of mucus secretion.

Indeed, it is this lack of cellular adhesion that highlights the principal limitation of this study- the use of only one donor. In order to utilise primary cells that had not been yet exposed to atRA at any stage in *in vitro* culture following the cell isolation, the ATCC was selected as a supplier for primary tracheobronchial epithelial cells for the study in this chapter. Although it was clear that the attachment of cells on atRA-CHyA-B scaffolds was low, it is important to note that histological and electron microscopic analyses also captured a lack of cell attachment and the absence of a confluent epithelial layer on CHyA-B scaffolds at day 21. This is in stark contrast to the findings of multiple experiments using two donors in Chapter 4 that visualised cell layers across the CHyA-B scaffolds at an even later time point of day 28. atRA is not essential for primary epithelial cells to maintain viable in culture [69, 333] and thus, the only major difference between the scaffold cultures in Chapters 4 and 5 is the source of the primary cells. Accordingly, future studies with a newly identified source of NHBEs that have not been exposed to atRA (Lonza, catalogue CC-2541) could provide clarity on the effects of atRA incorporation on cell adhesion and monolayer formation. Of course, while the batch of cells actually used in this study may have had poor adherence and growth characteristics, they still served to highlight the significant inductive effect of the atRA-CHyA-B scaffold on goblet cell differentiation and most notably, its significantly inductive effect on genes for both mucus secretion and ciliation that was superior to an atRA-free biomaterial.

5.5. Conclusion

In conclusion, the results presented in this chapter have described the development and characterisation of a novel all-*trans* retinoic acid-eluting bilayered scaffold with potential for tracheal tissue regeneration. The drug-loaded film layer of this scaffold can enhance the mucociliary differentiation of tracheobronchial epithelial cells which could contribute to the provision of a protective and functional cellular barrier along the scaffold surface. While future studies are required to fully confirm its applicability as a novel *in vivo* implant, this drug-loaded scaffold can potentially pioneer the development of a novel and biocompatible device to address a currently unmet clinical need in tracheal replacement.

Chapter 6: Thesis discussion and conclusions

6.1. Overview	221
6.2. Chapter 2: The assessment of CG scaffolds as a 3D substrate for the growth and differentiation of a bronchial epithelial cell line	223
6.3. Chapter 3: The development of a bilayered CG scaffold as a substrate for a bronchial epithelial cell line 3D <i>in vitro</i> co-culture model	225
6.4. Chapter 4: The development of a 3D primary tracheobronchial epithelial cell-derived co-culture system for application in respiratory <i>in vitro</i> modelling	227
6.5. Chapter 5: The manufacture of an all- <i>trans</i> retinoic acid-eluting bilayered scaffold as a platform technology for airway tissue regeneration.....	229
6.6. Future work	231
6.7. Thesis conclusions.....	234

6.1. Overview

Current therapies for chronic respiratory disease serve to modify disease progression, provide symptomatic relief and reduce the incidence of exacerbations. However, incurable airway conditions such as chronic obstructive pulmonary disease (COPD), cystic fibrosis (CF) and idiopathic pulmonary fibrosis (IPF) remain associated with a high mortality worldwide, in addition to the economic burden that their clinical management puts on healthcare systems [1-4]. In cases where these diseases or other trauma cause extensive tracheobronchial injury, surgical treatment by lesion removal and use of prosthetic implants is limited by a number of complications, including device failure and inadequate epithelialisation [41]. Epithelial cell dysfunction and persistent inflammatory damage to respiratory tissue play a central role in the pathophysiology of respiratory disease and .therefore the development of novel therapeutics that target epithelial tissue to restore its normal function could lead to the generation of curative drugs. However, while current *in vitro* and *in vivo* respiratory drug development and disease models have greatly assisted in providing the treatments that are available to respiratory medicine, the simplistic nature of current cell culture models, combined with the inherent differences of disease phenotype and treatment response between humans and animals [32, 75, 313], can increase the risk of drug candidate failure due to inadequate data on the safety and efficacy of the candidate. Ultimately, this culminates in great expense and time lost that impedes the development of new medicines. With this in mind, complex, physiologically-representative *in vitro* models must be developed to address the inadequacies of current model platforms. Accordingly, the overall objective in this PhD project was to develop a novel *in vitro* 3D model of the tracheobronchial region for applications both in respiratory drug development and as a potential therapeutic in respiratory tissue regeneration.

Tissue engineering (TE), a field generally concerned with the reconstruction of tissue equivalents to replace or restore physiologic tissue through the use of biomaterial scaffold templates, cells and signalling mechanisms [95], has the potential to overcome the shortcomings of current respiratory *in vitro* models. This thesis investigated the biofabrication of a three-dimensional (3D) scaffold that can integrate tracheobronchial tissue architecture and co-culture of multiple cell types,

in the desired spatial pattern, to form an organotypic *in vitro* model with native tissue composition and structure. In order to address the limitations of mechanically weak collagen hydrogels that have been extensively investigated as tissue-engineered models, as well as the supply limitations of donor tissue-derived scaffold models, Chapter 2 evaluated the ability of collagen-chondroitin-6-sulphate (CCS) scaffolds, a well-characterised type of collagen-glycosaminoglycan (CG) scaffold [255-259], to support the growth and differentiation of tracheobronchial respiratory epithelial cells. In the first instance, the Calu-3 bronchial epithelial cell line was used because it is well-established for respiratory drug development models. Scaffolds not only supported cell line growth, but also had a direct influence on increasing epithelial mucin secretion when compared to their culture on standard on polymeric cell inserts at an air-liquid interface (ALI). This highlighted that the scaffold could induce a different phenotype within bronchial cells, but the key barrier function that an intact respiratory epithelium provides was absent on the porous scaffolds, prompting the decision to tailor a novel scaffold that could better facilitate such monolayer formation at the ALI.

Thus, in order to design a novel type of CG scaffold to resemble the anatomical architecture of tracheobronchial tissue more accurately, Chapter 3 focused on the manufacture of a bilayered scaffold structure. This bilayered collagen-hyaluronate (CHyA-B) scaffold was composed of a thin film top-layer for epithelial monolayer culture and a porous submucosal layer for 3D co-culture with lung fibroblasts. The novel design succeeded in resolving the major limitation of the CCS scaffold from Chapter 2 by facilitating the formation of a pseudostratified, confluent and continuous Calu-3 cell monolayer with suitable barrier integrity. Overall, the 3D CHyA-B model was validated as a 3D substrate for *in vitro* modelling and in Chapter 4 it was then used as a template to co-culture primary tracheobronchial epithelial cells with lung fibroblasts using this scaffold in Chapter 4. While complex culture conditions and the rapid *in vitro* dedifferentiation of these primary cells is challenging, the CHyA-B scaffold was found to be a favourable substrate for organotypic primary epithelium culture. Interestingly, while the scaffold composition had a greater influence on Calu-3 epithelial cell phenotype than co-cultured fibroblasts did, the CHyA-B scaffold and fibroblasts were both required to maximise the differentiation of primary epithelial cells towards a phenotype

representative of the *in vivo* epithelium. Ultimately, a 3D primary tracheobronchial epithelial cell-derived co-culture system using CHyA-B scaffolds was successfully developed that has the capacity to act as a physiologically-representative drug discovery platform.

The final objective of this thesis, the assessment of the potential of the CHyA-B scaffold for tracheal tissue regeneration, involved the incorporation of all-*trans* retinoic acid (atRA) into the scaffold as a potential enhancer of mucociliary epithelialisation on a cell-free scaffold implant [69, 341]. Primary tracheobronchial epithelial cells cultured on atRA-CHyA films exhibited greater ciliary protein expression and elevated mucociliary gene expression compared to atRA-free films. When the atRA-loaded film was incorporated into the bilayered scaffold, however, no increase in BIV expression was detected, despite the continued upregulation of key ciliation and mucin genes. Regardless, the atRA-loaded CHyA-B scaffold exhibited potential as a novel medical device for tracheal tissue regeneration.

In summary, this thesis has adapted a porous biomaterial previously optimised for other tissue engineering applications, resulting in a versatile new technology with potential for both *in vitro* modelling and tissue regeneration. The remainder of this chapter summarises the key findings and implications from each individual results chapter within this thesis and reviews outstanding questions and possible future directions which have arisen from this research.

6.2. Chapter 2: The assessment of CG scaffolds as a 3D substrate for the growth and differentiation of a bronchial epithelial cell line

Collagen-chondroitin-6-sulphate (CCS) scaffolds, an extensively-characterised type of CG scaffold [255, 256], have consistently demonstrated the ability to facilitate cell growth and differentiation of osteoblasts [276], mesenchymal stem cells (MSCs; [258, 259, 281] and endothelial cells [346], but they had not yet been examined for tracheobronchial cell culture. Therefore, the major aim of Chapter 2 was to evaluate their ability to support the growth and differentiation of tracheobronchial epithelial cells under two sets of respiratory culture conditions: air-liquid interface (ALI) culture and liquid-liquid interface (LLI) culture. Additionally, CCS scaffolds with two mean pore sizes were examined in order to assess

whether smaller and larger pores, as well as the resultant surface area for cell attachment, influenced Calu-3 culture on the biomaterial.

When seeded on CCS scaffolds, Calu-3 cells exhibited significant proliferation in ALI culture when compared to LLI culture over a 28-day period. This occurred in scaffolds with mean pore size diameters of both 120µm and 325µm, indicating that the most important factor affecting cellular viability and growth on the scaffold was the presence of an ALI. Of even more interest was the finding that the CCS scaffold had a direct influence on increasing epithelial mucin secretion under ALI conditions. A mucus barrier of approximately 150-200µm in height was detected in ALI culture that was absent in LLI culture on the CCS scaffolds. ALI conditions have previously been shown to improve Calu-3 expression of mucin [53], but this height was much greater than reports of 15µm in Calu-3 cells grown on cell inserts and the physiological height of airway surface liquid which has been estimated to range from 5-58µm, depending on the method of measurement [289, 290]. While the argument could be made that this thicker mucus layer could be a function of a greater cell number on CCS scaffolds than on cell inserts, analysis of normalised mucin gene expression showed that cells cultured on CCS scaffolds of both mean pore diameters had elevated MUC5AC mRNA levels relative to the cell insert culture. This highlighted that the scaffold could induce a greater degree of mucus secretion within bronchial cells than cell insert culture, whether representative of the physiological environment or reflective of a hypersecretory pathology, and that this phenotype could be of interest for improving respiratory epithelial differentiation or for assessing inhaled drug transport.

The formation of a contiguous Calu-3 epithelial layer across the entire apical scaffold surface and epithelial ciliation, however, did not occur on the porous CCS scaffolds, even when cultured at an ALI. While bands of ZO-1, the tight junction protein that signifies strong intercellular connections, were detected between adjacent Calu-3 cells along the scaffold struts, microscopic analysis confirmed that the cells were incapable of forming a consistent barrier along the porous scaffold surface. Given that the basic prerequisite for any epithelial cell coating of tissue is to provide a protective barrier function [6], it was clear that the scaffold substrate could not facilitate this essential property as long as it remained fully porous in architecture. Furthermore, ciliation of Calu-3 cells at the ALI was not observed on

CCS scaffolds but microvilli extensions were detected in cells cultured on cell inserts. We hypothesised that the lack of signalling mechanisms induced by a tightly formed barrier contributed to this finding [297].

Thus, this chapter confirmed that CG scaffolds supported the growth and differentiation of the Calu-3 bronchial epithelial cell line, particularly with ALI culture conditions, and were a suitable substrate to bring forward as a scaffold template for a novel tracheobronchial *in vitro* model. However, the porous nature of the CCS scaffold demonstrated the requirement for a new structural form of the CG scaffold that could better facilitate epithelial monolayer formation at the ALI. This was the subject of Chapter 3.

6.3. Chapter 3: The development of a bilayered CG scaffold as a substrate for a bronchial epithelial cell line 3D *in vitro* co-culture model

In order to mimic the anatomical architecture of tracheobronchial tissue more accurately, the major objective of Chapter 3 was to engineer a bilayered collagen-hyaluronate (CHyA-B) scaffold as a tissue-engineered template for the development of a physiologically-representative 3D *in vitro* tracheobronchial epithelial co-culture model. Two central modifications from the scaffold used in Chapter 2 were considered. Firstly, a bilayered scaffold structure was proposed that consisted of a thin film top-layer for epithelial monolayer culture and a porous sub-layer to represent the submucosal extracellular matrix (ECM) and allow 3D co-culture with lung fibroblasts. Secondly, the glycosaminoglycan used in the scaffold, chondroitin-6-sulphate, was switched to hyaluronate (HyA) to better emulate the native tracheobronchial ECM composition.

The CHyA-B scaffold was successfully constructed through modification of a lyophilisation technique whereby a CHyA film was manufactured separately, rehydrated and lyophilised with an overlying CHyA suspension to create fusion of the film layer with an interconnected porous 3D sub-layer. The two layers of the scaffold adhered to each other during lyophilisation and maintained this connection during physical manipulation and handling in experiments. Furthermore, a carbodiimide crosslinking step to mechanically strengthen the scaffold was identified as a critical requirement for formation of a confluent, continuous monolayer by Calu-3 cells. As a result, this chemically-crosslinked

CHyA-B scaffold succeeded in resolving the major design limitation of the CCS scaffold for respiratory culture identified in Chapter 2 but still contained the porous and cartilaginous CHyA sub-layer [298, 299] that can enhance 3D co-culture beneath the epithelium. Accordingly, the CHyA-B scaffold was brought forward for further Calu-3 cell studies in monoculture and in co-culture with the Wi38 lung fibroblast cell line.

Having modified the CG scaffold substrate for epithelial cell culture to achieve the desired cell localisation and morphology across the film top-layer, the next stage was to ascertain the scaffold effect on mucin secretion and also to investigate whether the new scaffold had a positive influence on epithelial barrier formation and ciliation. Analysis of MUC5AC gene and glycoprotein expression confirmed that the bilayered scaffold maintained a stimulatory effect on Calu-3 mucus secretion that aligned with data from CCS scaffold culture in Chapter 2. Unlike the CCS scaffold, however, an interconnected mesh-like distribution of ZO-1 protein between the cells showed universal intercellular junctions across the apical side of the CHyA-B scaffold, while ultrastructural analysis visualised a pseudostratified epithelial monolayer that had a cobblestone morphology and longer cilia than that observed in cell insert culture. The robust integrity of the barrier was verified by transepithelial electrical resistance (TEER) and by paracellular transport of fluorescein isothiocyanate (FITC)-labelled dextran. Moreover, analysis of FOXJ1, a genetic regulator of ciliation, found that the CHyA-B scaffold induced ciliation at a faster rate in cells than synthetic polymeric membranes did. Therefore, not only did the CHyA-B scaffold address the limitations of the CCS scaffold design in Chapter 2, but it also stimulated the differentiation of Calu-3 cells into an organotypic representation of the tracheobronchial epithelium to a degree that was not observed in a standard respiratory culture model.

The third objective of this chapter was to develop an epithelial-fibroblast co-culture model with improved physiological tissue architecture. To this end, Calu-3 cells were cultured together with Wi38 fibroblasts on CHyA-B scaffolds with the latter cell population seeded into the porous sublayer of the scaffold to permit 3D culture. The fibroblasts remained viable in culture with the Calu-3 cells and served to add another layer of physiological complexity to the tissue engineered-model. Mucus secretion, barrier formation and ciliation continued to be exhibited by Calu-

3 cells in scaffold co-culture, though reduced MUC5AC glycoprotein expression was noted. Interestingly, TEER readings in both monoculture and co-culture on CHyA-B scaffolds were closer to the estimated range of 300-650 Ω cm² of native tracheobronchial tissue [54] than for those observed in cell insert culture, once again indicating a more physiologically-relevant epithelium in scaffold culture.

The results in this chapter have interesting implications for the use of CHyA-B scaffolds with Calu-3 cells as a respiratory drug development *in vitro* model. Depending on whether monoculture with the scaffold biomaterial is performed or fibroblasts are co-cultured in the scaffold sublayer, different barrier phenotypes can potentially be represented, facilitating *in vitro* investigations of different environments in the respiratory tract. For instance, the use of Calu-3 cells in monoculture on CHyA-B scaffolds could be useful for examining drug permeation through thicker mucus barriers as a putative disease model to bring analyses beyond non-diseased models [308]. On the other hand, introducing fibroblasts reduces the levels of MUC5AC and might provide a more accurate representation of the healthy tracheobronchial tract with physiological TEER that could be useful for toxicological studies. Indeed, the CHyA-B scaffold model provides a versatile means of utilising a well-established bronchial epithelial cell line to obtain valuable data for drug discovery and toxicology.

This study has validated the 3D CHyA-B scaffold as a 3D substrate for *in vitro* modelling using Calu-3 cells. However, the use of primary cells, without the inherent abnormalities of immortalised cells [310], holds the potential to further improve this novel 3D culture system as a true representation of the conducting respiratory region and to improve the primary cell culture environment to prevent dedifferentiation. Therefore, the decision was made to progress to primary tracheobronchial epithelial cell co-culture with lung fibroblasts using this scaffold in Chapter 4.

6.4. Chapter 4: The development of a 3D primary tracheobronchial epithelial cell-derived co-culture system for application in respiratory *in vitro* modelling

The major objective of Chapter 4 was, using CHyA-B scaffolds, to develop a 3D primary tracheobronchial epithelial cell-derived co-culture system for applications

in respiratory *in vitro* modelling. To this end, normal human bronchial epithelial (NHBE) cells derived from two donors were sourced commercially for evaluation of 3D culture on CHyA-B scaffolds. In contrast to the Calu-3 cell line, the use of the CHyA-B scaffold in monoculture was insufficient to induce the formation of a pseudostratified ciliated epithelium from seeded NHBE cells. The NHBE cells adopted a flattened and squamous morphology in monoculture on scaffolds, with no ciliation of the epithelial cells evident. In fact, the squamoid respiratory epithelial cell morphology present on the CHyA-B scaffold more closely resembled an *in vitro* representation of squamous metaplasia [322, 323]. Although ZO-1 bands were present and peak TEER values were observed on scaffolds that were greater than in cell insert monoculture, the barrier integrity was negligible by day 28. Thus, in the case of the transition from a cell line to primary cells, scaffold culture was not superior to cell insert culture and the action was taken to investigate the inclusion of fibroblasts.

Following the addition of Wi38 fibroblasts, the benefit of the CHyA-B scaffold as a culture substrate became evident. In short, a major effect on the development of a pseudostratified ciliated epithelium was observed when the fibroblasts were co-cultured in the porous scaffold region underneath the epithelial layer. The epithelial layer thickened and became pseudostratified in morphology, and cilia were also expressed across the cell monolayer on CHyA-B samples. Most significantly, this ciliation did not occur in cell insert culture, even when Wi38 cells were co-cultured on the underside of the polymeric membrane. In addition to enhancing ciliation, the CHyA-B co-culture model exhibited an average TEER value within physiological ranges on day 28 ($423\Omega\text{cm}^2$), rendering it the only culture group that was in the physiological range at the final time point when compared to cell insert monoculture, cell insert co-culture and scaffold monoculture. These results were reinforced by the analysis of gene expression, where upregulation of genes for tight junctions and ciliation were seen in scaffold co-culture. Taken together, these data confirmed that the 3D CHyA-B substrate holds a clear advantage over the standard cell insert conditions for primary tracheobronchial epithelial co-culture.

While Calu-3 cell culture on CHyA-B scaffolds has been discussed for improved drug transport analysis and for toxicological analysis, the use of NHBE 3D co-culture models using the tissue-engineered scaffold could be even more useful.

Discrepancies in the magnitude of toxicological response of cell lines and primary cell cultures [55] could have far-reaching implications in the analysis of safety of investigational new drugs or nanoparticulate materials and poor *in vitro-in vivo* correlation. On the other hand, physiologically-relevant *in vitro* iterations of the tracheobronchial region, such as the primary epithelial CHyA-B scaffold co-culture model in this study, could be invaluable early in the drug development process to provide accurate *in vitro* data and improve successful clinical translation of worthwhile drug candidates. The response of co-cultured cells to drug exposure can also be obtained from the CHyA-B scaffold co-culture system, further enhancing data output from this model. Indeed, the establishment of this model is the first step in the application of a tissue engineering approach to address the current inadequacies of respiratory drug development and drug discovery models. In summary, Chapters 3 and 4 have developed a bilayered collagen-glycosaminoglycan scaffold which, as a 3D substrate for *in vitro* modelling, provides a physiologically relevant composition, architecture and organotypic mucosal and submucosal co-culture of the tracheobronchial region that has not been comprehensively modelled *in vitro* to date. This novel scaffold can therefore provide a new platform for applications in respiratory drug development and disease modelling.

6.5. Chapter 5: The manufacture of an all-*trans* retinoic acid-eluting bilayered scaffold as a platform technology for airway tissue regeneration

Having established the CHyA-B scaffold as a novel 3D *in vitro* model for applications in respiratory drug development, the final chapter of this thesis investigated the scaffold's potential for respiratory tissue regeneration. CHyA-B scaffolds can support the respiratory epithelial cell and fibroblast co-culture, once the cells are seeded on the scaffold in an *in vitro* setting (Chapter 4). However, the epithelialisation of tracheal medical devices *in vivo* is an important factor for clinical success. As discussed by Delaere and van Raemdonck [347], the luminal side of the respiratory tract belongs to the external environment and healing at the anastomotic sites between implants and tissue will not occur if bacterial colonisation takes place. The use of a medical device that can rapidly support the formation of an epithelium with mucociliary function could prevent such colonisation. To this end, all-*trans* retinoic acid (atRA), a small molecule drug

known to stimulate mucociliary differentiation of tracheobronchial epithelial cells [69], was incorporated into the film layer of the scaffold as a potential enhancer of functional epithelialisation of the CHyA-B scaffold. The film layer was loaded with a range of concentrations of the drug through the use of a homogenising blender prior film drying, though losses of 80-85% of loaded atRA occurred. While these losses appeared high as a percentage of the initial suspensions used in fabrication, the absolute quantity of atRA in the resultant film was similar to biomaterials in another successful study of atRA-loaded membranes [341]. Furthermore, atRA-loaded materials were stable after manufacture and contained the drug until hydration in physiological fluids, when rapid release would occur.

Following extensive characterisation of atRA encapsulation and release from drug-loaded films, the bioactive effects on primary tracheobronchial epithelial cells cultured on atRA-CHyA films were analysed. The presence of atRA was found to increase the expression of the ciliary protein β -tubulin IV (BIV) and mucus secretion, in addition to increasing mucociliary gene expression. These effects were dose-dependent and accordingly, atRA loading of a specific concentration (10 μ g/ml) gave the greatest enhancement of mucociliary expression and maintenance of epithelial cell viability. Thereafter, this 10 μ g/ml concentration was carried forward for incorporation of the atRA-loaded films into the bilayered scaffold manufacture process.

These atRA-CHyA films were integrated into the optimised freeze-dry process established in Chapter 3 to successfully yield an atRA-loaded bilayered collagen-hyaluronate (atRA-CHyA-B) scaffold. The freeze-drying process did not reduce the concentration of atRA loaded in the film layer significantly and these scaffolds were stable in cold storage as dry materials. As an “off-the-shelf” medical device, this stable storage would be of great advantage in the future, particularly when compared to decellularised tissue that is more challenging to preserve over time [229]. However, despite the fact that the atRA-CHyA-B scaffold and 10 μ g/ml atRA-CHyA films had equivalent composition and atRA content, cellular attachment and distribution was reduced when primary cells were cultured on scaffold samples. Clusters of attached cells expressed more mucin when atRA was loaded into the bilayered scaffold, but a continuous cell layer was not observed along the film layer. Furthermore, no cilia were detected, despite the continued upregulation of

the key ciliation gene FOXJ1. As observed within Chapter 2 and Chapter 3, the lack of cell signalling induced by a tightly formed barrier could have contributed to the absence of ciliation [297]. The poor cell attachment on the scaffold in this study could be simply a result of the quality of primary cells that were used for these experiments, given that attachment was also sparse on atRA-free CHyA-B scaffold controls that were consistently shown in Chapter 4 to form a continuous monolayer on the film top-layer. Irrespective of this possibility, the tracheobronchial epithelial cell culture on atRA-CHyA-B scaffolds did demonstrate enhanced mucociliary signalling and mucin secretion, albeit with an incomplete cell monolayer. Thus, while an incomplete epithelial layer formed on the atRA-CHyA-B scaffold, this biomaterial has the key characteristics that could potentially pioneer the development of a novel device to address a currently unmet clinical need in tracheal replacement.

Moreover, as found in Chapter 4, fibroblast factors from co-cultured cells could also be required to achieve full ciliation of the cells. Regarding how this could affect the potential of atRA-CHyA-B scaffolds as a future regenerative implant, the porous sub-layer of the atRA-CHyA-B scaffold facilitates epithelial wound healing in its own right [279] and has previously demonstrated the ability to support *in vivo* mesenchymal cell recruitment and bone tissue regeneration as a cell-free scaffold [260]; therefore, in this implantation scenario, such cell recruitment could ultimately provide stem cells and fibroblasts whose paracrine signalling could work synergistically with local atRA release and maximise functional epithelialisation. Cell recruitment could also be boosted through the intraoperative addition of pharmacological agents [215]. In this regard, the atRA-loaded CHyA-B scaffold displays potential as a novel cell-free medical device for tracheal tissue regeneration. Taken together with the evidence of its ability to culture a 3D *in vitro* tracheobronchial model that resembles native tissue, the bilayered collagen-hyaluronate scaffold developed in this PhD thesis can also be applied to respiratory tissue regeneration in addition to operating as a novel biofabricated template for applications in respiratory drug development.

6.6. Future work

- ◁ This thesis has demonstrated that the CHyA-B scaffold enhanced the formation of a pseudostratified epithelium in a 3D co-culture *in vitro* model, particularly

with the expression of cilia that only occurred when both the scaffold and fibroblasts were utilised. It can be argued, however, that the cilia formed were not fully mature in structure. Motile cilia in the respiratory tract are typically 7µm in length [332] and longer cilia have been visualised in other studies than the cilia observed in Chapter 4 [60, 100, 294]. The exact concentration of atRA used for the NHBE cells is withheld by the supplier, but future optimisation of its concentration in the co-culture media has the potential to even further enhance ciliation within the 3D CHyA-B co-culture model.

- ◁ The CHyA-B scaffold primary 3D co-culture *in vitro* model was successfully validated in this thesis by analysis of markers of differentiation, quantification of TEER and analysis of fluorescein isothiocyanate (FITC)-labelled dextran of an average weight of 70,000 Daltons. The use of a paracellular marker of this molecular weight is a very useful indicator of epithelial barrier integrity in its own right, but it would be interesting in the future to expand on this work and characterise a battery of paracellular and transcellular transport markers and drug molecules across this novel co-culture model. For example, a recent publication by Reus et al. has examined the transport of a range of aqueous-soluble and lipophilic drugs in the MucilAir® primary culture system [72], and similar analyses of such drug compounds and dextrans of other molecular weights [53] would be a worthwhile next step with this model to attain comprehensive validation of drug absorption.

- ◁ The CHyA-B scaffold primary 3D co-culture *in vitro* model was established in this thesis using tracheobronchial epithelial cells from healthy donors. Future studies involving the culture of cells obtained from diseased tissue or sufferers of chronic respiratory conditions are two applications where this respiratory model, complete with a prominent extracellular component and other cell types, could excel as a disease model. The increased mucus secretion that has been induced in Calu-3 cells, for instance, could translate through to primary asthmatic epithelial cells and propagate the hypersecretory phenotype observed in large airway obstruction [8, 11], while for fibrotic conditions like IPF, examination of how diseased fibroblasts responses affect remodelling of

the local tissue matrix and aberrant epithelial signalling [4, 100, 202] could advance our understanding of disease progression. This in turn could lead to the identification of new pathways for reversing the progression of such diseases, or even to their eradication.

- ◁ While more focus was given in this thesis to the development of a 3D *in vitro* tracheobronchial model for respiratory drug development, the concluding chapter has highlighted the opportunity to investigate CHyA-B scaffolds for tracheal tissue regeneration. An important first step towards this goal would be to fabricate the CHyA-B scaffold as a tubular scaffold. This could then be cultured *ex vivo* to form a cell-seeded construct for *in vivo* implantation, or fabricated as a tubular atRA-CHyA-B scaffold for implantation as a cell-free biomedical device. Within our laboratory, bilayered scaffolds composed of collagen and elastin were developed in tandem with the CHyA-B biomaterial for applications in cardiovascular blood vessel modelling; these scaffolds, of course, are of a much smaller dimension than what would be required for a human trachea, but with rescaling, as well as the use of a bioreactor, epithelial cells and mesenchymal stem cells (MSCs; [97, 348]), could pave the way for an “off-the-shelf” variant of the CHyA-B scaffold that can be customised and seeded with autologous cells for the regeneration of damaged tracheal tissue.

- ◁ Finally, while this thesis has developed the CHyA-B scaffold for applications in tracheobronchial tissue engineering and regenerative medicine, this bilayered scaffold has the potential to be a springboard platform technology for other epithelial co-culture systems. The development of a system for gastrointestinal drug development or disease modelling, for instance, could be of interest for the formulation of novel drugs that can be orally administered for patient convenience or used to treat chronic inflammatory conditions of the intestine. Recent studies have investigated the use of decellularised tissue [349], but as with the case of respiratory tissue, bilayered collagen-based scaffolds can provide a more readily available and scalable biomaterial for such purposes.

6.7. Thesis conclusions

In conclusion, this thesis has successfully developed a bilayered collagen-glycosaminoglycan scaffold with applications in airway modelling and tissue regeneration. This CHyA-B scaffold can be applied as a novel biofabricated template that provides a physiologically-relevant 3D *in vitro* model with the potential to develop novel therapeutics, perform toxicological analysis of inhalable formulations and generate more sophisticated disease models for understanding and treating respiratory disease. Ultimately, this innovative platform can overcome the simplistic nature of current respiratory cell culture models and improve *in vitro-in vivo* correlations in respiratory drug development and disease modelling. Additionally, this scaffold can also be applied as a novel technology with enhanced functional epithelialisation for tracheal tissue regeneration, As an advanced medical device, the atRA-CHyA-B scaffold can potentially overcome the limitations of current synthetic tracheal implants and tissue engineering approaches with decellularised tissue.

The specific conclusions from this study are as follows:

- ◁ The research in this thesis initially demonstrated the potential of a fully-porous collagen-chondroitin-6-sulphate scaffold as a 3D substrate for the growth and differentiation of the Calu-3 bronchial epithelial cell line. This confirmed the biomaterial's potential as a core substrate component of a novel *in vitro* model, particularly when used with airway culture-enhancing ALI conditions. In particular, the use of this natural scaffold increased the ability of these cells to express mucin when compared to standard cell insert culture which is an integral feature of the tracheobronchial epithelium in native tissue.

- ◁ The research presented has also led to the development of a bilayered collagen-hyaluronate scaffold that surpassed the fully-porous scaffolds as a 3D *in vitro* model of the tracheobronchial region of the respiratory tract. The novel bilayered scaffold combines a film layer for the epithelial cell culture and a porous 3D sub-layer for co-culture with other cell types with effective mimicry of the tracheobronchial ECM composition and tissue architecture. This scaffold

has demonstrated the ability to support the growth and differentiation of the Calu-3 bronchial cell line in addition to epithelial-fibroblast co-culture. Most notably, this novel material has maintained the mucin-secreting effect mentioned above and also enhanced ciliation and pseudostratification of Calu-3 cells at an ALI. It has therefore acted as an adequate submucosal analogue upon which a ciliated and robust epithelial barrier layer has formed with organotypic features of the native tracheobronchial epithelium.

- ◁ As well as supporting a bronchial epithelial cell line, the bilayered collagen-hyaluronate scaffold also supported the growth and differentiation of primary tracheobronchial epithelial cells in the successful development of an organotypic 3D co-culture model. The use of primary cells circumvented the inherent abnormalities of immortalised cell lines and provided an even more physiologically-representative *in vitro* model that can provide improved data for *in vitro-in vivo* correlation in drug development and disease modelling. Of critical importance, the formation of a pseudostratified epithelium with organotypic markers of differentiation and a barrier strength matching that of native tissue was achieved through the synergistic combination of the biomaterial scaffold and 3D co-culture of lung fibroblasts.

- ◁ Finally, this thesis also developed a novel all-*trans* retinoic acid-eluting bilayered scaffold with potential for tracheal tissue regeneration. Incorporation of this drug can enhance the epithelialisation of the scaffold with mucociliary function and advances its potential as an *in vivo* scaffold implant for tracheal regeneration. With future studies, this scaffold can potentially pioneer the development of a novel and biocompatible “off-the-shelf” medical device for implantation to address a currently unmet clinical need in tracheal replacement.

Bibliography

- [1] Global Strategy for the Diagnosis, Management and Prevention of COPD, Global Initiative for Chronic Obstructive Lung Disease (GOLD) 2015. Available from: <http://www.goldcopd.org>. Accessed 7/4/16.
- [2] Dodge JA, Lewis PA, Stanton M, Wilsher J. Cystic fibrosis mortality and survival in the UK: 1947-2003. *The European respiratory journal* 2007;29:522-6.
- [3] Cystic Fibrosis Foundation. Cystic fibrosis foundation patient registry: 2013 annual data report to the center directors. Bethesda, Maryland: 2014.
- [4] King TE, Jr., Pardo A, Selman M. Idiopathic pulmonary fibrosis. *Lancet* 2011;378:1949-61.
- [5] Mathers CD, Loncar D. Projections of global mortality and burden of disease from 2002 to 2030. *PLoS medicine* 2006;3:e442.
- [6] Knight DA, Holgate ST. The airway epithelium: structural and functional properties in health and disease. *Respirology* 2003;8:432-46.
- [7] Tam A, Wadsworth S, Dorscheid D, Man SF, Sin DD. The airway epithelium: more than just a structural barrier. *Therapeutic advances in respiratory disease* 2011;5:255-73.
- [8] Holgate ST. The sentinel role of the airway epithelium in asthma pathogenesis. *Immunological reviews* 2011;242:205-19.
- [9] Hartl D, Gaggar A, Bruscia E, Hector A, Marcos V, Jung A, et al. Innate immunity in cystic fibrosis lung disease. *Journal of cystic fibrosis* 2012;11:363-82.
- [10] Gunther A, Korfei M, Mahavadi P, von der Beck D, Ruppert C, Markart P. Unravelling the progressive pathophysiology of idiopathic pulmonary fibrosis. *European respiratory review* 2012;21:152-60.
- [11] Blume C, Davies DE. In vitro and ex vivo models of human asthma. *European journal of pharmaceuticals and biopharmaceutics* 2013;84:394-400.
- [12] Breeze RG, Wheeldon EB. The cells of the pulmonary airways. *The American review of respiratory disease* 1977;116:705-77.
- [13] Klein SG, Hennen J, Serchi T, Blomeke B, Gutleb AC. Potential of coculture in vitro models to study inflammatory and sensitizing effects of particles on the lung. *Toxicology in vitro* 2011;25:1516-34.

- [14] Kleinstreuer C, Zhang Z, Donohue JF. Targeted drug-aerosol delivery in the human respiratory system. *Annual review of biomedical engineering* 2008;10:195-220.
- [15] Huang S, Wiszniewski L., Constant S. The use of *in vitro* 3D cell models in drug development for respiratory diseases. In: Kapetanovic IM, editor. *Drug Discovery and Development- Present and Future*. Croatia: InTech; 2011. p. 169-90.
- [16] McGowan SE. Extracellular matrix and the regulation of lung development and repair. *FASEB journal* 1992;6:2895-904.
- [17] Dunsmore SE, Rannels DE. Extracellular matrix biology in the lung. *The American journal of physiology* 1996;270:L3-27.
- [18] Weaver M, Dunn NR, Hogan BL. Bmp4 and Fgf10 play opposing roles during lung bud morphogenesis. *Development* 2000;127:2695-704.
- [19] Papakonstantinou E, Karakiulakis G. The 'sweet' and 'bitter' involvement of glycosaminoglycans in lung diseases: pharmacotherapeutic relevance. *British journal of pharmacology* 2009;157:1111-27.
- [20] Drake RL, Vogl W, Mitchell AWM, Gray H. *Gray's anatomy for students*. 2e Philadelphia: Elsevier/Churchill Livingstone; 2005.
- [21] Temenoff JS, Mikos AG. Review: tissue engineering for regeneration of articular cartilage. *Biomaterials* 2000;21:431-40.
- [22] Belsey R. Resection and reconstruction of the intrathoracic trachea. *The British journal of surgery* 1950;38:200-5.
- [23] Crapo JD, Barry BE, Gehr P, Bachofen M, Weibel ER. Cell number and cell characteristics of the normal human lung. *The American review of respiratory disease* 1982;126:332-7.
- [24] Rooney SA, Young SL, Mendelson CR. Molecular and cellular processing of lung surfactant. *FASEB journal* 1994;8:957-67.
- [25] Lopez-Rodriguez E, Perez-Gil J. Structure-function relationships in pulmonary surfactant membranes: from biophysics to therapy. *Biochimica et biophysica acta* 2014;1838:1568-85.
- [26] Dunsmore SE. Treatment of COPD: a matrix perspective. *International journal of chronic obstructive pulmonary disease* 2008;3:113-22.

- [27] von der Mark K, Park J. Engineering biocompatible implant surfaces: Part II: Cellular recognition of biomaterial surfaces: Lessons from cell–matrix interactions. *Progress in Materials Science* 2013;58:327-81.
- [28] Suki B, Ito S, Stamenovic D, Lutchen KR, Ingenito EP. Biomechanics of the lung parenchyma: critical roles of collagen and mechanical forces. *Journal of applied physiology* 2005;98:1892-9.
- [29] Suki B, Bates JH. Lung tissue mechanics as an emergent phenomenon. *Journal of applied physiology* 2011;110:1111-8.
- [30] Abraham T, Hirota JA, Wadsworth S, Knight DA. Minimally invasive multiphoton and harmonic generation imaging of extracellular matrix structures in lung airway and related diseases. *Pulmonary pharmacology & therapeutics* 2011;24:487-96.
- [31] Walker R, Whittlesea C. *Clinical pharmacy and therapeutics*. 5 ed. Edinburgh: Churchill Livingstone; 2012.
- [32] O'Sullivan BP, Freedman SD. Cystic fibrosis. *Lancet* 2009;373:1891-904.
- [33] Kreuter M, Bonella F, Wijsenbeek M, Maher TM, Spagnolo P. Pharmacological treatment of idiopathic pulmonary fibrosis: current approaches, unsolved Issues, and future perspectives. *BioMed research international* 2015;2015:329481.
- [34] British Thoracic Society and the Scottish Intercollegiate Guidelines Network. *British guideline on the management of asthma*. United Kingdom: 2014.
- [35] Van Goor F, Hadida S, Grootenhuis PD, Burton B, Cao D, Neuberger T, et al. Rescue of CF airway epithelial cell function in vitro by a CFTR potentiator, VX-770. *Proceedings of the National Academy of Sciences of the United States of America* 2009;106:18825-30.
- [36] Ramsey BW, Davies J, McElvaney NG, Tullis E, Bell SC, Drevinek P, et al. A CFTR potentiator in patients with cystic fibrosis and the G551D mutation. *The New England journal of medicine* 2011;365:1663-72.
- [37] Orenstein DM, O'Sullivan BP, Quinton PM. Cystic fibrosis: breakthrough drugs at break-the-bank prices. *Global advances in health and medicine* 2015;4:8-57.
- [38] Pinsonneault C, Fortier J, Donati F. Tracheal resection and reconstruction. *Canadian journal of anaesthesia* 1999;46:439-55.
- [39] Grillo HC. Tracheal replacement: a critical review. *The Annals of thoracic surgery* 2002;73:1995-2004.

- [40] Haykal S, Salna M, Waddell TK, Hofer SO. Advances in tracheal reconstruction. *Plastic and reconstructive surgery* 2014;2:e178.
- [41] Walles T. Tracheobronchial bio-engineering: biotechnology fulfilling unmet medical needs. *Advanced drug delivery reviews* 2011;63:367-74.
- [42] Trotter MA, Hopkins PM. Advanced therapies for COPD-what's on the horizon? Progress in lung volume reduction and lung transplantation. *Journal of thoracic disease* 2014;6:1640-53.
- [43] Hayanga JW, D'Cunha J. The surgical technique of bilateral sequential lung transplantation. *Journal of thoracic disease* 2014;6:1063-9.
- [44] Steger V, Hampel M, Trick I, Muller M, Walles T. Clinical tracheal replacement: transplantation, bioprotheses and artificial grafts. *Expert review of medical devices* 2008;5:605-12.
- [45] Willmann JK, van Bruggen N, Dinkelborg LM, Gambhir SS. Molecular imaging in drug development. *Nature reviews Drug discovery* 2008;7:591-607.
- [46] Ledford H. Translational research: 4 ways to fix the clinical trial. *Nature* 2011;477:526-8.
- [47] Baxter K, Horn E, Gal-Edd N, Zonno K, O'Leary J, Terry PF, et al. An end to the myth: there is no drug development pipeline. *Science translational medicine* 2013;5:171cm1.
- [48] Kola I. The state of innovation in drug development. *Clinical pharmacology and therapeutics* 2008;83:227-30.
- [49] Shoyele SA, Slowey A. Prospects of formulating proteins/peptides as aerosols for pulmonary drug delivery. *International journal of pharmaceutics* 2006;314:1-8.
- [50] Nahar K, Gupta N, Gauvin R, Absar S, Patel B, Gupta V, et al. In vitro, in vivo and ex vivo models for studying particle deposition and drug absorption of inhaled pharmaceuticals. *European journal of pharmaceutical sciences* 2013;49:805-18.
- [51] Patel B, Gauvin R, Absar S, Gupta V, Gupta N, Nahar K, et al. Computational and bioengineered lungs as alternatives to whole animal, isolated organ, and cell-based lung models. *American journal of physiology Lung cellular and molecular physiology* 2012;303:L733-47.
- [52] BeruBe K, Aufderheide M, Breheny D, Clothier R, Combes R, Duffin R, et al. In vitro models of inhalation toxicity and disease. The report of a FRAME workshop. *Alternatives to laboratory animals* 2009;37:89-141.

- [53] Grainger CI, Greenwell LL, Lockley DJ, Martin GP, Forbes B. Culture of Calu-3 cells at the air interface provides a representative model of the airway epithelial barrier. *Pharmaceutical research* 2006;23:1482-90.
- [54] Forbes B, Ehrhardt C. Human respiratory epithelial cell culture for drug delivery applications. *European journal of pharmaceuticals and biopharmaceutics* 2005;60:193-205.
- [55] Balharry D, Sexton K, BeruBe KA. An in vitro approach to assess the toxicity of inhaled tobacco smoke components: nicotine, cadmium, formaldehyde and urethane. *Toxicology* 2008;244:66-76.
- [56] Fogh J, Fogh JM, Orfeo T. One hundred and twenty-seven cultured human tumor cell lines producing tumors in nude mice. *Journal of the National Cancer Institute* 1977;59:221-6.
- [57] Cozens AL, Yezzi MJ, Kunzelmann K, Ohrui T, Chin L, Eng K, et al. CFTR expression and chloride secretion in polarized immortal human bronchial epithelial cells. *American journal of respiratory cell and molecular biology* 1994;10:38-47.
- [58] Ehrhardt C, Kneuer C, Fiegel J, Hanes J, Schaefer UF, Kim KJ, et al. Influence of apical fluid volume on the development of functional intercellular junctions in the human epithelial cell line 16HBE14o-: implications for the use of this cell line as an in vitro model for bronchial drug absorption studies. *Cell and tissue research* 2002;308:391-400.
- [59] Forbes B, Shah A, Martin GP, Lansley AB. The human bronchial epithelial cell line 16HBE14o- as a model system of the airways for studying drug transport. *International journal of pharmaceuticals* 2003;257:161-7.
- [60] Pohl C, Hermanns MI, Uboldi C, Bock M, Fuchs S, Dei-Anang J, et al. Barrier functions and paracellular integrity in human cell culture models of the proximal respiratory unit. *European journal of pharmaceuticals and biopharmaceutics* 2009;72:339-49.
- [61] Reddel RR, Ke Y, Gerwin BI, McMenamin MG, Lechner JF, Su RT, et al. Transformation of human bronchial epithelial cells by infection with SV40 or adenovirus-12 SV40 hybrid virus, or transfection via strontium phosphate coprecipitation with a plasmid containing SV40 early region genes. *Cancer research* 1988;48:1904-9.

- [62] Foster KA, Avery ML, Yazdanian M, Audus KL. Characterization of the Calu-3 cell line as a tool to screen pulmonary drug delivery. *International journal of pharmaceuticals* 2000;208:1-11.
- [63] Gazdar AF, Linnoila RI, Kurita Y, Oie HK, Mulshine JL, Clark JC, et al. Peripheral airway cell differentiation in human lung cancer cell lines. *Cancer research* 1990;50:5481-7.
- [64] Hermanns MI, Unger RE, Kehe K, Peters K, Kirkpatrick CJ. Lung epithelial cell lines in coculture with human pulmonary microvascular endothelial cells: development of an alveolo-capillary barrier in vitro. *Laboratory investigation* 2004;84:736-52.
- [65] Kasper J, Hermanns MI, Bantz C, Utech S, Koshkina O, Maskos M, et al. Flotillin-involved uptake of silica nanoparticles and responses of an alveolar-capillary barrier in vitro. *European journal of pharmaceuticals and biopharmaceuticals* 2013;84:275-87.
- [66] Giard DJ, Aaronson SA, Todaro GJ, Arnstein P, Kersey JH, Dosik H, et al. In vitro cultivation of human tumors: establishment of cell lines derived from a series of solid tumors. *Journal of the National Cancer Institute* 1973;51:1417-23.
- [67] Lieber M, Smith B, Szakal A, Nelson-Rees W, Todaro G. A continuous tumor-cell line from a human lung carcinoma with properties of type II alveolar epithelial cells. *International journal of cancer* 1976;17:62-70.
- [68] Rothen-Rutishauser BM, Kiama SG, Gehr P. A three-dimensional cellular model of the human respiratory tract to study the interaction with particles. *American journal of respiratory cell and molecular biology* 2005;32:281-9.
- [69] Gray TE, Guzman K, Davis CW, Abdullah LH, Nettekheim P. Mucociliary differentiation of serially passaged normal human tracheobronchial epithelial cells. *American journal of respiratory cell and molecular biology* 1996;14:104-12.
- [70] Fulcher ML, Gabriel S, Burns K, Yankaskas J, Randell S. Well-differentiated human airway epithelial cell cultures. In: Picot J, editor. *Human Cell Culture Protocols* 2005. New York: Springer Protocols. p. 183-206.
- [71] Berube K, Pitt A, Hayden P, Prytherch Z, Job C. Filter-well technology for advanced three-dimensional cell culture: perspectives for respiratory research. *Alternatives to laboratory animals* 2010;38 Suppl 1:49-65.

- [72] Reus AA, Maas WJ, Jansen HT, Constant S, Staal YC, van Triel JJ, et al. Feasibility of a 3D human airway epithelial model to study respiratory absorption. *Toxicology in vitro* 2014;28:258-64.
- [73] Davenport EA, Nettlesheim P. Regulation of mucociliary differentiation of rat tracheal epithelial cells by type I collagen gel substratum. *American journal of respiratory cell and molecular biology* 1996;14:19-26.
- [74] Cryan SA, Sivadas N, Garcia-Contreras L. In vivo animal models for drug delivery across the lung mucosal barrier. *Advanced drug delivery reviews* 2007;59:1133-51.
- [75] Zosky GR, Sly PD. Animal models of asthma. *Clinical and experimental allergy* 2007;37:973-88.
- [76] Tardif SD, Coleman K, Hobbs TR, Lutz C. IACUC review of nonhuman primate research. *ILAR journal / National Research Council, Institute of Laboratory Animal Resources* 2013;54:234-45.
- [77] Leberl M, Kratzer A, Taraseviciene-Stewart L. Tobacco smoke induced COPD/emphysema in the animal model-are we all on the same page? *Frontiers in physiology* 2013;4:91.
- [78] March TH, Cossey PY, Esparza DC, Dix KJ, McDonald JD, Bowen LE. Inhalation administration of all-trans-retinoic acid for treatment of elastase-induced pulmonary emphysema in Fischer 344 rats. *Experimental lung research* 2004;30:383-404.
- [79] Scherliess R, Monckedieck M, Young K, Trows S, Buske S, Hook S. First in vivo evaluation of particulate nasal dry powder vaccine formulations containing ovalbumin in mice. *International journal of pharmaceutics* 2015;479:408-15.
- [80] Ghasemian E, Vatanara A, Rouini MR, Rouholamini Najafabadi A, Gilani K, Lavasani H, et al. Inhaled sildenafil nanocomposites: lung accumulation and pulmonary pharmacokinetics. *Pharmaceutical development and technology* 2015:1-11.
- [81] de Jong PM, van Sterkenburg MA, Hesseling SC, Kempenaar JA, Mulder AA, Mommaas AM, et al. Ciliogenesis in human bronchial epithelial cells cultured at the air-liquid interface. *American journal of respiratory cell and molecular biology* 1994;10:271-7.
- [82] Kirkpatrick CJ, Fuchs S, Unger RE. Co-culture systems for vascularization — Learning from nature. *Advanced drug delivery reviews* 2011;63:291-9.

- [83] Kirkpatrick CJ. Developing cellular systems in vitro to simulate regeneration. *Tissue engineering Part A* 2014;20:1355-7.
- [84] Kim SW, Park KC, Kim HJ, Cho KH, Chung JH, Kim KH, et al. Effects of collagen IV and laminin on the reconstruction of human oral mucosa. *Journal of biomedical materials research* 2001;58:108-12.
- [85] Lin YM, Zhang A, Rippon HJ, Bismarck A, Bishop AE. Tissue engineering of lung: the effect of extracellular matrix on the differentiation of embryonic stem cells to pneumocytes. *Tissue engineering Part A* 2010;16:1515-26.
- [86] Sorkio A, Hongisto H, Kaarniranta K, Uusitalo H, Juuti-Uusitalo K, Skottman H. Structure and barrier properties of human embryonic stem cell-derived retinal pigment epithelial cells are affected by extracellular matrix protein coating. *Tissue engineering Part A* 2014;20:622-34.
- [87] Crapo JD, Young SL, Fram EK, Pinkerton KE, Barry BE, Crapo RO. Morphometric characteristics of cells in the alveolar region of mammalian lungs. *The American review of respiratory disease* 1983;128:S42-6.
- [88] Liu X, Engelhardt JF. The glandular stem/progenitor cell niche in airway development and repair. *Proceedings of the American Thoracic Society* 2008;5:682-8.
- [89] Suntharalingam G, Perry MR, Ward S, Brett SJ, Castello-Cortes A, Brunner MD, et al. Cytokine storm in a phase 1 trial of the anti-CD28 monoclonal antibody TGN1412. *The New England journal of medicine* 2006;355:1018-28.
- [90] Holmes AM, Solari R, Holgate ST. Animal models of asthma: value, limitations and opportunities for alternative approaches. *Drug discovery today* 2011;16:659-70.
- [91] Russell WMS, Burch RL. *The Principles of Humane Experimental Technique*. University of Michigan: Methuen & Co.; 1959.
- [92] Wells DJ. Animal welfare and the 3Rs in European biomedical research. *Annals of the New York Academy of Sciences* 2011;1245:14-6.
- [93] Huh D, Matthews BD, Mammoto A, Montoya-Zavala M, Hsin HY, Ingber DE. Reconstituting organ-level lung functions on a chip. *Science* 2010;328:1662-8.
- [94] Benam KH, Villenave R, Lucchesi C, Varone A, Hubeau C, Lee HH, et al. Small airway-on-a-chip enables analysis of human lung inflammation and drug responses in vitro. *Nature methods* 2016;13:151-7.
- [95] Langer R, Vacanti JP. *Tissue engineering*. *Science* 1993;260:920-6.

- [96] Douglas WH, Moorman GW, Teel RW. The formation of histotypic structures from monodisperse fetal rat lung cells cultured on a three-dimensional substrate. *In vitro* 1976;12:373-81.
- [97] Macchiarini P, Jungebluth P, Go T, Asnaghi MA, Rees LE, Cogan TA, et al. Clinical transplantation of a tissue-engineered airway. *Lancet* 2008;372:2023-30.
- [98] Gonfiotti A, Jaus MO, Barale D, Baiguera S, Comin C, Lavorini F, et al. The first tissue-engineered airway transplantation: 5-year follow-up results. *Lancet* 2014;383:238-44.
- [99] Pfenninger C, Leinhase I, Endres M, Rotter N, Loch A, Ringe J, et al. Tracheal remodeling: comparison of different composite cultures consisting of human respiratory epithelial cells and human chondrocytes. *In vitro cellular & developmental biology (Animal)* 2007;43:28-36.
- [100] Pageau SC, Sazonova OV, Wong JY, Soto AM, Sonnenschein C. The effect of stromal components on the modulation of the phenotype of human bronchial epithelial cells in 3D culture. *Biomaterials* 2011;32:7169-80.
- [101] Rhee S. Fibroblasts in three dimensional matrices: cell migration and matrix remodeling. *Experimental & molecular medicine* 2009;41:858-65.
- [102] O'Brien FJ. Biomaterials & scaffolds for tissue engineering. *Materials today* 2011;14:88-95.
- [103] Hutmacher DW. Scaffolds in tissue engineering bone and cartilage. *Biomaterials* 2000;21:2529-43.
- [104] Hogan BL, Barkauskas CE, Chapman HA, Epstein JA, Jain R, Hsia CC, et al. Repair and regeneration of the respiratory system: complexity, plasticity, and mechanisms of lung stem cell function. *Cell stem cell* 2014;15:123-38.
- [105] Crosby LM, Waters CM. Epithelial repair mechanisms in the lung. *American journal of physiology Lung cellular and molecular physiology* 2010;298:L715-31.
- [106] Kajstura J, Rota M, Hall SR, Hosoda T, D'Amario D, Sanada F, et al. Evidence for human lung stem cells. *The New England journal of medicine* 2011;364:1795-806.
- [107] Warburton D, El-Hashash A, Carraro G, Tiozzo C, Sala F, Rogers O, et al. Chapter Three - Lung Organogenesis. In: Peter K, editor. *Current topics in developmental biology*. United States: Academic Press; 2010. p. 73-158.

- [108] Beers MF, Morrisey EE. The three R's of lung health and disease: repair, remodeling, and regeneration. *The Journal of clinical investigation* 2011;121:2065-73.
- [109] Hong KU, Reynolds SD, Watkins S, Fuchs E, Stripp BR. Basal cells are a multipotent progenitor capable of renewing the bronchial epithelium. *The American journal of pathology* 2004;164:577-88.
- [110] Rock JR, Onaitis MW, Rawlins EL, Lu Y, Clark CP, Xue Y, et al. Basal cells as stem cells of the mouse trachea and human airway epithelium. *Proceedings of the National Academy of Sciences of the United States of America* 2009;106:12771-5.
- [111] Rawlins EL, Okubo T, Xue Y, Brass DM, Auten RL, Hasegawa H, et al. The role of Scgb1a1+ Clara cells in the long-term maintenance and repair of lung airway, but not alveolar, epithelium. *Cell stem cell* 2009;4:525-34.
- [112] Uhal BD. Cell cycle kinetics in the alveolar epithelium. *The American journal of physiology* 1997;272:L1031-45.
- [113] Rock JR, Hogan BL. Epithelial progenitor cells in lung development, maintenance, repair, and disease. *Annual review of cell and developmental biology* 2011;27:493-512.
- [114] Mercer RR, Russell ML, Roggli VL, Crapo JD. Cell number and distribution in human and rat airways. *American journal of respiratory cell and molecular biology* 1994;10:613-24.
- [115] Evans MJ, Van Winkle LS, Fanucchi MV, Plopper CG. Cellular and molecular characteristics of basal cells in airway epithelium. *Experimental lung research* 2001;27:401-15.
- [116] Rock J, Konigshoff M. Endogenous lung regeneration: potential and limitations. *American journal of respiratory and critical care medicine* 2012;186:1213-9.
- [117] Adamson IY, Bowden DH. Derivation of type 1 epithelium from type 2 cells in the developing rat lung. *Laboratory investigation* 1975;32:736-45.
- [118] Rock JR, Barkauskas CE, Cronic MJ, Xue Y, Harris JR, Liang J, et al. Multiple stromal populations contribute to pulmonary fibrosis without evidence for epithelial to mesenchymal transition. *Proceedings of the National Academy of Sciences of the United States of America* 2011;108:E1475-83.

- [119] Barkauskas CE, Cronce MJ, Rackley CR, Bowie EJ, Keene DR, Stripp BR, et al. Type 2 alveolar cells are stem cells in adult lung. *The Journal of clinical investigation* 2013;123:3025-36.
- [120] Kim CF, Jackson EL, Woolfenden AE, Lawrence S, Babar I, Vogel S, et al. Identification of bronchioalveolar stem cells in normal lung and lung cancer. *Cell* 2005;121:823-35.
- [121] Chapman HA, Li X, Alexander JP, Brumwell A, Lorzio W, Tan K, et al. Integrin alpha6beta4 identifies an adult distal lung epithelial population with regenerative potential in mice. *The Journal of clinical investigation* 2011;121:2855-62.
- [122] Kumar PA, Hu Y, Yamamoto Y, Hoe NB, Wei TS, Mu D, et al. Distal airway stem cells yield alveoli in vitro and during lung regeneration following H1N1 influenza infection. *Cell* 2011;147:525-38.
- [123] Moodley Y. Evidence for human lung stem cells. *The New England journal of medicine* 2011;365:464; author reply 5-6.
- [124] Siti-Ismael N, Samadikuchaksaraei A, Bishop AE, Polak JM, Mantalaris A. Development of a novel three-dimensional, automatable and integrated bioprocess for the differentiation of embryonic stem cells into pulmonary alveolar cells in a rotating vessel bioreactor system. *Tissue engineering Part C, Methods* 2012;18:263-72.
- [125] Sun H, Quan Y, Yan Q, Peng X, Mao Z, Wetsel RA, et al. Isolation and characterization of alveolar epithelial type II cells derived from mouse embryonic stem cells. *Tissue engineering Part C, Methods* 2014;20:464-72.
- [126] Samadikuchaksaraei A, Cohen S, Isaac K, Rippon HJ, Polak JM, Bielby RC, et al. Derivation of distal airway epithelium from human embryonic stem cells. *Tissue engineering* 2006;12:867-75.
- [127] Wong AP, Bear CE, Chin S, Pasceri P, Thompson TO, Huan LJ, et al. Directed differentiation of human pluripotent stem cells into mature airway epithelia expressing functional CFTR protein. *Nature biotechnology* 2012;30:876-82.
- [128] Carraro G, Perin L, Sedrakyan S, Giuliani S, Tiozzo C, Lee J, et al. Human amniotic fluid stem cells can integrate and differentiate into epithelial lung lineages. *Stem cells* 2008;26:2902-11.

- [129] Albera C, Polak JM, Janes S, Griffiths MJ, Alison MR, Wright NA, et al. Repopulation of human pulmonary epithelium by bone marrow cells: a potential means to promote repair. *Tissue engineering* 2005;11:1115-21.
- [130] Kassmer SH, Bruscia EM, Zhang PX, Krause DS. Nonhematopoietic cells are the primary source of bone marrow-derived lung epithelial cells. *Stem cells* 2012;30:491-9.
- [131] Seguin A, Baccari S, Holder-Espinasse M, Bruneval P, Carpentier A, Taylor DA, et al. Tracheal regeneration: Evidence of bone marrow mesenchymal stem cell involvement. *Journal of thoracic and cardiovascular surgery* 2013;145:1297-304 e2.
- [132] Elliott MJ, De Coppi P, Spegginorin S, Roebuck D, Butler CR, Samuel E, et al. Stem-cell-based, tissue engineered tracheal replacement in a child: a 2-year follow-up study. *Lancet* 2012;380:994-1000.
- [133] Bara JJ, Richards RG, Alini M, Stoddart MJ. Concise review: Bone marrow-derived mesenchymal stem cells change phenotype following in vitro culture: implications for basic research and the clinic. *Stem cells* 2014;32:1713-23.
- [134] Yamanouchi H, Fujita J, Yoshinouchi T, Hojo S, Kamei T, Yamadori I, et al. Measurement of hepatocyte growth factor in serum and bronchoalveolar lavage fluid in patients with pulmonary fibrosis. *Respiratory medicine* 1998;92:273-8.
- [135] Plantier L, Marchand-Adam S, Marchal-Somme J, Leseche G, Fournier M, Dehoux M, et al. Defect of hepatocyte growth factor production by fibroblasts in human pulmonary emphysema. *American journal of physiology Lung cellular and molecular physiology* 2005;288:L641-7.
- [136] Crestani B, Marchand-Adam S, Quesnel C, Plantier L, Borensztajn K, Marchal J, et al. Hepatocyte growth factor and lung fibrosis. *Proceedings of the American Thoracic Society* 2012;9:158-63.
- [137] Dohi M, Hasegawa T, Yamamoto K, Marshall BC. Hepatocyte growth factor attenuates collagen accumulation in a murine model of pulmonary fibrosis. *American journal of respiratory and critical care medicine* 2000;162:2302-7.
- [138] Watanabe M, Ebina M, Orson FM, Nakamura A, Kubota K, Koinuma D, et al. Hepatocyte growth factor gene transfer to alveolar septa for effective suppression of lung fibrosis. *Molecular therapy* 2005;12:58-67.
- [139] Gazdhar A, Fachinger P, van Leer C, Pierog J, Gugger M, Friis R, et al. Gene transfer of hepatocyte growth factor by electroporation reduces bleomycin-

induced lung fibrosis. American journal of physiology Lung cellular and molecular physiology 2007;292:L529-36.

[140] Hegab AE, Kubo H, Yamaya M, Asada M, He M, Fujino N, et al. Intranasal HGF administration ameliorates the physiologic and morphologic changes in lung emphysema. Molecular therapy 2008;16:1417-26.

[141] Gazdhar A, Temuri A, Knudsen L, Gugger M, Schmid RA, Ochs M, et al. Targeted gene transfer of hepatocyte growth factor to alveolar type II epithelial cells reduces lung fibrosis in rats. Human gene therapy 2013;24:105-16.

[142] Chakraborty S, Chopra P, Hak A, Dastidar SG, Ray A. Hepatocyte growth factor is an attractive target for the treatment of pulmonary fibrosis. Expert opinion on investigational drugs 2013;22:499-515.

[143] Gazdhar A, Susuri N, Hostettler K, Gugger M, Knudsen L, Roth M, et al. HGF expressing stem cells in usual interstitial pneumonia originate from the bone marrow and are antifibrotic. PloS one 2013;8:e65453.

[144] Warburton D, Bellusci S. The molecular genetics of lung morphogenesis and injury repair. Paediatric respiratory reviews 2004;5 Suppl A:S283-7.

[145] Masterson JC, Molloy EL, Gilbert JL, McCormack N, Adams A, O'Dea S. Bone morphogenetic protein signalling in airway epithelial cells during regeneration. Cellular signalling 2011;23:398-406.

[146] Abe E. Function of BMPs and BMP antagonists in adult bone. Annals of the New York Academy of Sciences 2006;1068:41-53.

[147] McKay B. Local sustained delivery of recombinant human bone morphogenetic protein-2 (rhBMP-2). Conference proceedings : Annual International Conference of the IEEE Engineering in Medicine and Biology Society IEEE Engineering in Medicine and Biology Society Conference 2009;2009:236-7.

[148] Weaver M, Yingling JM, Dunn NR, Bellusci S, Hogan BL. Bmp signaling regulates proximal-distal differentiation of endoderm in mouse lung development. Development 1999;126:4005-15.

[149] Lynn TM, Molloy EL, Masterson JC, Glynn SF, Costello RW, Avdalovic MV, et al. SMAD signaling in the airways of healthy versus asthmatic rhesus macaques highlights a relationship between inflammation and BMPs. American journal of respiratory cell and molecular biology 2015.

- [150] Molloy EL, Adams A, Moore JB, Masterson JC, Madrigal-Estebas L, Mahon BP, et al. BMP4 induces an epithelial-mesenchymal transition-like response in adult airway epithelial cells. *Growth factors* 2008;26:12-22.
- [151] McCormack N, Molloy EL, O'Dea S. Bone morphogenetic proteins enhance an epithelial-mesenchymal transition in normal airway epithelial cells during restitution of a disrupted epithelium. *Respiratory research* 2013;14:36.
- [152] Urist MR. Bone: formation by autoinduction. *Science* 1965;150:893-9.
- [153] Ware LB, Matthay MA. Keratinocyte and hepatocyte growth factors in the lung: roles in lung development, inflammation, and repair. *American journal of physiology Lung cellular and molecular physiology* 2002;282:L924-40.
- [154] Chedid M, Rubin JS, Csaky KG, Aaronson SA. Regulation of keratinocyte growth factor gene expression by interleukin 1. *The Journal of biological chemistry* 1994;269:10753-7.
- [155] Hicks WL, Jr., Hall LA, 3rd, Hard R, Gardella J, Bright F, Parashurama N, et al. Keratinocyte growth factor and autocrine repair in airway epithelium. *Archives of otolaryngology--head & neck surgery* 2004;130:446-9.
- [156] Waters CM, Savla U, Panos RJ. KGF prevents hydrogen peroxide-induced increases in airway epithelial cell permeability. *The American journal of physiology* 1997;272:L681-9.
- [157] Gomperts BN, Belperio JA, Fishbein MC, Keane MP, Burdick MD, Strieter RM. Keratinocyte growth factor improves repair in the injured tracheal epithelium. *American journal of respiratory cell and molecular biology* 2007;37:48-56.
- [158] Yildirim AO, Veith M, Rausch T, Muller B, Kilb P, Van Winkle LS, et al. Keratinocyte growth factor protects against Clara cell injury induced by naphthalene. *The European respiratory journal* 2008;32:694-704.
- [159] Lo-Coco F, Hasan SK, Montesinos P, Sanz MA. Biology and management of therapy-related acute promyelocytic leukemia. *Current opinion in oncology* 2013;25:695-700.
- [160] Malpel S, Mendelsohn C, Cardoso WV. Regulation of retinoic acid signaling during lung morphogenesis. *Development* 2000;127:3057-67.
- [161] Massaro GD, Massaro D. Retinoic acid treatment abrogates elastase-induced pulmonary emphysema in rats. *Nature medicine* 1997;3:675-7.

- [162] Mao JT, Goldin JG, Dermand J, Ibrahim G, Brown MS, Emerick A, et al. A pilot study of all-trans-retinoic acid for the treatment of human emphysema. *American journal of respiratory and critical care medicine* 2002;165:718-23.
- [163] Lucey EC, Goldstein RH, Breuer R, Rexer BN, Ong DE, Snider GL. Retinoic acid does not affect alveolar septation in adult FVB mice with elastase-induced emphysema. *Respiration* 2003;70:200-5.
- [164] Ishizawa K, Kubo H, Yamada M, Kobayashi S, Numasaki M, Ueda S, et al. Bone marrow-derived cells contribute to lung regeneration after elastase-induced pulmonary emphysema. *FEBS letters* 2004;556:249-52.
- [165] Roth MD, Connett JE, D'Armiento JM, Foronjy RF, Friedman PJ, Goldin JG, et al. Feasibility of retinoids for the treatment of emphysema study. *Chest* 2006;130:1334-45.
- [166] Gray T, Koo JS, Nettesheim P. Regulation of mucous differentiation and mucin gene expression in the tracheobronchial epithelium. *Toxicology* 2001;160:35-46.
- [167] Huang TW, Cheng PW, Chan YH, Yeh TH, Young YH, Young TH. Regulation of ciliary differentiation of human respiratory epithelial cells by the receptor for hyaluronan-mediated motility on hyaluronan-based biomaterials. *Biomaterials* 2010;31:6701-9.
- [168] O'Leary C, Gilbert JL, O'Dea S, O'Brien FJ, Cryan SA. Respiratory tissue engineering: current status and opportunities for the future. *Tissue engineering Part B, Reviews* 2015;21:323-44.
- [169] Blau H, Guzowski DE, Siddiqi ZA, Scarpelli EM, Bienkowski RS. Fetal type 2 pneumocytes form alveolar-like structures and maintain long-term differentiation on extracellular matrix. *Journal of cellular physiology* 1988;136:203-14.
- [170] Mondrinos MJ, Koutzaki S, Jiwanmall E, Li M, Dechadarevian JP, Lelkes PI, et al. Engineering three-dimensional pulmonary tissue constructs. *Tissue engineering* 2006;12:717-28.
- [171] Mondrinos MJ, Koutzaki S, Lelkes PI, Finck CM. A tissue-engineered model of fetal distal lung tissue. *American journal of physiology Lung cellular and molecular physiology* 2007;293:L639-50.
- [172] Sugihara H, Toda S, Miyabara S, Fujiyama C, Yonemitsu N. Reconstruction of alveolus-like structure from alveolar type II epithelial cells in three-dimensional collagen gel matrix culture. *The American journal of pathology* 1993;142:783-92.

- [173] Ott HC, Clippinger B, Conrad C, Schuetz C, Pomerantseva I, Ikonomidou L, et al. Regeneration and orthotopic transplantation of a bioartificial lung. *Nature medicine* 2010;16:927-33.
- [174] Petersen TH, Calle EA, Zhao L, Lee EJ, Gui L, Raredon MB, et al. Tissue-engineered lungs for in vivo implantation. *Science* 2010;329:538-41.
- [175] Price AP, England KA, Matson AM, Blazar BR, Panoskaltsis-Mortari A. Development of a decellularized lung bioreactor system for bioengineering the lung: the matrix reloaded. *Tissue engineering Part A* 2010;16:2581-91.
- [176] Cortiella J, Niles J, Cantu A, Brettler A, Pham A, Vargas G, et al. Influence of acellular natural lung matrix on murine embryonic stem cell differentiation and tissue formation. *Tissue engineering Part A* 2010;16:2565-80.
- [177] Bonvillain RW, Danchuk S, Sullivan DE, Betancourt AM, Semon JA, Eagle ME, et al. A nonhuman primate model of lung regeneration: detergent-mediated decellularization and initial in vitro recellularization with mesenchymal stem cells. *Tissue engineering Part A* 2012;18:2437-52.
- [178] Nichols JE, Niles J, Riddle M, Vargas G, Schilagard T, Ma L, et al. Production and assessment of decellularized pig and human lung scaffolds. *Tissue engineering Part A* 2013;19:2045-62.
- [179] Gilpin SE, Guyette JP, Gonzalez G, Ren X, Asara JM, Mathisen DJ, et al. Perfusion decellularization of human and porcine lungs: bringing the matrix to clinical scale. *The Journal of heart and lung transplantation* 2014;33:298-308.
- [180] Douglas WH, Teel RW. An organotypic in vitro model system for studying pulmonary surfactant production by type II alveolar pneumocytes. *The American review of respiratory disease* 1976;113:17-23.
- [181] Andrade CF, Wong AP, Waddell TK, Keshavjee S, Liu M. Cell-based tissue engineering for lung regeneration. *American journal of physiology Lung cellular and molecular physiology* 2007;292:L510-8.
- [182] Chen P, Marsilio E, Goldstein RH, Yannas IV, Spector M. Formation of lung alveolar-like structures in collagen-glycosaminoglycan scaffolds in vitro. *Tissue engineering* 2005;11:1436-48.
- [183] Cortiella J, Nichols JE, Kojima K, Bonassar LJ, Dargon P, Roy AK, et al. Tissue-engineered lung: an in vivo and in vitro comparison of polyglycolic acid and pluronic F-127 hydrogel/somatic lung progenitor cell constructs to support tissue growth. *Tissue engineering* 2006;12:1213-25.

- [184] Crapo PM, Gilbert TW, Badylak SF. An overview of tissue and whole organ decellularization processes. *Biomaterials* 2011;32:3233-43.
- [185] Wagner DE, Bonenfant NR, Parsons CS, Sokocevic D, Brooks EM, Borg ZD, et al. Comparative decellularization and recellularization of normal versus emphysematous human lungs. *Biomaterials* 2014;35:3281-97.
- [186] Daly AB, Wallis JM, Borg ZD, Bonvillain RW, Deng B, Ballif BA, et al. Initial binding and recellularization of decellularized mouse lung scaffolds with bone marrow-derived mesenchymal stromal cells. *Tissue engineering Part A* 2012;18:1-16.
- [187] Petersen TH, Calle EA, Colehour MB, Niklason LE. Matrix composition and mechanics of decellularized lung scaffolds. *Cells, tissues, organs* 2012;195:222-31.
- [188] Wallis JM, Borg ZD, Daly AB, Deng B, Ballif BA, Allen GB, et al. Comparative assessment of detergent-based protocols for mouse lung decellularization and re-cellularization. *Tissue engineering Part C, Methods* 2012;18:420-32.
- [189] Bonenfant NR, Sokocevic D, Wagner DE, Borg ZD, Lathrop MJ, Lam YW, et al. The effects of storage and sterilization on de-cellularized and re-cellularized whole lung. *Biomaterials* 2013;34:3231-45.
- [190] Sokocevic D, Bonenfant NR, Wagner DE, Borg ZD, Lathrop MJ, Lam YW, et al. The effect of age and emphysematous and fibrotic injury on the re-cellularization of de-cellularized lungs. *Biomaterials* 2013;34:3256-69.
- [191] Carvalho TC, Peters JI, Williams RO, 3rd. Influence of particle size on regional lung deposition--what evidence is there? *International journal of pharmaceutics* 2011;406:1-10.
- [192] Paquette JS, Tremblay P, Bernier V, Auger FA, Laviolette M, Germain L, et al. Production of tissue-engineered three-dimensional human bronchial models. *In vitro cellular & developmental biology (Animal)* 2003;39:213-20.
- [193] Vaughan MB, Ramirez RD, Wright WE, Minna JD, Shay JW. A three-dimensional model of differentiation of immortalized human bronchial epithelial cells. *Differentiation* 2006;74:141-8.
- [194] Wang Y, Wong LB, Mao H. Creation of a long-lifespan ciliated epithelial tissue structure using a 3D collagen scaffold. *Biomaterials* 2010;31:848-53.

- [195] Hughes CS, Postovit LM, Lajoie GA. Matrigel: a complex protein mixture required for optimal growth of cell culture. *Proteomics* 2010;10:1886-90.
- [196] Delgado O, Kaisani AA, Spinola M, Xie XJ, Batten KG, Minna JD, et al. Multipotent capacity of immortalized human bronchial epithelial cells. *PloS one* 2011;6:e22023.
- [197] Wu X, Peters-Hall JR, Bose S, Pena MT, Rose MC. Human bronchial epithelial cells differentiate to 3D glandular acini on basement membrane matrix. *American journal of respiratory cell and molecular biology* 2011;44:914-21.
- [198] Choe MM, Sporn PH, Swartz MA. An in vitro airway wall model of remodeling. *American journal of physiology Lung cellular and molecular physiology* 2003;285:L427-33.
- [199] Darveau ME, Jacques E, Rouabhia M, Hamid Q, Chakir J. Increased T-cell survival by structural bronchial cells derived from asthmatic subjects cultured in an engineered human mucosa. *The Journal of allergy and clinical immunology* 2008;121:692-9.
- [200] Risbud M, Endres M, Ringe J, Bhonde R, Sittinger M. Biocompatible hydrogel supports the growth of respiratory epithelial cells: possibilities in tracheal tissue engineering. *Journal of biomedical materials research* 2001;56:120-7.
- [201] Cornelissen CG, Dietrich M, Kruger S, Spillner J, Schmitz-Rode T, Jockenhoevel S. Fibrin gel as alternative scaffold for respiratory tissue engineering. *Annals of biomedical engineering* 2012;40:679-87.
- [202] Kobayashi K, Suzuki T, Nomoto Y, Tada Y, Miyake M, Hazama A, et al. Potential of heterotopic fibroblasts as autologous transplanted cells for tracheal epithelial regeneration. *Tissue engineering* 2007;13:2175-84.
- [203] Naito H, Tojo T, Kimura M, Dohi Y, Zimmermann WH, Eschenhagen T, et al. Engineering bioartificial tracheal tissue using hybrid fibroblast-mesenchymal stem cell cultures in collagen hydrogels. *Interactive cardiovascular and thoracic surgery* 2011;12:156-61.
- [204] Hong HJ, Lee JS, Choi JW, Min BH, Lee HB, Kim CH. Transplantation of autologous chondrocytes seeded on a fibrin/hyaluronan composite gel into tracheal cartilage defects in rabbits: preliminary results. *Artificial organs* 2012;36:998-1006.
- [205] Hong HJ, Chang JW, Park JK, Choi JW, Kim YS, Shin YS, et al. Tracheal reconstruction using chondrocytes seeded on a poly(L-lactic-co-glycolic acid)-

fibrin/hyaluronan. *Journal of biomedical materials research Part A* 2014;102:4142-50.

[206] Chang JW, Park SA, Park JK, Choi JW, Kim YS, Shin YS, et al. Tissue-engineered tracheal reconstruction using three-dimensionally printed artificial tracheal graft: preliminary report. *Artificial organs* 2014;38:E95-E105.

[207] Brown RA. In the beginning there were soft collagen-cell gels: towards better 3D connective tissue models? *Experimental cell research* 2013;319:2460-9.

[208] Salinas CN, Anseth KS. Mesenchymal stem cells for craniofacial tissue regeneration: designing hydrogel delivery vehicles. *Journal of dental research* 2009;88:681-92.

[209] Gao J, Liu R, Wu J, Liu Z, Li J, Zhou J, et al. The use of chitosan based hydrogel for enhancing the therapeutic benefits of adipose-derived MSCs for acute kidney injury. *Biomaterials* 2012;33:3673-81.

[210] Mathieu E, Lamirault G, Toquet C, Lhommet P, Rederstorff E, Sourice S, et al. Intramyocardial delivery of mesenchymal stem cell-seeded hydrogel preserves cardiac function and attenuates ventricular remodeling after myocardial infarction. *PloS one* 2012;7:e51991.

[211] Curley GF, Scott JA, Laffey JG. Therapeutic potential and mechanisms of action of mesenchymal stromal cells for acute respiratory distress syndrome. *Current stem cell research & therapy* 2014;9:319-29.

[212] Antunes MA, Laffey JG, Pelosi P, Rocco PR. Mesenchymal stem cell trials for pulmonary diseases. *Journal of cellular biochemistry* 2014;115:1023-32.

[213] Macchiarini P, Walles T, Biancosino C, Mertsching H. First human transplantation of a bioengineered airway tissue. *Journal of thoracic and cardiovascular surgery* 2004;128:638-41.

[214] Go T, Jungebluth P, Baiguero S, Asnaghi A, Martorell J, Ostertag H, et al. Both epithelial cells and mesenchymal stem cell-derived chondrocytes contribute to the survival of tissue-engineered airway transplants in pigs. *Journal of thoracic and cardiovascular surgery* 2010;139:437-43.

[215] Jungebluth P, Bader A, Baiguera S, Moller S, Jaus M, Lim ML, et al. The concept of in vivo airway tissue engineering. *Biomaterials* 2012;33:4319-26.

[216] Jungebluth P, Moll G, Baiguera S, Macchiarini P. Tissue-engineered airway: a regenerative solution. *Clinical pharmacology and therapeutics* 2012;91:81-93.

- [217] Delaere P, Vranckx J, Verleden G, De Leyn P, Van Raemdonck D. Tracheal allotransplantation after withdrawal of immunosuppressive therapy. *The New England journal of medicine* 2010;362:138-45.
- [218] Delaere PR, Vranckx JJ, Den Hondt M. Tracheal allograft after withdrawal of immunosuppressive therapy. *The New England journal of medicine* 2014;370:1568-70.
- [219] Martinod E, Zegdi R, Zakine G, Aupeple B, Fornes P, D'Audiffret A, et al. A novel approach to tracheal replacement: the use of an aortic graft. *Journal of thoracic and cardiovascular surgery* 2001;122:197-8.
- [220] Martinod E, Seguin A, Pfeuty K, Fornes P, Kambouchner M, Azorin JF, et al. Long-term evaluation of the replacement of the trachea with an autologous aortic graft. *The Annals of thoracic surgery* 2003;75:1572-8; discussion 8.
- [221] Martinod E, Seguin A, Holder-Espinasse M, Kambouchner M, Duterque-Coquillaud M, Azorin JF, et al. Tracheal regeneration following tracheal replacement with an allogenic aorta. *The annals of thoracic surgery* 2005;79:942-8; discussion 9.
- [222] Azorin JF, Bertin F, Martinod E, Laskar M. Tracheal replacement with an aortic autograft. *European journal of cardio-thoracic surgery* 2006;29:261-3.
- [223] Wurtz A, Porte H, Conti M, Desbordes J, Copin MC, Azorin J, et al. Tracheal replacement with aortic allografts. *The New England journal of medicine* 2006;355:1938-40.
- [224] Seguin A, Radu D, Holder-Espinasse M, Bruneval P, Fialaire-Legendre A, Duterque-Coquillaud M, et al. Tracheal replacement with cryopreserved, decellularized, or glutaraldehyde-treated aortic allografts. *The annals of thoracic surgery* 2009;87:861-7.
- [225] Makris D, Holder-Espinasse M, Wurtz A, Seguin A, Hubert T, Jaillard S, et al. Tracheal replacement with cryopreserved allogenic aorta. *Chest* 2010;137:60-7.
- [226] Hopitaux de Paris. Airway and/or Pulmonary Vessels Transplantation (TRACHBRONCAR) trial. Available at <http://clinicaltrials.gov>. Identifier: NCT01331863. Accessed 7/4/16.
- [227] Partington L, Mordan NJ, Mason C, Knowles JC, Kim HW, Lowdell MW, et al. Biochemical changes caused by decellularization may compromise mechanical integrity of tracheal scaffolds. *Acta biomaterialia* 2013;9:5251-61.

- [228] Haykal S, Soleas JP, Salna M, Hofer SO, Waddell TK. Evaluation of the structural integrity and extracellular matrix components of tracheal allografts following cyclical decellularization techniques: comparison of three protocols. *Tissue engineering Part C, Methods* 2012;18:614-23.
- [229] Baiguera S, Del Gaudio C, Jaus MO, Polizzi L, Gonfiotti A, Comin CE, et al. Long-term changes to in vitro preserved bioengineered human trachea and their implications for decellularized tissues. *Biomaterials* 2012;33:3662-72.
- [230] Lyons F, Partap S, O'Brien FJ. Part 1: scaffolds and surfaces. *Technology and health care* 2008;16:305-17.
- [231] Harrington H, Cato P, Salazar F, Wilkinson M, Knox A, Haycock JW, et al. Immunocompetent 3D model of human upper airway for disease modeling and in vitro drug evaluation. *Molecular pharmaceutics* 2014;11:2082-91.
- [232] Luo X, Liu Y, Zhang Z, Tao R, He A, Yin Z, et al. Long-term functional reconstruction of segmental tracheal defect by pedicled tissue-engineered trachea in rabbits. *Biomaterials* 2013;34:3336-44.
- [233] Ajallouelian F, Lim ML, Lemon G, Haag JC, Gustafsson Y, Sjoqvist S, et al. Biomechanical and biocompatibility characteristics of electrospun polymeric tracheal scaffolds. *Biomaterials* 2014;35:5307-15.
- [234] Jungebluth P, Alici E, Baiguera S, Le Blanc K, Blomberg P, Bozoky B, et al. Tracheobronchial transplantation with a stem-cell-seeded bioartificial nanocomposite: a proof-of-concept study. *Lancet* 2011;378:1997-2004.
- [235] Vogel G. Regenerative medicine. Report finds misconduct by surgeon. *Science* 2015;348:954-5.
- [236] Vogel G. Regenerative medicine. Trachea surgeon cleared of misconduct. *Science* 2015;349:1035.
- [237] Vogel G. Karolinska Institute has 'lost confidence' in Paolo Macchiarini, says it won't renew his contract. *Science*; 2016. Available at <http://sciencemag.org>. Accessed 7/4/16.
- [238] Vogel G. Karolinska Institute vice-chancellor resigns in wake of Macchiarini scandal. *Science*; 2016. Available at <http://sciencemag.org>. Accessed 7/4/16.
- [239] Macchiarini P. Tracheobronchial transplantation. *Lancet* 2016;387:339.
- [240] Hersel U, Dahmen C, Kessler H. RGD modified polymers: biomaterials for stimulated cell adhesion and beyond. *Biomaterials* 2003;24:4385-415.

- [241] Bryers JD, Giachelli CM, Ratner BD. Engineering biomaterials to integrate and heal: The biocompatibility paradigm shifts. *Biotechnology and bioengineering* 2012;109:1898-911.
- [242] Sung HJ, Meredith C, Johnson C, Galis ZS. The effect of scaffold degradation rate on three-dimensional cell growth and angiogenesis. *Biomaterials* 2004;25:5735-42.
- [243] Hinderer S, Schesny M, Bayrak A, Ibold B, Hampel M, Walles T, et al. Engineering of fibrillar decorin matrices for a tissue-engineered trachea. *Biomaterials* 2012;33:5259-66.
- [244] Lin CH, Hsu SH, Huang CE, Cheng WT, Su JM. A scaffold-bioreactor system for a tissue-engineered trachea. *Biomaterials* 2009;30:4117-26.
- [245] Ghezzi CE, Marelli B, Donelli I, Alessandrino A, Freddi G, Nazhat SN. The role of physiological mechanical cues on mesenchymal stem cell differentiation in an airway tract-like dense collagen-silk fibroin construct. *Biomaterials* 2014;35:6236-47.
- [246] Ziegelaar BW, Aigner J, Staudenmaier R, Lempart K, Mack B, Happ T, et al. The characterisation of human respiratory epithelial cells cultured on resorbable scaffolds: first steps towards a tissue engineered tracheal replacement. *Biomaterials* 2002;23:1425-38.
- [247] Nomoto Y, Kobayashi K, Tada Y, Wada I, Nakamura T, Omori K. Effect of fibroblasts on epithelial regeneration on the surface of a bioengineered trachea. *The annals of otology, rhinology, and laryngology* 2008;117:59-64.
- [248] Kobayashi K, Suzuki T, Nomoto Y, Tada Y, Miyake M, Hazama A, et al. A tissue-engineered trachea derived from a framed collagen scaffold, gingival fibroblasts and adipose-derived stem cells. *Biomaterials* 2010;31:4855-63.
- [249] Tani A, Tada Y, Takezawa T, Imaizumi M, Nomoto Y, Nakamura T, et al. Regeneration of tracheal epithelium using a collagen vitrigel-sponge scaffold containing basic fibroblast growth factor. *The annals of otology, rhinology, and laryngology* 2012;121:261-8.
- [250] Takezawa T, Ozaki K, Nitani A, Takabayashi C, Shimo-Oka T. Collagen vitrigel: a novel scaffold that can facilitate a three-dimensional culture for reconstructing organoids. *Cell transplantation* 2004;13:463-73.

- [251] Hamilton NJ, Kanani M, Roebuck DJ, Hewitt RJ, Cetto R, Culme-Seymour EJ, et al. Tissue-Engineered Tracheal Replacement in a Child: A 4-Year Follow-Up Study. *American journal of transplantation* 2015.
- [252] Friess W. Collagen – biomaterial for drug delivery. *European Journal of Pharmaceutics and Biopharmaceutics* 1998;45:113-36.
- [253] Stamov DR, Pompe T. Structure and function of ECM-inspired composite collagen type I scaffolds. *Soft Matter* 2012;8:10200-12.
- [254] Knight CG, Morton LF, Peachey AR, Tuckwell DS, Farndale RW, Barnes MJ. The collagen-binding A-domains of integrins alpha(1)beta(1) and alpha(2)beta(1) recognize the same specific amino acid sequence, GFOGER, in native (triple-helical) collagens. *The Journal of biological chemistry* 2000;275:35-40.
- [255] O'Brien FJ, Harley BA, Yannas IV, Gibson L. Influence of freezing rate on pore structure in freeze-dried collagen-GAG scaffolds. *Biomaterials* 2004;25:1077-86.
- [256] O'Brien FJ, Harley BA, Yannas IV, Gibson LJ. The effect of pore size on cell adhesion in collagen-GAG scaffolds. *Biomaterials* 2005;26:433-41.
- [257] Cunniffe GM, O'Brien FJ. Collagen scaffolds for orthopedic regenerative medicine. *Journal of the metals, minerals and materials Society* 2011;63:66-73.
- [258] Duffy GP, McFadden TM, Byrne EM, Gill SL, Farrell E, O'Brien FJ. Towards in vitro vascularisation of collagen-GAG scaffolds. *European cells & materials* 2011;21:15-30.
- [259] Tierney EG, Duffy GP, Cryan SA, Curtin CM, O'Brien FJ. Non-viral gene-activated matrices: next generation constructs for bone repair. *Organogenesis* 2013;9:22-8.
- [260] Lyons FG, Al-Munajjed AA, Kieran SM, Toner ME, Murphy CM, Duffy GP, et al. The healing of bony defects by cell-free collagen-based scaffolds compared to stem cell-seeded tissue engineered constructs. *Biomaterials* 2010;31:9232-43.
- [261] David F, Levingstone TJ, Schneeweiss W, de Swarte M, Jahns H, Gleeson JP, et al. Enhanced bone healing using collagen-hydroxyapatite scaffold implantation in the treatment of a large multiloculated mandibular aneurysmal bone cyst in a thoroughbred filly. *Journal of tissue engineering and regenerative medicine* 2015;9:1193-9.

- [262] Levingstone TJ, Thompson E, Matsiko A, Schepens A, Gleeson JP, O'Brien FJ. Multi-layered collagen-based scaffolds for osteochondral defect repair in rabbits. *Acta biomaterialia* 2016;32:149-60.
- [263] Levingstone TJ, Ramesh A, Brady RT, Brama PA, Kearney C, Gleeson JP, et al. Cell-free multi-layered collagen-based scaffolds demonstrate layer specific regeneration of functional osteochondral tissue in caprine joints. *Biomaterials* 2016;87:69-81.
- [264] Curtin CM, Cunniffe GM, Lyons FG, Bessho K, Dickson GR, Duffy GP, et al. Innovative collagen nano-hydroxyapatite scaffolds offer a highly efficient non-viral gene delivery platform for stem cell-mediated bone formation. *Advanced materials* 2012;24:749-54.
- [265] Mencia Castano I, Curtin CM, Shaw G, Murphy JM, Duffy GP, O'Brien FJ. A novel collagen-nanohydroxyapatite microRNA-activated scaffold for tissue engineering applications capable of efficient delivery of both miR-mimics and antagomiRs to human mesenchymal stem cells. *Journal of controlled release* 2015;200:42-51.
- [266] Fitzgerald KA, Guo J, Tierney EG, Curtin CM, Malhotra M, Darcy R, et al. The use of collagen-based scaffolds to simulate prostate cancer bone metastases with potential for evaluating delivery of nanoparticulate gene therapeutics. *Biomaterials* 2015;66:53-66.
- [267] Quinlan E, Lopez-Noriega A, Thompson EM, Hibbitts A, Cryan SA, O'Brien FJ. Controlled release of vascular endothelial growth factor from spray-dried alginate microparticles in collagen-hydroxyapatite scaffolds for promoting vascularization and bone repair. *Journal of tissue engineering and regenerative medicine* 2015.
- [268] Quinlan E, Thompson EM, Matsiko A, O'Brien FJ, Lopez-Noriega A. Long-term controlled delivery of rhBMP-2 from collagen-hydroxyapatite scaffolds for superior bone tissue regeneration. *Journal of controlled release* 2015;207:112-9.
- [269] Quinlan E, Thompson EM, Matsiko A, O'Brien FJ, Lopez-Noriega A. Functionalization of a collagen-hydroxyapatite scaffold with osteostatin to facilitate enhanced bone regeneration. *Advanced healthcare materials* 2015;4:2649-56.
- [270] Ryan AJ, O'Brien FJ. Insoluble elastin reduces collagen scaffold stiffness, improves viscoelastic properties, and induces a contractile phenotype in smooth muscle cells. *Biomaterials* 2015;73:296-307.

- [271] Brougham CM, Levingstone TJ, Jockenhoevel S, Flanagan TC, O'Brien FJ. Incorporation of fibrin into a collagen-glycosaminoglycan matrix results in a scaffold with improved mechanical properties and enhanced capacity to resist cell-mediated contraction. *Acta biomaterialia* 2015;26:205-14.
- [272] Tierney EG. Non-viral gene-activated matrices for bone repair applications (PhD thesis). Dublin: Royal College of Surgeons in Ireland; 2012.
- [273] Tierney EG, Duffy GP, Cryan SA, Curtin CM, O'Brien FJ. Non-viral gene-activated matrices-next generation constructs for bone repair. *Organogenesis* 2013;9.
- [274] Haugh MG, Murphy CM, McKiernan RC, Altenbuchner C, O'Brien FJ. Crosslinking and mechanical properties significantly influence cell attachment, proliferation, and migration within collagen glycosaminoglycan scaffolds. *Tissue engineering Part A* 2011;17:1201-8.
- [275] Haugh MG, Murphy CM, O'Brien FJ. Novel freeze-drying methods to produce a range of collagen-glycosaminoglycan scaffolds with tailored mean pore sizes. *Tissue engineering Part C, Methods* 2010;16:887-94.
- [276] Murphy CM, Haugh MG, O'Brien FJ. The effect of mean pore size on cell attachment, proliferation and migration in collagen-glycosaminoglycan scaffolds for bone tissue engineering. *Biomaterials* 2010;31:461-6.
- [277] Engler AJ, Sen S, Sweeney HL, Discher DE. Matrix elasticity directs stem cell lineage specification. *Cell* 2006;126:677-89.
- [278] Olde Damink LH, Dijkstra PJ, van Luyn MJ, van Wachem PB, Nieuwenhuis P, Feijen J. Cross-linking of dermal sheep collagen using a water-soluble carbodiimide. *Biomaterials* 1996;17:765-73.
- [279] Yannas IV, Lee E, Orgill DP, Skrabut EM, Murphy GF. Synthesis and characterization of a model extracellular matrix that induces partial regeneration of adult mammalian skin. *Proceedings of the National Academy of Sciences of the United States of America* 1989;86:933-7.
- [280] Tierney CM, Haugh MG, Liedl J, Mulcahy F, Hayes B, O'Brien FJ. The effects of collagen concentration and crosslink density on the biological, structural and mechanical properties of collagen-GAG scaffolds for bone tissue engineering. *Journal of the mechanical behavior of biomedical materials* 2009;2:202-9.
- [281] Farrell E, O'Brien FJ, Doyle P, Fischer J, Yannas I, Harley BA, et al. A collagen-glycosaminoglycan scaffold supports adult rat mesenchymal stem cell

- differentiation along osteogenic and chondrogenic routes. *Tissue engineering* 2006;12:459-68.
- [282] Lemmer HJ, Hamman JH. Paracellular drug absorption enhancement through tight junction modulation. *Expert opinion on drug delivery* 2013;10:103-14.
- [283] Haugh MG, Jaasma MJ, O'Brien FJ. The effect of dehydrothermal treatment on the mechanical and structural properties of collagen-GAG scaffolds. *Journal of biomedical materials research Part A* 2009;89:363-9.
- [284] Thornton DJ, Sheehan JK. From mucins to mucus: toward a more coherent understanding of this essential barrier. *Proceedings of the American Thoracic Society* 2004;1:54-61.
- [285] Choksi SP, Lauter G, Swoboda P, Roy S. Switching on cilia: transcriptional networks regulating ciliogenesis. *Development* 2014;141:1427-41.
- [286] Ali MS, Pearson JP. Upper airway mucin gene expression: a review. *The Laryngoscope* 2007;117:932-8.
- [287] Livak KJ, Schmittgen TD. Analysis of relative gene expression data using real-time quantitative PCR and the $2^{-\Delta\Delta C(T)}$ Method. *Methods* 2001;25:402-8.
- [288] Gruenert DC, Finkbeiner WE, Widdicombe JH. Culture and transformation of human airway epithelial cells. *The American journal of physiology* 1995;268:L347-60.
- [289] Widdicombe J. Airway and alveolar permeability and surface liquid thickness: theory. *Journal of applied physiology* 1997;82:3-12.
- [290] Widdicombe JH, Bastacky SJ, Wu DX, Lee CY. Regulation of depth and composition of airway surface liquid. *The European respiratory journal* 1997;10:2892-7.
- [291] Kim V, Rogers TJ, Criner GJ. New concepts in the pathobiology of chronic obstructive pulmonary disease. *Proceedings of the American Thoracic Society* 2008;5:478-85.
- [292] Fiegel J, Ehrhardt C, Schaefer UF, Lehr CM, Hanes J. Large porous particle impingement on lung epithelial cell monolayers--toward improved particle characterization in the lung. *Pharmaceutical research* 2003;20:788-96.
- [293] Hutter V, Chau DY, Hilgendorf C, Brown A, Cooper A, Zann V, et al. Digoxin net secretory transport in bronchial epithelial cell layers is not exclusively mediated

by P-glycoprotein/MDR1. *European journal of pharmaceutics and biopharmaceutics* 2014;86:74-82.

[294] Huang TW, Chan YH, Cheng PW, Young YH, Lou PJ, Young TH. Increased mucociliary differentiation of human respiratory epithelial cells on hyaluronan-derivative membranes. *Acta biomaterialia* 2010;6:1191-9.

[295] Stentebjerg-Andersen A, Notlevsen IV, Brodin B, Nielsen CU. Calu-3 cells grown under AIC and LCC conditions: Implications for dipeptide uptake and transepithelial transport of substances. *European journal of pharmaceutics and biopharmaceutics* 2011;78:19-26.

[296] You Y, Huang T, Richer EJ, Schmidt JE, Zabner J, Borok Z, et al. Role of f-box factor foxj1 in differentiation of ciliated airway epithelial cells. *American journal of physiology Lung cellular and molecular physiology* 2004;286:L650-7.

[297] Paz AC, Soleas J, Poon JC, Trieu D, Waddell TK, McGuigan AP. Challenges and opportunities for tissue-engineering polarized epithelium. *Tissue engineering Part B, Reviews* 2013.

[298] Matsiko A, Levingstone TJ, O'Brien FJ, Gleeson JP. Addition of hyaluronic acid improves cellular infiltration and promotes early-stage chondrogenesis in a collagen-based scaffold for cartilage tissue engineering. *Journal of the mechanical behavior of biomedical materials* 2012;11:41-52.

[299] Murphy CM, Matsiko A, Haugh MG, Gleeson JP, O'Brien FJ. Mesenchymal stem cell fate is regulated by the composition and mechanical properties of collagen-glycosaminoglycan scaffolds. *Journal of the mechanical behavior of biomedical materials* 2012;11:53-62.

[300] Levingstone TJ, Matsiko A, Dickson GR, O'Brien FJ, Gleeson JP. A biomimetic multi-layered collagen-based scaffold for osteochondral repair. *Acta biomaterialia* 2014;10:1996-2004.

[301] Hayflick L, Moorhead PS. The serial cultivation of human diploid cell strains. *Experimental cell research* 1961;25:585-621.

[302] Freyman TM, Yannas IV, Yokoo R, Gibson LJ. Fibroblast contraction of a collagen-GAG matrix. *Biomaterials* 2001;22:2883-91.

[303] Caliarì SR, Ramirez MA, Harley BA. The development of collagen-GAG scaffold-membrane composites for tendon tissue engineering. *Biomaterials* 2011;32:8990-8.

- [304] Bridge JC, Aylott JW, Brightling CE, Ghaemmaghami AM, Knox AJ, Lewis MP, et al. Adapting the electrospinning process to provide three unique environments for a tri-layered in vitro model of the airway wall. *Journal of visualized experiments* 2015.
- [305] Melo E, Kasper JY, Unger RE, Farre R, Kirkpatrick CJ. Development of a bronchial wall model: triple culture on a decellularized porcine trachea. *Tissue engineering Part C, Methods* 2015;21:909-21.
- [306] Lee CR, Grodzinsky AJ, Spector M. The effects of cross-linking of collagen-glycosaminoglycan scaffolds on compressive stiffness, chondrocyte-mediated contraction, proliferation and biosynthesis. *Biomaterials* 2001;22:3145-54.
- [307] Thornton DJ, Rousseau K, McGuckin MA. Structure and function of the polymeric mucins in airways mucus. *Annual review of physiology* 2008;70:459-86.
- [308] Schuster BS, Suk JS, Woodworth GF, Hanes J. Nanoparticle diffusion in respiratory mucus from humans without lung disease. *Biomaterials* 2013;34:3439-46.
- [309] Ivanov AI, Parkos CA, Nusrat A. Cytoskeletal regulation of epithelial barrier function during inflammation. *The American journal of pathology* 2010;177:512-24.
- [310] Pezzulo AA, Starner TD, Scheetz TE, Traver GL, Tilley AE, Harvey BG, et al. The air-liquid interface and use of primary cell cultures are important to recapitulate the transcriptional profile of in vivo airway epithelia. *American journal of physiology Lung cellular and molecular physiology* 2011;300:L25-31.
- [311] Chan BP, Leong KW. Scaffolding in tissue engineering: general approaches and tissue-specific considerations. *European spine journal* 2008;17 Suppl 4:467-79.
- [312] Ong HX, Traini D, Young PM. Pharmaceutical applications of the Calu-3 lung epithelia cell line. *Expert opinion on drug delivery* 2013;10:1287-302.
- [313] Berube K, Prytherch Z, Job C, Hughes T. Human primary bronchial lung cell constructs: the new respiratory models. *Toxicology* 2010;278:311-8.
- [314] Kaliner M, Marom Z, Patow C, Shelhamer J. Human respiratory mucus. *The Journal of allergy and clinical immunology* 1984;73:318-23.
- [315] Tadokoro T, Wang Y, Barak LS, Bai Y, Randell SH, Hogan BL. IL-6/STAT3 promotes regeneration of airway ciliated cells from basal stem cells. *Proceedings of the National Academy of Sciences of the United States of America* 2014;111:E3641-9.

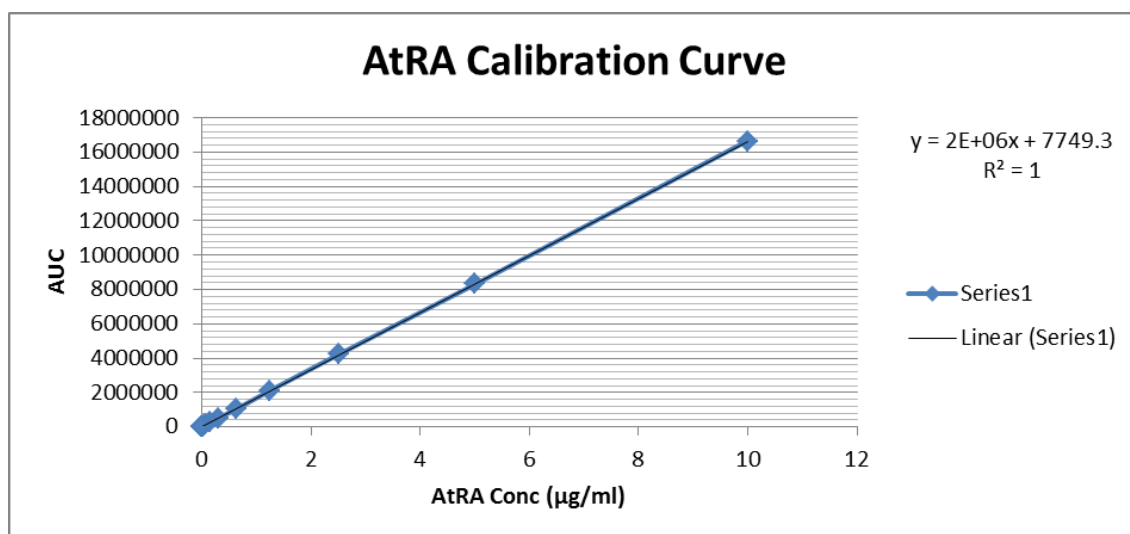
- [316] Yaghi A, Zaman A, Dolovich M. Primary human bronchial epithelial cells grown from explants. *Journal of visualized experiments* 2010.
- [317] Endres M, Leinhase I, Kaps C, Wentges M, Unger M, Olze H, et al. Changes in the gene expression pattern of cytokeratins in human respiratory epithelial cells during culture. *European archives of oto-rhino-laryngology* 2005;262:390-6.
- [318] Le Visage C, Dunham B, Flint P, Leong KW. Coculture of mesenchymal stem cells and respiratory epithelial cells to engineer a human composite respiratory mucosa. *Tissue engineering* 2004;10:1426-35.
- [319] Yuan S, Sun Z. Expanding horizons: ciliary proteins reach beyond cilia. *Annual review of genetics* 2013;47:353-76.
- [320] Fahy JV. Goblet cell and mucin gene abnormalities in asthma. *Chest* 2002;122:320S-6S.
- [321] Orlando RC. Review article: oesophageal mucosal resistance. *Alimentary pharmacology & therapeutics* 1998;12:191-7.
- [322] Herfs M, Hubert P, Poirrier AL, Vandevenne P, Renoux V, Habraken Y, et al. Proinflammatory cytokines induce bronchial hyperplasia and squamous metaplasia in smokers: implications for chronic obstructive pulmonary disease therapy. *American journal of respiratory cell and molecular biology* 2012;47:67-79.
- [323] Gray AC, McLeod JD, Clothier RH. A review of in vitro modelling approaches to the identification and modulation of squamous metaplasia in the human tracheobronchial epithelium. *Alternatives to laboratory animals* 2007;35:493-504.
- [324] Hovenberg HW, Davies JR, Carlstedt I. Different mucins are produced by the surface epithelium and the submucosa in human trachea: identification of MUC5AC as a major mucin from the goblet cells. *The biochemical journal* 1996;318 (Pt 1):319-24.
- [325] Htwe SS, Harrington H, Knox A, Rose F, Aylott J, Haycock JW, et al. Investigating NF-kappaB signaling in lung fibroblasts in 2D and 3D culture systems. *Respiratory research* 2015;16:144.
- [326] Skibinski G, Elborn JS, Ennis M. Bronchial epithelial cell growth regulation in fibroblast cocultures: the role of hepatocyte growth factor. *American journal of physiology Lung cellular and molecular physiology* 2007;293:L69-76.
- [327] Chambers-Fox S. Remington Education: Pharmaceuticals. 1 ed. United Kingdom: Pharmaceutical Press; 2014.

- [328] Man Y, Hart VJ, Ring CJ, Sanjar S, West MR. Loss of epithelial integrity resulting from E-cadherin dysfunction predisposes airway epithelial cells to adenoviral infection. *American journal of respiratory cell and molecular biology* 2000;23:610-7.
- [329] Lin H, Li H, Cho HJ, Bian S, Roh HJ, Lee MK, et al. Air-liquid interface (ALI) culture of human bronchial epithelial cell monolayers as an in vitro model for airway drug transport studies. *Journal of pharmaceutical sciences* 2007;96:341-50.
- [330] Hardyman MA, Wilkinson E, Martin E, Jayasekera NP, Blume C, Swindle EJ, et al. TNF-alpha-mediated bronchial barrier disruption and regulation by src-family kinase activation. *The Journal of allergy and clinical immunology* 2013;132:665-75 e8.
- [331] Pothoven KL, Norton JE, Hulse KE, Suh LA, Carter RG, Rocci E, et al. Oncostatin M promotes mucosal epithelial barrier dysfunction, and its expression is increased in patients with eosinophilic mucosal disease. *The Journal of allergy and clinical immunology* 2015;136:737-46 e4.
- [332] Sears PR, Thompson K, Knowles MR, Davis CW. Human airway ciliary dynamics. *American journal of physiology Lung cellular and molecular physiology* 2012.
- [333] Sachs LA, Finkbeiner WE, Widdicombe JH. Effects of media on differentiation of cultured human tracheal epithelium. *In vitro cellular & developmental biology (Animal)* 2003;39:56-62.
- [334] Vogel G. Trachea transplants test the limits. *Science* 2013;340:266-8.
- [335] National Center for Biotechnology Information PubChem Compound Database. Retinoic Acid. Available at <http://pubchem.ncbi.nlm.nih.gov/compound/444795>. Accessed 7/4/16.
- [336] Martindale: The Complete Drug Reference [online]. London: Pharmaceutical Press. Accessed 7/4/16.
- [337] Jeong YI, Song JG, Kang SS, Ryu HH, Lee YH, Choi C, et al. Preparation of poly(DL-lactide-co-glycolide) microspheres encapsulating all-trans retinoic acid. *International journal of pharmaceutics* 2003;259:79-91.
- [338] Cirpanli Y, Unlu N, Calis S, Hincal AA. Formulation and in-vitro characterization of retinoic acid loaded poly (lactic-co-glycolic acid) microspheres. *Journal of microencapsulation* 2005;22:877-89.

- [339] Puppi D, Piras AM, Detta N, Dinucci D, Chiellini F. Poly(lactic-co-glycolic acid) electrospun fibrous meshes for the controlled release of retinoic acid. *Acta biomaterialia* 2010;6:1258-68.
- [340] Almouazen E, Bourgeois S, Boussaid A, Valot P, Malleval C, Fessi H, et al. Development of a nanoparticle-based system for the delivery of retinoic acid into macrophages. *International journal of pharmaceutics* 2012;430:207-15.
- [341] Huang TW, Chan YH, Su HW, Chou YS, Young TH. Increased mucociliary differentiation and aquaporins formation of respiratory epithelial cells on retinoic acid-loaded hyaluronan-derivative membranes. *Acta biomaterialia* 2013;9:6783-9.
- [342] Muyonga JH, Cole CGB, Duodu KG. Fourier transform infrared (FTIR) spectroscopic study of acid soluble collagen and gelatin from skins and bones of young and adult Nile perch (*Lates niloticus*). *Food Chemistry* 2004;86:325-32.
- [343] Gopinath D, Ahmed MR, Gomathi K, Chitra K, Sehgal PK, Jayakumar R. Dermal wound healing processes with curcumin incorporated collagen films. *Biomaterials* 2004;25:1911-7.
- [344] Vidal Bde C, Mello ML. Collagen type I amide I band infrared spectroscopy. *Micron (Oxford, England : 1993)* 2011;42:283-9.
- [345] Aulton ME. *Aulton's pharmaceutics: the design and manufacture of medicines*. 4e. Edinburgh: Churchill Livingstone; 2007.
- [346] McFadden TM, Duffy GP, Allen AB, Stevens HY, Schwarzmaier SM, Plesnila N, et al. The delayed addition of human mesenchymal stem cells to pre-formed endothelial cell networks results in functional vascularization of a collagen-glycosaminoglycan scaffold in vivo. *Acta biomaterialia* 2013;9:9303-16.
- [347] Delaere PR, Van Raemdonck D. The trachea: the first tissue-engineered organ? *Journal of thoracic and cardiovascular surgery* 2014;147:1128-32.
- [348] Asnaghi MA, Jungebluth P, Raimondi MT, Dickinson SC, Rees LE, Go T, et al. A double-chamber rotating bioreactor for the development of tissue-engineered hollow organs: from concept to clinical trial. *Biomaterials* 2009;30:5260-9.
- [349] Pusch J, Votteler M, Gohler S, Engl J, Hampel M, Walles H, et al. The physiological performance of a three-dimensional model that mimics the microenvironment of the small intestine. *Biomaterials* 2011;32:7469-78.

Appendices

Appendix 1:



Sample calibration curve used in the high performance liquid chromatographic (HPLC) analysis of all-*trans* retinoic acid (atRA). Standard solutions of atRA were serially diluted to provide a concentration range of 10µg/ml to 0.00056µg/ml for resultant analysis of samples for atRA *in vitro* release and encapsulation efficiency studies. Preparation of standard curves was performed with occasional contributions from Ms. Gemma O'Connor and Ms. Christina Payne, RCSI.